INFORMATION TO USERS

This manuscript has been reproduced from the microfilm master. UMI films the text directly from the original or copy submitted. Thus, some thesis and dissertation copies are in typewriter face, while others may be from any type of computer printer.

The quality of this reproduction is dependent upon the quality of the copy submitted. Broken or indistinct print, colored or poor quality illustrations and photographs, print bleedthrough, substandard margins, and improper alignment can adversely affect reproduction.

In the unlikely event that the author did not send UMI a complete manuscript and there are missing pages, these will be noted. Also, if unauthorized copyright material had to be removed, a note will indicate the deletion.

Oversize materials (e.g., maps, drawings, charts) are reproduced by sectioning the original, beginning at the upper left-hand corner and continuing from left to right in equal sections with small overlaps. Each original is also photographed in one exposure and is included in reduced form at the back of the book.

Photographs included in the original manuscript have been reproduced xerographically in this copy. Higher quality 6" x 9" black and white photographic prints are available for any photographs or illustrations appearing in this copy for an additional charge. Contact UMI directly to order.

UMI®

Bell & Howell Information and Learning
300 North Zeeb Road, Ann Arbor, MI 48106-1346 USA
800-521-0600

Photogeneration and Chemistry of Quinone Methides from Hydroxybenzyl Alcohols

by

Li Diao
B.Sc., Beijing University of Aeronautics and Astronautics, 1990
M.Sc., Institute of Photographic Chemistry, Chinese Academy of Science, 1993

A Dissertation Submitted in Partial Fulfillment of the
Requirements for the Degree of

DOCTOR OF PHILOSOPHY

in the Department of Chemistry

We accept this dissertation as conforming
to the required standard

Dr. P. C. Wan, Supervisor (Department of Chemistry)

Dr. C. Bohne, Department Member (Department of Chemistry)

Dr. D. J. Berg, Department Member (Department of Chemistry)

Dr. J. Ausio, Outside Member (Department of Biochemistry and Microbiology)

Dr. R. A. McClelland, External Examiner (University of Toronto)

Supervisor: Dr. P. C. Wan

Abstract

The photosolvolysis of a series of hydroxy-substituted benzyl alcohols ($ArCH_2OH$) has been studied. Photomethanolysis of these alcohols showed exceptionally higher efficiencies for methyl ether formation (in 1:1 H_2O-MeOH) than the corresponding methoxybenzyl alcohols. UV-Vis absorption spectra of photogenerated transients were recorded in aqueous solution and had similar appearance to the carbocations that are observable from the methoxybenzyl alcohols, but with much longer lifetimes. These transients were also observable in neat organic solution for the ortho isomers. The yields of all these transients increased with increasing water content. The highest yields were observed in basic aqueous solution when pH > $pK_a(S_o)$ (of the phenol moiety). In addition, photolysis of the appropriate coumaranones gave the same transient absorption as that from the corresponding *o*-hydroxybenzyl alcohols. Since photolysis of coumaranones are known to give *o*-quinone methide (*o*-QM) intermediates (via loss of CO), the transients observed for the *o*-hydroxybenzyl alcohols are assigned to *o*-QMs. The transients observed for the *m* and *p*-isomers are assigned to the corresponding *m* and *p*-QMs. The quantum efficiencies for QMs generation from hydroxybenzyl alcohols are in the order as $o > m >> p$, in agreement with Zimmerman's ortho-meta activation theory.

The mechanism proposed at pH < $pK_a(S_o)$ involves adiabatic deprotonation of the ArOH moiety in the first excited singlet state (S_1) followed by heterolytic cleavage of the C-O bond of the hydroxymethyl group. In basic media, direct excitation of the phenolate

ion results in the loss of hydroxide ion to generate QMs. Subsequent nucleophilic trapping of these QMs by solvent results in the observed solvolysis product. *o*-QMs were also generated in neat organic solution. The proposed mechanism involves adiabatic deprotonation of phenol moiety facilitated by either intermolecular or intramolecular hydrogen bonding with a benzylic OH group.

This Thesis has demonstrated that a simple and general method is available for the photogeneration of all the QM isomers. Notably, the method is applicable to *m*-QMs, which have previously required more elaborate methods for their generation. A polymerization reaction of *m*-QMs has been discovered in basic media during investigations of their chemistry.

Dr. P. C. Wan, Supervisor (Department of Chemistry)

Dr. C. Bohne, Department Member (Department of Chemistry)

Dr. D. J. Berg, Department Member (Department of Chemistry)

Dr. J. Ausio, Outside Member (Department of Biochemistry and Microbiology)

Dr. R. A. McClelland, External Examiner (University of Toronto)

Table of Contents

List of Figures

List of Tables

List of Abreviations

BQ	Benzoquinone
CIP	Contact ion pair
DPMC	Diphenylmethyl chloride
ESPT	Excited state proton transfer
ET	Electron transfer
EVE	Ethyl vinyl ether
GRP	Geminate radical pair
HFIP	1,1,1,3,3,3-Hexafluoroisopropyl alcohol
HOMO	Highest occupied molecular orbital
ISC	Intersystem crossing
LCAO	Linear combination of atomic orbitals
LFP	Laser flash photolysis
LUMO	Lowest unoccupied molecular orbital
***m*-NQM**	*m*-Naphthoquinomethane
MO	Molecular orbital
NBMO	Nonbonding molecular orbitals
OMA	Optical multichannel analyzers
PMT	Photomultiplier tubes
PR	Pulse radiolysis
QDM	Quinone dimethide
QM	Quinone methide
SSIP	Solvent solvated ion pairs
TAM	Triarylmethyl
TFE	2,2,2-Trifluoroethanol
VBCM	Valence-bond configuration mixing model

Acknowledgements

I would like to express my great thankfulness to my supervisor Dr. Peter Wan for his thoughtful guidance and contributions to this work. His spirit of scientific inquiry will benefit me throughout my whole life. I would also like to thank my colleagues, Dr. Dave Budac, Dr. Yijian Shi, Maike Fischer, Darryl Brousmiche, Christy Chen, Kai Zhang, Beverly Barker and Sarah Baker, who made my life in Victoria so enjoyable. My special thanks goes to Dr. Cornelia Bohne and her group members: Luis Netter, Mark Kleinman and Scott Murphy for their generous help in laser photolysis system. I appreciate the friendship and generosity I received from everyone in the Department of Chemistry. The funding by NSERC and the University of Victoria is gratefully acknowledged.

My great appreciation goes to XiangZhou, my husband, for his understanding, help and patience. My parents also deserve great thanks for their year long encouragement and support.

Dedication

To

my husband

and my parents

Chapter 1

Introduction

1.1 Prologue

In organic photochemical reactions, the molecular species involved is electronically excited and generally will have an electronic configuration significantly changed from that of its ground state progenitor. As a consequence, photochemical reactions can occur via entirely different pathways from those encountered in the ground state and afford different products in general.

An understanding of structure-reactivity relationships from mechanistic studies enables photochemists to deduce the electronic structures of excited states.[1] The ground state electronic configuration of organic molecules consists of bonding molecular orbitals (MOs) each with a pair of electrons and unoccupied antibonding MOs. The absorption of light causes excitation of an electron from the highest occupied MO (HOMO) to the lowest unoccupied MO (LUMO), thereby creating an electronically excited state. Electronically excited molecules are short-lived and will dissipate the excess energy to go back to the stable ground state. The dissipation processes can be either radiative or non-radiative. Among the non-radiative pathways, organic chemists are interested in chemical processes including unimolecular reactions (fragmentations and molecular

isomerizations) and bimolecular photochemical reactions (such as electron transfer to or from the excited species, intermolecular hydrogen abstraction, etc.).

Since excited state σ-bond cleavage reactions will be the main theme of this Thesis, it is necessary to briefly introduce their mechanistic possibilities. The three most commonly cited bond fragmentation process in the literature are (i) homolysis, where the bonding electron pair is equally apportioned between the two departing fragments; (ii) heterolysis, where the bonding electron pair remains with one fragment; and (iii) mesolytic cleavage, which involves the fragmentation of radical ions, formed as a result of electron transfer. The particular pathway followed by a given molecule is governed by a number of factors including the nature of the solvent, the leaving group, and the excited state (singlet versus triplet) from which the reaction is taking place.

Most of the intermediates involved in photochemistry are short-lived. Although a large amount of conventional studies have laid the foundation for understanding the details of photochemical reactions, relatively fast techniques[2a] based on lasers have provided crucial new information on understanding these reactions, by direct observations and kinetic studies. Time-resolved techniques, including emission lifetime measurements, laser flash photolysis (LFP) and pulse radiolysis (PR) have been utilized for studying these short-lived transients. Data from these techniques have contributed to the elucidation of photochemical reaction mechanisms. For excited state lifetime measurements, photon pulses (micro to nanojoules) of short duration (pico to nanoseconds) are used to excite molecules, whose subsequent emission can then be

monitored directly by fast detectors, namely, photomultiplier tubes (PMT) and optical multichannel analyzers (OMA). In LFP, laser pulses (pico- to nanoseconds) of higher energy (usually millijoules) are used to produce photoexcited states at micromolar concentrations. Intermediates generated via these excited states are observed through absorbance changes on pico- to microsecond time scales. In PR,[2b] the interaction of a high-energy pulse of electrons (usually of nanosecond duration) with a solution gives rise to solvated electrons and solvent-derived cations (holes), which react further to produce reactive intermediates which are used for modeling the behavior of those obtained from photolysis.

1.2 Photosolvolysis

Ground state nucleophilic displacement reactions based on the S_N1-S_N2 framework of Ingold and co-workers[3] were among the first to be studied in detail and form one of the cornerstones of physical organic chemistry. The term "solvolysis" was introduced by Steigman and Hammett[4] to describe kinetically first-order reactions which involve formal heterolytic cleavage of a σ-bond between a carbon atom and a hetero atom (such as oxygen, sulfur or halogen) in large excess of solvent. The carbocationic species thus generated can be trapped by the nucleophilic solvent to give the solvolysis product. Carbocations are important intermediates in organic chemistry and hence have been extensively studied.[5,6] Their existence and role in a variety of ground state (thermal) reactions such as rearrangements, nucleophilic substitutions, and eliminations are well established.[5-7]

In organic photochemistry, the term "photosolvolysis" is used for a reaction where heterolytic cleavage followed by reaction with the solvent is initiated by photoexcitation. These reactions can be generally illustrated in their simplest form by Eq. 1.1, path a. However, in early studies, heterolytic bond cleavage reactions were not commonly encountered in organic photochemistry. The main reason is that much of the early work in photochemistry was carried out in the gas phase or in non-polar solvents where bond homolysis (Eq. 1.1, path b) is energetically preferred over bond heterolysis, considering the relatively small amounts of energy added photochemically (60-100 kcal mol^{-1}). In the absence of stabilizing solvent effects, it has been estimated[8] that heterolytic cleavage of a carbon-chlorine bond requires ≈170 kcal mol^{-1}; whereas, the homolytic bond dissociation energy is only about 80 kcal mol^{-1}. As a result, the majority of reactions in the gas phase or non-polar solvents reported in the photochemical literature involve bond homolysis and hence radical intermediates.[9-11] On the other hand, in polar solvents (such as acetonitrile, water, and alcohols) in which ions and ion pairs can be solvated, the reduced energy difference between the two processes could lead to bond heterolysis rather than homolysis. Investigations in polar solvents have made photosolvolysis a well-documented reaction.[12,13]

$$\mathrm{R{-}X} \xrightarrow{h\nu} \mathrm{R{-}X^*} \begin{cases} \xrightarrow{a} \mathrm{R^+\ X^-} \xrightarrow{\mathrm{Sol\ H}} \mathrm{H{-}X + R{-}Sol} \\ \xrightarrow{b} \mathrm{R^{\cdot}\ {\cdot}X} \longrightarrow \mathrm{R{-}R + RH + HX} \end{cases} \qquad (1.1)$$

Since the early report by Zimmerman and Sandel[14] on the photosolvolysis of benzyl acetates ($ArCH_2$-OAc) in nucleophilic solvents, considerable efforts in elucidating

the scope and mechanistic details of this type of reaction have since ensued in benzyl derivatives.[12,13] Substantial data now exists on the photosolvolysis of this system. In the early stages of the investigation, the main issues were determining whether a carbocationic intermediate was involved and from what multiplicity of the excited state it arose. Other concerns were substituent and leaving group effects. With the advent of LFP, the overall mechanism, including solvent effects and the reactivity of the photogenerated carbocation, has attracted even more attention.[15]

1.2.1 Photoheterolysis of Triarylmethyl Leuco Dyes

One of the earliest examples of photoheterolysis was reported by Lifschitz and Joffé in 1919:[16] irradiation of colorless triarylmethyl (TAM) leuco base **1a** in ethanol led to the formation of carbocation **2a** with its characteristic dye color via efficient loss of cyanide ion. Cabocation **2a** then recombines with the cyanide ion to regenerate **1a** (Eq. 1.2). Crystal violet and malachite green leucocyanide (**1b**, **1c**) behaved similarly. Both **1b** and **1c** were shown to produce the corresponding carbocations with a quantum efficiency of close to unity in ethanol. Therefore, malachite green leucocyanide has been used as a chemical actinometer.[17,18] Further investigation by Holmes[19a] showed that the photolysis of **1c** in aqueous ethanol resulted in formation of the corresponding solvolysis products **3c** and **4c** via the carbocation intermediate **2c**. Holmes[19b] also demonstrated similar photo-ion production with two additional triarylmethyl leucocyanides **1d** and **1e**. Herz[20] and others[21] have delineated that the singlet excited state of **1c** is the precursor of the dye cation.

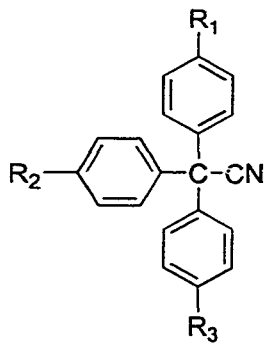

1a $R_1 = R_2 = R_3 = NH_2$
1b $R_1 = R_2 = R_3 = NMe_2$
1c $R_1 = R_2 = NMe_2$, $R_3 = H$
1d $R_1 = NMe_2$, $R_2 = R_3 = H$
1e $R_1 = R_2 = R_3 = t$-Bu

By employing picosecond LFP, Cremers and Cremers[22] have investigated the ultra-fast ionic photodissociation dynamics of compound **1c** after 266 nm excitation in ethanol. A fast rise in the absorbance at 610 nm ($t_{1/2}$ < 50 ps) was followed by a slower rise ($t_{1/2}$=120 ps) to complete the formation of **2c**. Therefore, they concluded that **1c** undergoes a very fast cleavage in ethanol to give **2c**, initially in a pyramidal conformation (sp^3 at central carbon), which then forms the more stable propeller conformation (sp^2 at the central carbon). However, Peters and Manring[23] argued that these results may not be due to changes in hybridization at the central carbon but could rather be attributable to a two-photon process in which the initially obtained S_1 state is further excited to S_n, which gave rise to **2c** on the faster time scale (> 10^9 s^{-1}).

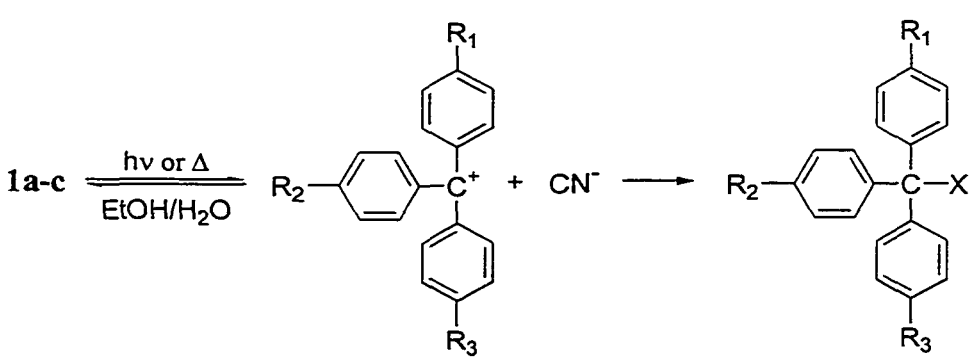

1a-c $\underset{EtOH/H_2O}{\overset{h\nu \text{ or } \Delta}{\rightleftharpoons}}$ **2a-e** (R_1, R_2, R_3 as defined for **1**) + CN^- → **3a-e** X = OH, **4a-e** X = OEt (R_1, R_2, R_3 as defined for **1**) (1.2)

Detailed mechanistic studies on **1c** were later carried out by Spears et al.[24] They agreed with Peters and Manring[23] that a higher energy excited state of **1c**, apparently accessible by absorption of a second photon from S_1, which undergoes ionic dissociation through an ionic transition state, rapidly dissociated into ions after radiationless conversion. The rate of ionization was modeled by using classical solvation energies of a dipole in a dielectric. The stability and hence ionization rate of such a transition state were determined by the solvent dielectric constant in aprotic solvents. The geometry change of the cation (**2c**, monitored at 600 nm) from an initial contact ion pair (tetrahedral) to a charge-delocalized, planar form had very fast conversion times in aprotic solvents that increased from 6 to 13 ps with increasing dielectric constant (explainable in terms of the solvent energetics).

1.2.2 Photosolvolysis of Benzyl Esters

1.2.2.1 The meta Effect

If the studies of TAM derivatives (**1a-e**) initiated considerable interest in photoheterolysis, the idea of meta activation proposed and quantified by Zimmerman and Sandel[14] gave a corresponding impetus to the investigation and understanding of photosolvolysis, as shown by the large number of papers which appeared afterwards. In their pioneering work, Zimmerman and Sandel[14] successfully revealed "the link between quantum mechanical description and experimental reality", by examining the electronic structure of mono-substituted benzenes after they recognized the importance of the idea that aromatic excited states may introduce a different reactivity from that of ground

states. The first example of this intriguing phenomenon was described by Havinga et al.[25] in a study of the photohydrolysis of the isomeric *m*- and *p*-nitrophenyl phosphate esters (**5** and **6**), as well as the corresponding sulfate esters. Curiously, the meta-isomers, which were stable in the dark, underwent facile photochemical hydrolysis, while the para isomers showed no greater reactivity than in the dark (Eqs. 1.3 and 1.4). This was the

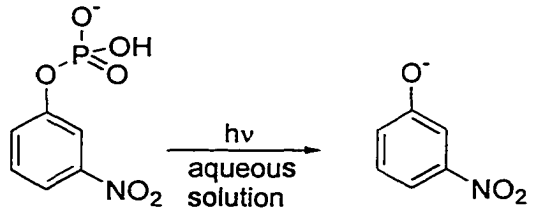

5 **(1.3)**

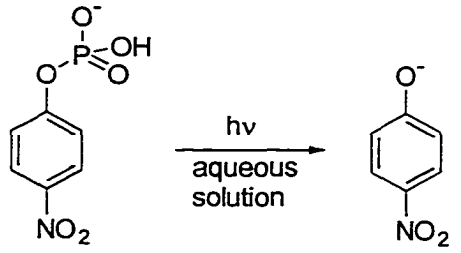

6 **(1.4)**

reverse of what is expected in the ground state (i.e., ortho-para electron transmission) and was not explicable on the basis of qualitative ground state resonance theory. Zimmerman and Somasekhara[26] provided supportive evidence by studying the photochemical solvolysis of isomeric *m*- and *p*-cyanophenyl trityl ethers **7** and **8** (Eqs. 1.5 and 1.6), in

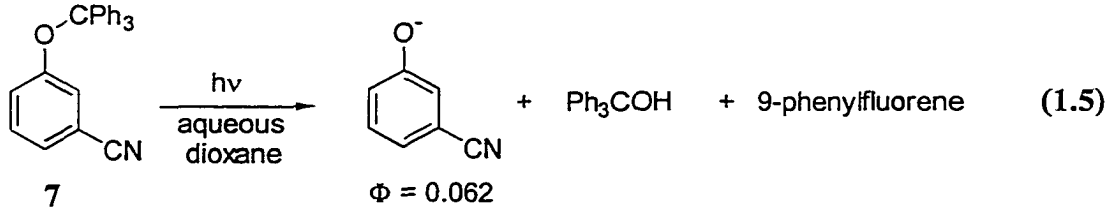

7 **(1.5)**

which the meta isomer reacted much more efficiently upon irradiation, in contrast to their ground state behavior. Molecular orbital calculations suggested preferential meta electron

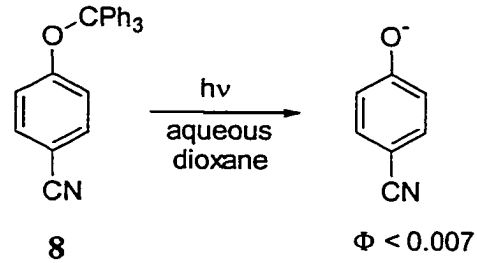

8 $\Phi < 0.007$ **(1.6)**

transmission in the singlet excited state. Havinga and coworkers[27] have subsequently reported many elegant examples of meta transmission in aromatic photosubstitution reactions of cyano-substituted aromatic compounds.

After further investigations on the photochemical reactivity of *m*- and *p*-methoxybenzyl acetates, Zimmerman and Sandel[14] coined the phrase "meta effect", which was defined at that time as the preferential transmission of electron density between meta situated groups on benzenoid compounds in the singlet excited state. Taking the electron-withdrawing group W as $-CH_2^+$ and the electron-donating group D as $-CH_2:^-$ for generality and simplicity, the aromatic compound then became the benzyl carbocation or the benzyl carbanion, respectively. Linear combination of atomic orbitals (LCAO) MO π-electron densities of the ground state and the first excited state are illustrated in Fig.1.1 for both types of aromatics and indicate a selective electron withdrawal from the *o*- and *m*-positions by W and a selective electron transmission to the *o*- and *m*-positions by D in the first excited state, in contrast to the long established ortho-para transmission in ground state chemistry. This novel ortho-meta transmission was predicted to be

characteristic of the first excited singlet state and not an isolated instance unique only to the benzyl system. A similar tendency can be seen in the LCAO MO calculations for anisole (Fig. 1.1) where the electron transmission to the *m*-position is even greater than to the *o*-position. This is the so-called "meta transmission effect".

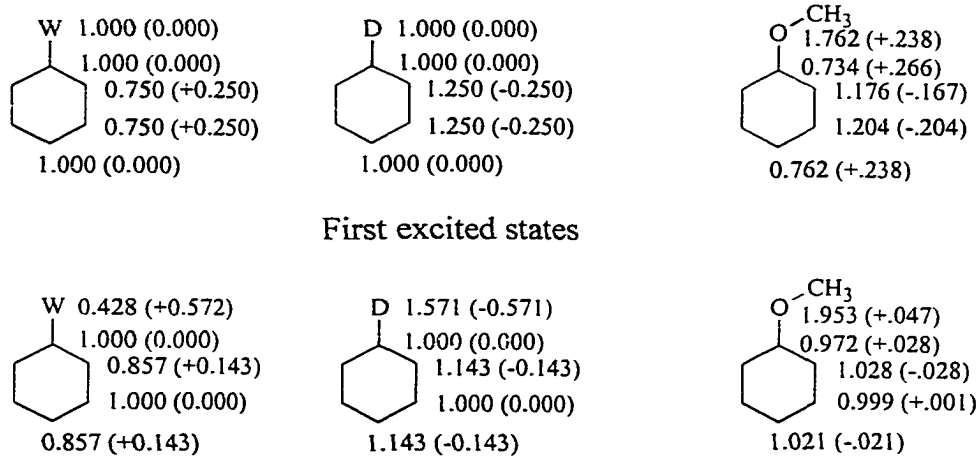

Fig. 1.1 Monosubstituted benzene electron densities (W = CH_2^+, D = $CH_2:^-$). Unparenthesized numbers are π-electron densities; parenthesized numbers are formal charges.[14]

Based on their theory, Zimmerman and Sandel[14] conceived that the placement of a $-CH_2-Y$ group at the *meta* position of anisole would possibly lead to an anionic expulsion of Y following excitation, to give entirely valence-bond structure **12** (a non-Kekulé structure), where $Y:^-$ might be chloride, acetate, etc. In striking agreement with theoretical suggestion, the photosolvolysis of the *meta*-isomer **10** in aqueous dioxane (Eq. 1.7) has a quantum yield of nearly ten times ($\Phi = 0.13$) that of the para isomer **11** ($\Phi = 0.016$). They described this effect in terms of an excited state **9** which has charge selectively transmitted to the meta position. Upon loss of ^-OAc, **12** is formed, which is

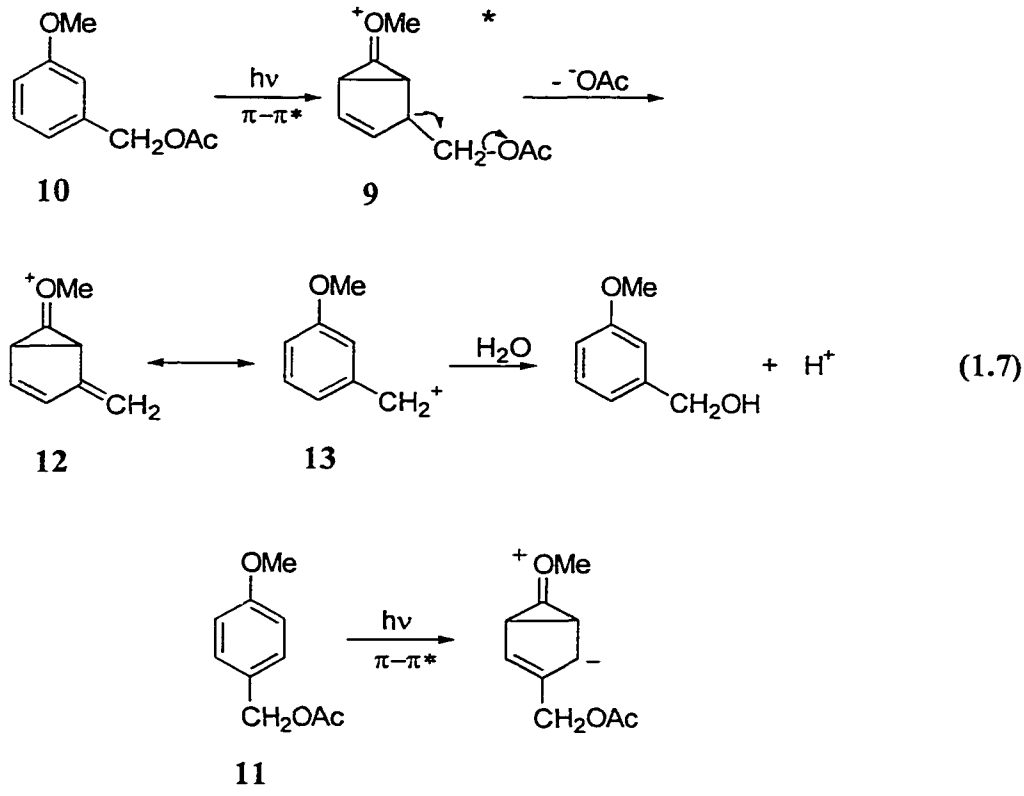

(1.7)

formally a resonance structure of the benzyl cation **13**, which then reacts with water to give the benzyl alcohol. Cristol and Bindel[12a] considered that it was more accurate to envision **12** as an excited state of **13**, i.e., **12** would have to first undergo radiationless decay to become **13**. Radical products, derived from homolysis of the C-OAc bond, were also observed. Irradiation of the 3,5-dimethoxy compound gave only the solvolysis product with even higher yield. Using a more sophisticated approach, the authors[14] calculated the π-electron energies for the first-excited states of a series of benzyl cations to describe the excited-state hypersurface. This enabled the authors to sequence the formation energy of an excited-state cation as 4-methoxybenzyl (-1.5597β) > 3-

methoxybenzyl (-1.7017β) > 3,5-dimethoxybenzyl (-1.7427β) which is consistent with the experimental results.

Recently, Zimmerman[28] has employed ab initio computations using GAUSSIAN92 to obtain more reliable results for the above systems. Three conclusions were drawn out of comparisons between the corresponding energy component of the radical and ion pairs. First, heterolysis had little energetic preference over homolysis for the *p*-methoxybenzyl isomer while the *m*-methoxybenzyl ion pair, and the 3,5-dimethoxybenzyl ion pair were energetically favored compared to the corresponding radical pair. The second concern was which ion pair for the monomethoxybenzyl species, meta or para, would make the heterolysis a preferred pathway in the S_1. The results from singlet energy calculation showed that *m*-methoxybenzyl S_1 cation formation from its singlet precursor was 15.9 kcal mol^{-1} lower in energy and had a distinct advantage over *p*-methoxybenzyl S_1 cation formation. The third comparison considered the homolysis from the S_1 state and found that the para isomer was slightly more favored by 1.68 kcal mol^{-1}.

Zimmerman and Sandel[14] emphasized the meta effect when they initially presented the calculations although it actually showed that both ortho- and meta-positions were activated in S_1 (Fig. 1.1). It was Wan and coworkers[29a] who first realized that it was actually an "ortho and meta effect" when they studied the relative reactivity of mono-methoxy-substituted benzyl alcohols. The intrinsic reactivity for these compounds was $o > m >> p$. After retackling the issue, Zimmerman[28] re-termed the "meta effect" as the "ortho-meta effect".

1.2.2.2 Multiplicity of the Excited State Precursor

In two papers published by Ivanov et al.,[30,31] controversal results regarding the multiplicity of the excited state precursor were reported for the photosolvolysis of methoxy-substituted benzyl, benzhydryl, and trityl acetates in aqueous methanol, and for the photosolvolysis of benzyl, 1-naphthylmethyl, 9-phenanthrylmethyl and 9-anthrylmethyl acetates in aqueous CH_3CN. For the first group of compounds, experiments involving quenching, sensitization, and heavy-atom effects gave the conclusion that the triplet state of these molecules was involved in the solvolysis.[30] Whereas for the second group of compounds, the interpretation of the results concluded that the first excited singlet state of these compounds was responsible for reaction.[31]

Recently, Pincock and coworkers[32] investigated the photosolvolysis of substituted benzyl acetates **14** and benzyl pivalates **15** in methanol. Selective quenching of the triplet

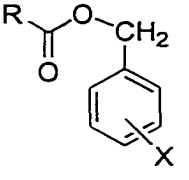

14 R = CH_3; **15** R = $C(CH_3)_3$

(X = *p*-OCH_3, CH_3, H, CF_3, CN; *m*-OCH_3)

state by 2,3-dimethylbutadiene showed that the irradiation with or without the quencher gave essentially the same values for product yields in almost all cases. Therefore, the triplet excited state was deemed unreactive and the formation of triplet radical pairs could be ignored. LFP studies[32b] of these acetates at 266 nm in methanol gave a strong

absorption in the 300-350 nm range which was assigned to the corresponding benzyl radical, and a weaker triplet-triplet absorption band of the acetates at ca. 400 nm. The benzyl radical absorption persisted even after all the triplets had been quenched by the added diene. This suggested that the singlet state of these acetates was the radical precursor.

1.2.2.3 Homolytic vs. Heterolytic Cleavage

LFP and product studies have adequately shown that a common feature in photosolvolysis is that heterolysis products are generally accompanied by products formed from radical intermediates.[12,13,15] According to Zimmerman,[14,28] competing pathways exist in the excited state. However, due to the energetic preference for heterolysis to give ion pairs, it is believed that ion pairs are generated from the singlet excited state in a primary photochemical step. Homolysis competes as an alternative primary photochemical pathway. Nevertheless, this interpretation has recently been challenged by Pincock and co-workers.[32] The major products of the photolysis of benzyl esters were formed from two critical intermediates—the ethers from the ion pair and all of the other products from the radical pair. The relative product yields depended strongly on the nature of the substituent. The explanation offered was that direct photolysis resulted in only an in-cage radical pair that in part undergoes electron transfer to give the ion pair (Scheme 1.1). Assuming that $k_{hom} >> k_{het}$ for all substitutents, the ratio of the ether product (via electron transfer) to the products derived from decarboxylation of $RCO_2^{\bullet}$ yielded k_{et} (rates of electron transfer). A plot of log k_{et} versus E° followed Marcus theory,

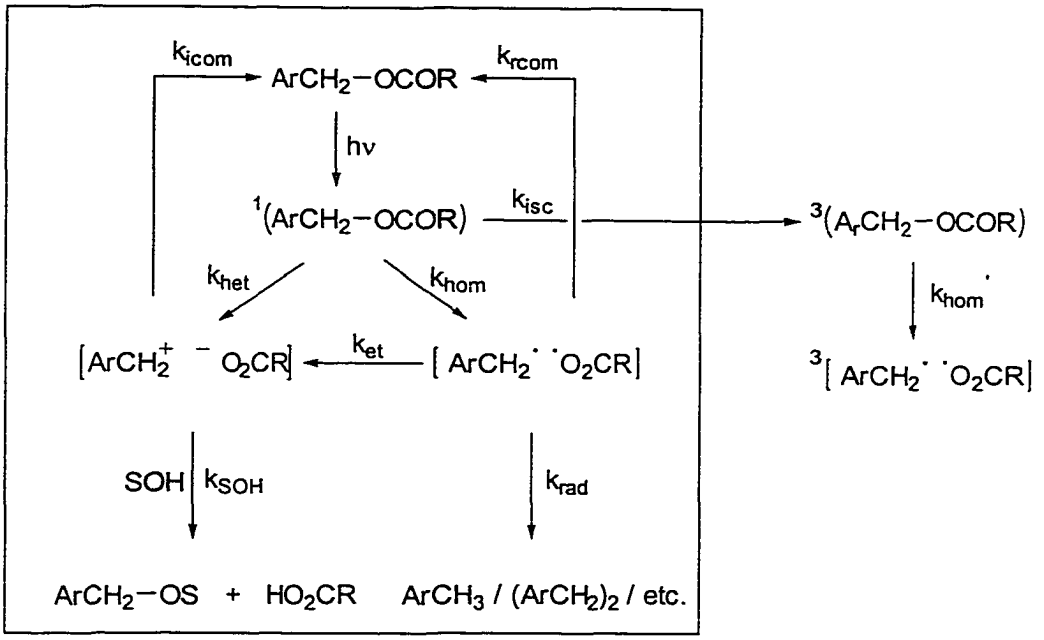

Scheme 1.1

including observation of the "inverted" region, as the process becomes more exothermic for the more easily oxidized radicals. Although the fact that the yield of ether produced from acetate esters varied from 2% for X = 4-OCH_3 to 32% for X = 3-OCH_3 could not be neglected, the authors argued that direct homolysis occurred predominantly from S_1, while direct heterolytic cleavage to form the ion pair was of minimal importance. Similar results were obtained by studying the photolysis of 1-naphthyl esters in methanol.[33]

Internal return of either the radical pair or the ion pair to the starting ester has also been investigated (Scheme 1.1). Jaeger[34] first demonstrated that photolysis of ^{18}O-labeled **16** (Scheme 1.2) in aqueous methanol resulted in the formation of the corresponding methyl ether via intermediacy of the carbocation. Some radical derived products are formed in this reaction. Photolysis of **16** and optically active **17** both showed complete

scrambling of ^{18}O in recovered substrate. Recovered **17** showed no loss of optical activity but yielded racemized methyl ether in aqueous methanol. These results are consistent with a mechanism in which the initially formed ion-pair can either cage escape to yield the solvolysis product, or collapse to give back the ^{18}O-scrambled **17** with total retention of configuration (Scheme 1.2). In effect, the ^{18}O-scrambling process only contributed to

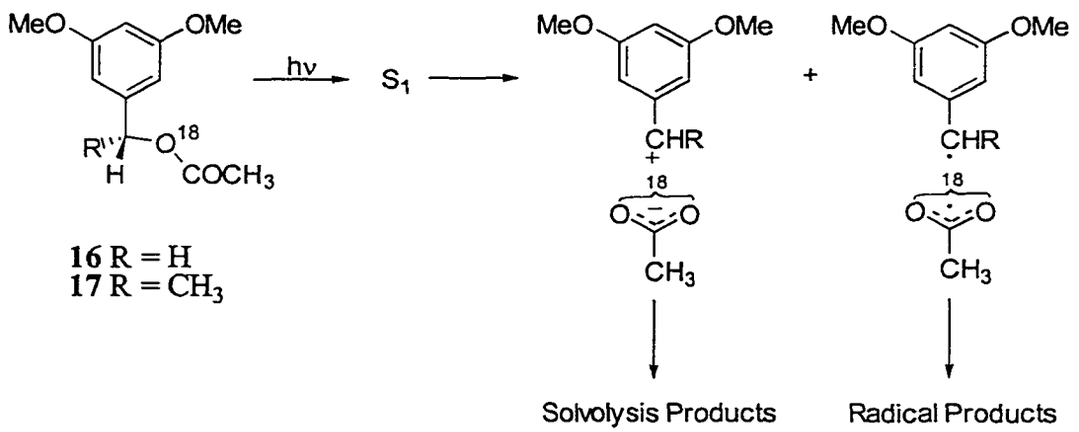

Scheme 1.2

the excited state decay and to a decreased quantum yield of product formation, without affecting the overall reactivity of either the radical or the ion pair.

1.2.3 Photosolvolysis of Benzyl Halides

Benzyl halides have been perhaps the most studied compounds to date in photosolvolysis. The multiplicity of their excited progenitor is the key question through almost all the investigations.[12] It has been found that, at least in the case of benzyl chloride, both singlet and triplet states are responsible for the formation of heterolysis products.

The investigation of 2-bromotriptycene (**18**) by Cristol and Schloemen[35] revealed, through the use of deuterium labeling, the clear participation of cationic intermediates in the acetone-sensitized photochemical solvolysis. It was also shown that direct irradiation afforded isomeric deuterium labeled alcohols **19** and **20** (Eq. 1.8) as products. It was rationalized that a vibrationally excited ground state was responsible for the reaction. A later study of benzyl chloride from the same group[36] reported that sensitization with acetone or acetophenone in methanol resulted in exclusive formation of the anticipated solvolysis product, which was absent upon direct irradiation. These results imply that some vibrational states formed from the reaction with the triplet sensitizer lead to heterolytic cleavage of the carbon-chlorine bond while the excited singlet state of benzyl chloride cleaves homolytically.

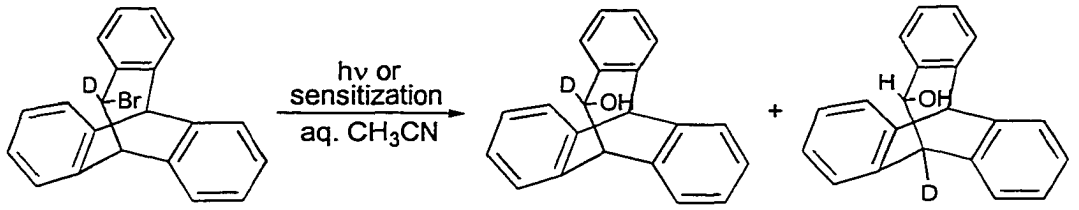

18 **19** **20** **(1.8)**

+ Radical products

Kuz'min and co-workers[37] observed that direct irradiation of benzyl chloride in alcohol-water solution gave high yield of the corresponding carbinol which was insensitive to the presence of oxygen. These authors suggested that photosolvolysis proceeded by direct heterolytic bond cleavage from the excited singlet state. A similar study of benzyl chloride carried out by Hyömäki and Koskikallio[38] in methanol-water

mixtures found both alcohol and ether products characteristic of heterolytic cleavage and radical coupling products from homolytic cleavage. Based on product ratio analysis with varying solvent compositions, the conclusion reached was that the initial photochemical reaction was homolytic cleavage from the excited singlet state followed by a competition between in-cage electron transfer to form ions and escape to give radical-derived products.

In McKenna and co-workers' hands,[39] direct irradiation of benzyl chloride in methanol afforded products characteristic of both ionic and radical pathways in yields quite similar to those reported by Hyömäki and Koskikallio.[38] Acetone-sensitized photolysis also gave both ionic and radical products, but in different proportions. Comparable results were found in the photolysis of the corresponding benzyl bromide and iodide. They were also consistent with the photochemistry of ammonium salts studied earlier.[40,41] Therefore, McKenna and coworkers[39] proposed that both the singlet and triplet excited states of benzyl chloride underwent only homolytic cleavage. The triplet radical pair can intersystem cross to the singlet radical pair, which equilibrates with the ion pairs by electron transfer.

Cristol and Bindel[42,43] have investigated the photosolvolysis of a number of benzyl chlorides in *tert*-butyl alcohol. Again, the products obtained were the same in both direct and acetone-sensitized irradiations but differ in observed ratio, i.e., sensitization favored free-radical derived products. Furthermore, a detailed quenching study of the sensitized reaction, using a combination of several techniques,[44,45,46] revealed that the state

responsible for the formation of ionic products in the sensitized reaction has a much shorter lifetime than the lowest triplet state of benzyl chloride. These authors concluded that an unspecified, short-lived upper triplet state (T_n) was formed in the sensitized reaction which was primarily responsible for the formation of ionic intermediates (Scheme 1.3).

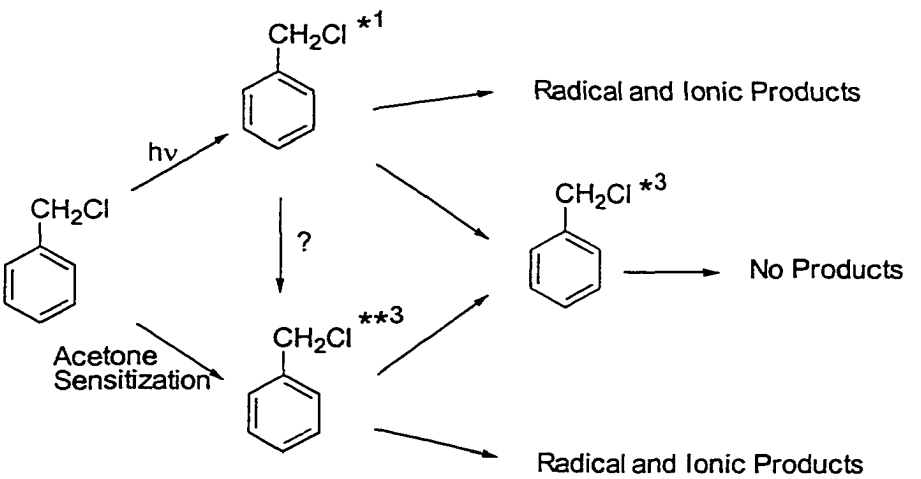

Scheme 1.3

McClelland and coworkers[47] provided convincing evidence for the involvement of the triplet excited state in the photosolvolysis of substituted benzhydryl chlorides in CH_3CN. It was shown that these compounds gave three transient absorptions upon direct photolysis in acetonitrile. They were assigned to diphenylmethyl cations with absorption maxima (λ_{max}) between 430-500 nm, and diphenylmethyl radicals with λ_{max} ca. 325-350 nm, produced from photo-induced heterolysis and homolysis, respectively. The weak absorptions at 350-400 nm belong to the excited radicals. Sensitization studies of the

same set of compounds with triplet acetophenone revealed that both cation and radical were produced as that from direct irradiation. Acetophenone triplet had a relatively slow decay which was in the same time scale as radical and cation formation from substrate. In the case of $(p\text{-ClPh})_2CHCl$, quantum yields for homolytic and heterolytic bond cleavage were found to be the same for both direct and sensitized experiments. However, for $(p\text{-MePh})_2CHCl$, much lower quantum yields for both ion and radical pairs were found under sensitization. Therefore, the substituents appear to influence not only the rates of homolysis and heterolysis from S_1, but also that from T_1, obtained from intersystem crossing of S_1. The only conclusion reached at this stage was that both singlet and triplet excited states of benzhydryl chlorides could be the precursors of cations and radicals.

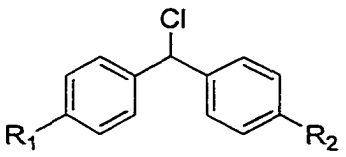

21 $R_1 = R_2 = H$
22 $R_1 = CH_3$, $R_2 = H$
23 $R_1 = OCH_3$, $R_2 = H$
24 $R_1 = R_2 = CH_3$
25 $R_1 = R_2 = OCH_3$

Using picosecond absorption spectroscopy, Peters and Li[48] examined the dynamics of radical and cation produced from the 266-nm photolysis of diphenylmethyl chloride (DPMC) in CH_3CN. Within the 20-ps time resolution of the equipment employed, both transients were fully formed with no indication of subsequent inter-conversion by electron transfer. In successive kinetic investigations of **21-25** in CH_3CN, Peters and coworkers[49,50] have revealed that both the geminate radical pair (GRP) and contact ion pair (CIP) were formed from the first excited singlet state in less than 20 ps (Scheme 1.4). In addition, the radical decayed on the time scale of 100 ps to a constant

absorbance and its kinetics followed the model depicted in Scheme 1.4. As a consequence, the GRP was consumed by electron transfer to form either the CIP or a covalent bond, as well as underwent diffusional separation to free radicals. The CIP, as described in Scheme 1.4, was formed either through direct dissociation of S_1 or from GIP through electron transfer. A parameter R (Eq. 1.9) was derived from the kinetic data to quantify the amount of CIP generated from each pathway. While all the CIP was derived from the first excited singlet state of DPMC **21** (R = 0.0), compounds **22-24** with electron donating substituents had R value ranging from 0.2 to 0.4, i.e., 20% to 40% of CIP came from the GRP. The CIP decayed either by diffusional separation to the solvent separated ion pair or by collapsing to form the carbon-chlorine bond.

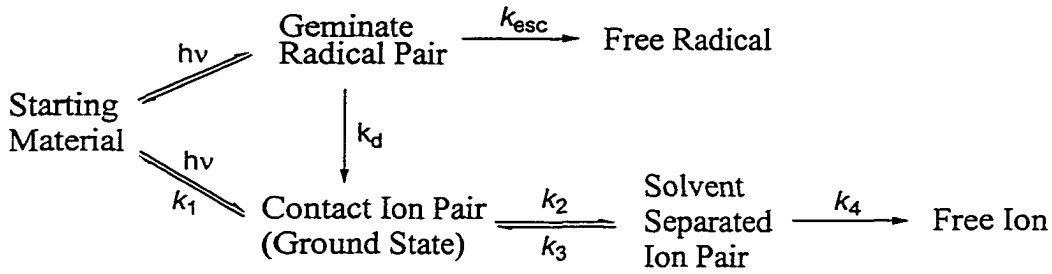

Scheme 1.4

$$R = [GRP]_0 / ([GRP]_0 + [CIP]_0) \qquad \textbf{(1.9)}$$

It is very convincing that both cation and radical are generated from the first excited state by direct photolysis of DPMC in CH_3CN. In fact, McClelland and coworkers[47] showed that the [cation]:[radical] ratio was higher for diphenylmethyl bromide than DPMC in direct photolysis. Assuming that heterolysis is less favored than homolysis and considering the heavy-atom effect, bromide should have higher

intersystem crossing (ISC) rate than chloride, which should lead to a lower [cation]:[radical] ratio. Since the opposite is observed, it at least suggests that ISC is not an efficient decay pathway in the direct photolysis. Nevertheless, there is no evidence against triplet DPMC being the corresponding precursor of cation and radical transients in sensitization experiments and this possible mechanism needs to be further investigated.

1.2.4 Photodehydroxylation

It is well known that hydroxide ion (HO^-) is not a very good leaving group in ground state solvolysis reactions under neutral conditions. Therefore, for quite a long time, there were very few cases of direct heterolysis of R-OH while extensive investigations were done on the photosolvolysis with a number of other leaving groups (such as halides, acetate, etc.), as discussed above. The formal loss of hydroxide ion in solvolysis reactions requires the assistance of strong acid in the ground state. That is, when protonated, the hydroxide ion (actually water) becomes a good leaving group. Such reactions of diaryl or triarylmethyl systems have been extensively studied and have served as an indicator of the relative stability of the corresponding carbocations.[51,52] Recently, it has been shown that HO^- can be a good leaving group in some photosolvolytic reactions under neutral conditions and have since then been termed as "photodehydroxylations".

An early example was reported by Rosenfeld et al.,[53] who showed the light induced heterolytic cleavage of a C-OH bond (photodehydroxylation). Their LFP studies of all-*trans*-retinol (**26**) resulted in transient absorptions at 405, 435 and 590 nm in

methanol. The transient absorbing at 435 nm was identified as the singlet state (S_1) and the 405-nm transient was ascribed to the triplet state of retinol (Scheme 1.5). The band at 590 nm was only observed in polar solvents (such as acetonitrile and water) with a concomitance increase in photoconductivity. The authors assigned this transient to the retinylic cation **27**, by comparing it with its known[54] spectrum and proposed a single step photodehydroxylation mechanism from photoexcited **26** (Scheme 1.5).

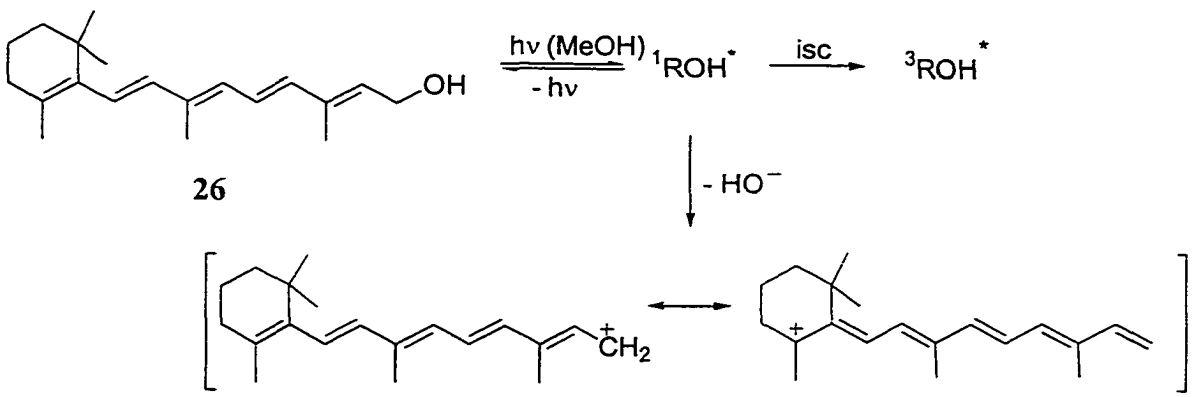

26 **27**

Scheme 1.5

Benzyl derivatives are the most widely studied systems that undergo photodehydroxylation reactions. Lin et al.[55] was the first to demonstrate that irradiation of (bichromophoric) benzyl alcohols **28** in methanol resulted in the overall heterolysis of the benzylic C-OH bond, generating 2,5-dimethoxystyrene, the crystal violet cation **29**, and rearranged **30**, which is the major product (Eq. 1.10). Photolysis of compound **31** in methanol gave 39% of the methyl ether **33** and only 5% of the fragmentation product **32** (Eq. 1.11). However, corresponding photo-induced ethers were not found upon

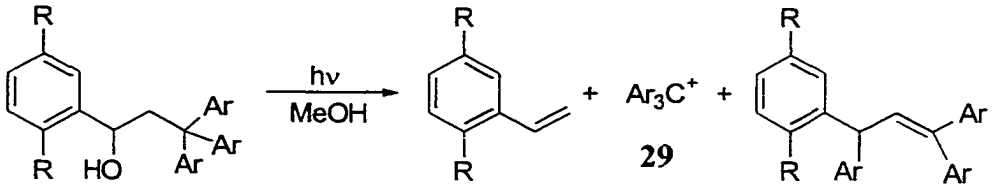

(1.10)

28a R = H
28b R = OCH_3
(Ar = *p*-$C_6H_4N(CH_3)_2$)

30a,b

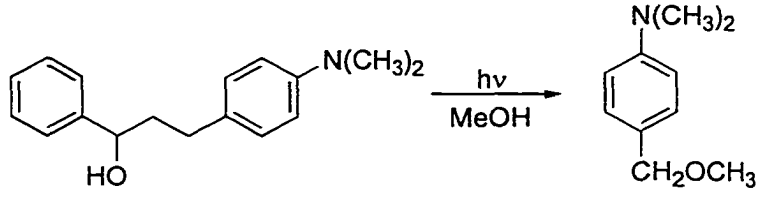

31 **32**

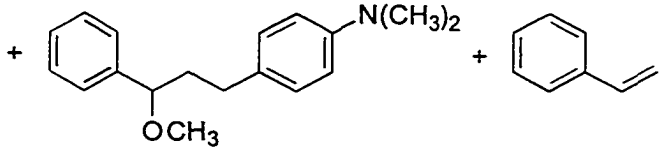

33

(1.11)

substitution of phenyl for dimethylaminophenyl or dimethylcarbinol for the benzylic alcohol group. Thus, the authors suggested that both electron acceptor (phenyl) and donor (dimethylamino) groups were required for the photodehydroxylation and a charge-transfer mechanism was proposed for the photofragmentation via the singlet excited state (Scheme 1.6). Presumably, the phenyl radical anion expels hydroxide ion to give a benzyl radical, which is oxidized by the electron deficient donor, to give a ground state carbocation.

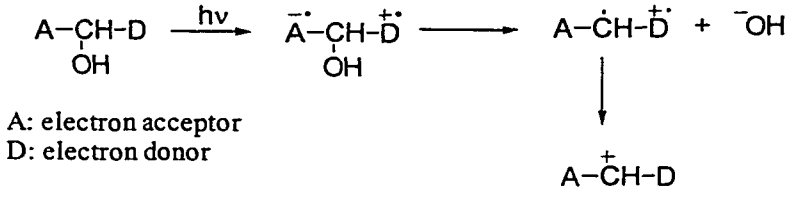

Scheme 1.6

Several other studies involving triarylmethanol derivatives (leucohydroxides) have also been reported. TAM derivative **34** is a well-known photochromic molecule, which dissociates into ion pairs very rapidly with high quantum yields[56,57] on UV irradiation, with generation of the colored triphenylmethyl cation **35**. The cation thermally recombines with the counterion, as shown in Eq. 1.12.[56] Basically, this

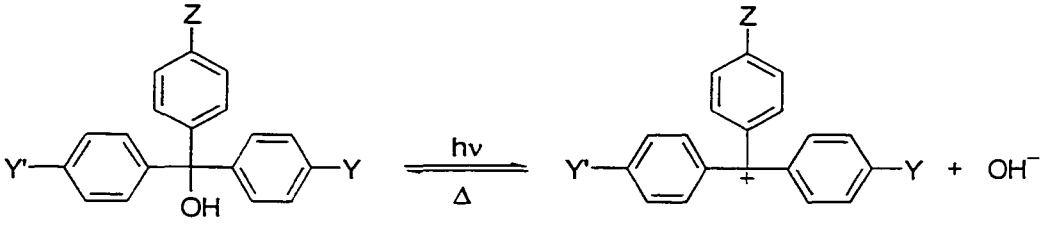

(1.12)

34 Y = Y' = $N(CH_3)_2$, Z = H
36 Y = $N(CH_3)_2$, Y' = $^+N(CH_3)_3$ I^-, Z = H
37 Y = Y' = $N(CH_3)_2$, Z = SO_3Na

35

derivative functions as a light-induced hydroxide ion emitter. For instance, irradiation of **34** and its derivatives, such as **36** and **37**, in aqueous solution results in an increase in pH, ranging from an initial pH of 5.4 to a final pH of 10.0.[58] The pH returned to its initial value within 15 minutes after the removal of light. The author ascribed this pH change on irradiation to the photodissociation of the leucohydroxide in the excited state.

Peters and Manring[23] have studied the dynamics of the photodissociation of TAM derivatives using picosecond LFP. Laser excitation of TAM **34** in CH_3CN generated a transient species with λ_{max} at 610 nm, observed 30 ps after the laser flash. After 2 ns, this transient absorption at 610 nm acquired the characteristic shape of the absorption spectrum of malachite green cation **35**. Excitation of **34** in the more polar solvent 9:1 CH_3CN-CH_3OH gave results similar to those of **34** in pure CH_3CN, except that the initial spectrum observed after 30 ps acquired the shape of **35** much sooner, namely within 300 ps. The authors noted that the results were consistent with initial formation of the first excited singlet state of **34**, which has an absorbance with λ_{max} at 610 nm based on the similarity between the transient absorption observed for **34** and *N*,*N*-dimethyl-*p*-toluidine. However, photolysis of **34** in cyclohexane only gave rise to the excited singlet state of **34** without forming **35** which is consistent with the anticipated instability of ion pairs in nonpolar solvents. Consequently, the authors concluded that the singlet excited species is the direct precursor of cation **35**.

A series of studies by Wan and coworkers[29,59,60] have shown that in many simple benzyl alcohol derivatives, the hydroxide ion behaves as an exceptionally good leaving group photochemically. Turro and Wan[59a] reported both the simple and proton-assisted photodehydroxylation of methoxybenzyl alcohols in aqueous solution, to generate the corresponding benzyl cations ($ArCH_2^+$). Photolysis of benzyl alcohols **38-40** in methanol-water or acetic acid-water resulted in the formation of methyl ether or acetate products. Only small amounts (≤5%) of dimeric products, resulting from C-OH bond homolysis,

were observed. Photolysis of **41**, however, does not give analogous products. It was further shown that the relative quantum efficiencies for methyl ether or acetate formation from **38-40** increased with decreasing pH, indicating that the process can be acid

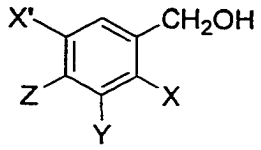

38 X = OCH_3; X' = Y = Z = H
39 Y = OCH_3; X = X' = Z = H
40 Y = X' = OCH_3; X = Z = H
41 Z = OCH_3; X = X' = Y = H

catalyzed. In the acidic pH region, fluorescence emission of **38** and **39** was quenched by protons ($k_q \approx 10^9$- 10^{10} M^{-1} s^{-1}). Nevertheless, *p*-methoxybenzyl alcohol (**41**) was still found to be unreactive under acidic conditions. Taking the rates of fluorescence quenching as being the proton catalyzed rate constants for the dehydroxylation, the authors found that *o*-methoxybenzyl alcohol (**38**) was 3 times more reactive than the corresponding *meta*-isomer **39**. On the basis of these observations, the possibility that the primary step involved the homolytic cleavage followed by rapid electron transfer (ET) was ruled out (Eq. 1.13). This mechanism can account for the acid-catalyzed formation of the methyl ether product if the k_p step is assumed to be acid-catalyzed. However, it cannot explain hydronium ion quenching of the fluorescence concurrent with acid catalyzed methyl ether formation since the primary step (k_i) is unimolecular and does not require proton assistance. The authors proposed a mechanism for photodehydroxylation shown in Scheme 1.7. The primary photochemical step involves water-assisted (k_s) and proton-assisted ($k_H[H^+]$) cleavage of the $ArCH_2$-OH bond from the singlet progenitor, to generate the corresponding benzyl cation $ArCH_2^+$ that can be trapped by an external nucleophile.

For benzyl alcohol **41** the results suggest that simple acid-catalyzed benzyl cation formation is not an important deactivational pathway.

$$[ArCH_2OH]^{\bullet} \xrightarrow{k_1} Ar\dot{C}H_2 \; \dot{O}H \overset{ET}{\rightleftharpoons} ArCH_2^{+} \; {}^{-}OH \xrightarrow{k_p} \text{Products} \qquad \textbf{(1.13)}$$

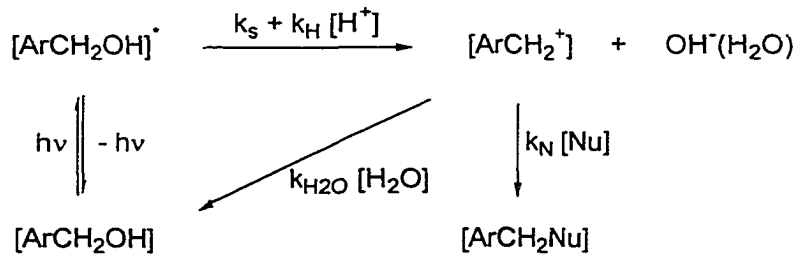

Scheme 1.7

Subsequent work by Wan et al.[29,59b,60] corroborated these initial observations. Methyl and fluoro substituted benzyl alcohols **42-45** were employed by Wan[60] to study

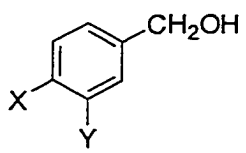

42 X = F, Y = H
43 X = H, Y = F
44 X = CH_3, Y = H
45 X = H, Y = CH_3

substituent effects. Based on fluorescence quenching results of **42-45** by the hydronium ion, it was shown that meta substituted benzyl alcohols **43** and **45** were more reactive compared to their para analogues **42** and **44**. Moreover, the photolysis of **45** in aqueous acetic acid (2:3 H_2SO_4(pH 0.2)-HOAc) gave 92% of the acetate **46** with only a small amount (<8%) of homolysis product **47** in low conversion experiments (<20%) while **44** failed to give any products under the same conditions (Eq. 1.14). A similar outcome was

obtained for compounds **42** and **43**. It should be noted here that, although the fluoro substituent at the meta position is an electron withdrawing group ($\sigma(m\text{-F}) = +0.34$) in the ground state, it effectively becomes an electron-donating group in S_1 (relative to the parent benzyl alcohol).

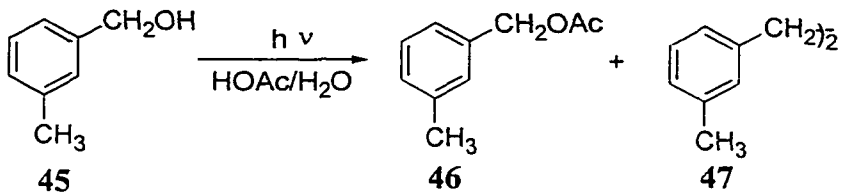

45 **46** **47** **(1.14)**

Wan and Chak[29] investigated the acid catalyzed photodehydroxylation of several methoxy-, dimethoxy-, and hydroxy-substituted benzyl alcohols **38-41** and **48-51** in

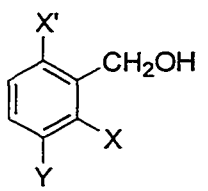

	X	X'	Y
48	OH	H	H
49	H	H	OH
50	OCH_3	H	OCH_3
51	OCH_3	OCH_3	H

aqueous solution. Combining fluorescence lifetimes and product quantum yields for the photodehydroxylation of these compounds, hydronium ion (k_H) and water-assisted rate constants (k_s) were obtained. Consistent with previous observations,[14] disubstituted methoxy benzyl alcohols in general react more efficiently than mono substituted derivatives, *i.e.*, substituent effects in the excited state (S_1) were additive. Within the mono-substituted series, the reactivity sequence follows *o-* > *m-* >> *p-* for the excited state molecules. The results of all these studies regarding substituent effects in the

photodehydroxylation of benzyl alcohols provided further evidence for the "meta electron transmission" effect proposed by Zimmerman and Sandel.[14]

Wan and Hall[61] have reported that arylmethanols **52-58** required the assistance of acid to effect photodehydroxylation but were otherwise photostable in neutral solution. They are much less reactive than methoxy-substituted benzyl alcohols. It would appear that without methoxy substituents, simple aryl groups do not have sufficient electron-donating power in the excited state to effect solvolysis with a poor leaving group such as the hydroxide ion. However, there is a degree of charge polarization in the excited singlet states of these systems that can initiate C-OH bond heterolysis in the presence of acid as catalyst (Scheme 1.7).

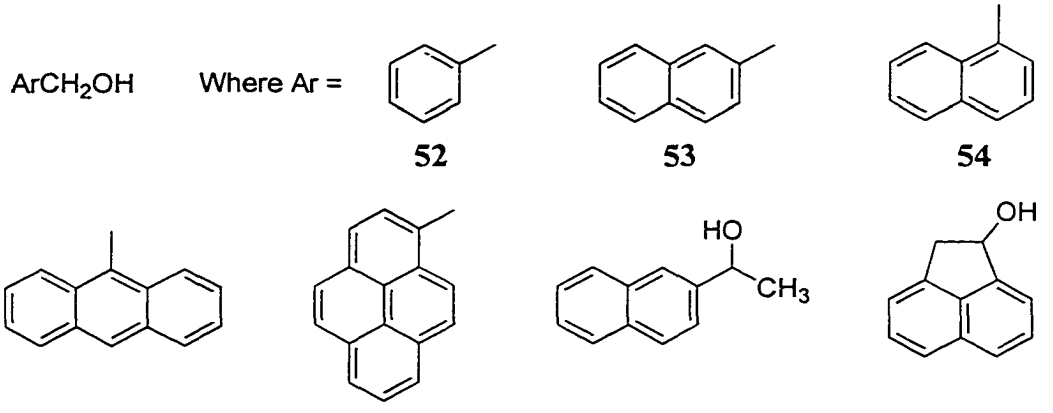

52 **53** **54** **55** **56** **57** **58**

So far, it has been demonstrated that the precursor alcohols may be viewed as very strong pseudo-bases in the excited state. Insight into these simple photoheterolysis pathways for the generation of carbocations will help in the understanding of how ground state and excited state reaction surfaces are related and help in the study of structure–reactivity relationships in ionic mechanisms.

1.2.5 General Survey of Photosolvolysis

1.2.5.1 Leaving Group Effects

Other than the systems discussed in the previous sections, numerous benzyl compounds with a variety of leaving groups,[12,13,15] including nitriles,[16] carbamates,[62] ethers, phosphonium salts,[63] trialkylammonium salts,[40] dialkylsulfonium salts[64] etc., have been studied during the last three decades exploring different aspects of photosolvolysis. Most of the work has demonstrated that individual leaving groups possess their own characteristic chemical behavior, which also depends on other factors such as solvent.[12]

Pincock and coworkers[65] studied fluorescence quenching rates and quantum yields of the products formed via heterolytic cleavage of the $ArCH_2$-X bond in the photosolvolysis of 1-naphthylmethyl derivatives **59** in methanol. They were able to determine the leaving group ability of various groups in the excited state (photofugacity) and proposed the following semi-quantitative scale:

$$S(CH_3)_2 > {}^-Cl \approx N(CH_3)_3 > {}^-O_2P(OEt)_2 > {}^-O_2CCH_3 > {}^-SO_2CH_3$$

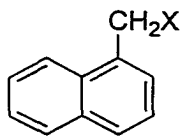

59

Generally, although very approximate, the nucleofugacity (leaving group ability in the ground state) of a group is inversely proportional to its basicity. The sequence given above shows that no such correlation can be made for the photofugacities of various groups in excited state photosolvolysis.

McClelland and coworkers[47,66] systematically studied the relative quantum efficiencies for photohomolysis and photoheterolysis for TAM and diarylmethyl compounds in CH_3CN and aqueous CH_3CN. Table 1.1 illustrates the effect of leaving groups (X) on both heterolysis and homolysis efficiencies of para-substituted diphenylmethyl derivatives in CH_3CN. Although there is a general trend that better leaving groups yield more of the cation and a higher ratio of heterolytic to homolytic products, the overall effect of the leaving group is highly attenuated relative to the situation found in ground state solvolysis.

Table 1.1 Quantum Yield of Intermediates Observed with ns LFP of Ph_2CH-X (R-X) in CH_3CN[a]

Leaving Group	$\Phi(R^+):\Phi(R^\bullet)$	$\Phi(R^+)$[b]	$\Phi(R^\bullet)$[c]
Bromide	0.63	0.12	0.19
Chloride	0.59	0.13	0.23
Fluoride	0.26	0.05	0.20
4-NCC_6H_4O	0.22	0.02	0.09
CF_3CO_2	0.14	0.04	0.31
4-$NO_2C_6H_4O$	< 0.1		
CH_3CO_2	< 0.08		
HO	< 0.03		0.04

[a] With 248 nm Irradiation. [b] Quantum yield of cation. [c] Quantum yield of radical.

1.2.5.2 Substituent Effects

Supporting evidence for the "meta effect" has appeared in a scattered manner within the studies concerning substituent effects.[14,32,33,40,41,67-69,70] As a matter of interest, Zimmerman and Sandel[14] also irradiated (*p*-methoxyphenyl)diphenylacetonitrile and (*m*-methoxyphenyl)diphenylacetonitrile in aqueous dioxane and found 42% and 62% of the

corresponding alcohols, respectively. Their results using benzhydryl and trityl derivatives, as well as theoretical calculations, suggested that the difference in energy among excited substrates were due to *meta vs. para* placement of the methoxy group. These differences became considerably smaller for the phenylated compounds, i.e. *m*- and *p*-substituted derivatives would not only both energetically favor, but also approach one another in ease of the heterolysis as well as the homolysis. It is interesting to note that *m*-methoxybenzyl chloride and *m*-N,N-dimethylaminobenzyl acetate were able to undergo photohydrolysis; whereas, *m*-methoxybenzyl methyl ether and *m*-methoxyphenylaceto-nitrile were unreactive, presumably due to the poorer leaving groups.[14] Although it is uncertain whether excited state reactants have thermal barriers of importance in general, it is quite clear that excited state reactions follow relatively low energy routes, or channels, along energy surfaces. Thus, in photochemical reactions, bonds are not randomly broken; in general, photochemical reactions seem to proceed with minimum electron localization. Phrased differently, photochemical reactions proceed by "smooth electron redistribution processes".[26,67,68]

Barltrop and Schofield[69] irradiated several substituted benzyloxycarbonylglycines **60** in aqueous alkaline solution. Products were benzyl alcohols and glycine, arising from heterolysis of the benzyl-oxygen bond. The quantum yields of glycine varied according to the nature of the substituent, with the highest value occurring for the *m*-methoxy substituted compound, as might be expected.

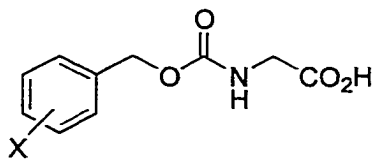

60

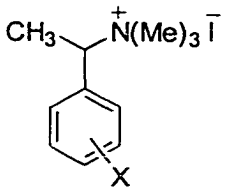

61

McKenna and coworkers[40,41] have demonstrated that the photosolvolysis efficiency of 1-phenylethyltrimethylammonium iodide (**61**) was greatly affected by the nature of the substituents present on the benzene ring. For instance, the quantum yields of the photosolvolysis of **61** remained more or less constant ($\Phi \sim 0.31$ to 0.39) for a variety of substituents (e.g., CH_3, OCH_3), but was very low ($\Phi \sim 0.005$) for *m*-cyano substitution, presumably due to the lower electron density at the carbon meta to the CN group ("meta effect").

In a series of studies by Pincock and coworkers,[32,33] all benzyl esters with *m*-methoxy substituents had exceptionally high yields of the heterolytic product, compared with the corresponding para substituted analog. Their additional report[70] of the photolysis of substituted 2,2-dimethyl-1-indanyl acetates **62** and pivalates **63** in methanol showed that the difference in relative excited-state reaction rate was 15:1 between the *m*- and *p*-methoxy substituted ester (quantum yield ratio). A higher value of 48:1 was obtained for the corresponding substituted benzyl acetates.[32] The larger difference in reaction rate for

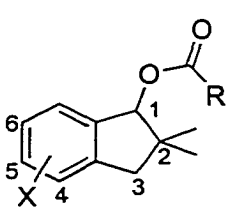

62 R = CH_3
63 R = $C(CH_3)_3$
(X = H, 6-OCH_3, 5-OCH_3)

the conformationally mobile benzylic esters was attributed to a higher population of the unreactive conformer for the *p*-methoxy substituted ester. The authors also concluded that substituents could increase the overall efficiency of the photoreaction by enhancing homolytic cleavage to afford a radical pair, which could convert to an ion pair through electron transfer. However, McClelland and coworkers[47] found that the quantum yields for homolysis (Φ = 0.2-0.4 of all these para-substituted diphenylmethyl halides, acetates and ethers) were rather independent of the nature of the substituent on the benzene ring; although, those for the heterolysis increased with increasing electron-donor strength, from $\leq$ 0.07 for CF_3, to 0.3 for OMe. The yield of the cation was found to be linearly related to the σ^+ values of the para-substituent as well as the pK_R^+ values (measure of the cation stability in solution) of the cation. According to Peters and coworkers[50] (Section 1.2.3), the electron donating substituent (in the ground state) should consistently enhance the conversion from GRP to CIP. Therefore, the overall picture would be that electron donating substituents increase both homolytic and electron transfer rate constants and, thereby, lead to an increase in the product yield originating from the ion pair.

1.2.5.3 Solvent Effects

The solvent effect has been an inevitable topic in the study of photosolvolysis, as well as for the corresponding ground state reaction. Using (4-methoxyphenyl)-diphenylacetonitrile as the substrate in aqueous acetonitrile, Ivanov et al.[71] have demonstrated that the yield of cations produced by flash photolysis and the photosolvolysis product yield increased as a function of water concentration. Several

other authors have also reported this same trend for the photosolvolysis of benzyloxycarbonylglycine ethyl ester in water and ethanol,[69] benzylammonium halides in ethanol and methanol,[72] and benzyl chloride in aqueous methanol.[38] Mckenna and coworkers,[73] found that benzyl acetate and benzyl iodide showed a much higher photosolvolysis efficiency in methanol than in *t*-butyl alcohol. Wan and Chak[29a] used MeOH-H_2O as solvent system for their studies of benzyl alcohols. Interestingly, the quantum yield of photomethanolysis reached an optimum point at 50-55% MeOH-H_2O mixture.

In a study by Peters and Manring[23] mentioned previously, it was found that the heterolytic cleavage of malachite green type compounds **64** showed a solvent dependence. In non-polar solvents such as cyclohexane, only S_1 was observed and no corresponding cation was formed from **64**. On the contrary, heterolytic cleavage was the predominant pathway in polar solvents such as MeOH and CH_3CN, leading to carbocationic intermediates.

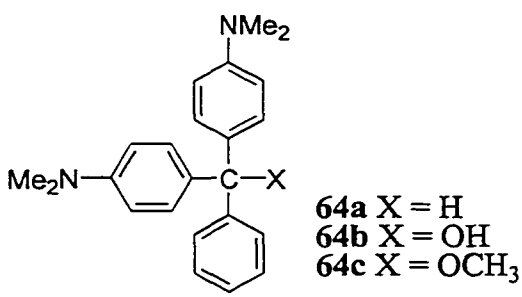

64a X = H
64b X = OH
64c X = OCH_3

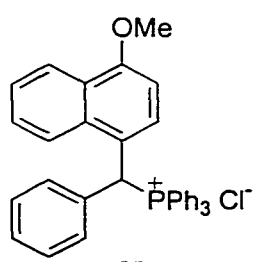

65

Scaiano and coworkers[74] have studied photolysis of phosphonium chloride **65** using LFP. The corresponding carbocation (λ_{max} ~500 nm) was the only transient obtained in either N_2 or O_2 purged 2,2,2-trifluoroethanol (TFE) or CH_3CN. The second

transient observed in CH_3CN-dioxane mixture (λ_{max} ~360 nm) was quenchable by O_2 but not by 1,3-cyclohexadiene, which favors the assignment to a radical. The relative yields of radical vs. cation varied considerably with the solvent composition, from 100% radical in 1-5% CH_3CN-dioxane to 100% cation in pure CH_3CN.

As for the homolytic process which generates a radical pair, McClelland and coworkers[47,66] showed homolysis product yields also increased with increasing CH_3CN content for (p-MeOPh)$_2$CHCl and Ph_2CHCl in CH_3CN-CH_2Cl_2 mixtures. In other words, for these two substrates, both homolysis and heterolysis benefited from the increasing polarity of the solvent although the reason for the decrease in bond cleavage yields with increasing CH_2Cl_2 content could be in part due to the singlet excited state being non-productively quenched by CH_2Cl_2.

A better understanding of the above solvent effects might come from analyzing the leaving group and solvent effect together. Peters and Manring[23] noted that photoheterolytic cleavage from **64b** (X = OH) was much faster than **64c** (X = OCH_3) and that no carbocation formation occurred for **64a** (X = H). These relative rates of heterolytic cleavages have been correlated to the higher electron affinity of $HO^{\bullet}$ (1.83 eV) compared to $CH_3O^{\bullet}$ (1.57 eV) and $H^{\bullet}$ (0.80 eV), although ion solvation energies of HO^- and CH_3O^- may also play a role. This rational was strengthened by the fact that the $PhCH_2$-OCH_3 bond (68-70 kcal mol^{-1}) is actually weaker than that of $PhCH_2$-OH (78 kcal mol^{-1}). Nevertheless, a similar investigation on a group of triphenylmethanes **66a-f** gave rather complicated results indicating that every individual compound has its own unique

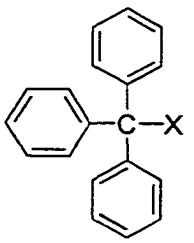

66a X = H
66b X = OH
66c X = OCH_3
66d X = Cl
66e X = Br
66f X = SCH_3

photochemical properties. In contrast to the results of Peters and Manning,[23] McClelland and coworkers[47,66] claimed that, for diphenylmethyl halides, the cation to radical ratios correlated with the pK_a values of the conjugate acids HX instead of the electron affinity of the halide radical. Also, heterolysis was much less endothermic than homolysis in CH_3CN. Thus, the solvent polarity must play an important role on the efficiency and yield of cation generation.

Recently, Peters and coworkers[50] used the kinetic information for the formation and decay of CIP and GIP for the development of potential energy surfaces for the S_N1 reaction for diphenylmethyl chlorides in polar solvents. The valence-bond configuration mixing model (VBCM) developed by Pross and Shaik[75] was used since it is a very successful theoretical perspective for examining organic reactivity in both gas and condensed phases. For the S_N1 reaction of alkyl halides, the two most important valence bond electronic configurations (the diabatic states) are the purely covalent state $R^{\bullet\bullet}X$, where the two active electrons are associated with R and X, respectively, and the purely ionic state R^+X^-, where both active electrons are associated with X. The reaction profile potential energy surfaces, the S_0 and S_1 adiabatic states, are developed by the mixing of these two diabatic states. In the gas phase, the ground state surface acquires some ionic

character resulting in a stabilization of S_0 relative to the diabatic surface $R^{\bullet\bullet}X$ and a destabilization of S_1 relative to the diabatic surface R^+X^- at bonding distances (Fig. 1.2). While in a polar solvent, the orders of stability of the two valence bond states are reversed as R and X become separated, leading to a curve crossing between the two diabatic states.[75] In the vicinity of this curve crossing, there is a large electronic coupling between the two diabatic surfaces leading to an avoided crossing between the two adiabatic surfaces S_0 and S_1. However, the dissociation pathways depend not only on the bond extension coordinate but also upon a solvent coordinate where the solvent structure continuously changes with bond extension, which is missing in Fig. 1.2. Furthermore, the solvation structure along the S_0 and S_1 surfaces would differ given the difference in ionic character for the two surfaces.

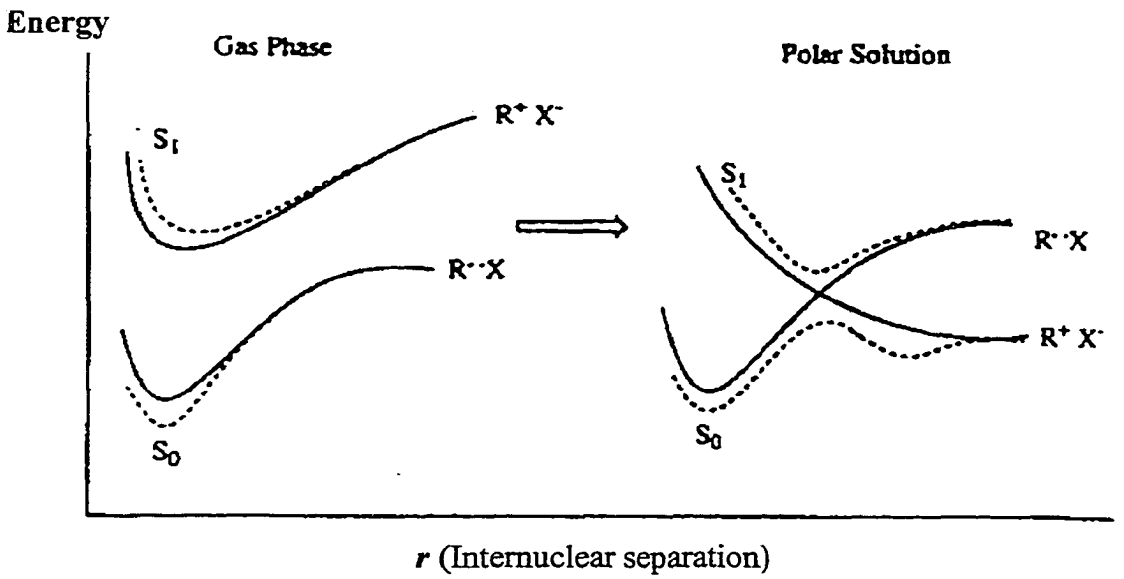

Fig. 1.2 Potential energy surfaces for homolysis and heterolysis in the gas phase and in polar solution. Solid curves: diabatic surfaces. Dashed curves: adiabatic surfaces.

Despite the difference between the fully equilibrated solvent structure for S_0 and S_1, this diagram provides important theoretical support for the product outcome of the photosolvolysis in polar solvents depicted in Scheme 1.4. It can be seen that a minimum is produced on the excited state surface and a maximum is produced on the S_0 surface, corresponding to the transition state for heterolytic dissociation from the mixing of the two diabatic states. Hence, excitation of benzylmethyl chloride could either lead to the formation of the GRP adiabatically on the S_1 surface, which might partially convert to CIP via electron transfer, or dissociate adiabatically to generate a CIP.

1.2.5.4 Reactivity of Photogenerated Carbocations

Generally, carbocations are short-lived species unless stabilized by strongly electron donating group. This makes direct observation and study of their reactivity a difficult task, although the development of LFP techniques has brought about a substantial improvement. A very important reason is that the polar solvents required for cation generation are also good nucleophiles and have a profound effect on the cation lifetime. It was found that protic solvents such as ROH reacted with a given cation in the order of methanol > ethanol > water >> TFE >> 1,1,1,3,3,3-hexafluoroisopropyl alcohol (HFIP). For example, the diphenylmethyl cation[76,77] becomes observable with ns LFP in TFE and is even long lived in HFIP. The 9-fluorenyl cation[78,79] required ps LFP even in TFE but is observable with ns LFP in HFIP. Therefore, weaker nucleophilic polar solvents such as TFE and HFIP are capable of promoting the formation of cations and also extend their lifetimes to a range detectable using slower apparatus.

McClelland and coworkers[66,15] have recorded absorption spectra of a series of 18 triarylmethyl cations and 10 diarylmethyl cations by nanosecond LFP of the cyanide, 4-cyanophenyl ether and acetate precursors in CH_3CN/water (AN/W) mixtures. The first-order rate constants (k_s) for these cations in 1:2 AN/W at 20 °C have been measured following the decay in their optical density. The triarylmethyl cations had k_s values ranging from 10 s^{-1} (for the 4,4',4"-$(MeO)_3$-substituted ion) to 9×10^6 s^{-1} (4,4'-$(CF_3)_2$), while diarylmethyl cations were less stable with k_s values ranging from 10^5 s^{-1} (for the 4,4'-$(MeO)_2$) to 3×10^7 s^{-1} (4,4'-Me_2). The parent diphenylmethyl cation and its derivative with one 4-methyl substituent had half-lives of less than 15 ns and are only observable when the water content was close to 0 %.

The effect of varying the alkyl group at the cation carbon center was also investigated. As expected, a methyl group can kinetically stabilize benzylic type cations and resulted in a decrease in the decay rate constant by a factor of 10-100.[76,80] However, the effect of the added methyl group diminished with increasing stability of the original cation. In the series benzyl, phenethyl and cumyl, the second methyl substituent had only about twice the effect of the first which was most likely due to a non-additive steric effect, i.e., the cumyl cation becomes too crowded for efficient solvent addition.[80] The fluorenyl cation with a 9-*t*-butyl substituent was less reactive than the methyl analog, but the methyl and *tert*-butyl substituents in the *p*-anisylethyl cation series had almost equal rate constants. According to the authors, the story with respect to alkyl substitution in

carbocations is far from complete and more studies are required for a satisfactory understanding.[15]

Electron withdrawing substituents are also of interest. Curiously, Richard and co-workers[81] found through the use of the "azide-clock" method that CF_3-substituted cations lacked kinetic destabilization. Later on, in collaboration with Richard's group, McClelland et al.[82] confirmed this effect through direct measurement. For example, the *p*-methoxycumyl cation decays in TFE with $k_{TFE} = 1.6 \times 10^4$ s^{-1}, while the cation *p*-$MeOC_6H_4C^+(CF_3)_2$, where both methyl groups have been replaced by CF_3 groups, is only slightly more reactive, with $k_{TFE} = 6.4 \times 10^4$ s^{-1}. Flash photolysis studies by other groups have shown a similar small effect upon substitution of the $COOCH_3$ group.[83,84] These substitutions did result in large decreases in thermodynamic stability, however.[81]

The LFP characterization of the vinyl cation has also been reported.[85] Photolysis of α-(2,6-dimethoxyphenyl)vinyl chloride in TFE solution at 25 °C was found to produce the α-(2,6-dimethoxyphenyl)vinyl cation as a transient species with a lifetime of 1 μs.

Highly stabilized dialkoxycarbocations, such as $(EtO)_2C^+$-H and $(iPro)_2C^+$-H, are ca. 1000 times less reactive when substituted with one methyl group.[86] Okuyama et al.[87] also have demonstrated that flash photolysis of aqueous solutions of **67** and other dithiolane derivatives generated the cation **68** as a very long-lived transient with a maximum absorption at 342 nm (Eq. 1.15). This dithiolanylium cation decayed with pseudo-first-order rate constants of 3.83 and 0.56 s^{-1} in 1:1 H_2O-EtOH and 1:1 H_2O-CH_3CN, respectively.

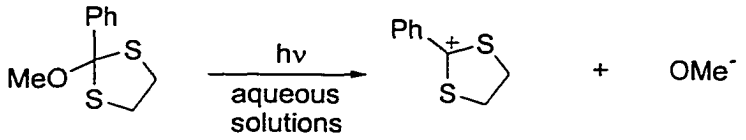

67 68 (1.15)

1.3 Excited State Acidity of Hydroxyarenes

It is well known that phenols, naphthols and other hydroxyarenes are considerably more acidic in S_1 than in the ground state.[88-90] The excited state proton transfer (ESPT) of these compounds has been extensively studied. Much of the earlier work was mainly concerned with the measuring their excited state pK_a's. The advent of picosecond LFP has enabled precise measurements of various kinetic parameters of these ESPT reactions, as well as providing new insights into the understanding of these photoprototropic equilibria.[91-95] For example, the excited singlet state acidity of 1-naphthol (**69**) and 2-naphthol (**70**) were found to be essentially identical ($pK_a^* \approx 2.8$)[89a] on the basis of simple Förster cycle analyses. However, using picosecond spectroscopy, Webb et al.[92] have shown that 1-naphthol (**69**) (p$K_a^* = 0.4$)[93] is much more acidic than 2-naphthol (**70**) (p$K_a^* = 2.78$).[93] Also, in contrast to 2-naphthol (**70**), the fluorescence emission from 1-naphthol (**69**) is either absent or very weak in aqueous solution,[92,94] which is mainly due to photoprotonation of the 5- and 8-positions, an important deactivational pathway operating only for 1-naphthol (**69**).[92] Presumably, these photoprotonations generate intermediate phototautomers such as **71**, which have not been directly observed.

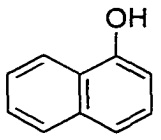

69

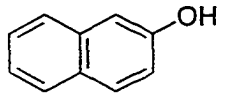

70

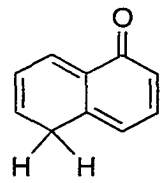

71

The enhanced acidity of excited state naphthols is capable of inducing a transient pH decrease ("pH jump").[96,97a] Clark et al.[96] reported that pulsed laser excitation of an aqueous solution (pH 7) of 2-hydroxynaphthene-6-sulfonate (**72**) at 266 nm resulted in rapid establishment of the excited state acid-base equilibrium ($k_f = 1.02 \times 10^9$ s^{-1}; $k_b = 9 \times 10^{10}$ s^{-1}) (Eq. 1.16). The calculated H_3O^+ concentration increased by > 10^{-4} M during the

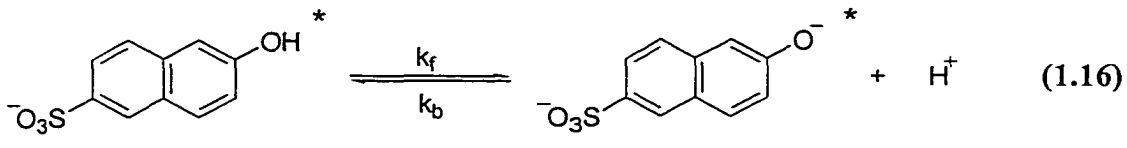

72 **73** **(1.16)**

excited state lifetime ($\tau \approx 10$ ns) of **72**. Thus, the pH 7 solution was rapidly modulated on laser excitation to a pH < 4 on a time scale governed by the proton-transfer rate. The pH jump technique has now been used to probe the microenvironments of biological systems[91,97b,c] as well as local structures of electrolyte solutions.[97d]

An attractive concept is to use the enhanced acidity of excited states of phenols and naphthols to initiate chemical reactions. An interesting possible example is the photocyclization of *o*-allylphenols (**74**) in a variety of solvents to yield a mixture of furanyl **75** and pyranyl ethers **76**[98a-d] (Eq. 1.17). In related work, Chow et al.[99] have reported that 1-allyl-2-naphthol (**77**) and 2-allyl-1-naphthol (**78**) undergo a similar

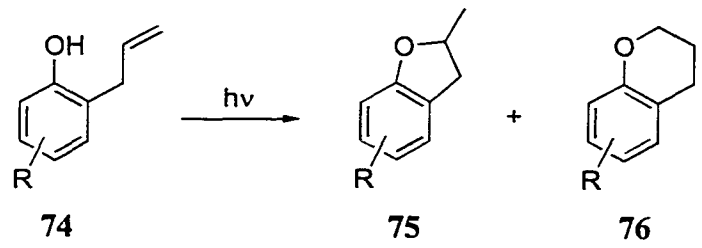

74 75 76 (1.17)

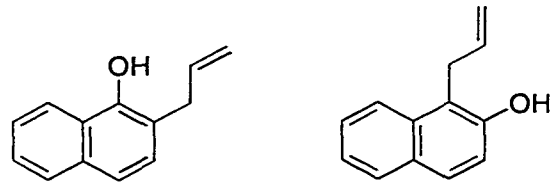

77 78

photocyclization to give the corresponding dihydrofuranyl and pyranyl ethers. It has been shown that the reaction is via the singlet excited state and that proton transfer from the naphthol is necessary for cyclization. The proposed mechanism is believed to involve initial intramolecular proton transfer to the alkene via two isomeric hydrogen-bonded complexes, to generate isomeric carbocation intermediates, which subsequently cyclize to the observed products (Eq. 1.17). This appealing mechanism is disputable since the alkene moiety (not photoexcited in the reaction) is such a weak base that the acidity change of phenols or naphthols is still insufficient to protonate the alkene. An alternative mechanism[98e,f] for the reaction is an initial electron transfer between the phenol and alkene moieties. The thus formed radical-ion pair reacts via proton transfer, leading to isomeric biradicals, which subsequently couple to give the observed products. A simpler hydrogen abstraction mechanism in which the alkene abstracts the hydrogen atom of the naphthol OH can also be envisaged, leading ultimately to products.

1.4 Quinone Methides

Quinone methides (QMs) (**79-81**, singlet and triplet forms),[100,101] unlike their structurally related benzoquinones (BQs) and quinone dimethides (QDMs, also known as *o*-xylylenes), are extensively polarized and hence tend to regain the aromatic phenol ring via either nucleophilic or electrophilic attack (Scheme 1.8).[100,101] The inherent driving

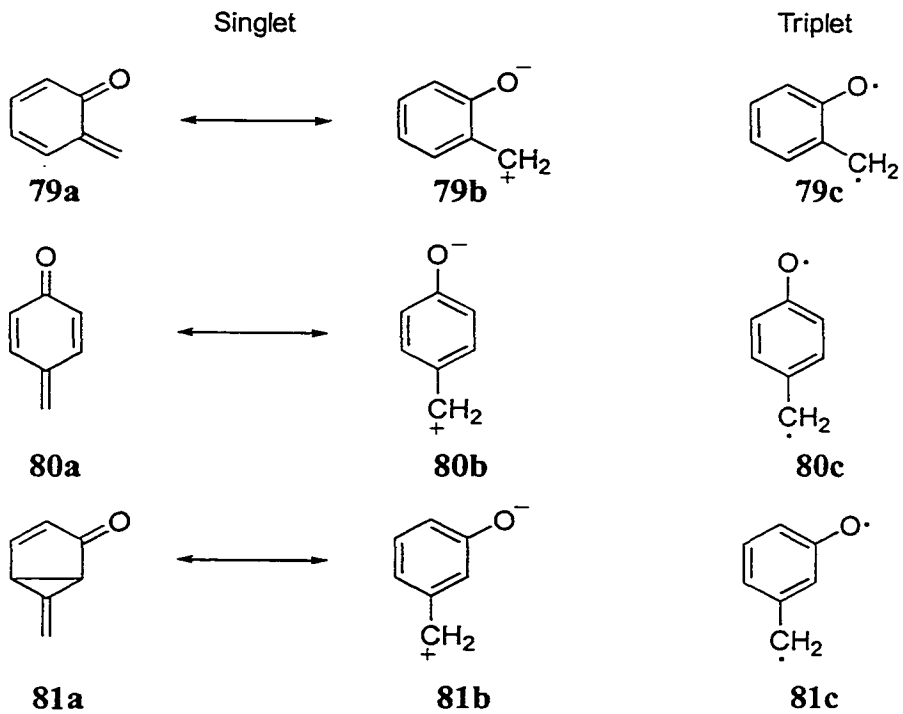

Scheme 1.8

force in this transformation makes QMs highly reactive. Recognized as early as 1907,[102-104] simple QMs are unstable molecules that self-condense spontaneously to form dimers and trimers even in dilute solution at room temperature. The addition of electron donating substituents on either the ring or the methylene group stablizes the quinone methide, making it less reactive.[105]

Among the three isomers, *ortho*- and *para*-QMs (2-methylene-3,5-cyclohexadien-1-one (**79a**) and 4-methylene-2,5-cyclohexadien-1-one (**80a**), respectively) are intermediates in a variety of important chemical and biochemical systems, while the *meta* isomers **81a** (**81b**, **c**) are mainly of theoretical interest (Scheme 1.8).[106]

1.4.1 *ortho*- and *para*-Quinone Methides

ortho-QMs are well known in organic synthesis for the construction of chroman ring systems.[100,101,107] Their characteristic reaction with electron-rich alkenes, namely "reverse electron demand" [4+2] cycloaddition to give chroman derivatives, has been employed as a key step in total synthesis, some representative examples are carpanone,[108] hexahydrocanabinol,[109] and thielocin A1β (Scheme 1.9).[110]

The [4+2] addition of *para*-QMs with dienes, which have also been used in

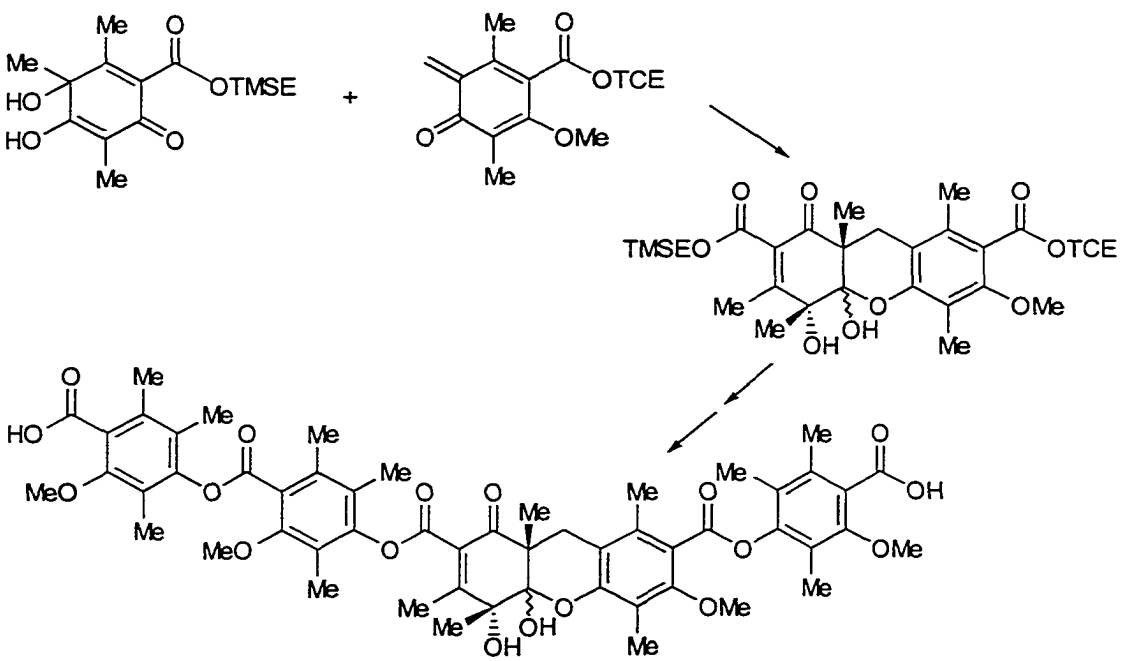

(thielocin A1β)

Scheme 1.9

synthesis, lead to spiro products.[111] Angle et al.[112] reported that *p*-QMs generated via Ag_2O oxidation of the corresponding *p*-substituted phenol react via a formal [3+2] cycladdition with a simple alkene intermolecularly to give indanes, or intramolecularly to give a variety of *p*-hydroxyphenyl-substituted ring systems.

In lignin chemistry,[113] *p*-QMs are believed to be crucial intermediates in their biosynthesis. The polymerization of coniferyl alcohol, the predominant *p*-coumaryl alcohol of softwood lignins, is conceived to start with initial coupling of two coniferyl alcohol phenoxyl radicals to give various *p*-QM structural isomers, which subsequently react further to yield lignin. The aging of lignin can also involve the intermediate formation of *p*-QMs.

In addition, QMs are involved in a number of biochemical processes. It has been found that QMs are able to alkylate cellular macromolecules such as proteins and DNA, and are the critical intermediates of several antitumor/antibiotic drugs.[114a] A typical example is the mode of action of Mitomycin C (a clinically used anticancer drug), which can be bioreduced (Scheme 1.10) followed by loss of CH_3OH and opening of the aziridine ring, to generate an *o*-QM, the active alkylation reagent of DNA.[114,115] For the same reason, *p*-QMs, generated by oxidation of phenols during the metabolic process, are responsible for the known toxicity of common phenols found in spices, flavoring agents, and food preservatives such as BHT (butylated hydroxytoluene).[114] Therefore, studies have been directed at sequence selective alkylation of duplex DNA using both thermally and photochemically generated QMs.[116]

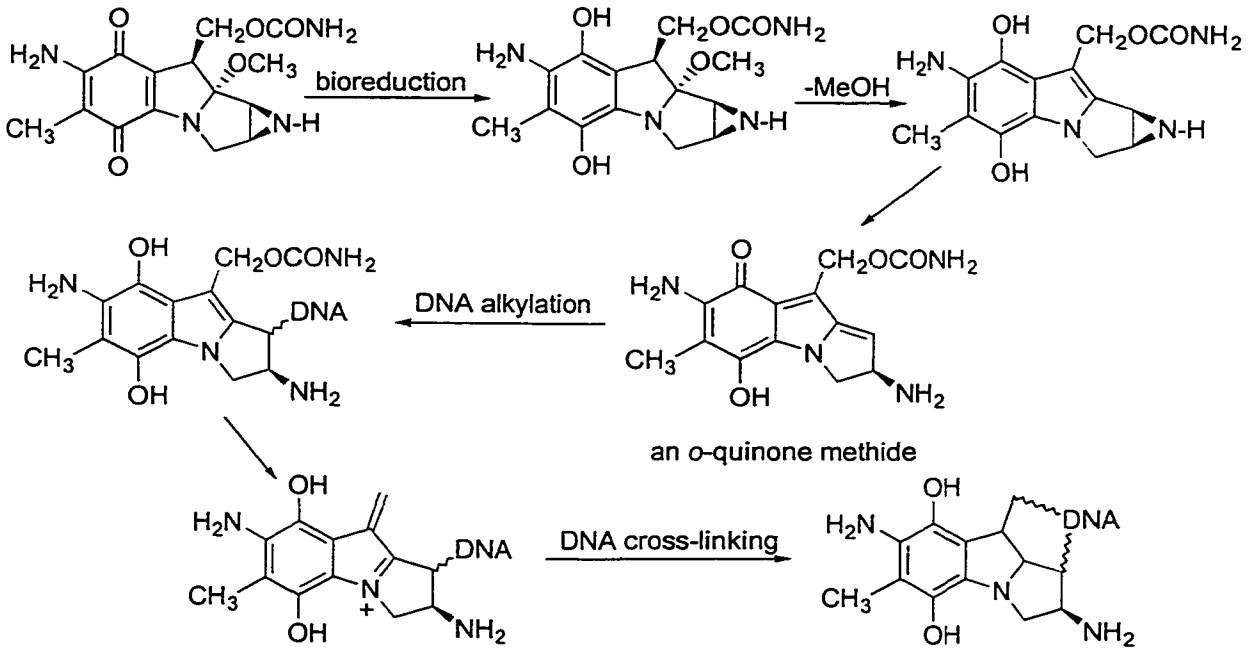

Scheme 1.10

In a newly devised technique, an *o*-QM has been used for identifying catalytic antibodies that accelerate certain biochemical reactions.[117] It has been shown that, if an antibody fragment in a library catalyzes cleavage of the glycosidic bond, a highly reactive *o*-QM is released from the trapping agent which reacts immediately with the antibody fragment, thereby trapping it covalently and hence making it identifiable.

Due to these applications, various thermal methods for generating QMs have been developed during the last two decades. The most widely used method is oxidation of phenols by metal oxides such as Ag_2O, PbO_2, etc.[118,119] The fact that Filar *et al.*[119] could prepare 2,6-dimethyl-*p*-QM by just shaking a solution of mesitol with Ag_2O indicated that *p*-QMs were inherently easier to access. Therefore, numerous spectroscopic information of *p*-QMs is available in the literature.[81b,c,82,118,119] In order to study the more

reactive *o*-QMs, other routes including high-temperature dehydration of *o*-hydroxybenzyl alcohols,[120] fluoride-induced desilylation of silyl ethers,[109] and thermal extrusion of small molecules[121] have been reported. The extrusion of phenyl boronic acid from 1,3,2-benzodioxaborins has been reported by Lau and Defresne and co-workers[122] as a simple and general method for making *o*-QMs suitable for synthesis (Scheme 1.11). The

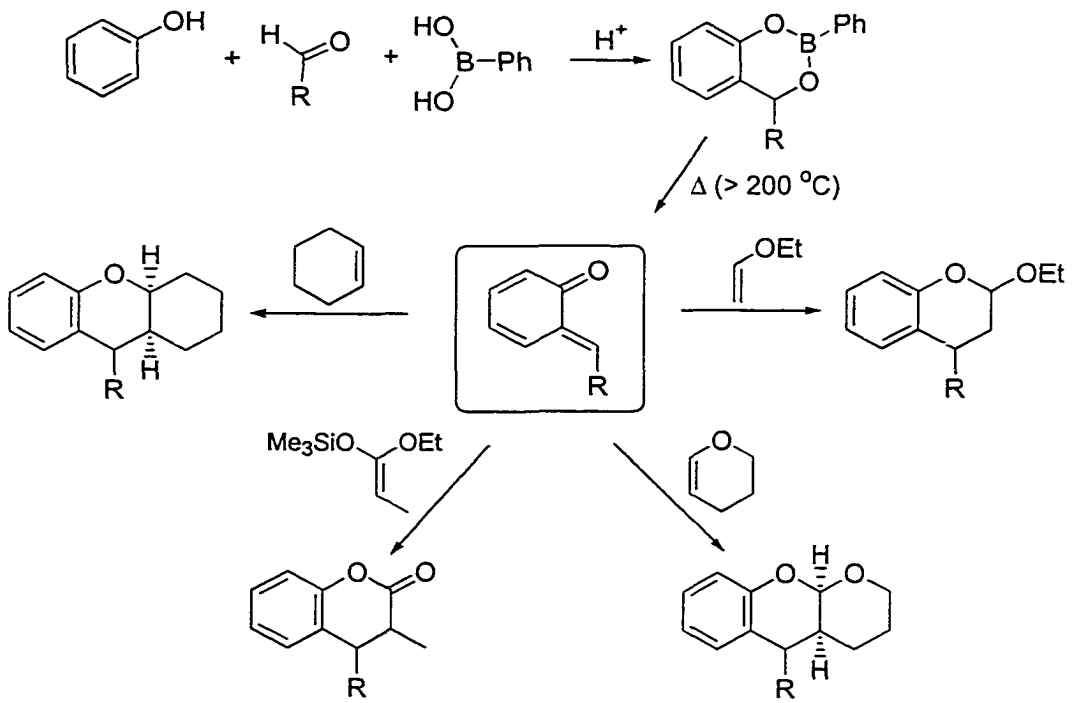

Scheme 1.11

precursors (1,3,2-benzodioxaborins) are readily made by condensation of phenylboronic acid with phenol and the required aldehyde. To confirm the formation of QMs, nucleophiles like alcohols and a variety of standard agents such as ethyl vinyl ether and ketene acetal have been used as trapping agents.

1.4.2 *meta*-Quinone Methides

General structural formulas for the biradicals **81c**, **82b** and **83b**, and for the conceivable fully covalent isomers **81a**, **82a** and **83a** of *m*-quinonoids are shown in Scheme 1.12. The covalent isomers have conventional Kekulé structures, whereas *m*-QM (**81c**), along with *m*-QDM (**82b**) and *m*-BQ (**83b**), are considered to be non-Kekulé molecules. Non-Kekulé molecules are defined as fully conjugated systems but each of whose Kekulé structures contains at least two atoms that are not π-bonded.[123a] On the basis of Hund's rule,[123b,c] Longuet-Higgins[123a] predicted that the ground state of a non-Kekulé hydrocarbon with *n* electrons in *n* π nonbonding molecular orbitals (NBMOs) would have a spin quantum number of S = *n*/2. Therefore, the diradical **82b** should have a triplet ground state (S = 1), in which the two nonbonding electrons occupy different NBMOs and have parallel spins. Thus, this diradical should be paramagnetic. It would violate Hund's rule if evidence is available indicating that it has a singlet ground state. A search for violations of Hund's rule accounts for the main stream of interest on research on non-Kekulé hydrocarbons. In addition, the paramagnetic property makes this species a promising candidate as an organic magnet.

Covalent singlet

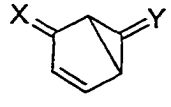

81a X = O, Y = CH_2
82a X = Y = CH_2
83a X = Y = O

Diradical triplet

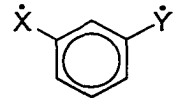

81c
82b
83b

Scheme 1.12

The same theoretical and practical expectations apply to *m*-QM (**81c**), another series of non-Kekulé molecules. Nevertheless, this polarized species is much more reactive than their *m*-QDM analogue and more difficult to generate. In principle, the biradical **81c** could be derived by cleavage of one bond of **81a** because the isomers of higher covalence generally tend to be more stable. However, in the case of the *m*-QM,[124] the covalent form (**81a**) is destabilized by strain, while the biradicaloid form (**81c**) is stabilized by resonance. Thus, the two forms may not differ greatly in energy. According to rough bond additivity calculations,[125] it actually suggests that, in the case of *m*-QM **81c**, the covalent tautomer **81a** is less stable than the biradical **81c** by ~ 4 kcal mol^{-1}. Clearly, it is a challenging task to experimentally investigate the existence of these highly unstable species. It was not until 1979 that enone **84**, the first covalent precursor of *m*-QMs, was synthesized by Berson *et al.*[126] Section 1.4.3.2 will illustrate that both pyrolysis and photolysis of this compound and other related derivatives led to efficient formation of *m*-QMs.

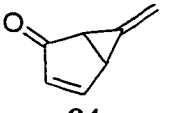

84

1.4.3 Photogeneration of Quinone Methides

1.4.3.1 *ortho*- and *para*-Quinone Methides

In view of the wide-spread relevance of QMs in organic and biological chemistry, it would be desirable to devise a general photochemical method for forming QMs since this would allow one to study their reaction dynamics without the encumbrance

associated with thermal methods. Occasional reports of QM photogeneration can be found in the literature. Some of these methods have involved (i) decarbonylation of lactones;[127] (ii) photolysis of *o*-hydroxy-triphenylmethanols;[128] (iii) photoisomerization of chromenes;[129] (iv) photolysis of benzoquinones and Vitamin K derivatives;[130] and (v) photolysis of bicyclic enones (for *m*-QMs).[106] None of these methods could be conceived as general since only selected QMs are photogenerated in each method.

During the studies of photodehydroxylation of benzyl alcohols, a very important observation noted by Wan *et al.*[29] was that the product quantum yield for *o*-hydroxybenzyl alcohol (**48**) was about five times that of *o*-methoxybenzyl alcohol (**38**). At that time, the proposed mechanism for **48** involved the intermediacy of an *o*-QM **79a** rather than a benzyl carbocation. The authors realized that a simple and general photochemical method might indeed be available using readily available substrates. Moreover, the method might allow the study of photogenerated *m*-QMs, in addition to the more common *ortho* and *para* isomers.

Further investigation using all three isomers of hydroxybenzyl alcohols provided additional evidence for the formation of **79a** from **48**.[131] Upon photolysis in basic aqueous solution, only **48** was able to photocondense to form phenol-formaldehyde resins. In the initial step of this process, **79a** was photochemically generated. After alkylation at the benzylic carbon by the substrate, the intermediate rearranged to the phenolate form, which can either give rise to a "dimer" of **48** with protonation or employed in a subsequent photoreaction to afford phenol-formaldehyde oligomers (Scheme 1.13).

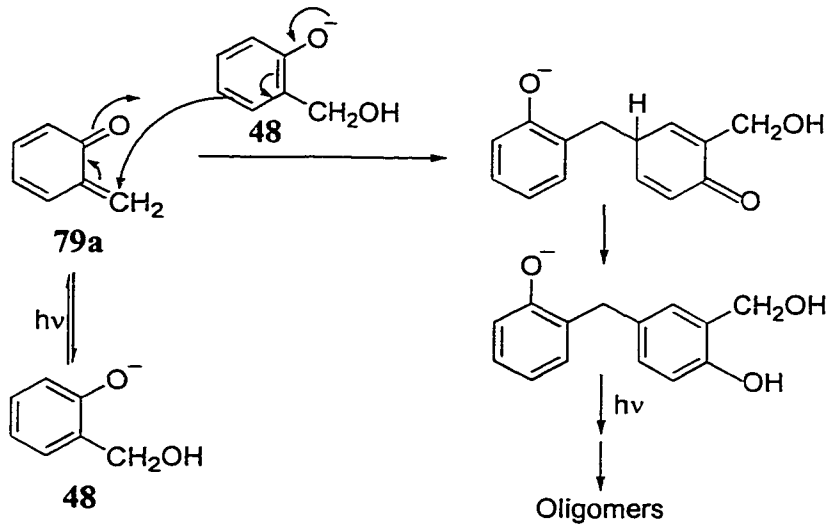

Scheme 1.13

As discussed in Section 1.3,[89,90] phenols ($pK_a \approx 10$ in the ground state) become much more acidic in the excited singlet state ($pK_a \approx 3$). The oxygen substituent in S_1 has enhanced electron-donating power which induces the acidity increase of the phenolic proton. Yates and coworkers[132,133] showed that an *o*-hydroxyl substituent results in more efficient photohydration of styrene and phenylacetylene. They attributed this enhanced reactivity to a fast intramolecular proton transfer from the more acidic ArOH to the alkyne or alkene moiety. Consequently, a similar mechanism was envisioned by Wan *et al.*[29a] for the photosolvolysis reaction of **48** in which the loss of the hydroxide ion is concerted with the deprotonation of the phenolic proton, giving rise to *o*-QM **79a**, via a more efficient reaction (Eq. 1.18). In the case of the meta and para isomers, it was believed that the phenolic OH group is too far removed from the reaction site to have this effect.

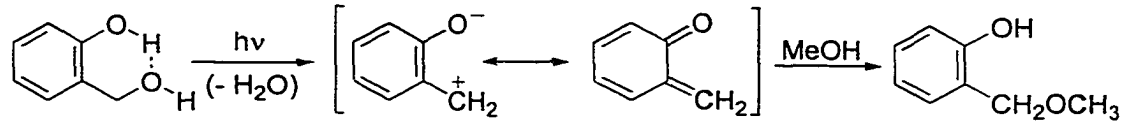

48 79a (1.18)

A venture by Wan *et al.*[134] into diaryl ether photochemistry led to the discovery of a method for photogenerating biphenyl quinone methides. They observed a curious rearrangement occurring on photolysis of xanthene (**85**) in aqueous solution via the biradical **86**. Instead of giving **87** (reduction via hydrogen abstraction from the solvent) as the major product, the reaction (Scheme 1.14) proceeded via attack of the phenyl radical at the *ortho* position of the other ring, to afford spiro ketone **88** and subsequently formed *o,o'*-biphenyl quinone methide **89**, which then reacted via electrocyclic ring closure to generate the major product 5*H*-dibenzo[*b,d*]pyran (**92**). When water or CH_3OH were used as co-solvents, **90** and **91** were also found as products, respectively.

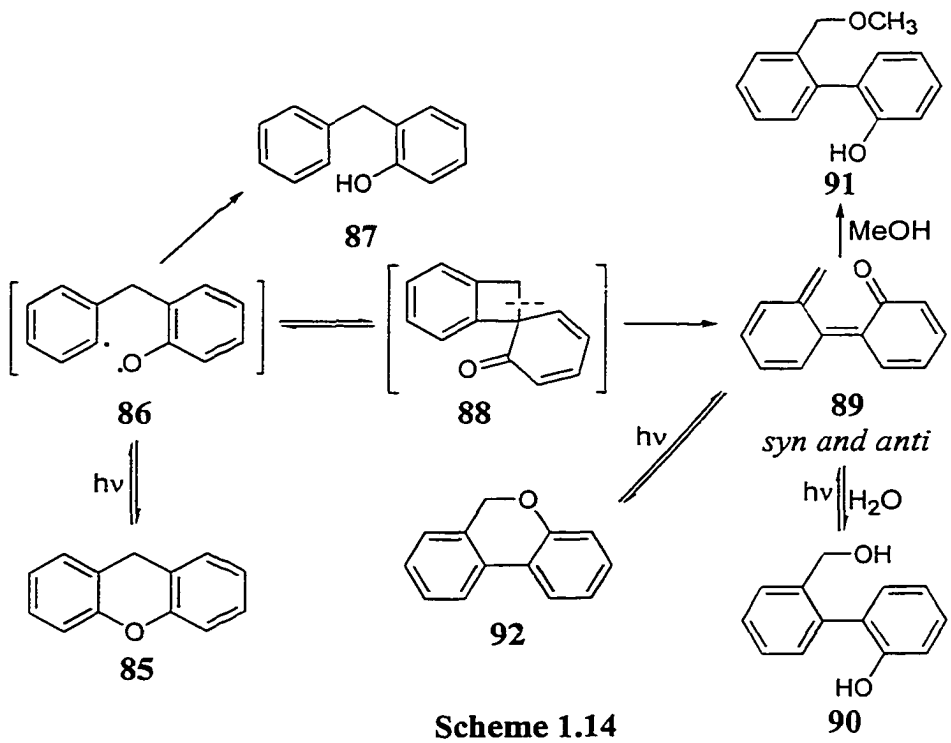

Scheme 1.14

In an attempt to answer the question of whether **89** could also be photogenerated by photolysis of **90** or **92**, the authors carried out a detailed mechanistic study of the photochemistry of 2-(2'-hydroxyphenyl)benzyl alcohol **90** and related compounds[135] (Scheme 1.15). The quantum yield for formation of **92** from **90** increased on increasing

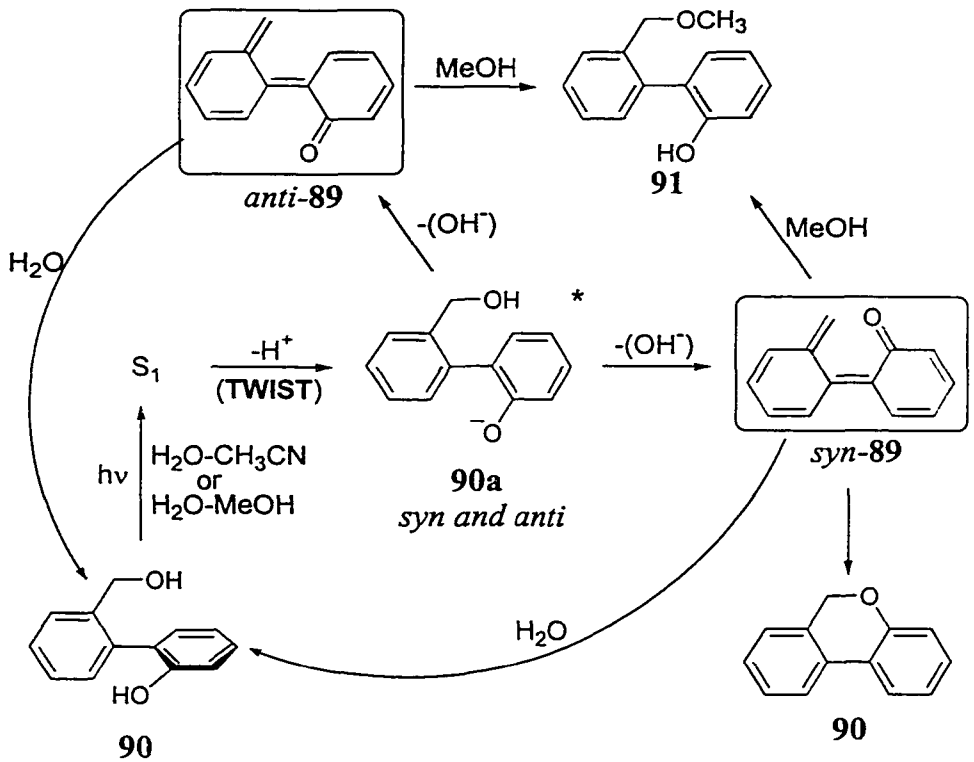

Scheme 1.15

pH and showed two sigmoidal curves at pH ≈ 1 ($pK_a(S_1)$) and at pH ≈ 10 ($pK_a(S_0)$), which implied the necessity of an electronically excited phenolate ion **90a** in the mechanism. Interestingly, an essentially planar product **92** is formed from a highly twisted precursor **90** (dihedral angle of 72° in the *syn* geometry by X-ray crystallography). The explanation given by the authors was that a fast twisting motion of

the bond joining the two benzene rings takes place on the S_1 surface before or during deprotonation of ArOH. LFP experiments failed to detect **89**, which probably indicate that such QMs are very reactive, and thus are very short lived (< 5 ns).

In order to test the generality of this reaction,[136] studies were extended to a variety of other biaryls incorporating naphthalene rings (Scheme 1.16). It was found that these biaryls indeed also undergo the photocyclization and the highest quantum efficiency belonged to the highly twisted binaphthyl system (dihedral angle ≈ 90°) which reacted to yield a much less twisted (dihedral angle ≈ 35°) binaphthyl pyran. These results are consistent with the well-known tendency of biaryls to twist to a more planar geometry upon electronic excitation.[135]

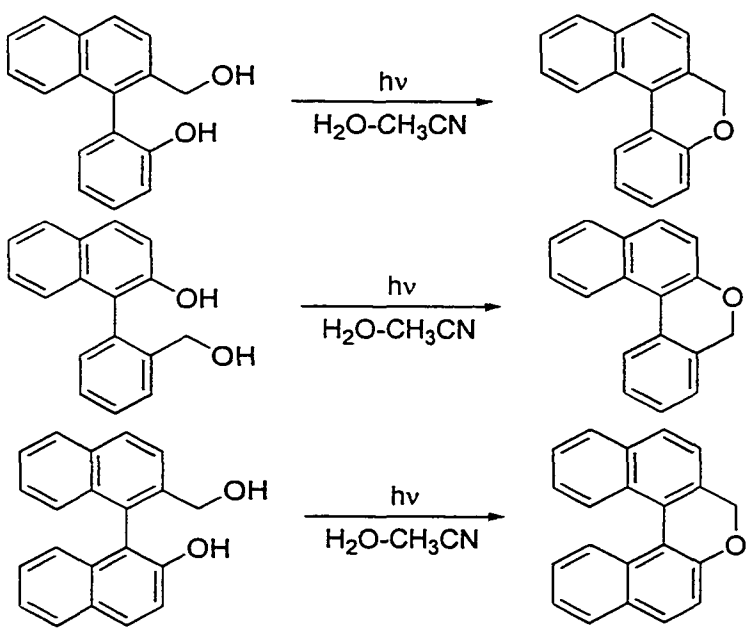

Qutantum Yield

0.11

0.02

0.17

Scheme 1.16

Prevention of the cyclization pathway using appropriately designed biaryl systems may extend the lifetimes of the photogenerated biphenyl quinone methides in aqueous solution and hence make them observable by LFP. This idea led the authors to synthesize biphenyl alcohols **93** and **95**.[136] Photolysis in CH_3OH-H_2O gave the expected methyl ether substitution products. LFP of these alcohols gave transients assigned to the corresponding biphenyl quinone methides **94** (λ_{max} = 570 nm, τ = 0.47 μs) and **96** (λ_{max} = 530 nm, τ = 67 μs) (Eqs. 1.19 and 1.20).

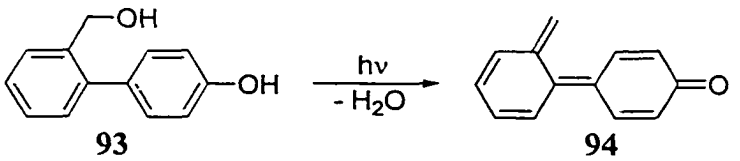

93 **94** **(1.19)**

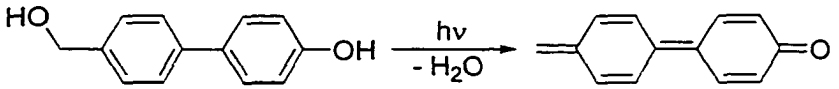

95 **96** **(1.20)**

Although formally antiaromatic in the ground state, fluorenyl quinone methide **98** was easily photogenerated using 1-hydroxy-9-fluorenol **97**.[137] Again, product studies using CH_3OH and ethyl vinyl ether produced high yields of the expected products. LFP of **97** in aqueous solution gave rise to a long-lived (τ > 2 ms) and strongly absorbing transient with λ_{max} = 450 nm, consistent with the formation of fluorenyl quinone methide **98** (Eq. 1.21).

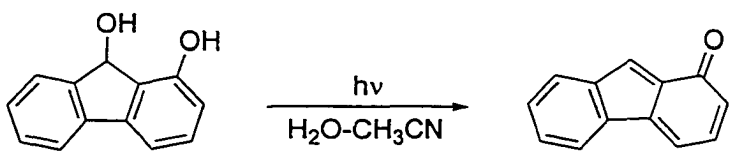

97 **98** **(1.21)**

1.4.3.2 *meta*-Quinone Methides

m-QMs, along with *m*-QDMs and *m*-BQs, are mainly of theoretical interest although they also could be candidates as organic magnets. The enone **84**[126] and its derivatives represent one important class of precursors for *m*-QMs generation, developed by Berson et al.[126] Pyrolysis of **84** (15min, 150°C) in ethylene glycol gave the ether **99a** in good yield (Eq. 1.22a), which is indicative of the intermediacy of a carbocationic

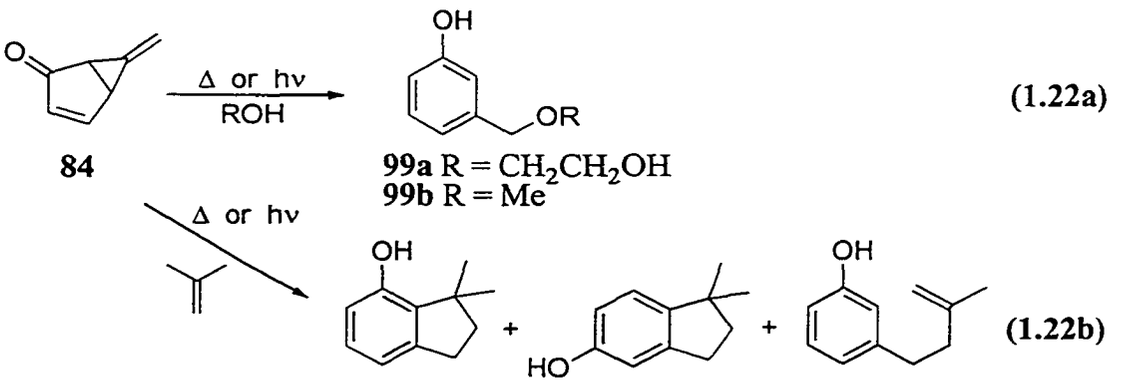

(1.22a)

(1.22b)

species. Similarly, **99a** and its analogue **99b** were the major products of the photolysis of **84** (350 nm, 0°C) in ethylene glycol or methanol, respectively. A well-defined triplet electron paramagnetic resonance (EPR) spectrum was obtained after a few minutes of irradiation at > 310 nm of a degassed, glassy 0.29 M solution of dienone **84** in 2-methyltetrahydrofuran at 11 K and was assigned to the triplet *m*-QM **81c**. The authors' confidence in its identification was substantiated by the photolysis of the benzo derivative **100** (Eq. 1.23),[138,139] where parallel results were obtained as that of **84**. In order to identify

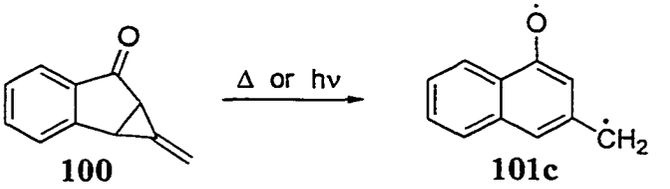

(1.23)

the total electronic spin of the ground state, they closely analyzed the EPR spectra of the photolysis product of **84** and **100** and found that their zero-field splitting parameter values ($|D|/hc$) are in agreement with semi-empirical molecular orbital calculations.[140] Further evidence is that the carrier of the EPR signal has substantial spin density on oxygen. Therefore, they conservatively estimated that the singlet *m*-naphthoquinomethanes (*m*-NQMs) cannot be lower in energy than the triplet by more than 0.01 kcal mol^{-1}. In another words, either the triplet and singlet are nearly degenerate or the triplet is the ground state. This demonstration of a low-lying triplet state for the biradicals **81c** and **101** parallels observations by Platz and Burns[141] in the case of 1-methylene-8-naphthiminyl **102**, which has been assigned a triplet ground state. Further investigations[142] revealed that

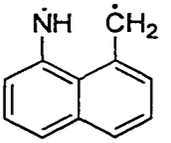

102

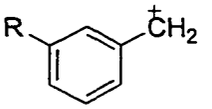

81b R = O^-
103 R = OH

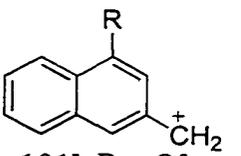

101b R = O^-
104 R = OH

both enones **84** and **100** can react smoothly with alcohols thermally, following clean pseudo-first-order kinetics to afford the corresponding ether products, or can carry out a series of [3+2] cycloadditions with electron-rich olefins under either thermal or photolytic conditions (Eq. 1.22b). Since the intermediates from **84** and **100** readily add nucleophiles such as amines, electron-rich olefins, and alcohols (i.e., as dipolar molecules), it was reasonable to speculate that these reactions might involve the singlet **81b** and **101** (the zwitterions **81b** and **101b**), or perhaps their protonated counterparts, **103** and **104**. Similar

studies on the isomeric pentacyclic diketones **105** and **108** yielded the triplets bis-*m*-QMs **106** and **109**, and subsequently the quintets **107** and **110**, respectively (Eqs. 1.24 and 1.25).

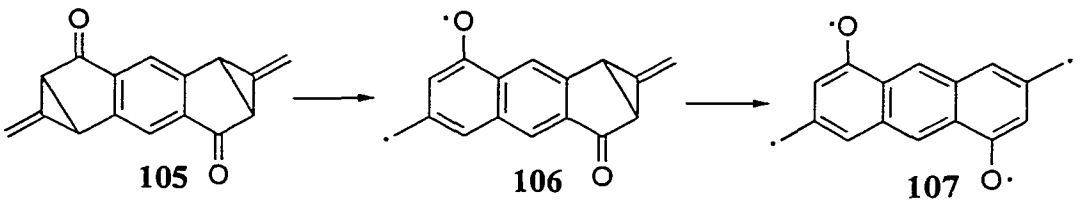

(1.24)

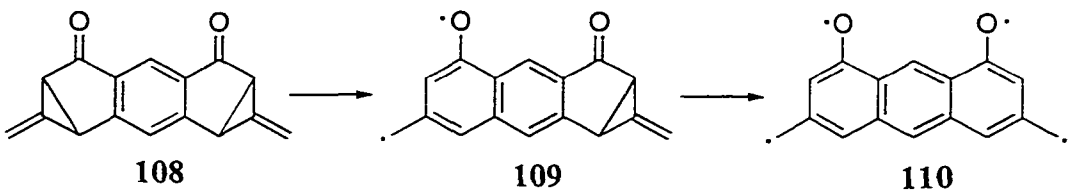

(1.25)

Picosecond LFP studies of enone **100** gave two absorption transients.[143] The authors considered that the absorption spectrum observed after 25 ps belonged to transient A (λ_{max} <450 nm in CH_3CN), which is red shifted in non polar solvents. This initial transient decayed to a new species (transient B, λ_{max} = 500 nm) that was stable within the nanosecond time scale and insensitive to solvent polarity. Following pseudo-first-order kinetics, transient A could be quenched by methanol without forming B. This suggested that A underwent unimolecular decay to generate B in the absence of methanol. With the assistance of an EPR spectrum, the transient A was assigned to singlet *m*-NQM, while the transient B to triplet *m*-NQM. UV spectra of triplet **81c** and **101** have also been recorded at low temperature and shown to have a similar 500 nm band for substrate **101** as seen in ps LFP.[144] Recently, Khan and Goodman[145] have managed to measure the

energy difference ΔE_{ST} between the singlet and the triplet state of *m*-NQM (18.5 kcal/mol) by utilizing picosecond optical grating calorimetry (Scheme 1.17).

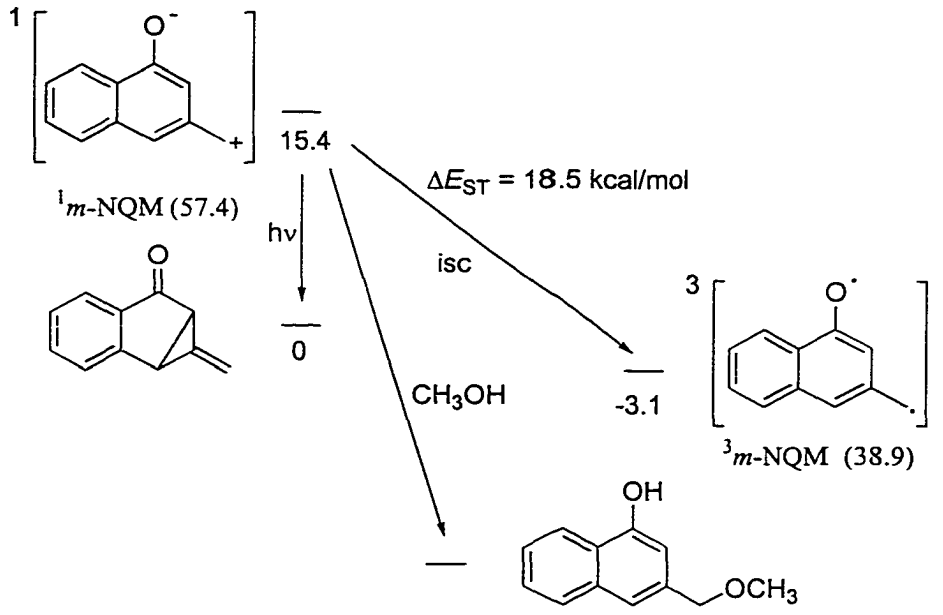

Scheme 1.17

1.5 Proposed Research

As discussed in the above sections, Wan and coworkers[29,131] have suggested the efficient formation of the parent *o*-QM (**79a**) from the photolysis of *o*-hydroxybenzyl alcohol (**48**) in aqueous solution which explains the facile photosolvolysis of this compound observed in 1:1 MeOH-H_2O (formation of the corresponding methyl ether). To further investigate the possibility of *o*-QM formation from various hydroxybenzyl alcohols as a general photochemical process, Yang[146,147] (a former member of the group) studied the photochemistry (using mostly product studies, along with steady state and transient fluorescence measurements) of a number of hydroxybenzyl alcohols including

48, **49**, **111** and **112**, as well the lactone **113** as an additional possible photochemical precursor to *o*-QM (**79a**).

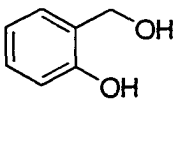

48

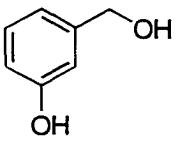

49

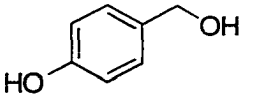

111

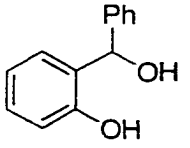

112

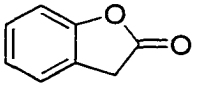

113

Based on product studies, Yang[146] found strong evidence for the efficient generation of *o*-QMs from photolysis of **48** and **112**, which included isolation of the [4+2] cycloaddition adduct (Eq. 1.26) in the presence ethyl vinyl ether (and other electron

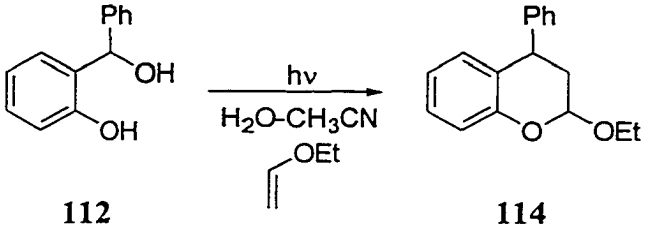

112 **114** **(1.26)**

rich alkenes). The much higher yield of methyl ether product observed on photolysis of **49** (in 1:1 MeOH-H_2O) compared to the photolysis of the methoxy derivative **39** suggested that *m*-QM (**81**) might also be the intermediate in the photosolvolysis of **49**.[147] This latter suggestion is an intriguing idea and needs to be further investigated.

The recent availability of LFP in this department provided an opportune time to systematically investigate the photochemistry of a variety of hydroxybenzyl alcohols in aqueous solution, to address the possibility that a general method for QM formation is

available from simple hydroxybenzyl alcohols. Although product studies have already suggested this to be the case for the ortho isomer, and possibly even the meta isomer, the detection of these and other QM intermediates by transient spectroscopy would be timely proof for their existence. Therefore, this Thesis will be primarily concerned with the photochemistry of hydroxybenzyl alcohols **112** and **115** to **120**, as well as **48**, **49** and **111**,

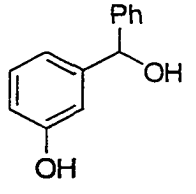

115

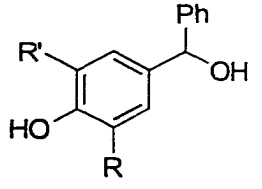

116 R = R' = H
117 R = H, R' = OMe
118 R = R' = *t*-Bu

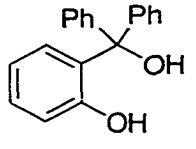

119

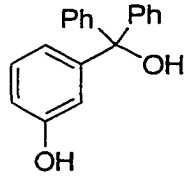

120

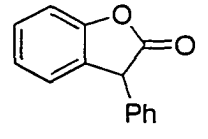

121

studied by LFP and product analysis. The addition of a phenyl substituent at the benzyl position of hydroxybenzyl alcohols was found to provide readily observable quinone methide transients in LFP studies. Lactones **113** and **121** were also strudied as alternate routes for *o*-QM formation, the results of which corroborate those observed for the corresponding *o*-hydroxybenzyl alcohols. Chapter 2 of this Thesis will present the results of photogeneration and chemistry of ortho and para QMs. Chapter 3 will address the success of the same method on the photogeneration of meta QMs and subsequent investigation of the chemistry of *m*-QMs. Chapter 4 will provide the experimental details.

Chapter 2

Photogeneration of *o*- and *p*-Quinone Methides From *o*- and *p*-Hydroxybenzyl Alcohols

2.1 Introduction

In continuing mechanistic studies of the photochemistry of the *o*-hydroxybenzyl alcohol system by the Wan group, Yang[146] provided initial evidence for the intermediacy of photogenerated *o*-QMs based on relative reactivity and product studies. Two compounds studied by Yang[146] were the parent *o*-hydroxybenzyl alcohol (**48**) and its α-phenyl substituted analog **112**, both of which reacted via efficient photosolvolysis in aqueous methanol resulting in the formation of the corresponding methyl ether in high yields (e.g., 65-70% for 10 min photolysis at 254 nm) (Eq. 2.1). Photolysis of these two compounds

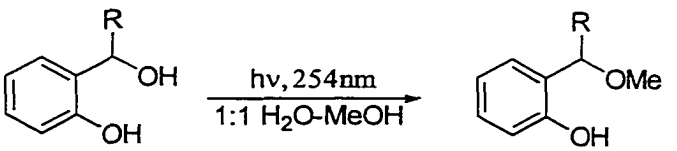

48 R = H
112 R = Ph

122 R = H
123 R = Ph

(2.1)

in the presence of electron-rich dienophiles such as ethyl vinyl ether and dihydropyran gave regiospecific [4+2] Diels-Alder type adducts (chroman derivatives) in high yields (~75% in one hour photolysis) (Eq. 1.26). Coumaranone (**113**), a well known photochemical precursor to the parent *o*-QM **79a** by decarbonylation,[127] was observed to undergo a similar photochemical reaction as described above for **48** (Eq. 2.2), which

supports the notion that *o*-QM **79a** is the key intermediate in the photochemistry of alcohol **48**.

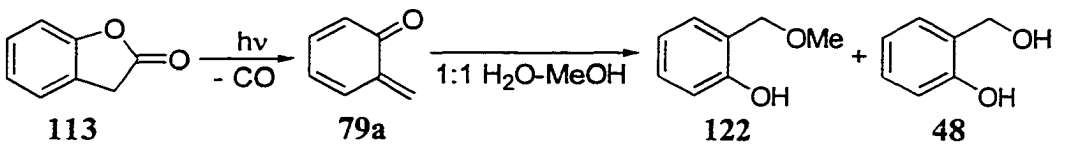

113 **79a** **122** **48** **(2.2)**

Yang[146] also found that both the fluorescence quantum yield (Φ_f) and the lifetime (τ) of phenol **48** were substantially diminished with the addition of water. Based on the well-known fact[90] that singlet excited phenols undergo efficient adiabatic deprotonation in aqueous solution, to give the corresponding singlet excited phenolates ($pK(S_1) \approx 2\text{-}4$)[90], Yang[146] proposed a mechanism of reaction involving initial formation of the excited state phenolate which subsequently reacted (via loss of hydroxide ion) to form the *o*-QMs **79a** and **124** (Scheme 2.1).

One assumption of this mechanism is that methanol is not involved in QM formation in the photomethanolysis, but just acts as a quencher of this transient since the fluorescence intensity was not affected by methanol addition. Consequently, the product quantum yield (Φ_p) for the photomethanolysis in aqueous MeOH solution is given by Eq. 2.3,[1751] where k_{MeOH} and k_{H2O} are the rate constants for nucleophilic attack of MeOH and H_2O towards *o*-QM, respectively, and Φ_{QM} is the quantum yield for formation of *o*-QM. The first bracketed quantity is the fraction of photogenerated *o*-QM that leads to the methyl ether product, which is set equal to α. Therefore, Φ_p is directly proportional to Φ_{QM} for the photomethanolysis.

$$\Phi_p = \left(\frac{k_{MeOH}\,[MeOH]}{k_{MeOH}\,[MeOH] + k_{H2O}\,[H_2O]}\right) \times \Phi_{QM} = \alpha\,\Phi_{QM} \qquad \textbf{(2.3)}$$

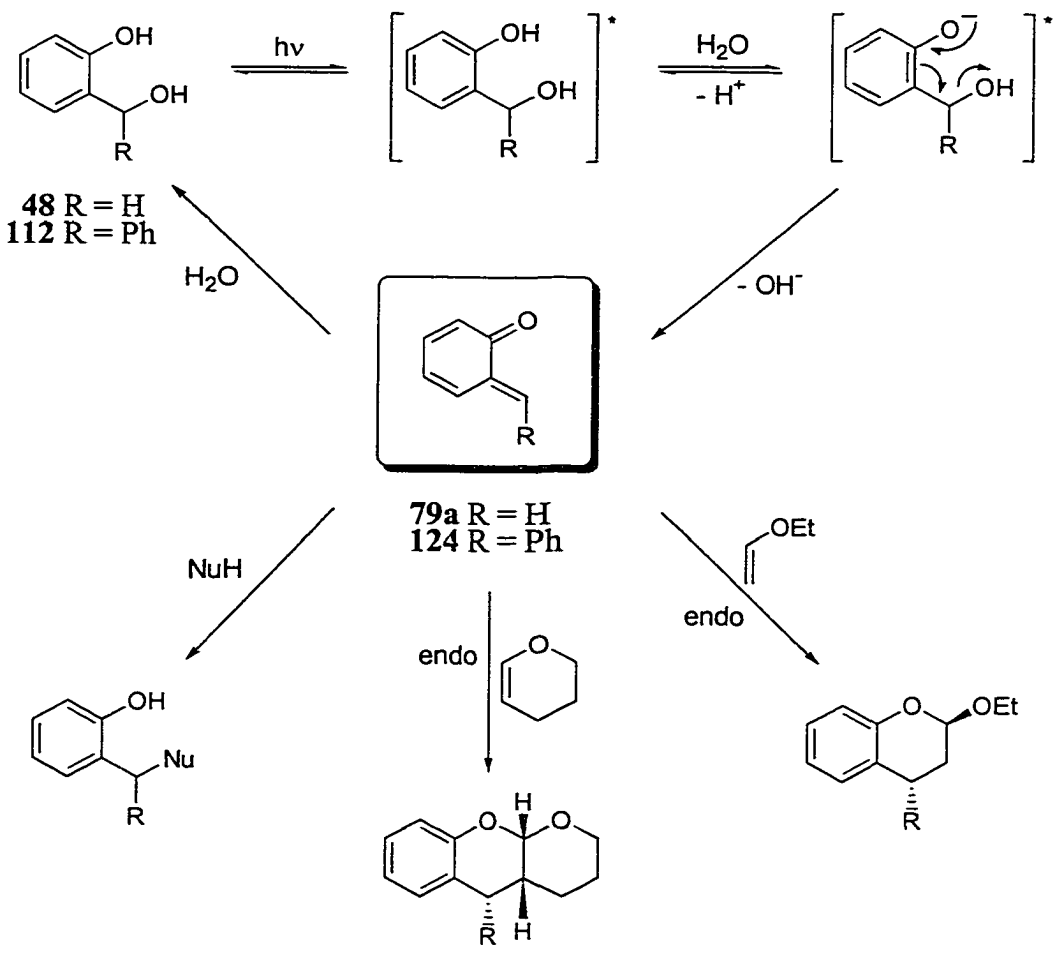

Scheme 2.1

Since the intermediacy of *o*-QMs was suggested in the photosolvolysis of *o*-hydroxybenzyl alcohols, it is important to investigate this further and collect more direct/indirect evidence for the proposed mechanism. This Chapter will describe the results of a mechanistic study of the photosolvolysis of a variety of *o*- and *p*-hydroxybenzyl alcohols and related compounds. In order to make the discussion easier to follow, hydroxybenzyl alcohols **48**, **49** and **111** will be called "parent alcohols", hydroxybenzhydrols **112** and **115-118** as "benzhydrols", and α-phenylhydroxybenzhydrols **119** and **120** as "triphenyl alcohols" in this and following chapters.

2.2 Materials

Hydroxybenzyl alcohols **48** and **111** and benzofuran-2(3*H*)-one (**113**) were commercially available and purified by recrystallization before use. *p*-Hydroxybenzhydrol (**116**) was prepared by reducing the corresponding benzophenone with sodium borohydride. *o*-Hydroxybenzhydrols **112** and **119** were made by the addition of phenylmagnesium bromide or phenyllithium to salicylaldehyde and methyl salicylate, respectively. Unlike the *para* isomers **111** and **116** (Fig. 2.1a), the ^{1}H NMR of **48** and **112** showed no readily assignable peak for either hydroxyl proton in acetone-d_6 or acetonitrile-d_3. Instead, one or two very broad bands, which were D_2O exchangeable, can be observed in the expanded spectra, hidden under other peaks between δ 4-9 (Fig. 2.1b for **112**). The X-ray structure of **112** (all X-ray structures were determined by Mr. Angus Mackinnon and Professor Judith Howard, University of Durham, U.K.) showed that it is extensively intermolecularly hydrogen bonded (Fig. 2.2). The two benzene rings are almost perpendicular to each other. Each phenol proton is pointed away from the benzylic carbon and hydrogen-bonded to the benzylic oxygen in a second molecule, which is similarly hydrogen-bonded with a third one, etc. The ^{1}H NMR of **119** showed two peaks at δ 5.2 and 8.2 assignable to the two hydroxyl protons. These two peaks are broad in a concentrated sample and sharp in a dilute one (Fig. 2.3). The X-ray structure of **119** showed that the molecule exists as an intermolecularly hydrogen-bonded dimer (phenol oxygen with proton of the benzylic hydroxyl group). The phenolic hydroxyl proton is also intramolecularly hydrogen-bonded with the oxygen of the benzylic hydroxy group (Fig. 2.4). The three benzene rings are positioned as a propeller.

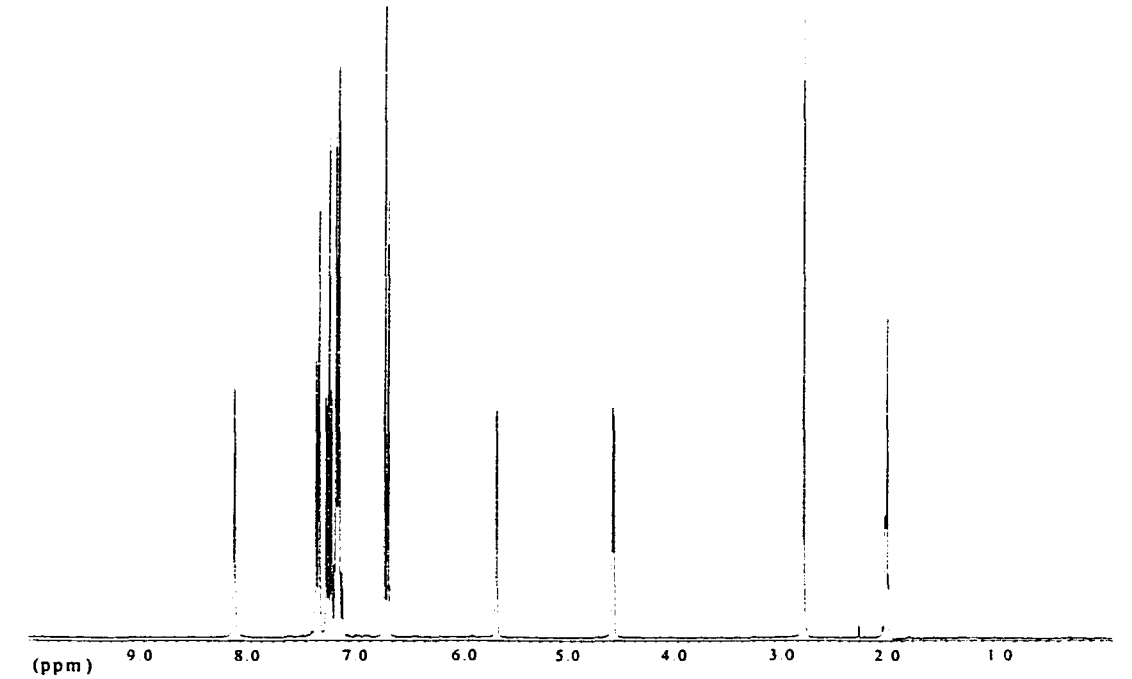

(a)

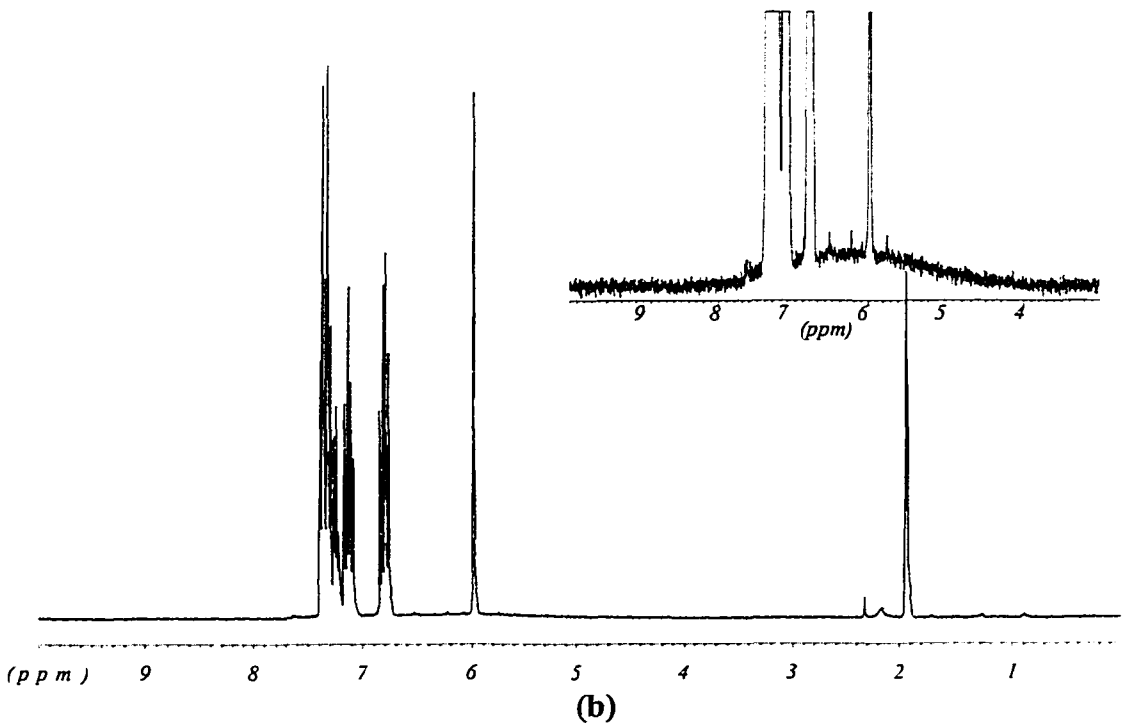

(b)

Fig. 2.1 Representative ^{1}H NMR spectrum of hydroxybenzyl alcohols (a) **116** and (b) **112**.

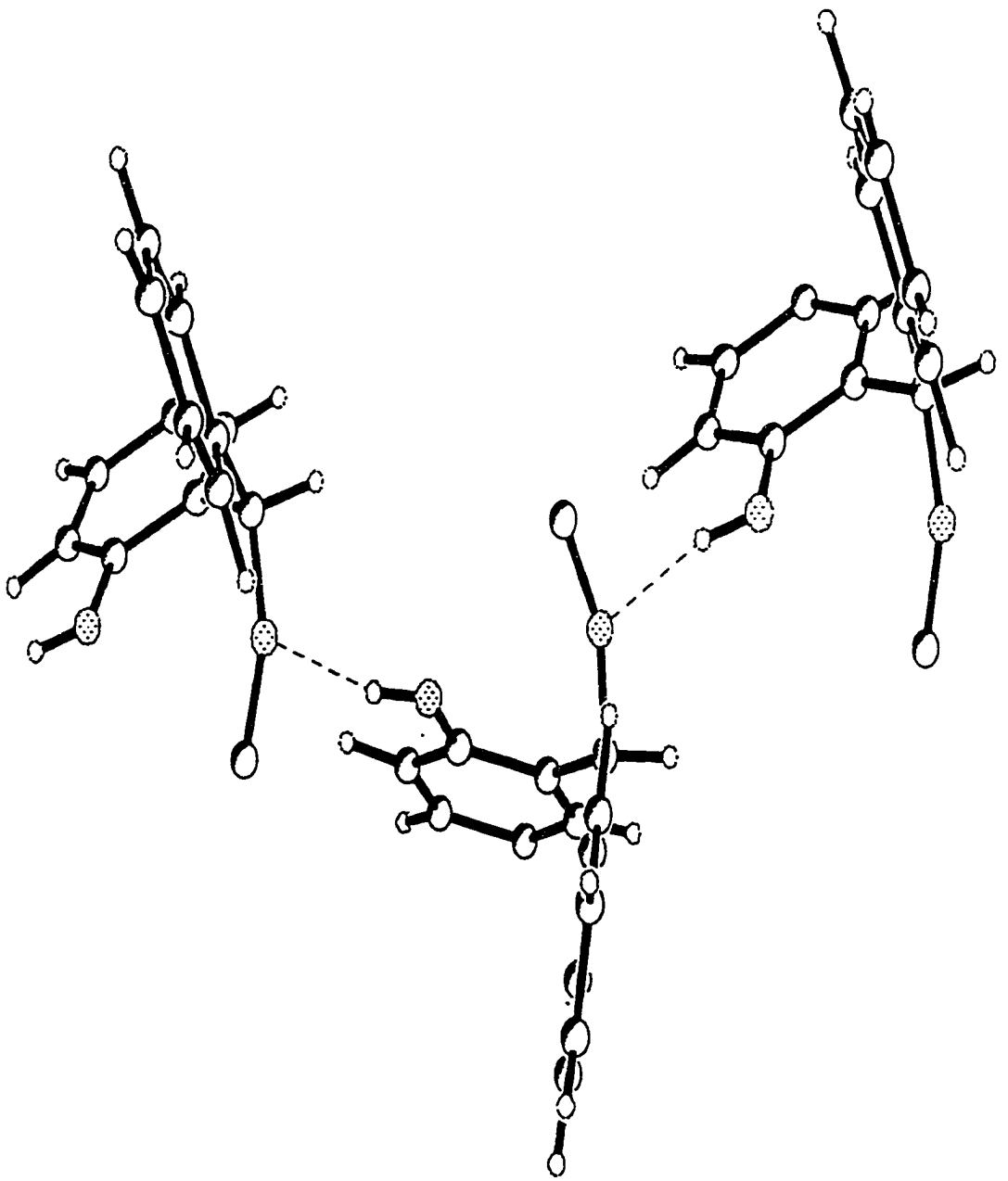

Fig. 2.2a X-ray structure of *o*-hydroxybenzhydrol (**112**).

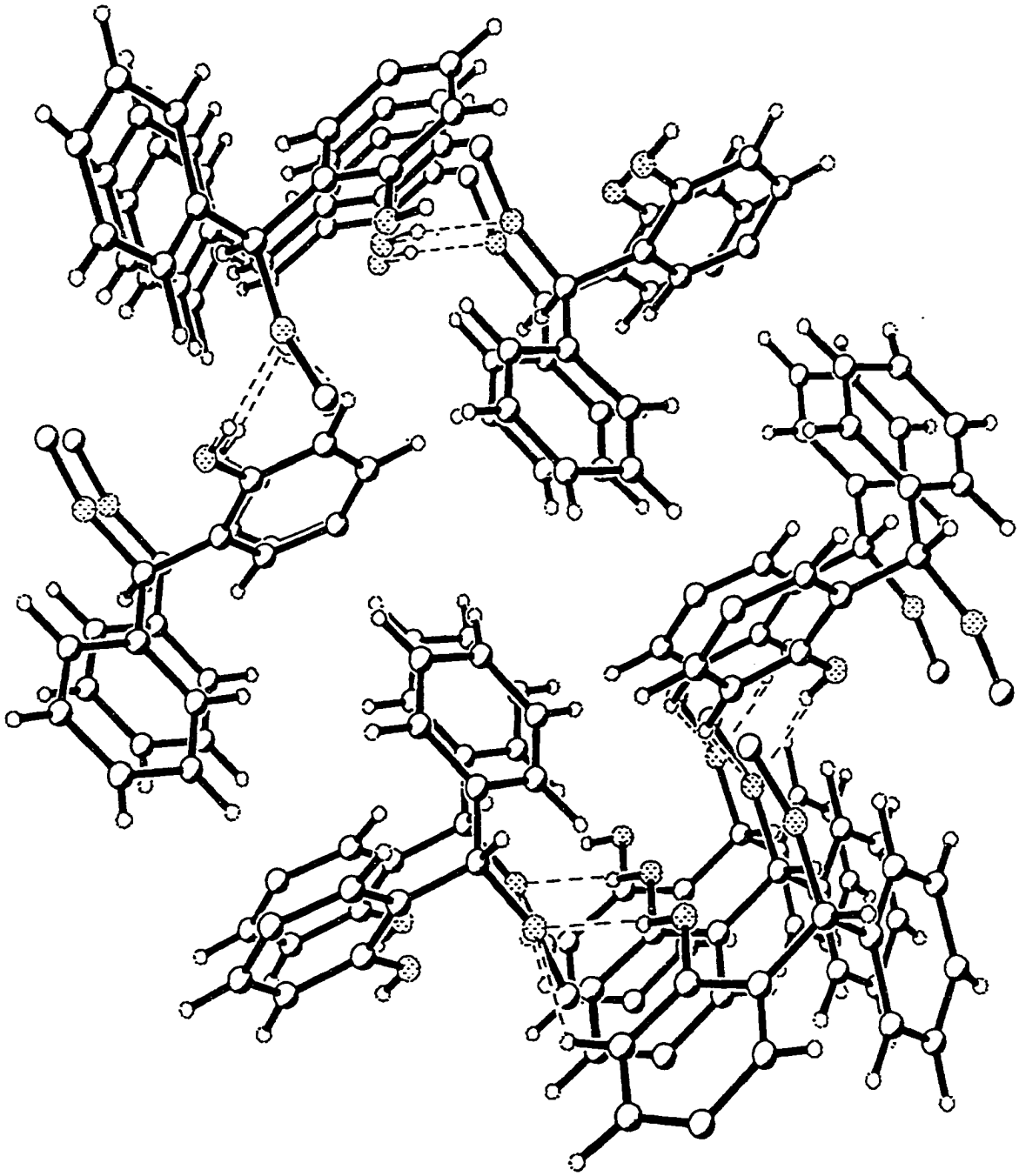

Fig. 2.2b X-ray structure of *o*-hydroxybenzhydrol (112).

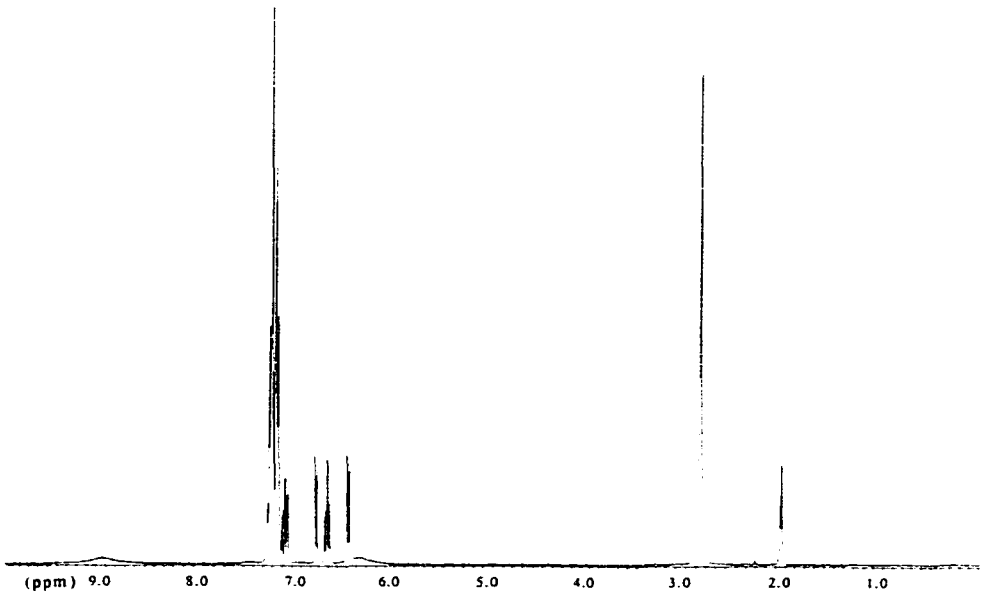

Fig. 2.3 ^{1}H NMR spectrum of α-phenyl-*o*-hydroxybenzhydrol (**119**).

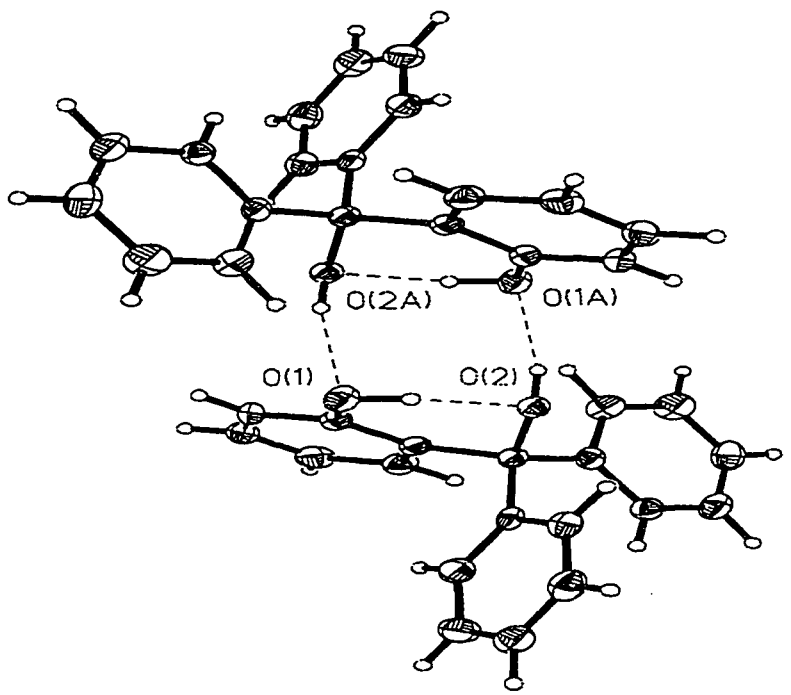

Fig. 2.4a X-ray structure of α-phenyl-*o*-hydroxybenzhydrol (**119**).

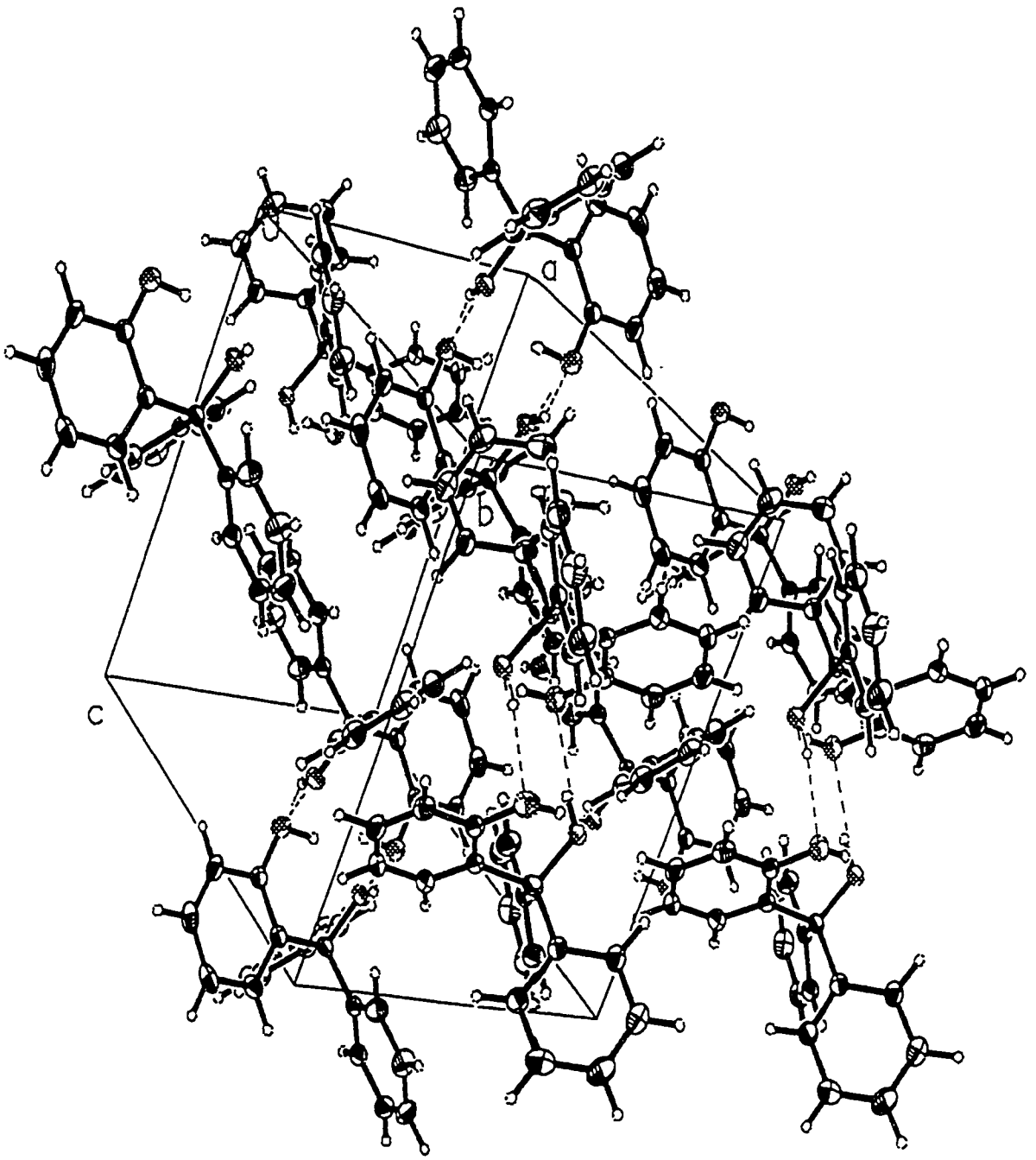

Fig. 2.4b X-ray structure of α-phenyl-*o*-hydroxybenzhydrol (119).

The addition of water (ca. 0.001mL to 0.02 mL) to a sample of **112** (Fig. 2.1b, 0.7 mL in acetonitrile-*d3* solution) did not affect the total appearance of the spectrum (Fig. 2.5a), but reduced slightly the intensity of the broad band, with a concomitant shift upfield. This indicates that there are interactions between substrate and water molecules. Sonification for 65 min. resulted in little change (Fig. 2.5b). Photolysis, however, resulted in the conversion of the broad band into initially two broad signals (Fig. 2.5c), and then to two sharp peaks (Fig. 2.5d) assignable to the two hydroxy protons, accompanied with a sharp water band. The broadening of the hydroxyl peaks is probably caused by extensive intermolecular hydrogen bonding even in solution, which is broken up effectively by photolysis but not by sonification.

Several derivatives related to the above compounds of interest were also studied. *o*-Methoxybenzhydrol (**125**) (available in this laboratory) was redistilled before use. Coumaranone **121** was synthesized according to the method of Padwa et al.[127b] *p*-Methoxybenzhydrol (**127**) was prepared by $NaBH_4$ reduction of the corresponding benzophenone. *o*-benzylphenol (**126**) was purchased from Aldrich and used as received. 3-Methoxy-*p*-hydroxybenzhydrol (**117**) and 3,5-di-*t*-butyl-*p*-hydroxybenzhydrol (**118**) were prepared by the addition of phenylmagnesium bromide to the corresponding benzaldehyde. 3-Methoxy-*p*-hydroxybenzyl alcohol (**128**) and 3,5-di-*t*-butyl-*p*-hydroxybenzyl alcohol (**129**) were obtained by $NaBH_4$ reduction of the corresponding benzaldehyde.

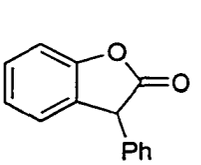

121

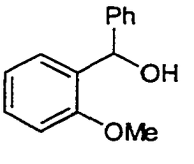

125

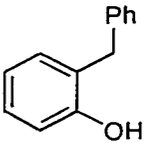

126

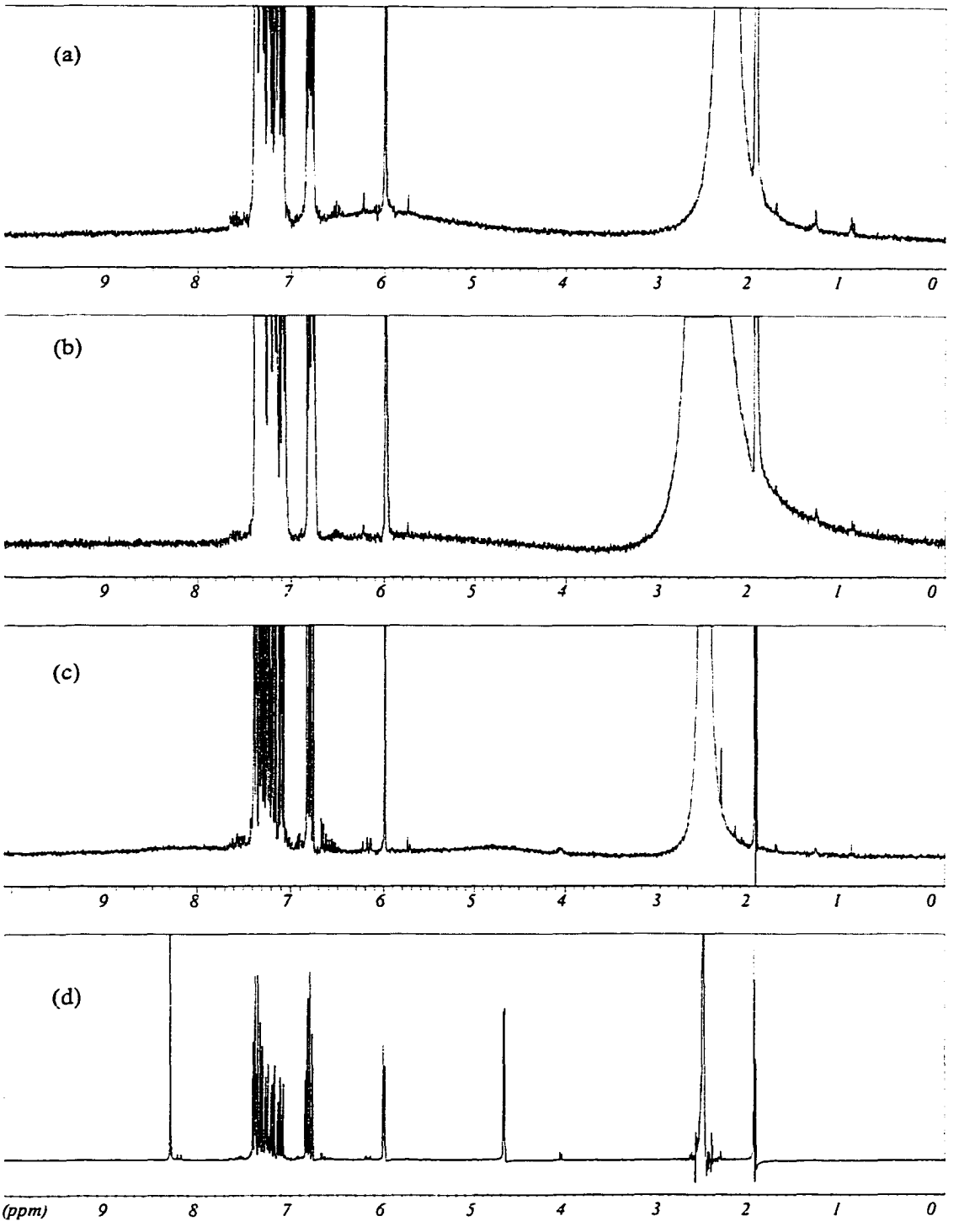

Fig. 2.5 ^{1}H NMR of **112** under various conditions in acetonitrile-d_3. From top to bottom: (a) 0.005 mL water added. (b) 0.02 mL water added and sonicated for 65 min. (c) 10 min. photolysis at 254 nm. d) 20 min. photolysis at 254 nm.

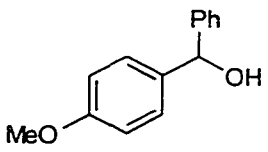

127

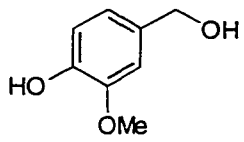

128

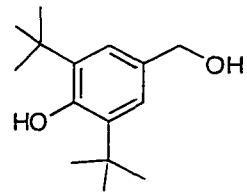

129

2.3 Photolysis in Aqueous Methanol

2.3.1 Product Studies

Photolysis (254 nm, 3 min) of *o*- and *p*-hydroxybenzhydrols (**112** and **116**) in 1:1 (*v*:*v*) H_2O-MeOH gave the corresponding methyl ethers **123** (17%) and **130** (7%) (Eq. 2.4), respectively, as the only products in low conversion runs (< 20%). The ^1H NMR of the reaction mixture showed the characteristic methoxy singlet of the methyl ether product at δ 3.4 (**123**) and 3.3 (**130**). Similar photolysis of their methoxy-substituted analogues **125** and **127** yielded ca. 4% and 0% of the corresponding methyl ethers (**131** and **132**) (Eq. 2.4),

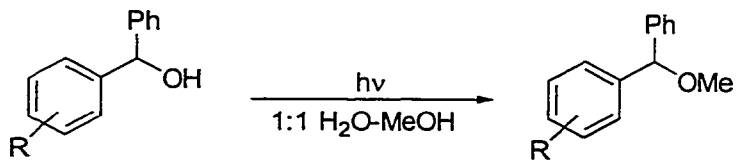

(2.4)

112 R = *o*-OH
116 R = *p*-OH
125 R = *o*-OMe
127 R = *p*-OMe

123 R = *o*-OH
130 R = *p*-OH
131 R = *o*-OMe
132 R = *p*-OMe

indicating that these are probably intrinsically much less reactive than **112** and **116**. Control experiments performed in the absence of light indicated that benzhydrols **112**, **116** and **125** were reactive (yield up to 5 %) if a small amount of $NaHCO_3$ was not added to the solution. Therefore, all runs (photochemical or thermal) using MeOH were carried out in the presence of a pinch of $NaHCO_3$, which resulted in negligible thermal reaction, under the

reaction condition employed for the photolysis. It is postulated that the observed thermal reaction in the absence of $NaHCO_3$ is due to the preexist acids from photo-oxidation of MeOH.

Prolonged photolysis (> 20 min) of **112** in 1:1 H_2O-MeOH gave increasing yields of the methyl ether **123** and also a secondary photoproduct, *o*-benzylphenol (**126**) (characteristic methylene singlet at δ 4.0) (Eq. 2.5). As shown in Fig. 2.6, the yield of **123**

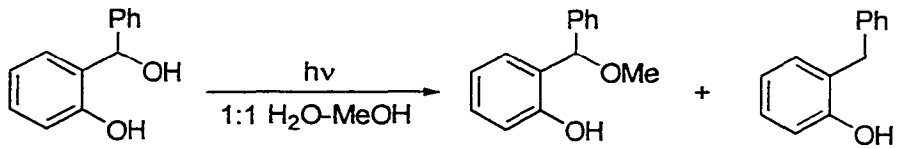

112 **123** **126** **(2.5)**

rises rapidly within the first 20 min of irradiation. However, its formation slows down and eventually levels off after 35 min irradiation (at 60% yield), while **126** builds up in the product mixture (< 10% after 60-min photolysis). Yang[146] observed similar results for **48** in 1:1 H_2O-MeOH (Eq. 2.6). He proposed that *o*-cresol (**133**), is produced exclusively from

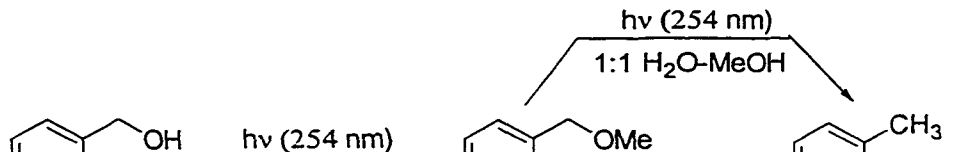

48 **122** **133** **(2.6)**

secondary photolysis of the primary methyl ether product **122**. This was demonstrated[146] by independent photolysis of an authentic sample of **122** in 1:1 H_2O-MeOH, which gave **133** exclusively. Likewise, it is reasonable to propose that **126** is the secondary product from photolysis of **123**. The mechanism probably involves initial homolytic cleavage of C-OMe

bond, followed by a disproportimation of the radical pair, to form **126** and formaldehyde.

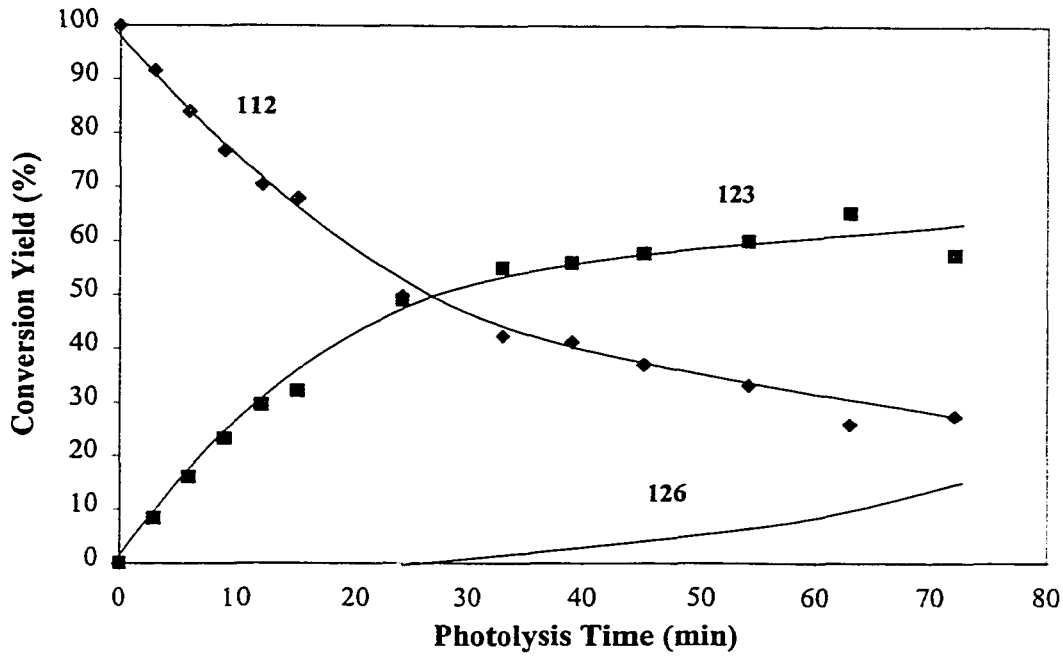

Fig. 2.6 Plot of the conversion of **112** to **123** and **126** in 1:1 H_2O-MeOH as a function of photolysis time.

Irradiation of coumaranone **121**, a known photo-progenitor[127b] of *o*-QM **124**, gave **123** as the only product (ca. 3 % yield) under identical conditions as used for **112** (however, the quantum yield for reaction of **121** is significantly lower than for **112**, *vide infra*). Extended photolysis (254 nm, 8 min), however, resulted in both methyl ether **123** (~ 13 %) and benzhydrol **112** (~ 9 %) as products (Eq. 2.7). These results are consistent with a mechanism of reaction via *o*-QM **124** from the photolysis of **121** via a standard photodecarbonylation mechanism. Since the photolysis of **112** resulted in similar products, it is reasonable to suggest that *o*-QM **124** is also the essential intermediate in the photolysis of **112**. Following this rationale, the photomethanolysis of **116** is proposed to proceed via *p*-QM **134** as the intermediate.

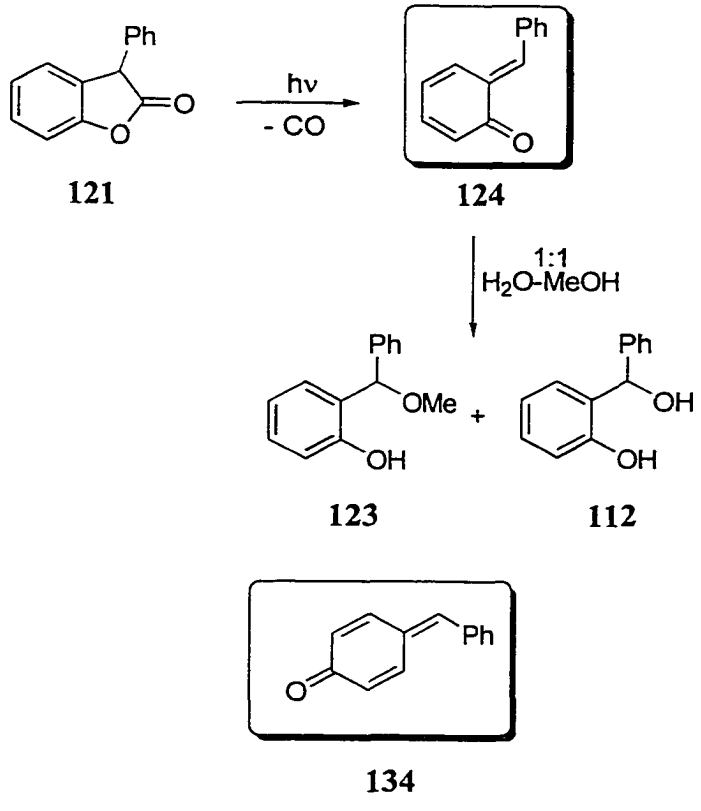

121 124 123 112 134 (2.7)

Yang[146] demonstrated that **48** and **113** gave up to 60% conversion in 1:1 H_2O-MeOH (1 hour irradiation), where the later compound generated both methyl ether **122** (56 %) and alcohol **48** (4 %) as products (Eq. 2.2). Apparently, the additional phenyl group of **121** results in a less reactive compound, perhaps due to the energy wasting chromophore of the additional benzene ring.

Photolysis of **112** was also carried out in basic H_2O-MeOH solutions (acidic solutions could not be used due to thermal reaction of **112**). The plot of the yield of **123** vs. pH (Fig. 2.7) showed a sigmoid curve in the basic pH region. It has an inflection point at around pH 12.5. Since phenols have $pK_a(S_0)$ of 9-12, the increase in the yield at high pH is consistent with higher reactivity of the photoexcited phenolate ion. This is corroborated by the fact that the UV-Vis spectrum of **112** gradually red shifted from 273 nm to 294 nm in

the same pH range (Fig. 2.8), with an estimated $pK_a(S_o) \approx 12$.

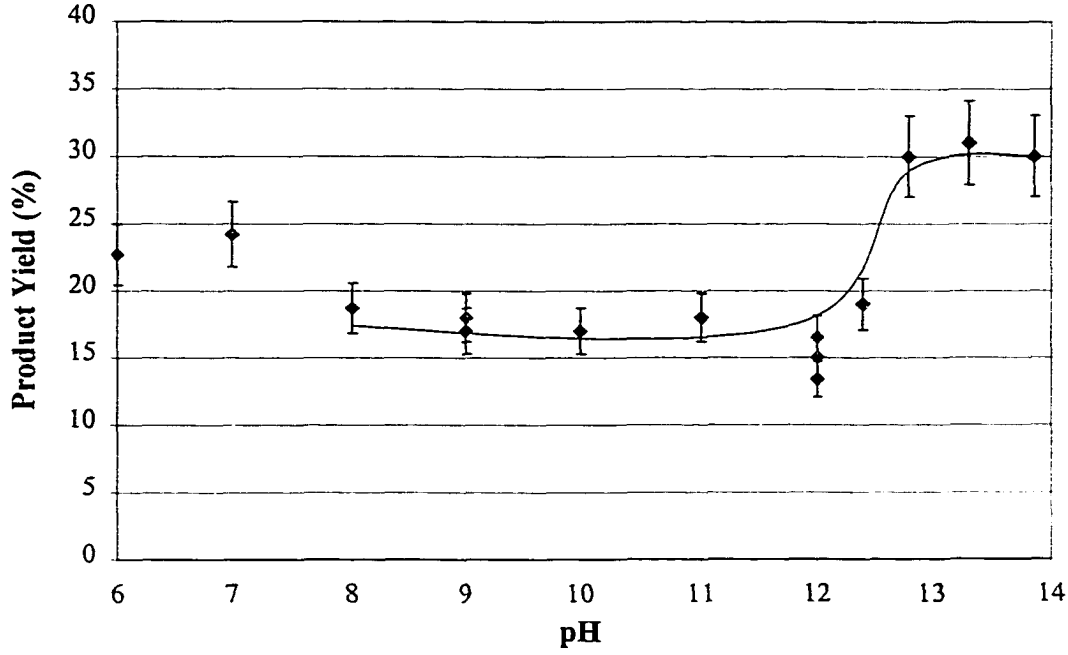

Fig. 2.7 pH Dependence of methyl ether **123** yield from photolysis of **112** in 1:1 H_2O-MeOH (pH is of the water portion).

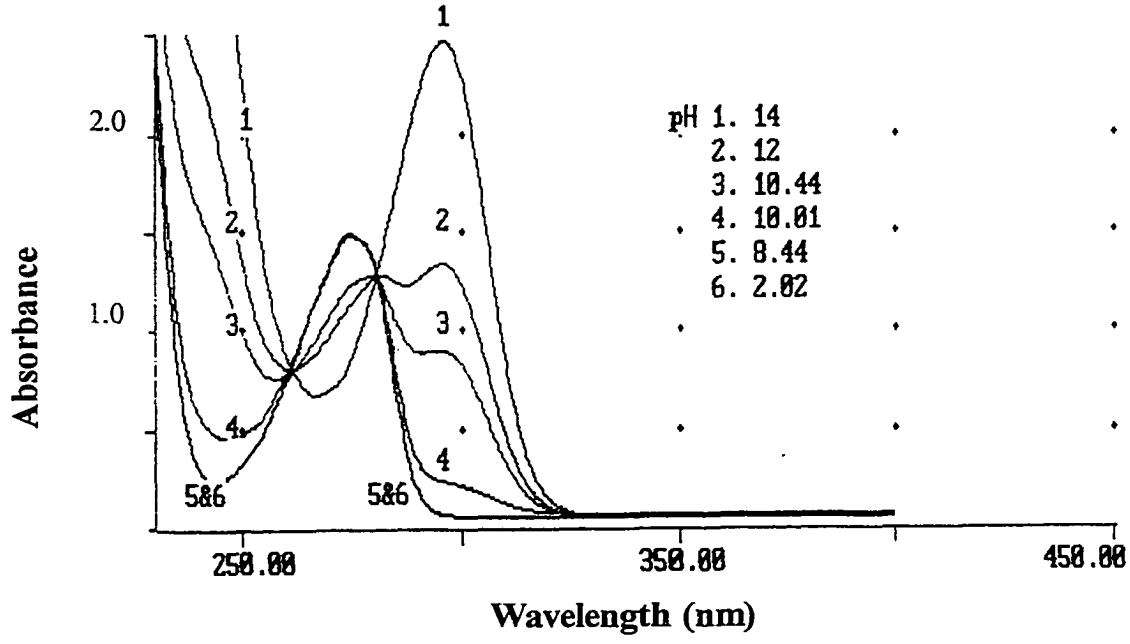

Fig. 2.8 UV-Vis Spectra of **112** vs. pH in 1:1 H_2O-MeOH (estimated $pKa(S_0) \approx 12$).

Photolysis of α-phenyl-*o*-hydroxybenzhydrol (**119**) in 1:1 H_2O-MeOH gave methyl ether **135** (^1H NMR and MS) as the only product in 28% yield under low conversion conditions (Eq. 2.8), which is significantly higher than observed for **112** under similar condition. Additionally, secondary photochemistry was not observed under the condition employed.

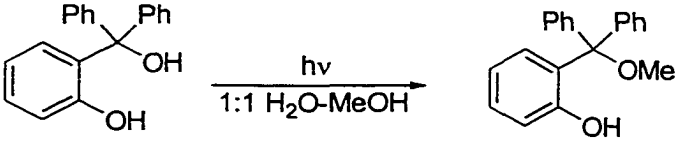

119 **135** **(2.8)**

2.3.2 Product Quantum Yields

The product quantum yield (Φ_p) for the methyl ether formation from **112** in 1:1 H_2O-MeOH has been measured by Yang[146] ($\Phi_p = 0.46 \pm 0.03$) using potassium ferrioxalate actinometry and GC for analysis. This reaction was subsequently used as the secondary actinometric standard for the determination of Φ_p's for the alcohols studied in this Thesis. ^1H NMR integration was employed for calculating the product conversions, which were subsequently converted to quantum yields (Table 2.1).

Although in general, product quantum yields cannot be used as a direct measure of reactivity, comparison of the Φ_p's in Table 2.1 reveal that the hydroxy-substituted alcohols (**112** and **116**) gave much higher yields than their methoxy-substituted counterparts (**125** and **127**). Within the *o*-hydroxybenzyl alcohol series, **119** gave the highest Φ_p suggesting that an additional phenyl group on the benzylic carbon enhances the reaction efficiency. Furthermore, the ortho-substituted substrates have more than twice the reactivity as their para analogues. These results are consistent with Zimmerman's "ortho-

meta effect"[14,26,28] and results obtained by Wan and Chak[29] on mono-substituted benzyl alcohols.

Table 2.1 Product Quantum Yields (Φ_p) for Methyl Ether Formation

Compound	Φ_p [b]	Compound	Φ_p [b]
112	0.46 ± 0.03[a]	**116**	0.19
125	0.11	**127**	0
121	0.08		
119	0.76		

[a] From Yang, reference 146.
[b] Measured using **112** as the secondary actinometric standard, using ^{1}H NMR integration. Photolysis carried out in a Rayonet RPR reactor (254 nm lamps). Estimated errors are 10-15% of quoted value due to uncertainties inherent in NMR integration. Conversions were kept < 30%.

2.4 UV-Vis Studies

The photosolvolysis of selected alcohols was studied using UV-Vis spectrophotometry in aqueous CH_3CN (to avoid complications from methyl ether formation if MeOH was used), to gain initial insight into whether the corresponding proposed QMs are observable without the need for laser flash photolysis (LFP).

Photolysis of **112** in neat acetonitrile (~10^{-2} M, 254 nm for ca. 1-5 min) in a quartz cuvette resulted in the formation of a yellow, then orange red, and eventually a deep red brown solution. UV-Vis spectra were recorded before and after photolysis (~5-10 °C) and are shown in Fig. 2.9 where the starting material absorbs only below 300 nm, with λ_{max} at 276 nm. On photolysis, the appearance of new absorption bands at 333 and 423 nm indicated the formation of a new species. This transient decayed slowly in neat CH_3CN; the yellow color remained even on sitting overnight. A similar transient was observed in

THF and cyclohexane (at ca. –15 °C) (Table 2.2). The red shift of λ_{max} on going to more polar solvents indicate that these transitions of π,π^* in character, consistent with a highly conjugated *o*-QM **124**.

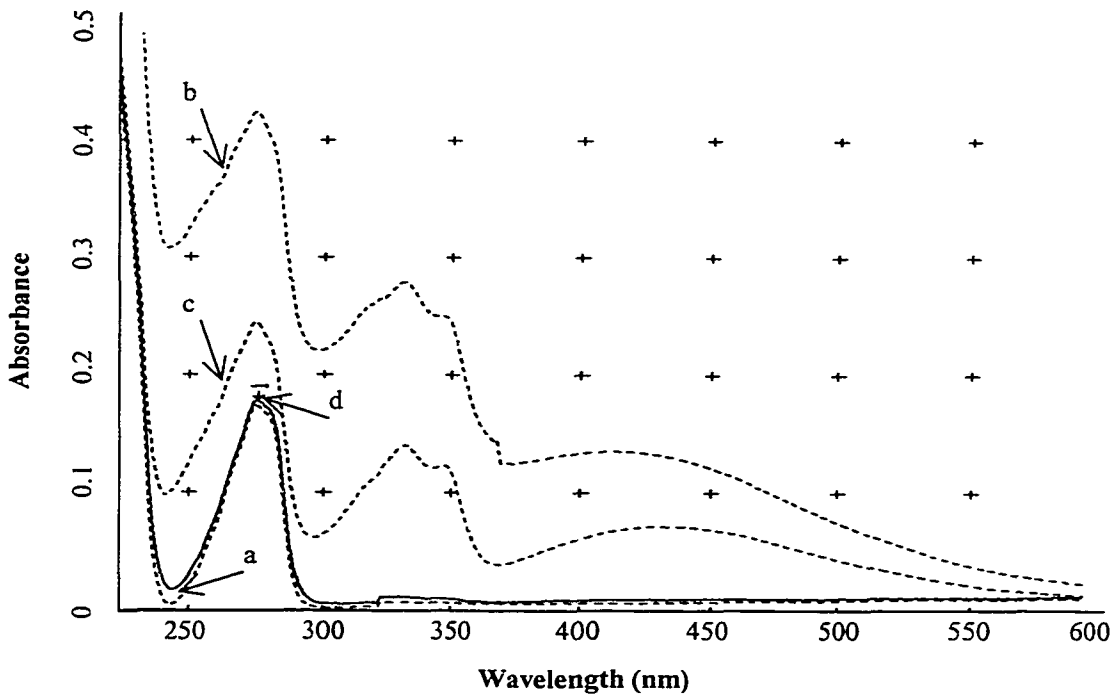

Fig. 2.9 Absorption spectra of **112** in pure acetonitrile (a) before photolysis; (b) immediately after 4-min photolysis (8 × 254 nm) at –15 °C; (c) on standing for 3 h; (d) standing overnight.

Table 2.2 Solvent Effect on Absorption Maxima (λ_{max}) for Species Photogenerated from **112**

Temperature	Solvent	λ_{max} (nm)	
< 0 °C [a]	Cyclohexane	333	410
	THF	333	427
	CH_3CN	332	434
ca. 5 °C	1:9 H_2O-CH_3CN[b]	333	438
ca. 20 °C	1:1 H_2O-CH_3CN[b]	345	455

[a] Irradiated in an ethylene glycol/dry ice slurry (ca. –15 °C).
[b] Results from LFP studies (vide infra).

Photolysis of **112** in 1:9 H_2O-CH_3CN at ~ 5 °C produced an orange-red solution, which was formed more efficiently than in neat acetonitrile but with similar λ_{max} (Table 2.2). Upon removal from the UV source, the color gradually faded ($\tau \approx 40$ sec; shorter at 20 °C) with complete recovery of the UV spectrum prior to irradiation. When photolyzed in essentially neat H_2O (< 5% CH_3CN as cosolvent), the same orange-red transient was generated but disappeared quickly (τ < 5 sec), prohibiting a UV-Vis spectrum to be recorded.

Photolysis of *p*-hydroxybenzhydrols **116-118** in aqueous acetonitrile also gave red colored transient, but none of them was capable of giving a colored transient when photolyzed in neat acetonitrile. The transient from **116** absorbed strongly at 372 nm in H_2O (< 5% CH_3CN) with a 10 sec lifetime. It was 20 times longer lived in 1:1 H_2O-CH_3CN (τ = 216 sec.). Similar transient absorptions were observed for **117** (at 377 nm) and for **118** (at 356 nm) in either neat water or in 1:1 H_2O-CH_3CN. Fig. 2.10 shows a typical absorption spectrum and its decay of the photogenerated transient from **117** in H_2O solution. Table 2.3 summarizes the λ_{max} and τ for the transients observed. The transients from **117** and **118** are much longer lived when less water is used.

All of the observed transients return to starting materials eventually. The transient from **116** has longer lifetime than that from **112**. Electron donating groups on the benzene ring (in **117** and **118**) produce transients that are even longer lived. All of these observations are consistent with the transients being assignable to the corresponding QMs.

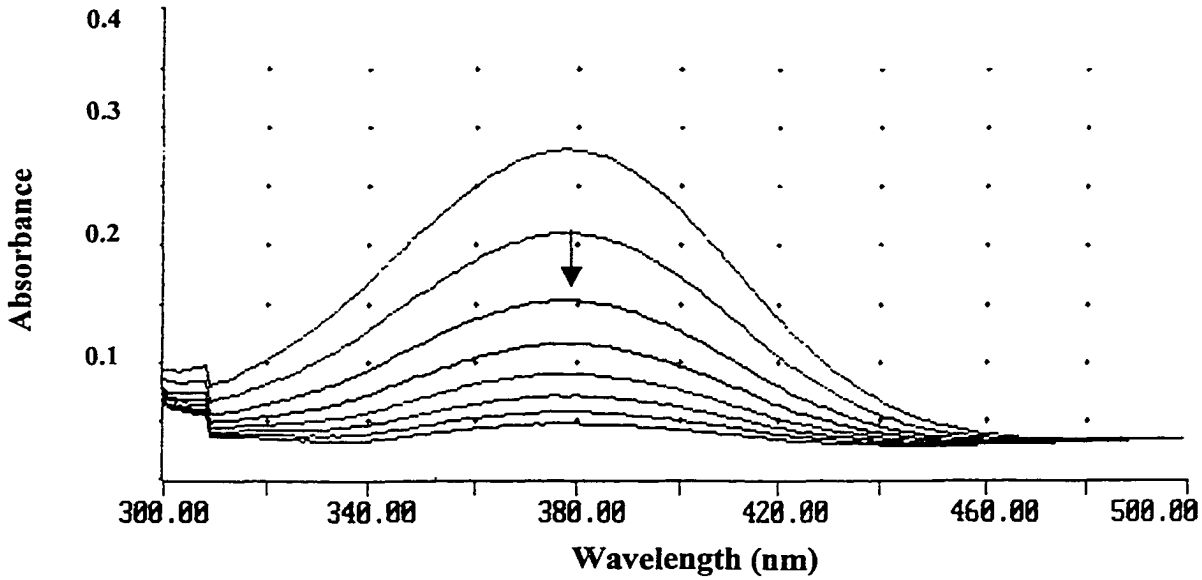

Fig. 2.10 Decay of transient generated on photolysis of **117** in 100% H_2O (transient taken at 1 min. intervals).

Table 2.3 Absorption Maxima (λ_{max}) and Estimated Lifetimes (τ) of Photogenerated Transients from Hydroxybenzhydrols

Compound	Solvent[a]	λ_{max} (nm)[b]	τ[c]
112	H_2O	333, 438	< 5 s
	1:9 H_2O-CH_3CN	333, 438	27 s
	1:9 H_2O-CH_3CN (~5 °C)	333, 438	40 s
116	H_2O	372	10 s
	1:1 H_2O-CH_3CN	360	216 s
	1:9 H_2O-CH_3CN	354	> 60 min
117	pH 7 buffer	377	130 s
	1:1 H_2O-CH_3CN	377	> 60 min
118	pH 7 buffer	356	> 60 min
	1:1 H_2O-CH_3CN	356	> 60 min

[a] At ~20 °C unless otherwise specified.
[b] Error is ca. 2nm.
[c] Estimated lifetime from a fit to a single exponential decay.

2.5 Laser Flash Photolysis

The laser flash photolysis (LFP) technique is now being utilized on a routine basis in photochemical studies. The above preliminary UV-Vis studies have shown that transients are photogenerated from benzhydrols **112** and **116-118**, which all have shorter lifetimes upon the addition of water. In order to investigate the chemical behavior of these transients in more detail, especially in aqueous solution, LFP experiments were carried out at ca. 20 °C using a nanosecond system with a YAG laser at 266 nm. Solutions were purged with N_2 or O_2 prior to and throughout the experiment when the flow cell was used, but only pre-purged for experiments using a static cell. flowing the solution had the advantage of avoiding complications arising from product photolysis and interference from long-lived species.

2.5.1 *o*-Substituted Benzhydrols

LFP of **112** in 1:1 H_2O-CH_3CN under either N_2 or O_2 gave the same strong signals as reported in Section 2.4 above, with no observable decay within the millisecond range, the limit of the nanosecond LFP system (Table 2.4). A significant amount of transient was also formed on photolysis in neat CH_3CN (under either N_2 or O_2), although the absorption bands were significantly blue shifted (the 455 and 345 nm bands were shifted to 410 and 330 nm, respectively).

Relative quantum yields for formation of the transients as a function of water content in CH_3CN were measured by monitoring the ΔA at both 350 and 450 nm (Fig. 2.11). Interestingly, the yield of the transient decreased initially (at low water content), followed by a dramatic increase with the increase in water concentration. The maximum

yield was reached in ca. 75% H_2O-CH_3CN which was followed by a slight drop on approaching 100% H_2O.

Transient spectra from **112** were also taken in neat H_2O of different pH with the same transient being observed in the whole pH range. A plot of ΔA (relative quantum yield) vs. pH (Fig. 2.12) showed two "titration" regions, at pH ~1-2, and at pH 11-12. The first of these approximately corresponds to the $pK_a(S_1)$ of phenols whereas the second corresponding to $pK_a(S_0)$. These results parallel those obtained in the product studies (Section 2.3.1) and are consistent with a mechanism for formation of the QM via an excited state phenolate.

Table 2.4 Absorption Maxima and Lifetimes for Transients Observed in LFP Experiments for Arylmethanols and Related Compounds[a]

	Compound	λ_{max} (nm)	Lifetime[b]
Benzhydrols	**112**	345, 455	~ 0.4 ms[c]
	125	420	13 ns, ~0.5 μs
	116	360	> 2 ms
	117	380	> 2 ms
	127	455	48 ns, 1.1 μs
Triphenyl Alcohols	**119**	350, 460	> 2 ms
Parent Alcohols	**111**	400	9.3 μs, > 2 ms
	128	390	27 μs, > 2 ms
	129	365	32 μs, > 2 ms
	48	379, 397	18 μs, > 2 ms
Coumaranones	**121**	340, 460	> 2 ms
	113	390	> 2 ms

[a] In 1:1 H_2O-CH_3CN. [b] Where two lifetimes are reported, a fit was carried out using the sum of the two single exponential decays. [c] In neat H_2O.

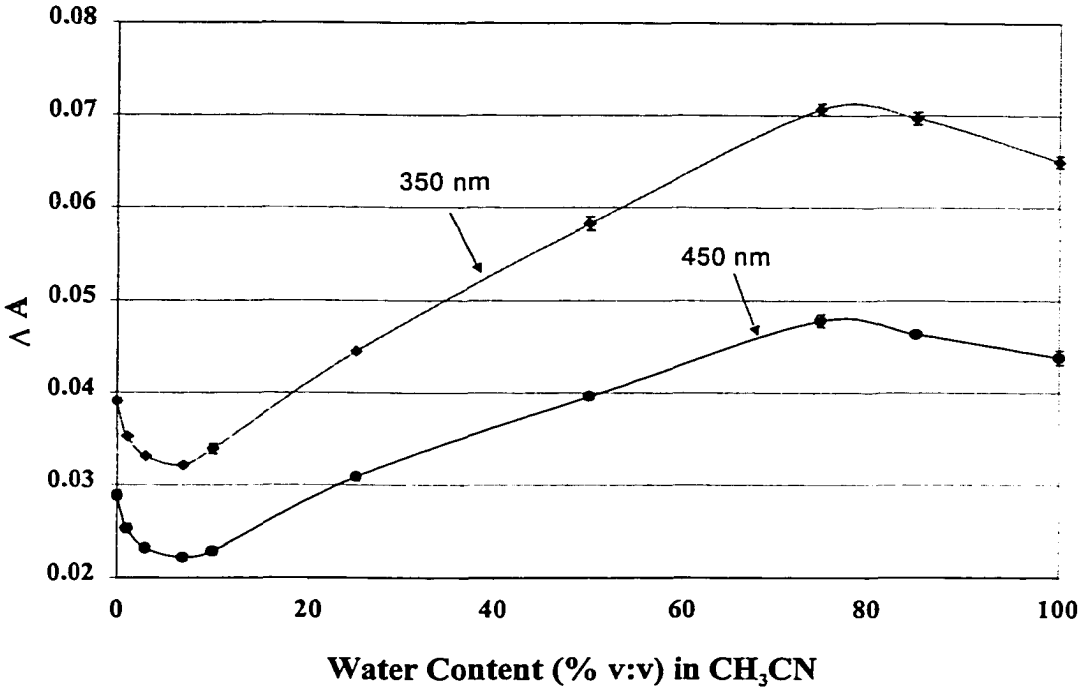

Fig. 2.11 Relative quantum yields for the formation of the transient from **112** as a function of water content in CH_3CN monitored at 350 and 450 nm, respectively.

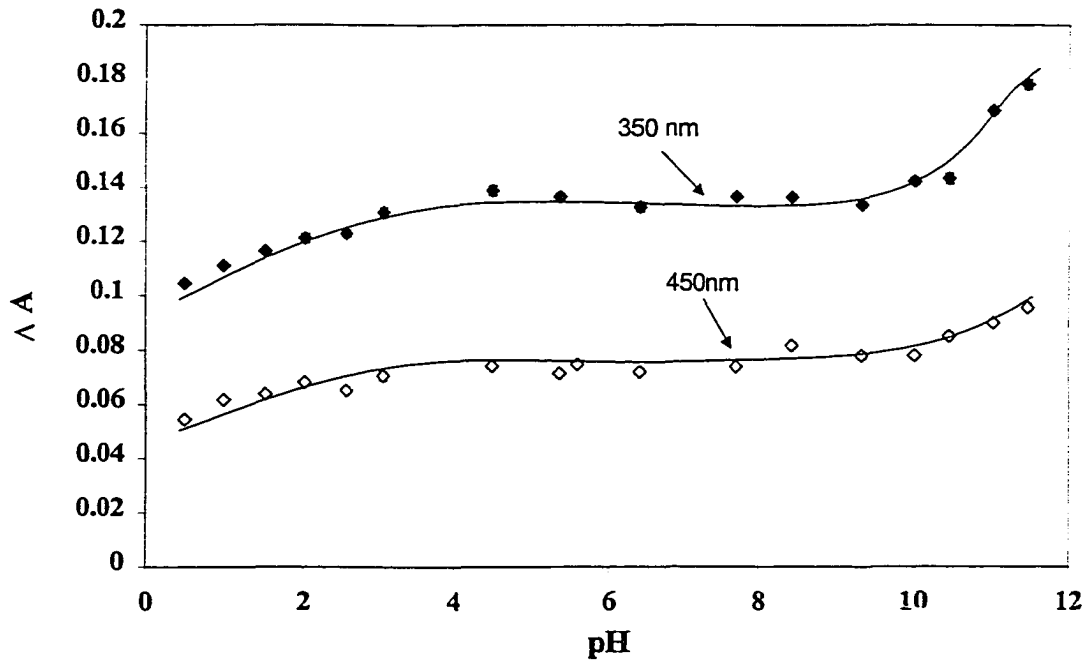

Fig. 2.12 Relative quantum yield (Δ A) for formation of transient for **112** vs. pH, monitored at 350 nm (♦) and 450 nm (◊) using LFP in neat H_2O.

The lifetime of this transient was measured in neat H_2O at different pH where possible (pH 0-5, pH > 12) (Fig. 2.13). At intermediate pHs, lifetimes were too long for the laser system employed. A plot of log k_{obs} vs. pH gave a slope of -1 at low pH and +1 at high pH (4.2E-11), indicating that the transient is quenchable by H^+ and OH^-. Equation 2.9 for k_{obs} may be used to quantify this behavior.

$$k_{obs} = k_{H+}[H^+] + k_{H2O}[H_2O] + k_{OH-}[OH^-] \quad \textbf{(2.9)}$$

In neutral solution with $[H^+]$ and $[OH^-]$ approaching zero, a slope of zero is expected. In either acidic or basic solution, $k_{H2O}[H_2O]$ is essentially a constant. At low pH, $k_{H2O}[H_2O] << k_{H+}[H^+]$, thus

$$\log k_{obs} = \log k_{H+} + \log [H^+] = \log k_{H+} - \text{pH} \quad \textbf{(2.10)}$$

Similarly, in basic solution, if $k_{OH-}[OH^-] >> k_{H2O}[H_2O]$, thus

$$\log k_{obs} = \log k_{OH-} + \log [OH^-] = (\log k_{OH-} + 14) + \text{pH} \quad \textbf{(2.11)}$$

Therefore, $k_{H+} = 1.0 \times 10^6\ M^{-1}s^{-1}$ and $k_{OH-} = 4.2 \times 10^3\ M^{-1}s^{-1}$ for **112**.

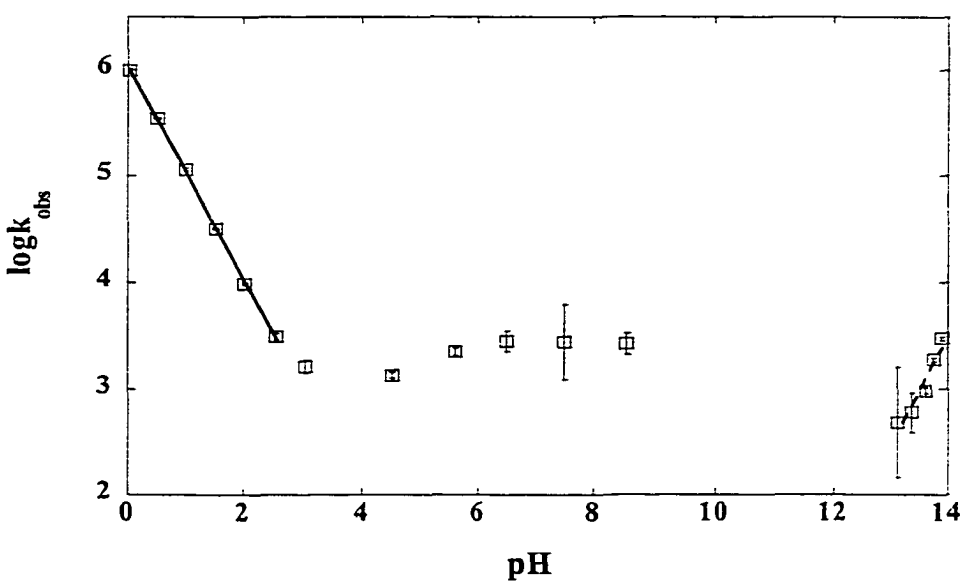

Fig. 2.13 A plot of log k_{obs} vs. pH (monitored at 350 nm) for the transient observed from **112** in neat H_2O.

The transient from **112** can also be quenched by added ethanolamine ($NH_2CH_2CH_2OH$). Additionally, UV spectra taken of **112** in 1:1 H_2O-CH_3CN with added ethanolamine showed that the corresponding phenolate ion is also generated with increasing ethanolamine concentration. However, LFP of these samples gave the same transient absorption spectrum as observed in the absence of ethanolamine. The lifetime of the transient from **112** was measured at different ethanolamine concentration (up to 0.4 M) in 1:1 H_2O-CH_3CN. A linear plot was observed between k_{obs} and $[NH_2CH_2CH_2OH]$. Fitting the data to $k_{obs} = k_{H2O}[H_2O] + k_{amine}[NH_2CH_2CH_2OH]$ gives $k_{amine} = 6.7 \times 10^3\ M^{-1}s^{-1}$ and $k_{H2O}[H_2O] = 1.2 \times 10^2\ s^{-1}$ for the transient from **112** (Fig. 2.14).

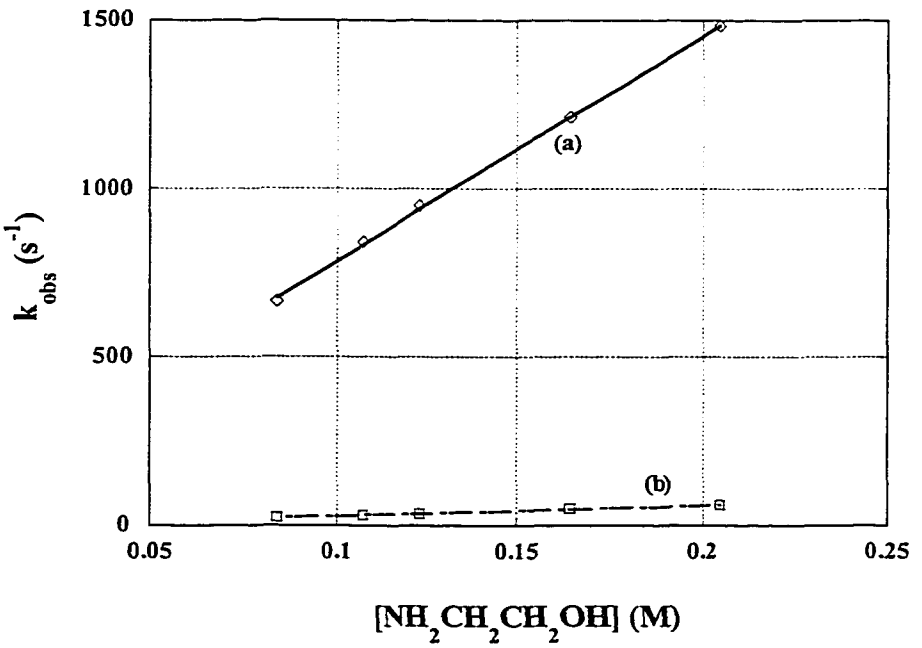

Fig. 2.14 Plot of k_{obs} vs. $[NH_2CH_2CH_2OH]$ for the transient obtained from **112** (a) and **116** (b).

LFP of **121** in 1:1 H_2O-CH_3CN afforded a transient spectrum essentially identical to that observed for **112** (Fig. 2.15), but with much weaker signal intensity, consistent with the

lower reactivity to photomethanolysis observed for **121**. This transient was also quenchable by added ethanolamine. Since **121** is known to give *o*-QM **124** upon photolysis,[127b] it is reasonable to infer that the transient from **112** is indeed *o*-QM **124**. However, one cannot rule out carbocation **136** at this stage since it would also absorb in the 400-500 nm region

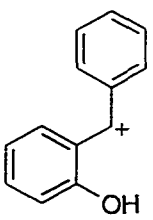

136

and be quenchable by nucleophiles such as water and ethanolamine. Nevertheless, experiments below help firm up the assignment to *o*-QM **124**.

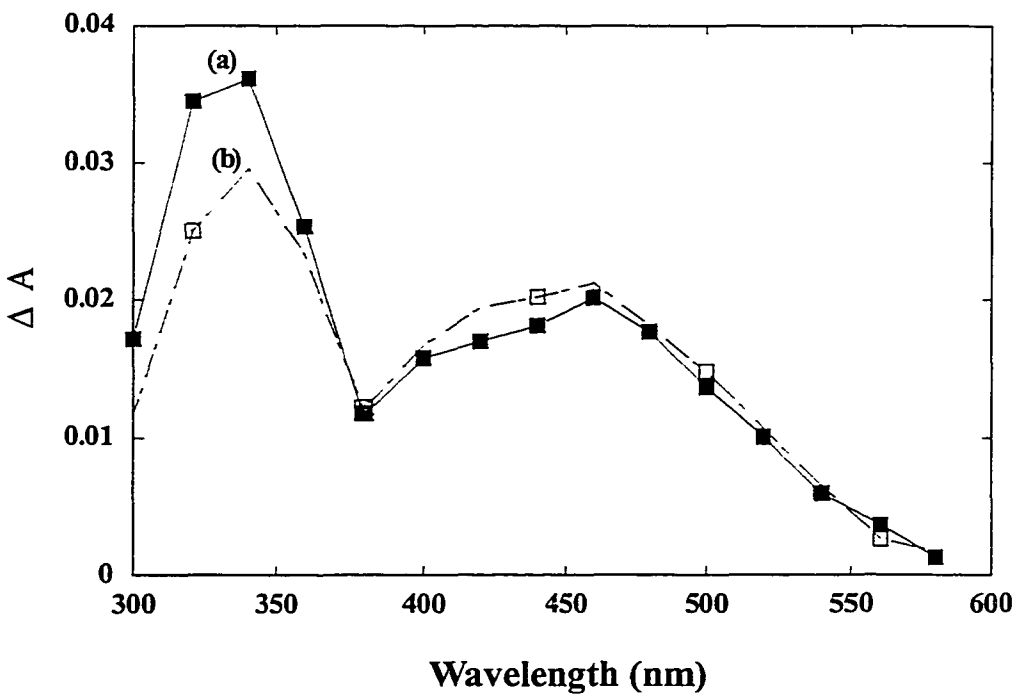

Fig. 2.15 Transient absorption spectra observed for **121** under (a) N_2, (b) O_2 in 1:1 H_2O-CH_3CN.

LFP of the *o*-methoxy derivative **125** 1:1 H_2O-CH_3CN gave a weak absorption at 420 nm, with a short-lived (13 ns) and a long-lived species (~0.5 μs) (fitted to the sum of two single exponential decays, Fig. 2.16) (Table 2.4). Chateauneuf[77] found that the diphenylmethyl cation (**137**) has λ_{max} at 435 nm with ca. 1 ns lifetime by using ps LFP, while McClelland et al.[47,66] reported that (*p*-methoxyphenyl)phenyl methyl cation (**138**) absorbs at 455 nm with a 0.5 μs lifetime in 2:1 H_2O-CH_3CN. Since the LFP system used by the McClelland group has a pulse of ~ 20 ns, they were unable to observe the short-lived species. Considering that substituents on the benzene ring have similar electron donating and withdrawing abilities at the ortho and para positions, it is reasonable to propose that the ortho-substituted diphenylmethyl cations also absorb in the 400-500 nm region and have μs lifetimes. Therefore, the long-lived (~ 0.5 μs) species observed from **125** is assigned to carbocation **139**. Since Peters and coworkers[48] showed that the contact ion pair from diphenyl chloride had lifetime 150 ps, the short-lived (13 ns) species may be a radical cation.

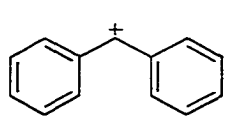

137

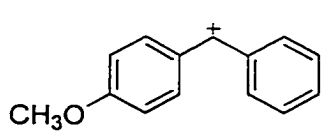

138

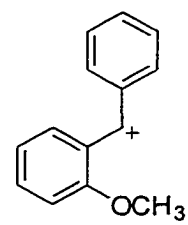

139

The transient from **112** has very different spectral characteristics compare to carbocation **139**. Moreover, it is much longer lived. Another argument against the carbocation assignment is that the transient from **112** is shorter lived in acidic solution, in accord with a QM structure.

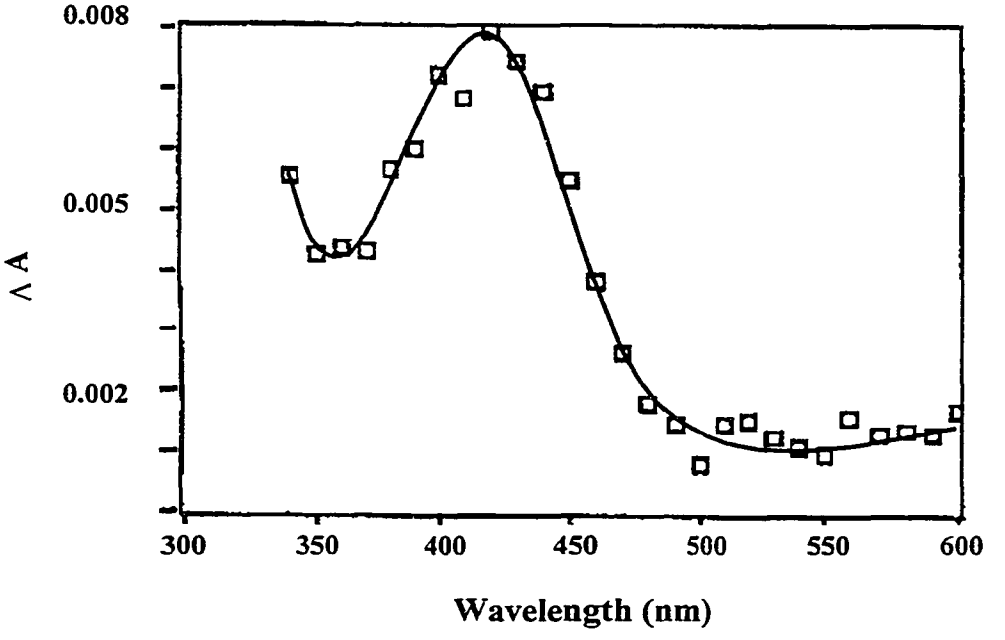

Fig. 2.16 Transient absorption spectra observed for **125** by LFP (under O_2) in 1:1 H_2O-CH_3CN.

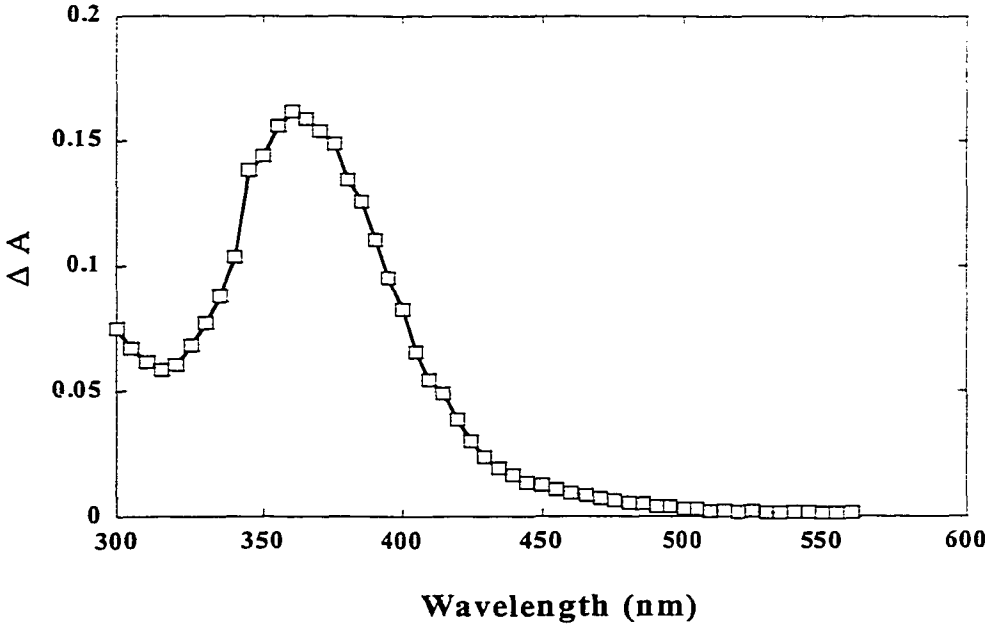

Fig. 2.17 Transient absorption spectrum observed for **116** by LFP in 1:1 H_2O-CH_3CN (under O_2).

2.5.2 *p*-Substituted Benzhydrols

LFP of *p*-hydroxybenzhydrol (**116**) gave one strong absorption band at 360 nm with no observable decay within ms range in 1:1 H_2O-CH_3CN, under either N_2 or O_2 (Fig. 2.17). The signal was also observed in 5% H_2O-CH_3CN but not in neat acetonitrile. The yield of the transient (as measured by ΔA) increased with the increase in the water content, to a maximum at 75% H_2O-CH_3CN (Fig. 2.18).

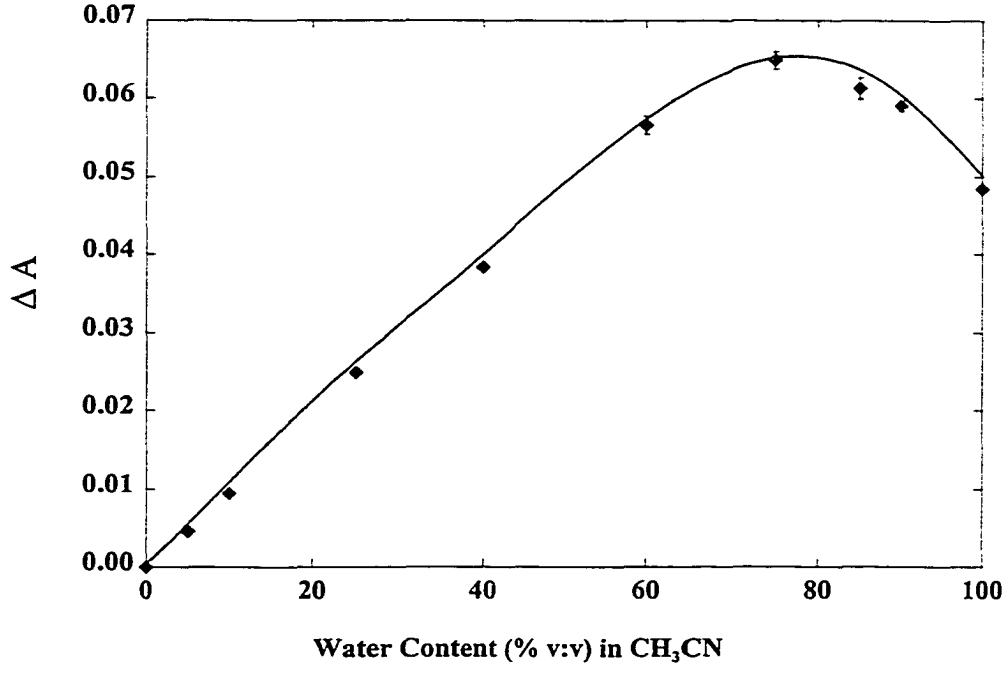

Fig. 2.18 Relative yield of transient obtained from **116** as a function of water content in CH_3CN (under O_2).

The transient from **116** was quenchable by ethanolamine. A fit to $k_{obs} = k_{H2O}[H_2O] + k_{amine}[NH_2CH_2CH_2OH]$ gave $k_{amine} = 3.1 \times 10^2\ M^{-1}s^{-1}$ and $k_{H2O}[H_2O] \approx 0\ s^{-1}$ for **116** (Fig. 2.14b).

The transient absorption spectrum observed for the *p*-methoxy analog **127** had a weak band at 455 nm with small shoulders at 340 and 360 nm. Monitored at 455 nm, the

decay consisted of two components, one with ~ 45 ns lifetime and another with a ~1 μs lifetime. The lifetime of the longer-lived species decreased significantly with increasing water content (Table 2.5). In 0.5 M NaOH, essentially no signal was observable in 400-500 nm region. These facts imply that the transient has cationic character. According to McClleland et al.,[47,66] (*p*-methoxyphenyl)phenyl methyl cation (**138**) has λ_{max} = 455 nm in CH_3CN (diarylmethyl chloride as precursor), which is also accompanied by the (*p*-methoxyphenyl)phenylmethyl radical at 340 nm. The cation has a lifetime of 0.5 μs in 2:1 H_2O-CH_3CN. The long-lived species generated from **127** has absorption characteristics and lifetime that matches those of the (*p*-methoxyphenyl)phenyl cation (**138**). Although the transient generated from **116** has similar absorption characteristics as cation **138** does, it is too long lived to be cation **140**. It seems reasonable that the transient is that of *p*-QM (**134**). Similarly, the transients observed for **117** and **118** (Section 2.4.2), which were quenchable by water and have even longer lifetimes than *p*-QM **134**, are also *p*-QMs (**141** and **142**, respectively).

Table 2.5 Effect of Water Content on the Lifetimes Observed for the Transient Generated from **127**

H_2O-CH_3CN	Lifetime τ[a]	
	(short-lived conponent, ns)	(long-lived conponent, ns)
1:4	22	2634
1:1	48	1090
4:1	28	545

[a] Monitored at 445 nm and fitted to the sum of two single exponential decays.

Filar[119] has successfully generated a series of *p*-QMs **143a-g**, by oxidizing the corresponding phenols (in isooctane and methanol). The absorption maxima of these *p*-

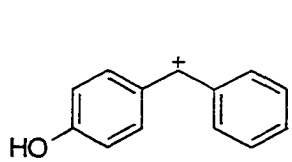

140

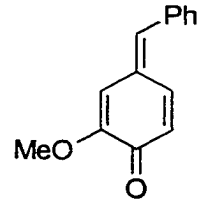

141

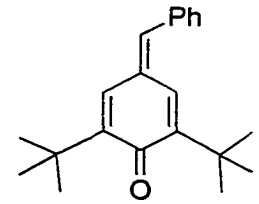

142

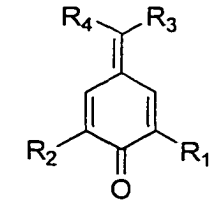

143

QMs are between 280-340 nm (Table 2.6). It is interesting to note that the methyl group on the benzylic carbon introduces at least 20 nm red-shift in λ_{max} without a significant change in their reactivity. A 50 nm shift is observed when a vinyl group is placed at the benzylic carbon (**143c**), presumably due to the added conjugation between the *p*-QM and the vinyl substituent. Following the same trend, a phenyl substitution on the benzylic carbon should lead to a substantial (≈ 100 nm) red shift. Indeed, the transients observed for *p*-hydroxybenzhydrols (**134**, **141** and **142**) have absorption maxima falling within this expected range. In addition, despite the difference in solvent, the lifetimes observed for **143** are in qualitative agreement with **134**, **141** and **142**.

Table 2.6 UV-Vis Absorption Data and Rate Constants for Decay of *p*-QMs[a]

	R_1	R_2	R_3	R_4	λ_{max} (Isooctane)	Log ε	λ_{max} (MeOH)	k (s^{-1})[b]
143a	CH_3	CH_3	H	H	283	4.46	ca. 290	$4.0e^{-2}$
143b	CH_3	CH_3	H	CH_3	297	4.40	ca. 312	$3.1e^{-2}$
143c	CH_3	CH_3	H	CH_2=CH	329	4.62	338	
143d	*t*-Bu	CH_3	H	H	285	4.35	290	$3.8e^{-3}$
143e	*t*-Bu	*t*-Bu	H	H	285	4.45	289	$9.4e^{-5}$
143f	*t*-Bu	*t*-Bu	H	CH_3	299	4.42	303	$5.5e^{-5}$
143g	*t*-Bu	*t*-Bu	CH_3	CH_3	314	4.40	322	$2.5e^{-5}$

[a] From Filar, reference 119. Generated from the correspond phenols via oxidative methods.

[b] First order rate constant for decay in MeOH.

2.5.3 Triphenyl alcohol 119

LFP of triphenyl alcohol **119** produced a strongly absorbing transient in either neat acetonitrile or in 1:1 H_2O-CH_3CN (Fig. 2.19), with no observable decay within 2 ms. The transient spectrum observed for **119** is almost identical to those obtained from **112** and **121**, indicating that a similar transient was being generated by all of these compounds and the additional phenyl substitution on benzylic carbon had little effect on absorption characteristics.

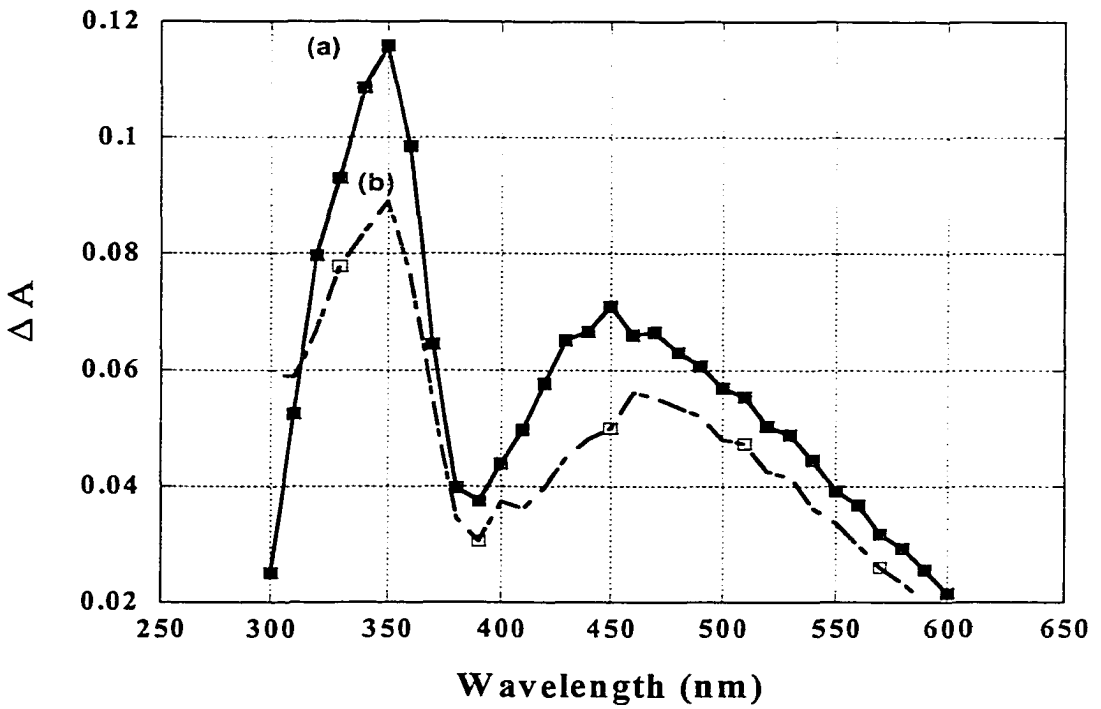

Fig. 2.19 The transient absorption spectra of **119** by LFP under O_2 in (a) pH 7 and (b) pH12 in 1:1 H_2O-CH_3CN.

The relative quantum yield for the formation of transient from **119** was monitored at 360 nm (Fig. 2.20) as a function of water content (in CH_3CN) and showed an increase with water content. The transient generated from triphenyl alcohol **119** is also sensitive towards

ethanolamine. McClelland et al.[66] have reported that the (*p*-methoxyphenyl)diphenylmethyl cation **144** has a lifetime of 0.71 ms in 2:1 H_2O-CH_3CN, which is much shorter than the transient observed from **119**. Using the same rationale as for the benzhydrols above, the transient observed for **119** is most likely *o*-QM **145**. Moreover, it is known that **119** and **146** show thermochromism[148] and photochromism in solution (Eq. 2.12).[128a,b] Hamai and Kokubun[128a] have assigned *o*-QMs **145** and **147** to the transients generated on photolysis of **121** and **149**, respectively, in either acetonitrile, benzene or *n*-hexane with very long lifetimes. The reported spectrum is essentially identical to that observed for the transient from **119**, i.e., bands at 340 and 440 nm.

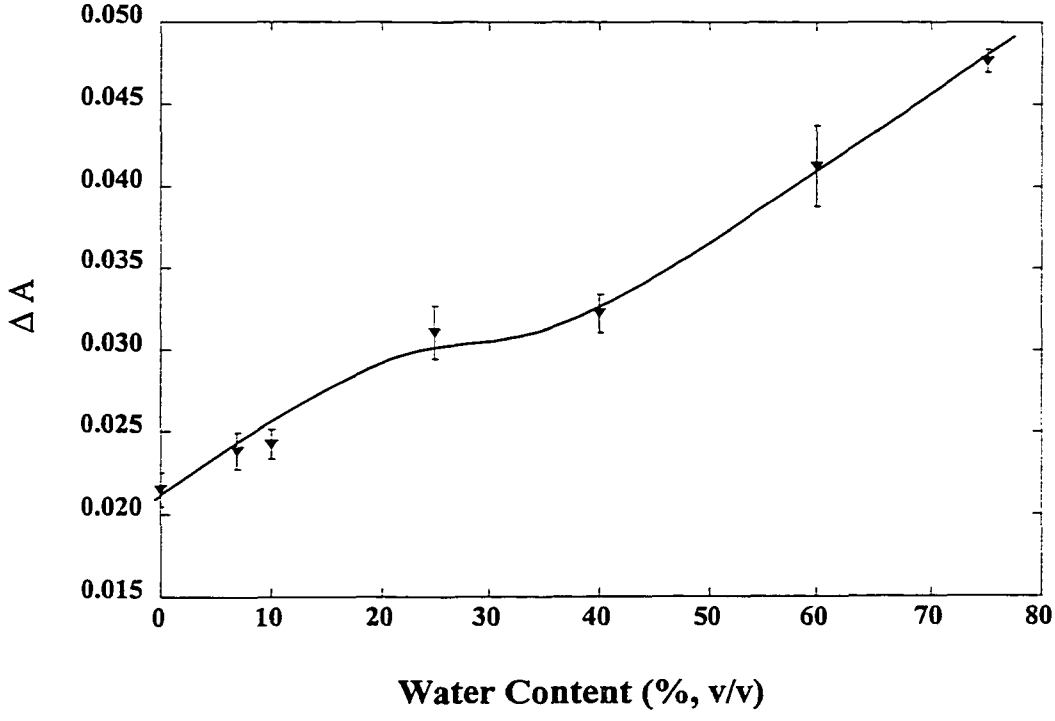

Fig. 2.20 Effect of water content (in CH_3CN) on relative quantum yield for the formation of the transient from **119**.

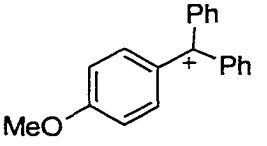

144

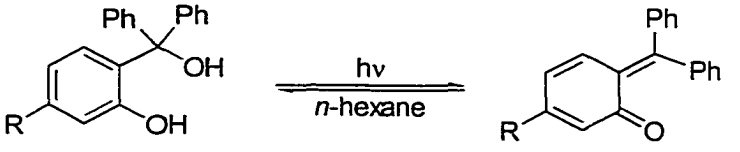

(2.12)

119 R = H
146 R = OMe

145 R = H
147 R = OMe

2.5.4 Parent Alcohols

LFP of **48** gave relatively weak signals in the 300-500 nm region (Fig. 2.21) compared to those observed for benzhydrols **112** and **116**. Similar but weaker spectra were also observed from *p*-hydroxybenzyl alcohols **111** and **128**, while **129** was able to afford absorption bands at 290 nm and 365 nm in aqueous solution. The decay trace of the corresponding transient from all these alcohols contained two first order components, a short-lived species with μs lifetime, which is sensitive to O_2 but unaffected by H_2O, and a long-lived species with $\tau > 2$ ms.

The transient spectrum of **48** is composed of a finely structured short-lived species (transient A) and a broad absorption underneath in the same region (transient B) (Fig. 2.21). Both are observed immediately after the laser pulse. Transient A decayed within ca. 50 μs (accelerated by O_2) and transient B did not decay within 2 ms. Transient A was generated with lower intensity in the presence of oxygen but was not affected by the addition of ethanolamine as nucleophile. In the presence of the O_2, the overall appearance

of the spectrum had less contribution of transient A, i.e., more B, which could also be shortened by the addition of ethanolamine (Fig. 2.22).

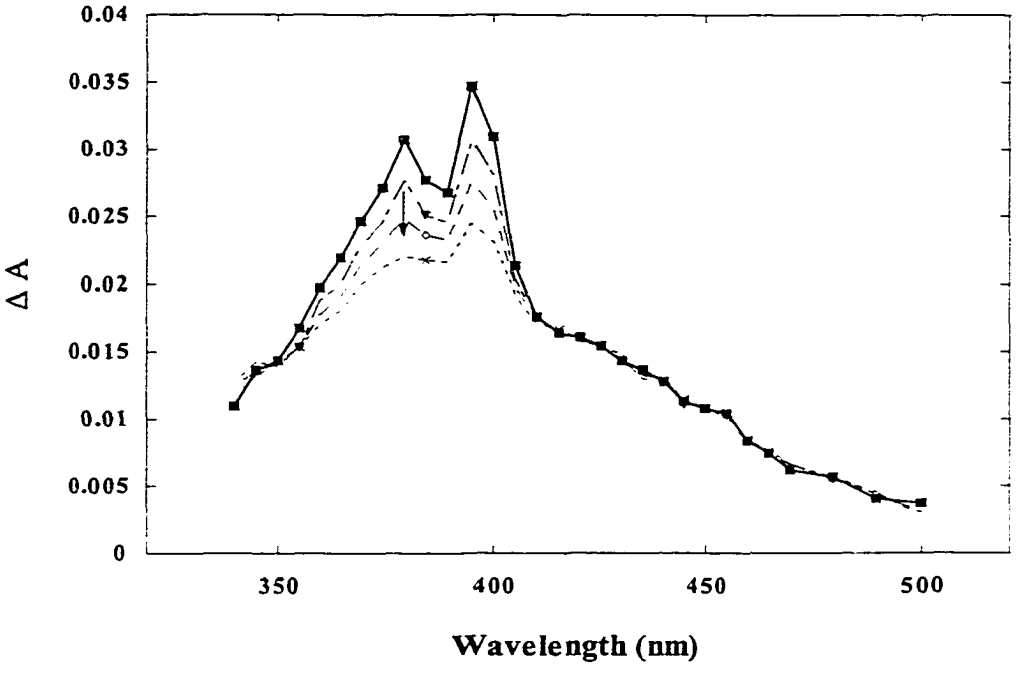

Fig. 2.21 Transient spectrum observed on LFP of **48** in neat H_2O (under O_2). Traces taken at 1.7, 6.0, 13 and 27 μs (Top to bottom) after laser pulse.

The relative yield of transient B to transient A was roughly calculated by using the formula $\Delta A_B/(\Delta A_{total}-\Delta A_B)$, where ΔA_{total} is the sum of the absorption of transient A and B and ΔA_B is the maximum absorption of the residue in the decay trace (in the absence of ethanolamine). This ratio was ca 0.60 in 100% CH_3CN, decreased to 0.48 in 10% H_2O-CH_3CN, followed by a continuous increase to 0.75 in 100% H_2O. The strongest residue signal (ΔA_B) from **48** was generated in 100% H_2O solution (Table 2.7). By increasing the basicity of aqueous solution, sharp peaks at 380 and 395 nm further diminished and left a broad band centered ca. 390 nm ($\tau \approx 0.15$ ms at pH 11) (Fig. 2.23a).

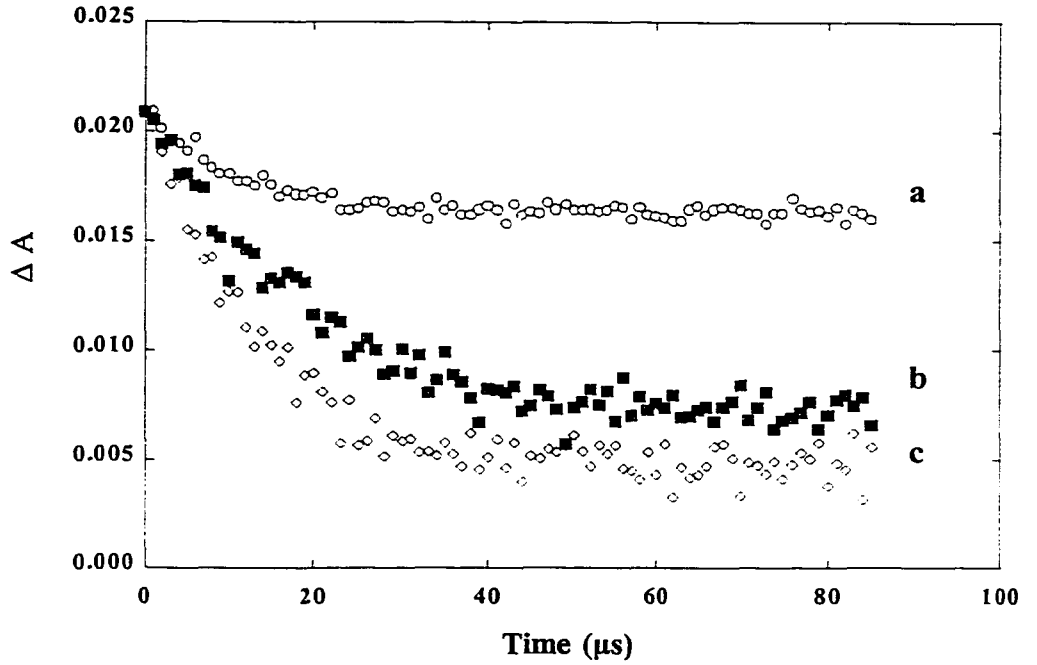

Fig. 2.22 Decay traces of the transient observed for **48** under O_2 in neat water upon addition of ethanolamine. a) 0 M; b) 0.0378M; c) 0.0757M.

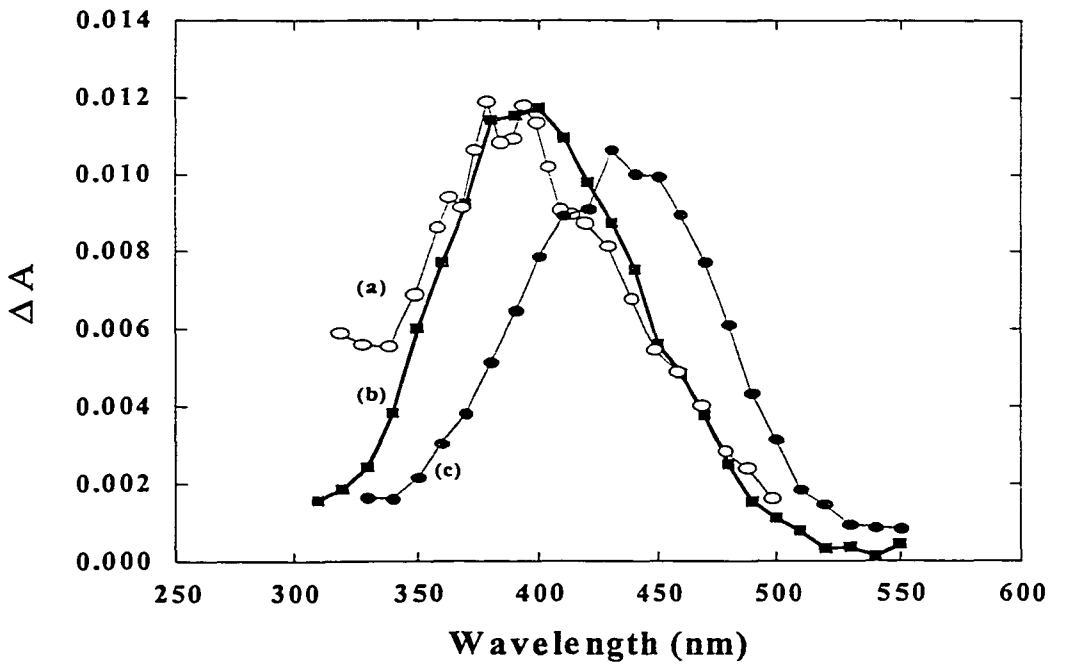

Fig. 2.23 Transient absorption spectrum of **48** (trace a), **113** (trace b) and **148** (trace c) in 100% H_2O under O_2.

Table 2.7 Effect of Water Content (in CH_3CN) on the Yield of The Long-lived Species Observed for **48**.

	100% CH_3CN	10 % H_2O-CH_3CN	50 % H_2O-CH_3CN	H_2O
ΔA_{380} ($\times 10^{-3}$)[a]	3.0	5.4	9.1	16
ΔA_{395} ($\times 10^{-3}$)[b]	1.6	5.7	9.9	18

[a] Monitored at 380 nm.
[b] Monitored at 395 nm.

LFP of **113** and **148**, which are known to photochemically give *o*-QMs **79a** and **149**,[127] respectively (Eq. 2.13), gave transients ($\tau > 2$ ms) at λ_{max} = 390 nm and 430 nm (Fig. 2.20b,c), respectively. Except for a slight difference in fine structure, the transient observed for **113** matches that observed for **48**. The presence of an electron-donating substituent in the hydroxy group of **149** is consistent with a 40-nm red shift observed for this *o*-QM.

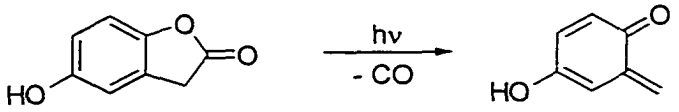

148 **149** **(2.13)**

The question arises as to the nature of the "fine structure" observed for **48** (Figs. 2.21 and 2.23). LFP studies of phenols in water have been extensively carried out (Table 2.8).[149] The transients generated are the corresponding phenoxyl radicals, which have finely structured absorption spectra and are quenchable by oxygen. Therefore, transient A observed from **48** is assignable to the corresponding phenoxyl radical **150**. Transient B, then is assigned to the parent *o*-QM **79a**. As discussed above, the red shift observed for **149** is probably the result of the additional electron-donating hydroxy group on the

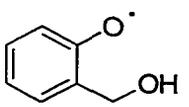

150

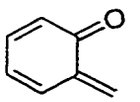

79a

phenyl ring. Creed[130a] reported the observation of a long-lived *o*-QM **152** (λ_{max} = 445 nm; τ = 12 s in ethanol) from photolysis of lactone **151**, which is even more red-shifted. In this case, there are three additional methyl groups on the ring.

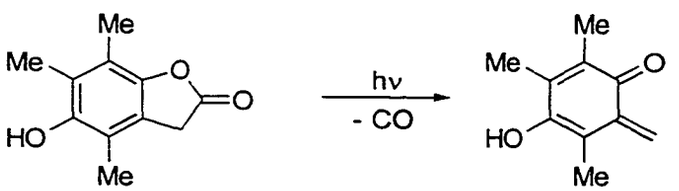

151 **152** **(2.14)**

Table 2.8 Transient Absorptions Observed from Benzyl Alcohols **48**, **111** and Related phenols

Compound (1:9 H_2O-CH_3CN)	λ_{max} (nm)	Compound (H_2O)	λ_{max}[149] (nm) (phenoxyl radical)
48	395	*o*-Cresol	395
	385		380
	365		363
	290		
111	410	*p*-Cresol	405
	390		385
			368
	300		
		Phenol	400
			382

As discussed above, McClelland et al.[66] have shown that diphenylmethyl cations **137** and **138** have lifetimes of ≈ 1 ns and 0.5 μs, respectively, in 2:1 H_2O-CH_3CN. One

would expect then that the phenylmethyl cation **153** would have a ps lifetime and that the lifetime of the *o*-hydroxyphenylmethyl cation **154** would be less than 10 ns, both of which would be too short to be observable in the LFP system employed. As a consequence, *o*-QM **79a** is the only reasonable candidate for transient B assignment.

LFP of **111** and **128** gave weaker signals than observed for **48** but with similar

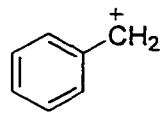

153

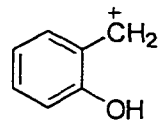

154

spectral features. The fine-structured component could be assigned to the corresponding phenoxyl radical. A second component of the transient has a maximum at ca. 290 nm, tailing to 400 nm, which could be quenched by ethanolamine. However, this component is dominated by the phenoxyl radical absorption. For compound **129**, the long-lived component has a weak broad band at 365 nm along with a stronger absorption at 290 nm. This is in agreement with Filar's[119] report for *p*-QM **143e** in methanol ($\lambda_{max} \approx 289$ nm; Table 2.6), although the weak 365 nm band was not mentioned, presumably because of its weak extinction coefficient. It is suggested that the long-lived components of these transient absorptions observed for *p*-hydroxybenzyl alcohols **111, 128** and **129** belong to

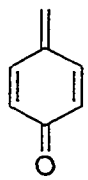

80a

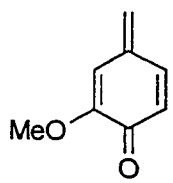

155

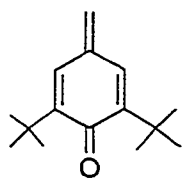

143e

p-QMs **80a**, **155** and **143e**, respectively.

2.5.5 The Quantum Yields of Photogenerated QMs

The quantum yields of QM could be estimated from the yield of photomethanolysis results (Table 2.1) using Eq. 2.3. According to Yang's results,[146] the nucleophilicity of H_2O was found to be about 0.08 times that of MeOH in 1:1 H_2O-MeOH. Then, $\alpha \approx 0.8$ can be deduced in such solution. Thus, the quantum yields Φ_{QM} for the formation of some QMs in the above solvent system was proportional to the corresponding quantum yield of photomethanolysis (Table 2.9).

Table 2.9 Quantum Yield (Φ_{QM}) of QMs from Photolysis of Benzyl Alcohols

Compound	Φ_{QM}	Compound	Φ_{QM}
112	0.58	**116**	0.24
121	0.10		
119	0.95		

2.6 Steady State Fluorescence Measurements

2.6.1 Water and pH Effects

o-hydroxybenzyl alcohols **48**, **112** and **119** gave similar intense emissions centered at ~ 300 nm in neat CH_3CN (Fig. 2.24, top trace). The fluorescence quantum yields (Φ_f), measured using anisole (Φ_f = 0.29 in cyclohexane) as secondary standard,[150] were drastically reduced by H_2O addition, accompanied with the red-shifted of emission maxima (Table 2.10). Among these three alcohols, the fluorescence intensity of **112** was affected the most where only a weak emission band was observed beside a clearly visible Raman band in 100% H_2O (Fig. 2.24). The fluorescence lifetimes (τ) of all these compounds were

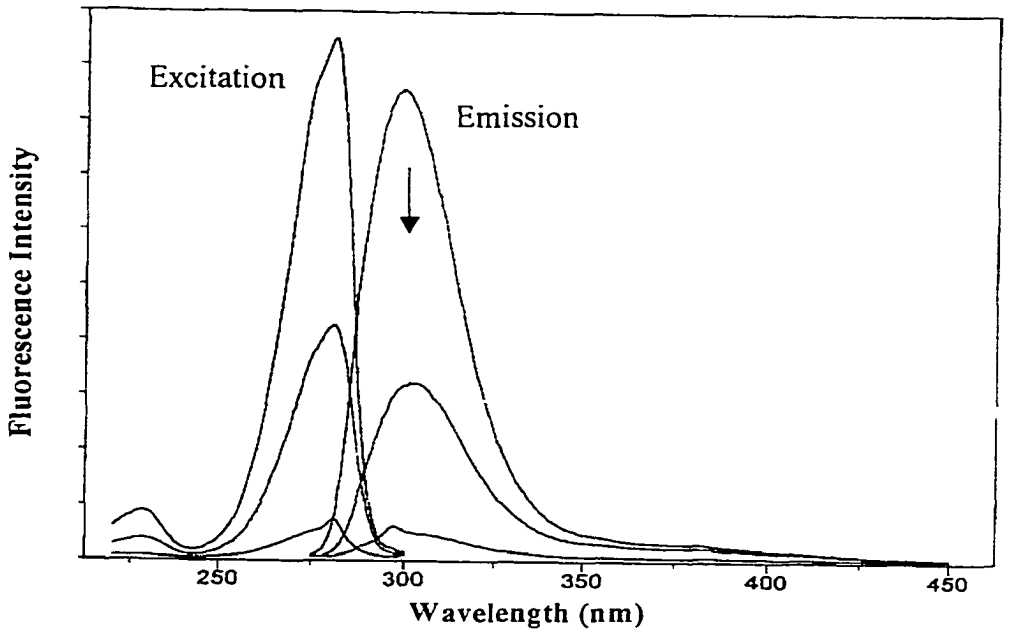

Fig. 2.24 The fluorescence emissions of **112** in 100 % CH_3CN (top), 1:1 CH_3CN-H_2O and 100% H_2O (bottom).

essentially the same in 100% CH_3CN but were drastically decreased with increased water concentration. The results of absorption maximum and lifetime for parent alcohol **48** are consistent with those reported by Yang.[146] However, more efficient quenching was observed for **112** and **119** since their lifetimes were about 3 times shorter with only 50% H_2O than that in 100% CH_3CN, compared to that of **48**.

Similar fluorescence emissions were obtained for two related derivatives (**125**, **126**) of **112** in the above mentioned solvent systems (Table 2.10). Measurement of Φ_f (Table 2.10) revealed that the fluorescence of **126** was quenched by 90% in 100% H_2O, while the fluorescence of **125** was much less sensitive to the presence of water than that of **112** and **126**. In addition, the emission of **125** did not red shift as all the other alcohols. The fluorescence lifetimes (τ) of **126** has an initial decrease to 3 ns in 1:1 H_2O-CH_3CN and then to < 2 ns in 100% H_2O, while the τ of **125** was almost unchanged by 50% water addition

and then dropped to 1.9 ns in 100% H_2O. Thus, the overall magnitude of water effect on these three compounds followed the order **112** > **126** > **125**. The lack of a fluorescence quenching effect for **125** can be attributed to its lack of a phenol moiety.

Table 2.10 Effect of H_2O Content in CH_3CN on Emission Maximum (λ_{max}), Fluorescence Quantum Yields[a] (Φ_f) and Lifetimes[b] (τ) of *ortho* Compounds

	Solvent	**48**	**112**	**119**	**125**	**126**
λ_{max}	100 % CH_3CN	299	298	299	299	297
	1:1 CH_3CN-H_2O	--	302	304	--	299
	100 % H_2O	300	--	--	300	--
Φ_f[c]	100 % CH_3CN	1 (0.19)[146]	1 (0.13)	1 (0.092)	1 (0.28)	1 (0.25)
	1:1 CH_3CN-H_2O	0.66	0.21	0.48	--	0.47
	100 % H_2O	0.37	0.04	0.12	0.62	0.10
τ[d] (ns)	100 % CH_3CN	4.7	4.5	4.6	5.3	5.1
	1:1 CH_3CN-H_2O	2.9	1.3	<2	4.6	3.0
	100 % H_2O	1.7	--	--	1.9	<1

[a] Excited at 270 nm.
[b] Excited at 275 nm.
[c] Measured using anisole (Φ_f = 0.29 in cyclohexane) as secondary standard. Absolute quantum yield quoted in brackets. All other numbers are relative yields.
[d] Measured using PTI LS-1 Time-Correlated Single Photon Counting system (> 2 ns) or picosecond laser flash photolysis system (< 2 ns).

Fluorescence emissions of **48**, **112** and **119** were also observed in aqueous solutions of different pH values (Table 2.11). However, their fluorescence emissions were in general so weak that it was not feasible to accurately measure the fluorescence quantum yield. Therefore, relative fluorescence intensity measurements (Φ_f°/Φ_f; Φ_f° = fluorescence quantum yield at pH 7) at ~ 290 nm were employed (λ_{ex} = 270 nm). No emission was observed in basic solution (0.1 N NaOH) for either ortho compound. Since their UV-Vis spectra showed growth of the absorption of the corresponding phenolate ion (~ 290 nm) in basic media (Fig. 2.8 for **112**), excitation at 290 nm gave weak emissions at ~ 350 nm,

which presumably are the fluorescence emissions of the corresponding phenolate. The parent alcohol **48** gave the strongest band amongst the three (Fig. 2.25a). Similar experiment with phenol gave weak emission at 335 nm (Fig. 2.25b), while *o*-cresol emit at 346 nm (Fig. 2.25c). The weak signals indicate that excited phenols are photochemically reactive, i.e. they decay through other routes competitive with fluorescence emission.

Table 2.11 pH Effect on Relative Fluorescence QuantumYields (Φ_f^o/Φ_f)[a] of ortho Alcohols and Related Compounds

Solvent	**48**	**112**	**119**	**125**	**126**
0.1 N H_2SO_4	0.30	1.07	1.30	0.97[b]	1
H_2O (pH 7)	1	1	1	1	1
0.1 N NaOH	~ 0	~ 0	~ 0	1.30[c]	~ 0

[a] OD_{270} is between 0.07 to 0.11, λ_{ex} = 270 nm, λ_{em} from 275 nm to 400 nm.
[b] pH 3 solution. [c] pH 11 solution.

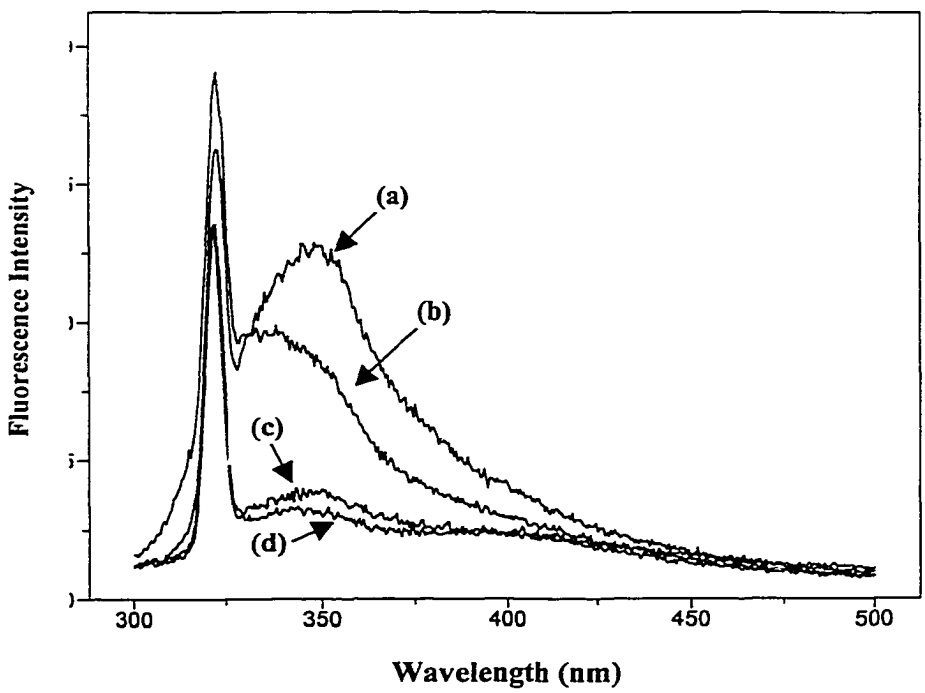

Fig. 2.25 Fluorescence emission in basic solution (0.1 N NaOH) (λ_{ex} = 270 nm). (a) **48**; (b) phenol; (c) *o*-cresol; (d) solvent blank.

o-Benzylphenol (**126**) gave strong emissions at ~ 290 nm (excited at 270 nm) in low pH solution and a weak emission band at ca. 350 nm at high pH. Excitation of **126** at 290 nm in different pH solutions gave the strongest phenolate emission in acidic solution and the weakest in basic media (Fig. 2.26). However, the emission of **125** increased with the increase of the pH of the solutions. Therefore, benzyl alcohols behave similarly as phenol **126**, indicating that phenol moieties in these compounds play an important role in the fluorescence quenching and transient formation mechanism.

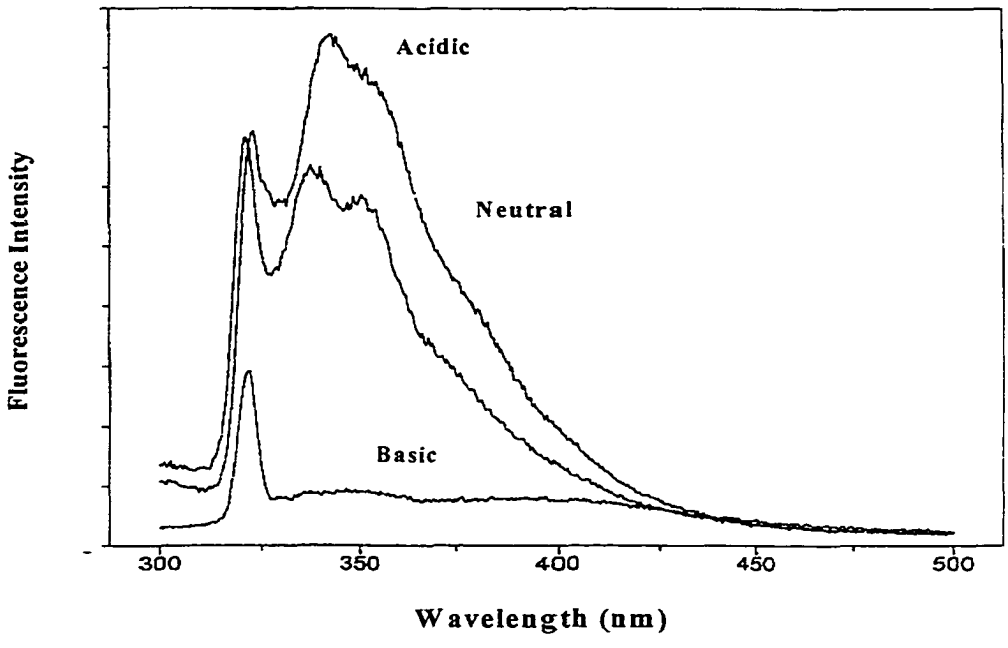

Fig. 2.26 pH dependence of the fluorescence emission of **126** in aqueous solution (λ_{ex} = 290 nm).

2.6.2 Stern-Volmer Plots

Relative fluorescence quantum yields (Φ_f^0/Φ_f; Φ_f^0 = fluorescence quantum yield in neat CH_3CN) of **48**, **112** and **119** (λ_{ex} = 270 nm) were measured in a series of H_2O-CH_3CN ($[H_2O] < 2$ **M**) solutions (Table 2.12). Unlike the bulk water effect reported earlier, Φ_f

increased with the increase of water concentration in all three cases. A similar effect on Φ_f for **116** was observed at these water concentrations (Table 2.12). These results prevent a Stern-Volmer analysis for fluorescence quenching using steady state data. However, fluorescence lifetimes (τ) of **112** decreased as expected with the addition of water (Fig. 2.27). A plot of τ_0/τ (τ_0 = lifetime in neat CH_3CN) vs. $[H_2O]$ give a linear plot with a quenching rate constant, $k_q = 2.0 \times 10^7\ M^{-1}\ s^{-1}$.

Table 2.12 Effect of Water Content in CH_3CN on Φ_f°/Φ_f[a] and λ_{max} of Benzyl Alcohols

$[H_2O]$ (M)		0	0.21	0.43	0.86	1.07	1.28	1.50	1.92
Φ_f°/Φ_f	**48**	1	--	0.97	1.01	--	1.07	--	1.04
	112	1	--	0.98	0.87	--	0.87	--	0.93
	119	1	--	0.97	0.96	--	0.94	--	0.96
	116	1	0.92	--	--	0.89	--	0.97	--
λ_{max} (nm)	**48**	297.2		297.8	298.0	--	298.6	--	298.3
	112	298.3	--	299.4	300.2	--	300.2	--	300.5
	119	297.5	--	298.3	298.3	--	299.1	--	299.1
	116	301.5	301.5	--	--	302.4	--	302.9	--

[a] Relative fluorescence quantum yuild where Φ_f° is the yield in neat CH_3CN.

The fluorescence of **112** reached maximum at around 2 **M** $[H_2O]$ followed by a consistent decrease to 100% H_2O (Fig. 2.28a). Similar trends were observed with **112** in D_2O-CH_3CN (Fig. 2.28b) and H_2O-THF (Table 2.13). Interestingly, there was basically no observable solvent isotope effect for **112** under 2 **M** $[H_2O]$. However, D_2O had less quenching efficiency at $[H_2O/\ D_2O] > 2$ **M**.

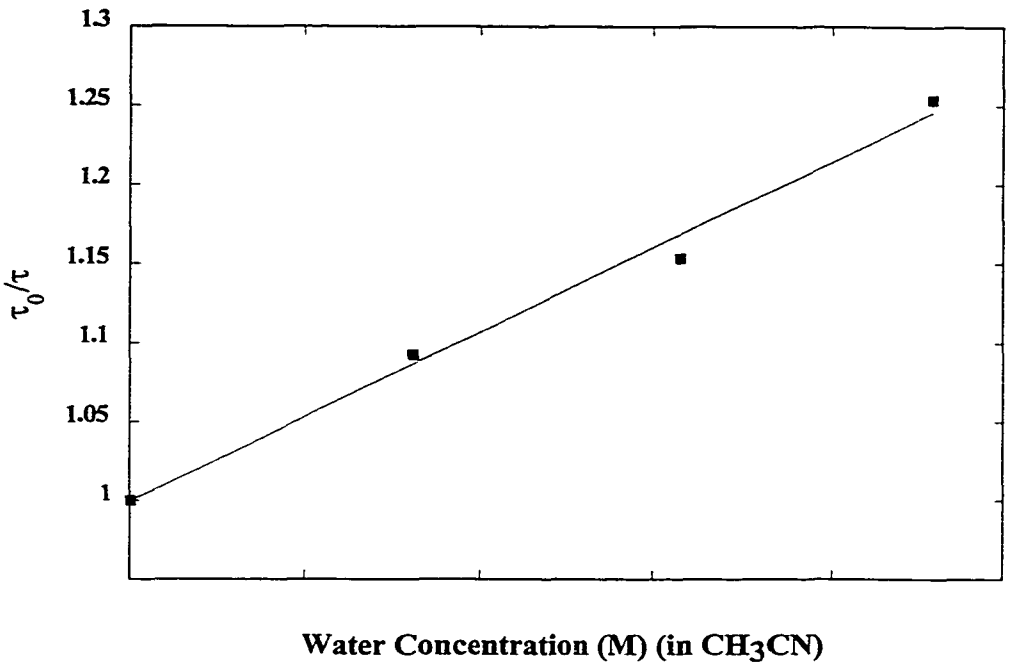

Fig. 2.27 A plot of τ_0/τ vs. water concentration (in CH_3CN) for **112**.

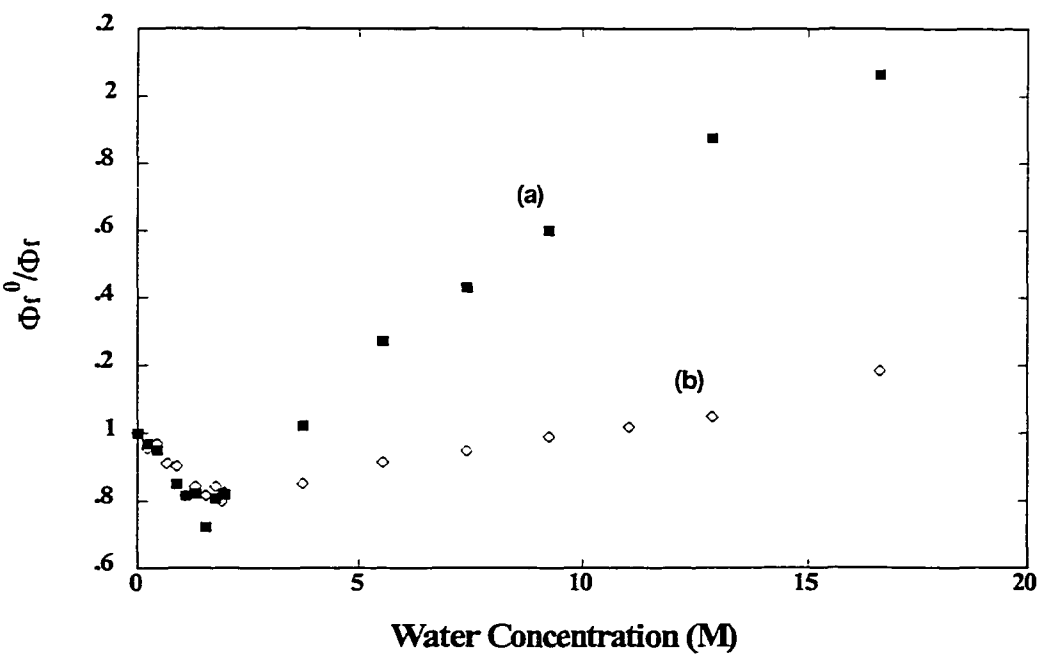

Fig. 2.28 Isotope effect on Φ_f°/Φ_f for **112**. (a) CH_3CN-H_2O; (b) CH_3CN-D_2O.

The Φ_f of compound **126** in H_2O-CH_3CN mixtures increased to the same extent at 1.84 M [H_2O] as **112**, but decreased to a less extent than that of **112** at higher H_2O content (Table 2.13). One result which is worth mentioning is that the λ_{max} of the emission bands of **112** and **126** red-shift gradually with increasing H_2O content (Table 2.14).

Table 2.13 Effect of Water Content (> 2M) on Φ_f^0/Φ_f[a] for **112** and **126**

[H_2O] **M**	**112** (H_2O-CH_3CN)	**112** (D_2O-CH_3CN)	**112** (H_2O-THF)	**126** (H_2O-CH_3CN)
0	1	1	1	1
1.84	0.93	0.80	0.92	0.93
3.69	1.02	0.85	0.96	0.96
5.54	1.27	0.92	1.02	1.02
7.38	1.43	0.95	1.08	1.03
9.22	1.60	0.99	1.15	1.05
12.9	1.88	1.05	1.23	1.14
16.6	2.06	1.18	1.32	1.16

[a] Φ_f^0 is the fluorescence quench yield in neat CH_3CN and THF, excited at 270 nm.

Table 2.14 Effect of Water Content (> 2 **M**) on λ_{max}[a] of the Fluorescence Emissions of **112** and **126**

[H_2O] M	**112** (H_2O-CH_3CN)	**112** (D_2O-CH_3CN)	**112** (H_2O-THF)	**126** (H_2O-CH_3CN)
0	298.4	298.6	299.3	296.4
1.84	300.9	300.3	301.0	298.3
3.69	300.9	301.1	301.5	298.8
5.54	301.7	301.1	301.5	299.1
7.38	301.7	301.4	301.5	299.1
9.22	302.0	301.1	301.5	299.1
12.9	302.5	301.7	302.1	299.6
16.6	302.5	301.7	302.4	299.4

[a] Excited at 270 nm.

The Φ_f of **112** was quenched by more than 50% with < 0.05 **M** [$NH_2CH_2CH_2OH$] in CH_3CN (Fig. 2.29), with no shift of the emission maximum. From the slope of a plot Φ_f^o/Φ_f vs. [$NH_2CH_2CH_2OH$], a quenching rate constant of $k_q = 3.8 \times 10^9$ M^{-1} s^{-1} was obtained (Fig. 2.29, inset). This value is more than two orders of magnitude higher than that observed using water as quencher (Fig. 2.27).

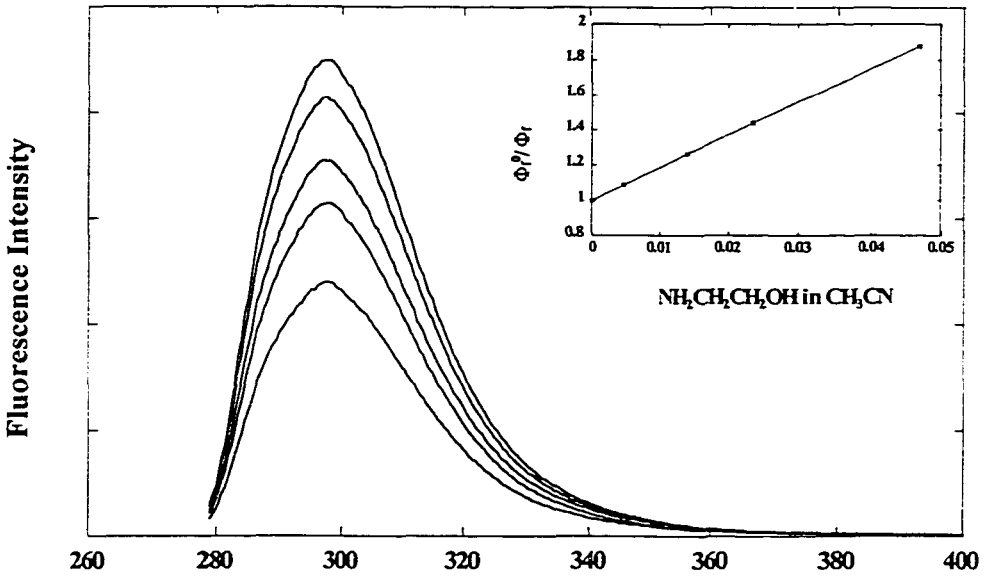

Fig. 2.29 Ethanolamine quenching of the fluorescence of **112**. Inset: a plot of Φ_f^o/Φ_f vs. [$NH_2CH_2CH_2OH$] (in CH_3CN).

2.7 Mechanism of Quinone Methide Photogeneration

2.7.1 Mechanism of Quinone Methide Photogeneration in Aqueous Solution

The conclusion was drawn in Section 2.4 that photolysis of *o*- and *p*-hydroxybenzyl alcohols in aqueous solution results in the formation of the corresponding QMs. Initial results showed, that while the quantum yields of QMs increased, the fluorescence intensity of the substrate decreased with the increasing water content (> 2 **M**), indicating that water is required for QM formation. Compared to **112**, model compounds **125** does not have a

phenol moiety and **126** lacks a hydroxy group on the benzyl carbon. Although fluorescence quantum yields (Φ_f) and lifetimes (τ) of both decreased with the addition of water, the decreases were notably less than observed for **112**.

As discussed previously, **125** can generate cation **137** in aqueous solution upon photolysis, presumably through dehydroxylation from S_1 (Scheme 2.2). As a result of this

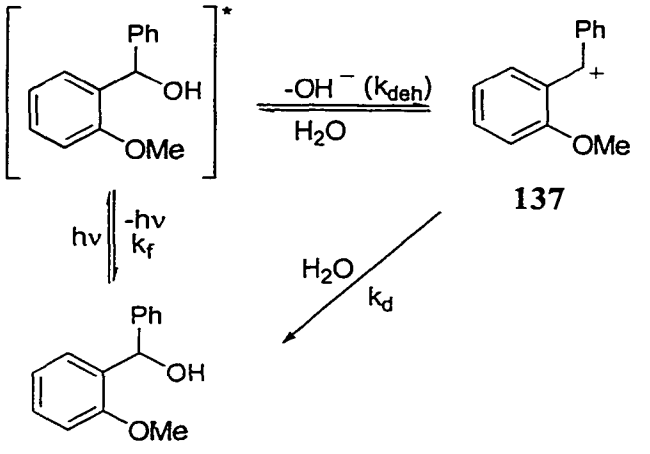

Scheme 2.2

decay pathway (k_{deh}, dehydroxylation rate constant), a decrease in Φ_f and τ was observed on the addition of water. Water quenching of phenol **126** could be attributed to proton transfer from singlet phenol to water (Scheme 2.3).[11] This deprotonation decay pathway (k_{dep}) accounts for the decrease of Φ_f and τ. Obviously, both hydroxy groups of **112** are required for QM formation in neutral solution. However, the relatively low fluorescence quenching efficiency by water observed for **125** is not comparable with that observed for **112**. On the contrary, water quenching of fluorescence observed for **126** is almost as efficient as that observed for **112**. Phenolate ion fluorescence emission was observed in basic solution for both **126** and **112**, but not for **125**. Moreover, the corresponding increase of the transient

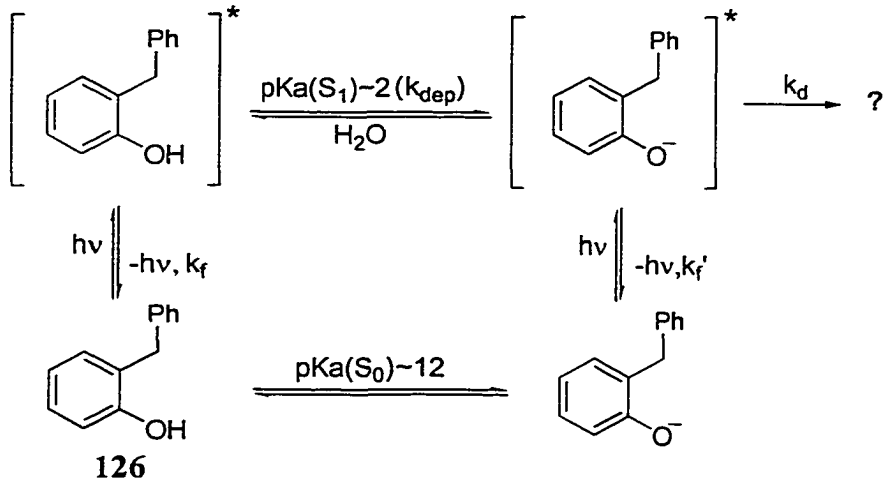

126

Scheme 2.3

yield in low pH region and the huge jump at high pH of both the methanolysis product quantum yield (Φ_p) and laser transient for **112** strongly suggest that the singlet phenolate ion is the crucial intermediate for QM formation. Thus, it is reasonable to propose that the adiabatic deprotonation of singlet phenol to establish equilibrium with singlet phenolate ion is the first step for the formation of *o*-QM **124** in neutral and acidic solution, as originally proposed by Yang[146] (Scheme 2.1). This proposal is also supported by the solvent isotope effect observed for **112**, where D_2O introduced less efficient quenching, and solvent polarity effect, in which a polar solvent resulted in more efficient quenching. A general mechanism is therefore proposed in which solvent water plays a crucial role (Scheme 2.4). Presumably, this mechanism is also suitable for *o*-QM **145** generation from alcohol **119** in high water content solution (> 2 **M**).

Following the same analogy, it is reasonable to believe that this is the general mechanism for the photogeneration of all *o*- and *p*-QMs discussed in this chapter (as shown in Scheme 2.5 for **116**).

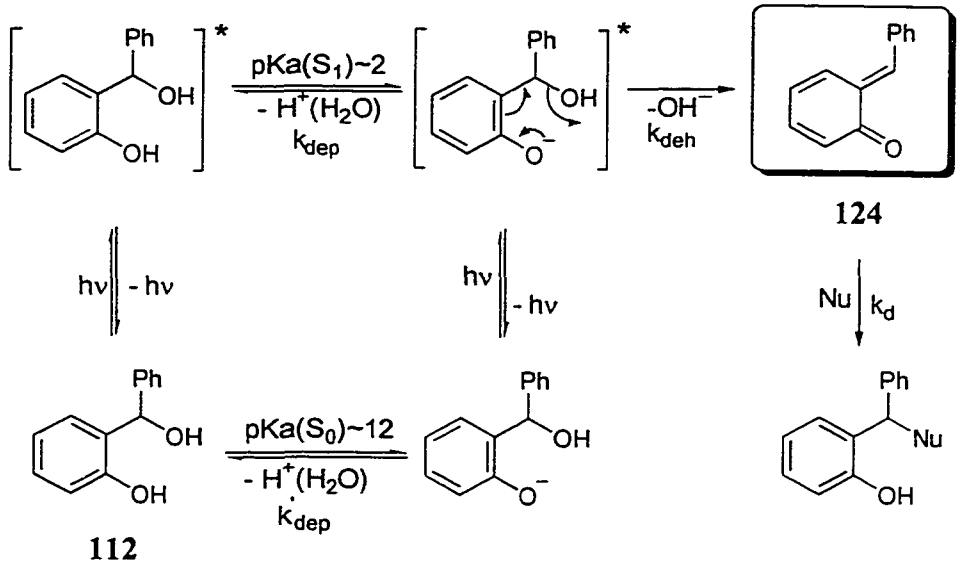

Scheme 2.4

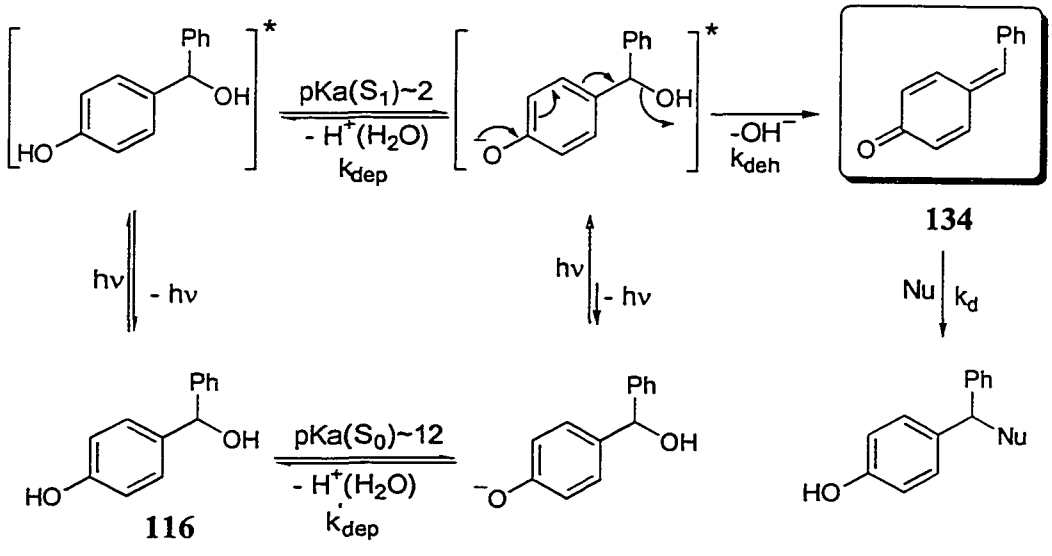

Scheme 2.5

However, this "water-assisted" mechanism can not explain the formation of *o*-QMs in neat CH_3CN as well as the decreasing *o*-QM yield at low water content. Alternative mechanisms need to be considered.

2.7.2 Mechanism of *o*-QMs Photogeneration in Neat CH_3CN and THF

As discussed in previous sections, *o*-QM **124** was generated from *o*-hydroxybenzhydrol (**112**) in neat CH_3CN or THF, and even in a non-polar solvent such as cyclohexane. LFP studies also showed that the yield of **124** decreased upon addition of small amounts of water to neat acetonitrile (Fig. 2.11). In parallel, the Φ_f of **112** showed an increase at these same water concentrations. In addition, a deuterium solvent effect on fluorescence intensity was not observable at these water concentrations (Fig. 2.28). Similar effects were observed when THF was used as the organic solvent (Table 2.13). *o*-QM **145** was also observed from LFP of compound **119** in neat CH_3CN (Fig. 2.20). However, no decrease in yield was observed upon addition of small amount of water. It is also interesting to note that none of the meta or para alcohols showed similar behaviors as **112**. Apparently, a new mechanism related to the unique structures is required to explain the reactivity of *o*-hydroxybenzyl alcohols in neat organic solvents. This is attempted in the section to follow.

2.7.2.1 *o*-Hydroxybenzyl Alcohols

o-Hydroxybenzhydrol (**112**) has unique ^1H NMR spectra, in which one or two broad bands represent phenol and benzylic hydroxyl protons (Fig. 2.1b). α-Phenyl-*o*-hydroxybenzhydrol (**119**) has two broad or sharp peaks, 1:1 in ratio depending on the concentration (Fig. 2.3). The broadening is attributed to hydrogen bonding in neat organic solvent or the water-substrate interaction in aqueous solution (Section 2.4.4). Indeed, the crystal structure of **112** shows that it is intermolecular hydrogen-bonded through the phenoxyl proton and the benzylic oxygen (Fig. 2.2). The bulkier **119** exists as a dimer in the solid state through intermolecular hydrogen bonding between benzylic hydroxyl proton and

phenol oxygen, while at the same time, the proton of the phenol is intramolecularly hydrogen-bonded to the benzylic oxygen (Fig. 2.4). Calculations using the Alchemy III program show that **112** has a smaller torsion angle between phenol proton and the benzylic oxygen (30°) than that of **119** (40°). The broadening of the hydroxyl proton signals observed for the parent alcohol **48** is similar to that of **112**. Therefore, it is reasonable to assume that **48** is also significantly hydrogen-bonded in the solid state.

2.7.2.2 Proposed Mechanism for 112

UV-Vis studies (both conventional and LFP) showed the formation of *o*-QM **124** from **112** in neat organic solvents. The yield of **124** was found to decrease with the addition of small amounts of water (Fig. 2.11), while Φ_f of **112** increased (Fig. 2.28). However, the fluorescence lifetime (τ) shortened with increasing water content (Fig. 2.27). Moreover, no solvent deuterium isotope effect for fluorescence quenching was observed at these water contents (Fig. 2.28). A simple and obvious explanation for this is that the protons of **112** are not readily exchangeable with solvent H_2O/D_2O at these concentrations and hence, no isotope effect would be observed. That is, **112** remains extensively intermolecular hydrogen-bonded in the neat organic solvents. Hydrogen bonding would weaken the strength of the phenol O-H bond and facilitate deprotonation on excitation. The resulting excited phenolate ion also has the benzylic oxygen hydrogen-bonded to a phenol proton which further facilitates it to react via the loss of water to form *o*-QM **124** (Scheme 2.6). An alternative is that the deprotonation and dehydration occurs simultaneously, i.e., a concerted pathway leading to the formation of *o*-QM **124**. We term this the "intermolecular proton transfer" mechanism.

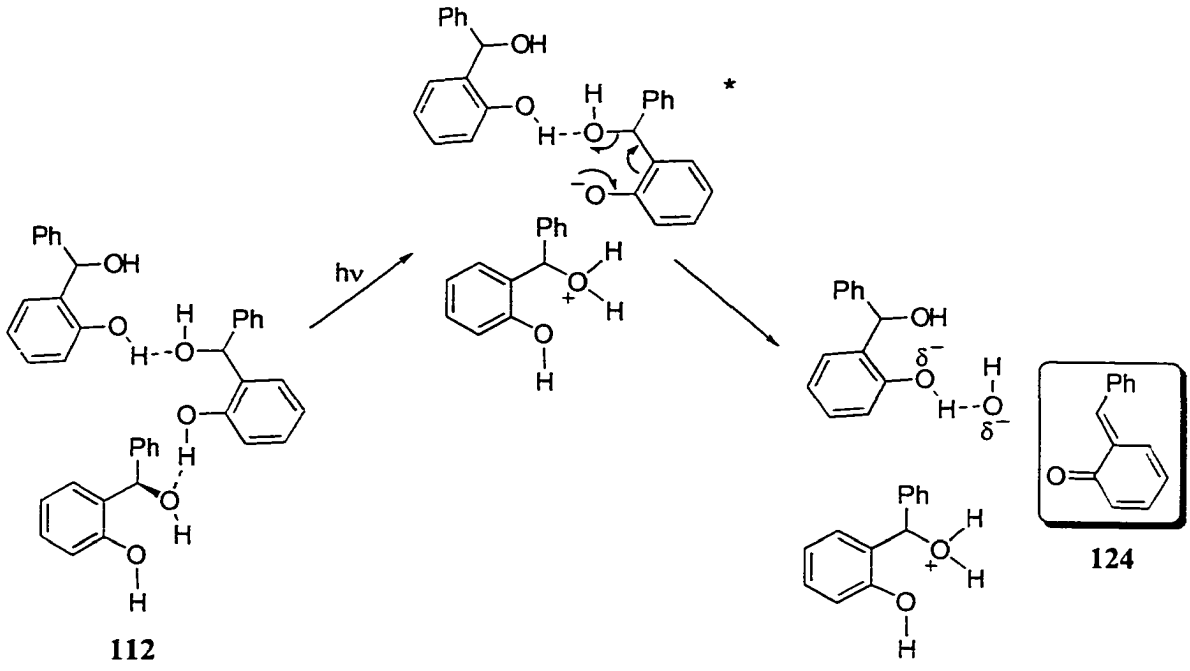

Scheme 2.6

The "water assisted" mechanism (Scheme 2.4) starts to operate when there is sufficient water in the system. The observed behavior in fluorescence intensity of **112** and **126** at low water concentration is indicative that water associates with substrate. The entire hydrogen bonded network of **112** is not disrupted until after the water content higher than 2 **M**, as evidenced by ^{1}H NMR and fluorescence data. At these water concentrations, both the "intermolecular proton transfer" and the "water-assisted" mechanism can in principle operate. However, the concentration of water is sufficiently low as to make the contribution from the "water-assisted" mechanism marginally important. The increase in fluorescence intensity and the diminished quantum yield of *o*-QM **124** in this region is consistent with this. The water molecule is a much better leaving group in the "intermolecular proton transfer" mechanism than hydroxide ion in the "water

assisted" mechanism, which accounts for these observations.

This mechanism is also consistent with the observation that monomeric **112** is formed on photolysis. That is, hydration of *o*-QM **124** in Scheme 2.6 by residual water in the system gives rise to solvated **112** by CH_3CN, which is no longer intermolecular hydrogen bonded.

2.7.2.3 Proposed Mechanism for 119

Photolysis of triphenyl alcohol **119** also generates *o*-QM **145** in neat organic solvents. The X-ray structure (Fig. 2.4) shows that it is intramolecularly hydrogen-bonded, phenolic proton with the benzylic oxygen, and intermolecular hydrogen bond, phenol oxygen with the proton of the benzylic oxygen. Upon photolysis, adiabatic deprotonation of singlet **119** generates an excited state phenolate ion, which then loses water to form *o*-QM **145** and **119** hydrogen-bonded to a water molecule. We term this as the "intramolecular proton transfer" mechanism (Scheme 2.7).

Interestingly, the quantum yield for the formation of **145** increased upon the addition of small amounts of water, unlike that observed for **112** (Fig. 2.20). However, the fluorescence quantum yield of **119** also increased slightly at low water content (Table 2.12). Therefore, addition of water appears to introduce the "water-assisted" mechanism for the generation of **145**, which competes effectively with the "intramolecular proton transfer" mechanism. It is not clear at this time why the fluorescence emission is enhanced in this region of water concentration. Obviously, another effect of water on the overall photophysics is occurring which is not easily visualized at this time.

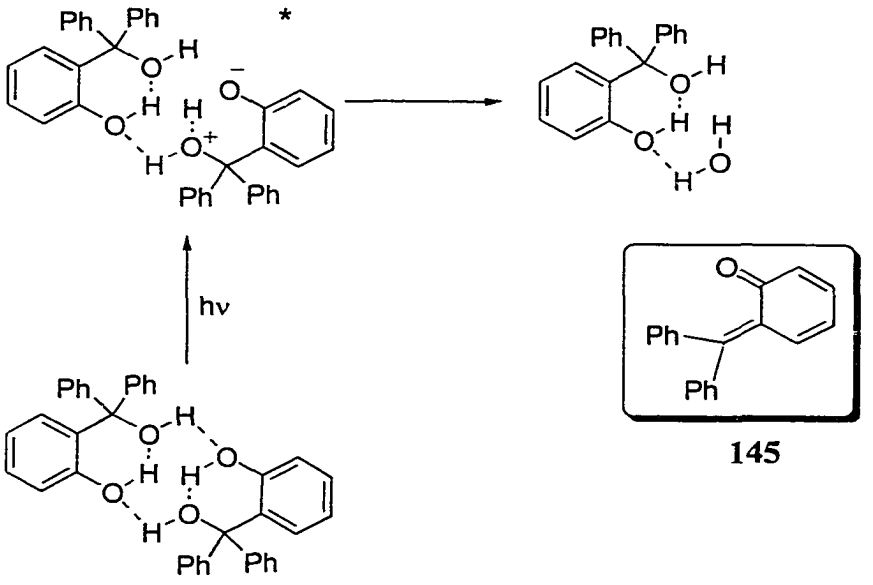

Scheme 2.7

2.7.3 Mechanism of Transients Generation from Parent Alcohols

The LFP of **48** gave *o*-QM **79a** and the phenoxyl radical **150** in 100% CH_3CN (Fig. 2.21). A higher *o*-QM: radical ratio was observed in neat CH_3CN than in 10% H_2O-CH_3CN, which increased with the further addition of water, indicating the *o*-QM formation is more efficient than that of the radical in neat organic solvent. Due to the fact that **48** has similar NMR behavior as **112**, it is reasonable to suggest that **48** is also intermolecularly hydrogen-bonded in the solid state and in neat organic solution. Consequently, it is possible that *o*-QM is generated via the "intermolecular proton transfer" mechanism (Scheme 2.6) in neat organic solvent. Nevertheless, the yield of **79a** increased upon the further addition of water (> 10 %) (Table 2.7). Conceivably, the "water assisted" mechanism (Scheme 2.4) is operating in such aqueous solution.

Land et al.[151] proposed that phenoxyl radicals are the primary intermediates in the photolysis of both phenol and phenolate ion, via hydrogen atom ejection (Scheme 2.8)

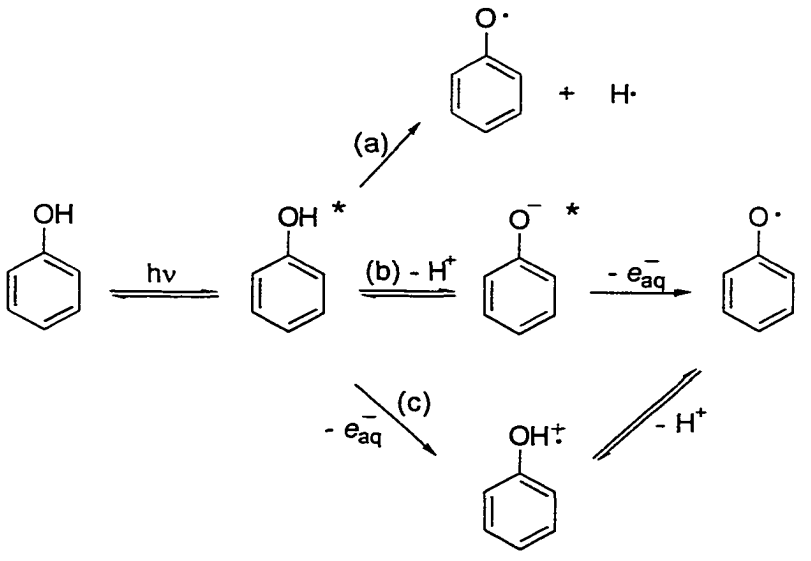

Scheme 2.8

and electron ejection (Scheme 2.8), respectively. It is easy to envision that the excited phenolate ion is responsible for the formation of phenoxyl radical by releasing electron to the solvent, i.e. hydrated electron as an initial product. In neutral solution, the possibility of electron ejection from phenol to give the phenoxyl radical cation followed by its equilibration with the neutral phenoxyl radical in protonic solvents was excluded (Scheme 2.8), although the authors observed the radical cation in solution at low acidity. On the other hand, fast equilibrium between singlet phenol and singlet phenolate ($pK_a(S_1)$ ~ 2-4) provide a feasible pathway for the radical generation. Our results showed that a broad band at 720 nm is observed in neutral solution under N_2, which disappeared with O_2 purging. Compared to the spectrum observed by Dobson et al.,[152] this band is assigned to e_{aq}^-. Yet, the lifetime of this species (0.3 μs) is much shorter than that reported by Dobson (ca. 20 μs), which might be caused by the higher substrate concentration employed in our LFP studies or insufficient removal of O_2. Although the formation of

phenoxyl radical **150** is competitive in neutral solution, its yield is much lower than that of **79a** in basic solution (pH > 10). Since these transients solely came from the excited phenolate ions in the latter, the appearance of phenoxyl radical implied that the path (b) (Scheme 2.8) was responsible for its formation and k_e (electron ejecting rate constant from singlet phenolate) is lower than k_{deh} (dehydroxylation rate constant) but competitive. The overall mechanism for photolysis of **48** is illustrated in Scheme 2.9. This mechanism equally applies to the other parent alcohols **49**, **111**, **128** and **129**.

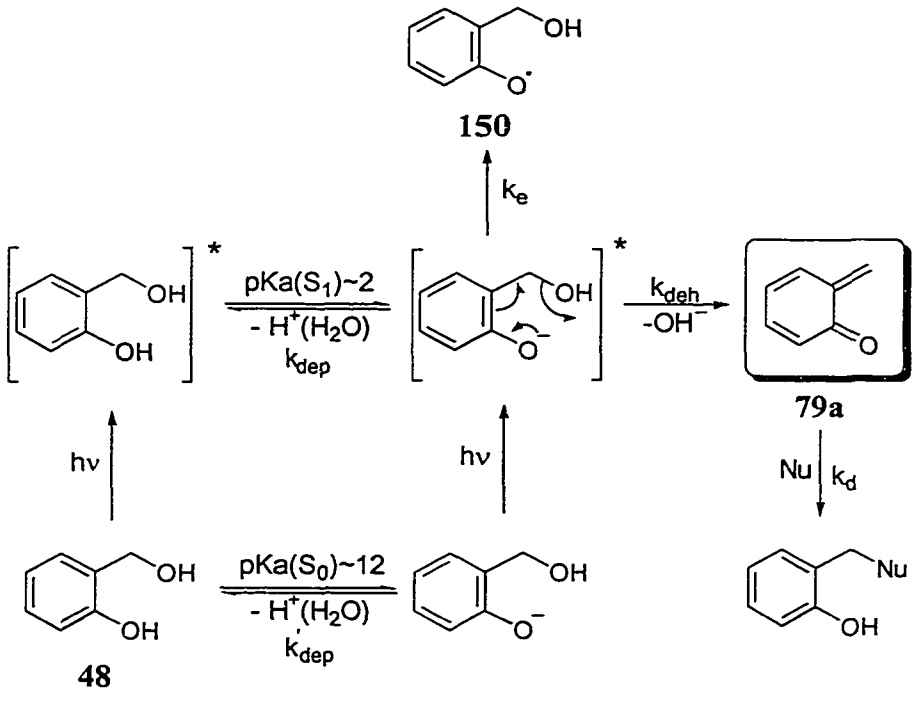

Scheme 2.9

2.8 Summary

Ortho and para-hydroxybenzyl alcohols are reactive upon photolysis in aqueous solution, to efficiently generate *o*- and *p*-QMs. Product studies gave the corresponding methyl ethers with high quantum yields in aqueous methanol, indicating the generation of

cationic species as intermediates. However, similar photolysis of the corresponding methoxy analogues gave much less or no methyl ether products. LFP studies in aqueous acetonitrile showed that strong and long-lived species were formed, which were inconsistent with the short-lived cationic species observed by McClelland et al.[47,66] for related diarylmethyl cations. LFP studies also showed that the quantum yield of transient increased with the addition of water (in acetonitrile), corresponding to a decrease of the fluorescence quantum yield. These transients can be quenched by both nucleophiles and electrophiles (H^+), consistent with their QM assignment. The proposed mechanism in aqueous solution is water assisted deprotonation of the singlet excited phenol at pH < $pK_a(S_0)$, to give the singlet excited phenolate ion as the key intermediate, which subsequently dehydroxlates. The competing formation of radicals probably involve electron ejection from the corresponding singlet excited phenolate ion.

Photolysis of *o*-hydroxybenzhydrols in neat organic solvents also gave observable QMs although in much lower yield compared to that observed in aqueous solution. For compound **112**, the mechanism probably involves formation of the key intermediate (singlet excited phenolate ion) with the aid of intermolecular hydrogen bonding with the benzyl hydroxy group from an adjacent molecule. While for **119**, the adiabatic deprotonation is facilitated by both inter and intramolecular hydrogen bonding within a dimer structure.

Chapter 3

Photogeneration of *m*-Quinone Methides From *m*-Hydroxybenzyl Alcohols

3.1 Introduction

Previous literature studies of *m*-QMs have shown that the generation of these non-Kekulé molecules is a difficult task (Section 1.4.2). Theoretical calculations have predicted[123] that *m*-QMs have triplet ground states and singlet excited states, both of which are intrinsically short-lived. Berson et al.[126,140,142] have provided evidence for the formation of *m*-QM **81** and *m*-NQM **101**, by pyrolysis and photolysis of enones **84** and **100**, respectively, in the presence of nucleophiles. Further studies[143-145] of compound **100** using LFP showed that **101** has a triplet ground state and a zwitterionic singlet state.

A preliminary study by Wan and Chak[29] showed that *m*-hydroxybenzyl alcohol **49** had a product quantum yield of photomethanolysis twice that of its methoxy analog **39**. It was proposed that carbocations **103** and **156** were the key intermediates. However, since OH and OMe have similar electron donating abilities, the relative yields of cations **103** and **156** should not differ much. In fact, they demonstrated that mono-substituted methoxybenzyl alcohols (**38**, **39** and **41**) follow the order $o > m >> p$ in relative reactivity. A similar trend was observed between ortho and meta hydroxybenzyl alcohols **48** and **49**. Yang[147] found that **49** was almost as reactive as **48** toward methanol as nucleophile and the

reactivities of three isomers (**48, 49** and **111**) followed the order *o* > *m* >> *p*. These facts reinforce the idea that the transient generated from **49** might not be the simple benzyl cation.

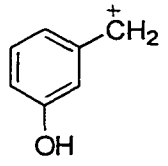

103

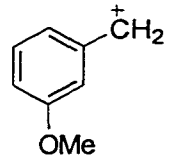

156

It has been shown in Chapter 2 that photolysis of ortho and para hydroxybenzyl alcohols efficiently generate the corresponding QMs through the excited phenolate ion. According to Zimmerman's *ortho-meta* activation theory (Section 1.2.2.1),[14,26] one would expect that the *meta*-substituted compounds (**49, 115** and **120**) could be promising precursors for the photogeneration of *m*-QMs. The results of this investigation will be discussed in the following sections.

3.2 Materials

m-Hydroxybenzhydrols **115** and **120** were made by the addition of a phenyl group to *m*-anisaldehyde and methyl *m*-hydroxybenzoate, respectively, using phenylmagnesium bromide. *m*-Methoxybenzhydrols **157** and **158** were prepared by either employing the same above methodology or by reducing the corresponding benzophenone with sodium borohydride. *m*-Hydroxybenzhydrol (**115**) was reduced (H_2/Pd) to afford *m*-benzylphenol (**159**), which was used as a control in mechanism studies.

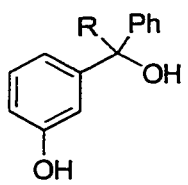

115 R = H
120 R = Ph

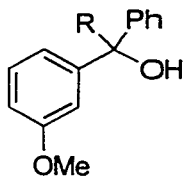

157 R = H
158 R = Ph

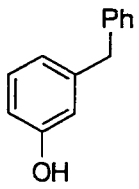

159

3.3 Product Studies

3.3.1 Photomethanolysis

Photolysis of *m*-hydroxybenzhydrol (**115**) in 1:1 H_2O-MeOH (10^{-3} M, 254 nm, 3 min) gave the corresponding methyl ether **160** as the only product at low conversion (~ 15%) (Eq. 3.1). The ^1H NMR showed the characteristic singlet at δ 3.3 (3H) and the

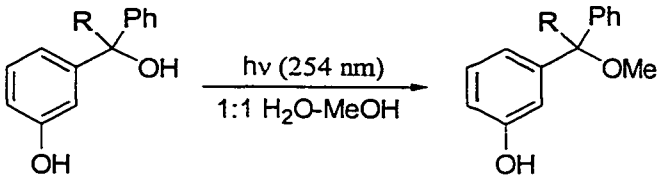

(3.1)

115 R = H
120 R = Ph

160 R = H
161 R = Ph

benzylic methine singlet at δ 5.2 (1H). Similar photomethanolysis of α-phenyl-*m*-hydroxybenzhydrol (**120**) afforded **161** (~ 10 % yield), as evident by the observation of the methoxy singlet at δ 3.2 (3H). Their methoxy analogues (**157, 158**) failed to produce observable products under the same conditions. Control experiments performed in the absence of light did not give any observable reaction.

Prolonged photolysis of **115** not only increased the yield of ether **160** (Table 3.1), which reached a maximum at 60%, but also gave a secondary photoproduct **159** (benzylic

methylene singlet at δ 3.9 (2H)) and trace amounts (< 2%) of products with higher molecular weights. Negative FAB spectra indicate that they are probably condensation products **162** and **163**. The yield of **159** increased with further photolysis (Table 3.1). Based on results observed for the *o*-hydroxybenzyl alcohols **48** and **112** (Section 2.3.1), it is reasonable to suggest that **159** is a secondary photoproduct of **160** (Eq. 3.2).

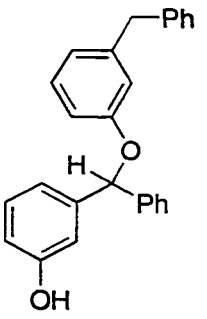

162

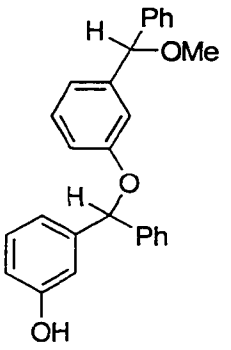

163

Table 3.1 Product Yields of Photomethanolysis of **115** As a Function of Photolysis Time[a]

Photolysis time (min.)	Yield (%)		
	115	**160**	**159**
0	100	0	0
5	80	20	0
5[b]	68	32	0
30	34	58	8
60	24	60	16

[a] In 1:1 H_2O-MeOH.
[b] 1 mL of 1N NaOH solution added.

Photomethanolysis of **115** carried out in basic 1:1 H_2O-MeOH gave a significantly higher yield of **160** than in neutral solution (Table 3.1). Photolysis of **120** yielded 41%, 59%

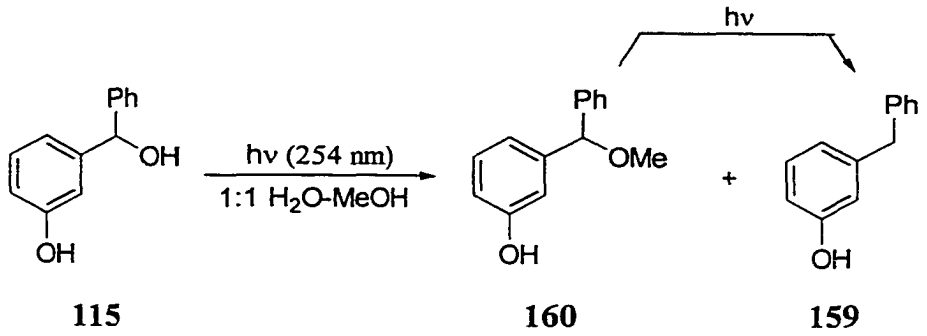

115 **160** **159** **(3.2)**

and 83% of methyl ether **161** in acidic (pH ~ 1), neutral and basic (pH ~ 13) 1:1 H_2O-MeOH, respectively. The resulting product solution of **120** in basic pH was observed to be a bit cloudy compared to similar runs under neutral and acidic conditions. The increase in yield for **160** and **161** with increasing pH correlates with the ground state pK_a (Fig. 3.1 for **115**) of the phenol moiety of **115** and **120**. The higher reactivity can be attributed to the more reactive excited phenolate ion.

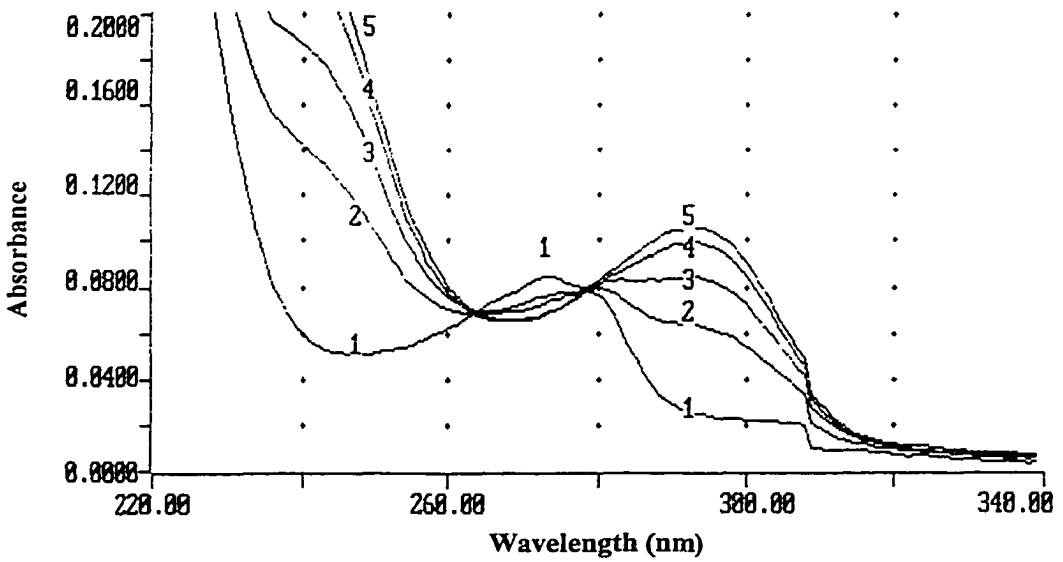

Fig. 3.1 Absorption spectra of **115** in aqueous solution at different pH. (Labels 1 to 5 are pHs 6, 10, 10.3, 10.7 and 11, respectively.)

Photolysis of **120** (10 min) in neat water at pH 12 resulted in a very cloudy solution, which was subsequently neutralized and extracted by CH_2Cl_2. The ^1H NMR of the product mixture showed a group of new peaks including two exchangeable protons (hydroxy singlets at δ 5.1 and δ 8.2) and a triplet near the aromatic region (δ 6.4), in addition to those expected for **120**. Prolonged irradiation (30 min) caused the formation of pale yellow flakes that precipitated out of solution and aggregated upon the addition of salt. This yellow substance gave a much cleaner ^1H NMR spectrum (Fig. 3.2) in which there are twice as many phenyl protons as hydroxyl protons than in the starting material, and a M^+-1 of 533 (negative FAB) indicative of a dimeric structure. In addition, only starting material **120** was obtained when this substance was stirred in acidic 1:1 H_2O-$(CH_3)_2CO$. The major component of this precipitate is assigned to the condensation product **164** (Scheme 3.1).

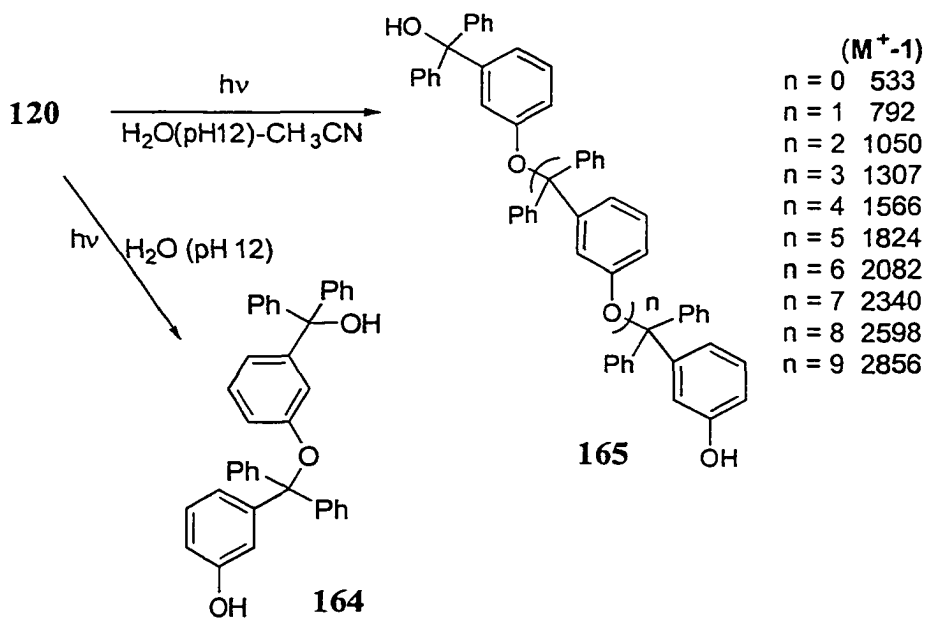

Scheme 3.1

Interestingly, similar photolysis of **120** in basic 1:1 H_2O-CH_3CN resulted in a yellow homogeneous solution after 30 min photolysis, which upon work-up was found to contain oligomers **165** of up to 10 units (Fig. 3.3, negative FAB).

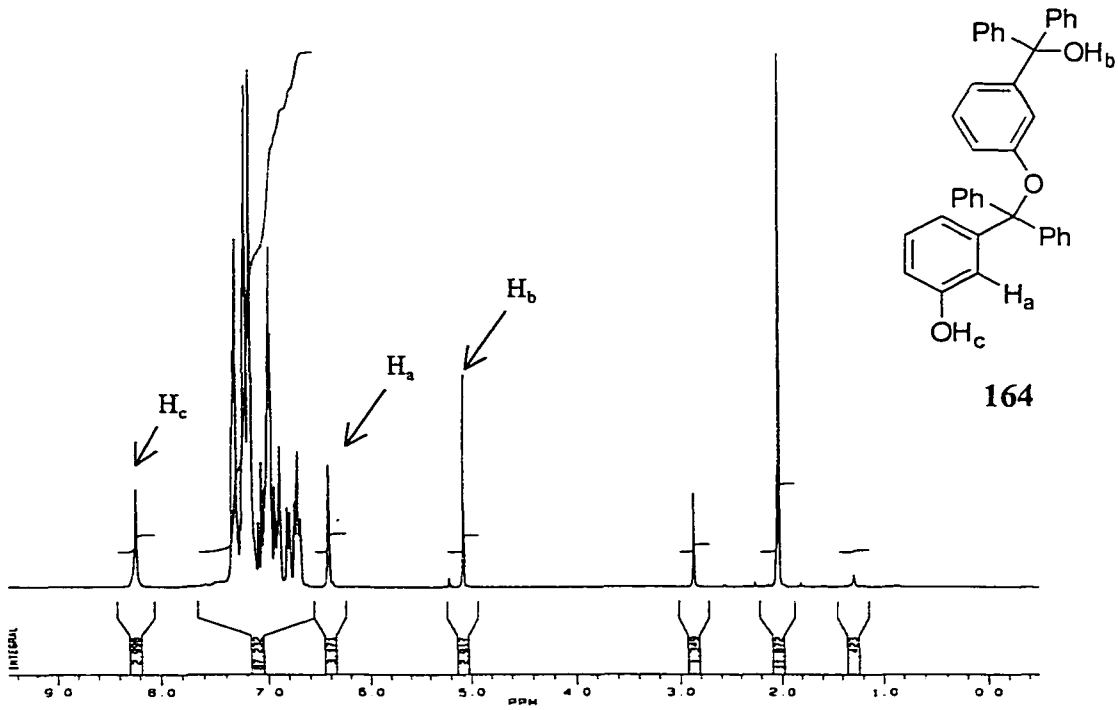

Fig. 3.2 ^{1}H NMR spectrum of the photoproduct **164** from **120** observed in basic neat water solution.

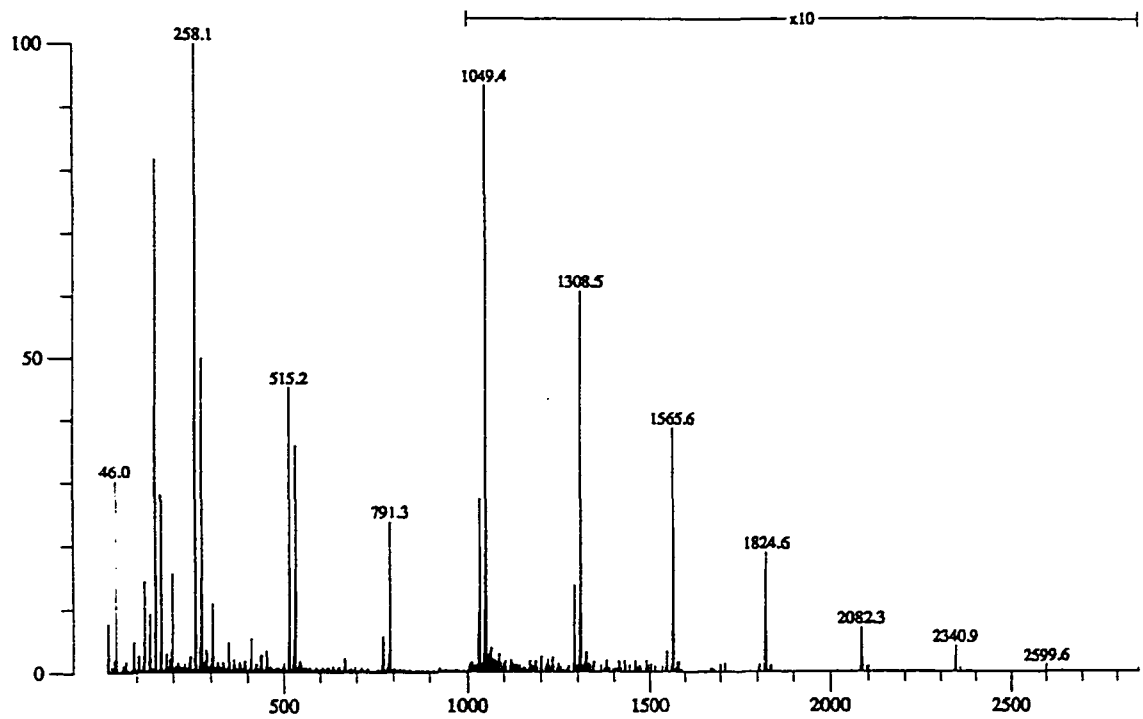

Fig. 3.3 Mass spectrum (Negative FAB) of photoproduct **165** from **120** in basic 1:1 H_2O-CH_3CN.

3.3.2 Photolysis of 115 with Ethyl Vinyl Ether

m-Hydroxybenzhydrol (**115**) was exhaustively photolyzed in the presence of ethyl vinyl ether (EVE), including variations in the excitation wavelength (254 nm and 300 nm), irradiation time, EVE concentration, as well as the H_2O-CH_3CN ratio. This was carried out to investigate the possibility that the intermediate photogenerated from **115** might react with EVE, which was the case observed for the ortho isomer (Scheme 2.1). Besides recovering some starting material and EVE polymer, two aldehydes **166** (a benzylic aldehyde singlet at δ 10.0; M^++1 of 123) and **167** (aldehyde triplet at δ 9.7; M^++1 = 227) were formed in low yields (< 5%) (Eq. 3.3). Formation of **167** is consistent with nucleophilic attack of the

benzyl cation from **115** by EVE followed by hydrolysis. However, **166** appears to be a photofragmentation product possibly arising via a photooxidation mechanism.

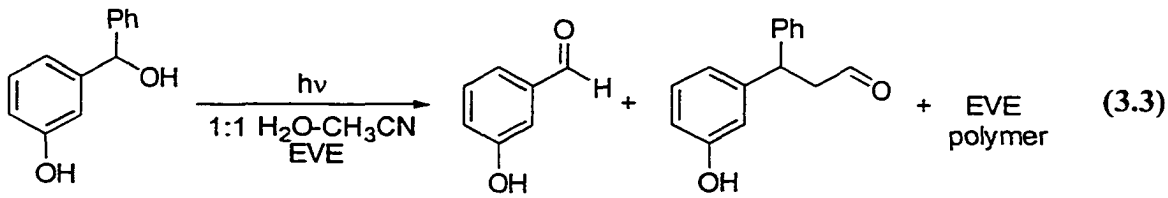

115 **166** **167** (3.3)

3.3.3 Photolysis of 160 in Aqueous Acetonitrile

To investigate the possibility that photomethanolysis of **115** might be photoreversible, photolysis of **160** was carried out in 1:1 H_2O-CH_3CN. Such a photolysis (20 min) generated **115** as the major product in 66% yield and small amounts of **159** and **166** (Eq. 3.4). An additional 20-min photolysis increased the yield of **115** to 87% and that of

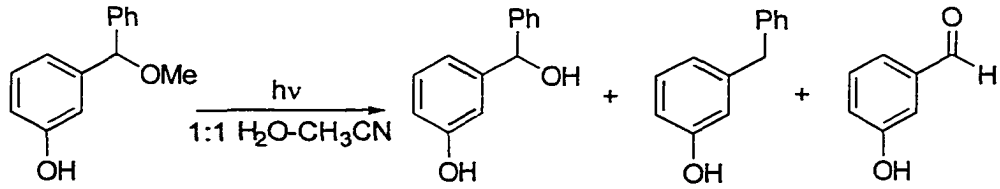

(3.4)

	160	**115**	**159**	**166**
20 min	29.6%	66.5%	3.0%	0.7%
40 min	7.9%	87.1%	3.8%	1.2%

159 to 3.8%. The high photoreactivity of **160** to afford **115** provokes the idea that this reaction can be used for the protection of alcohols, where photolysis of the ether in aqueous CH_3CN would easily release the alcohol and recover **115**.

3.4 Laser Flash Photolysis Studies

3.4.1 *m*-Hydroxybenzhydrol (115)

3.4.1.1 Transient Generation and Water Effect

LFP of **115** in 1:1 H_2O-CH_3CN (O_2 purged) generated a strongly absorbing but short-lived transient with λ_{max} = 440 nm and 30.1 ns lifetime (Fig. 3.4). This species was insensitive to oxygen and quenchable by water, added $NaBH_4$, and ethanolamine, (Fig. 3.4, inset). A weak residual signal (390 and 410 nm) was observable after the 440 nm transient had decayed (Fig. 3.4, bottom trace), which is more predominant with decreased water content.

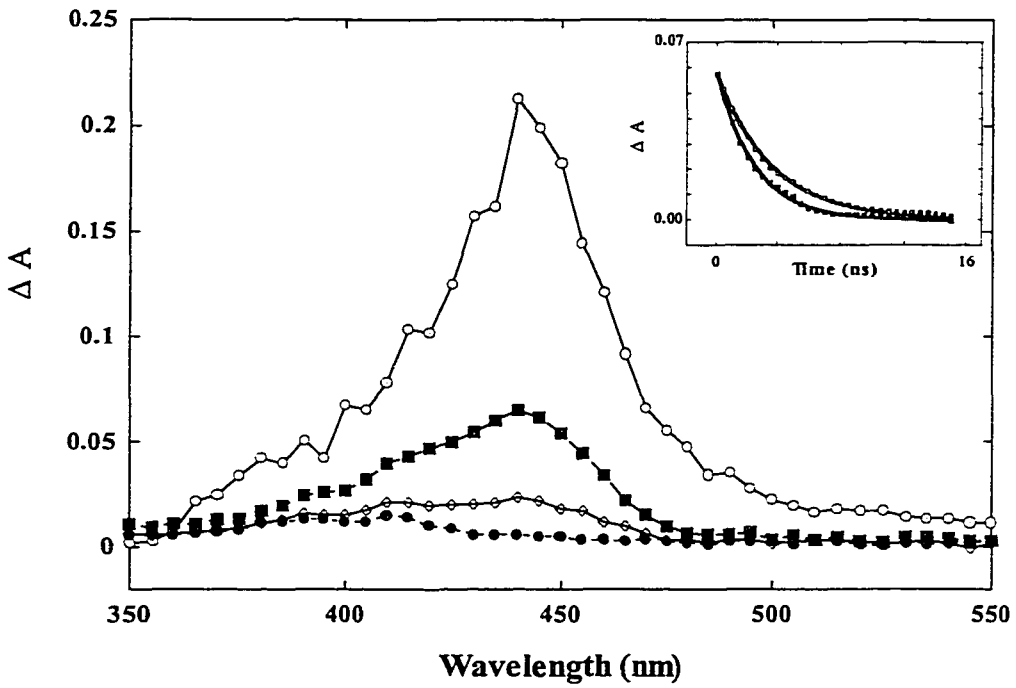

Fig. 3.4 Transient absorption spectra observed for **115** in 1:1 H_2O-CH_3CN (O_2). Top to bottom: recorded 10, 40 , 80 and 200 ns after the laser pulse. (Inset: top without ethanolamine and bottom with 0.24 **M** ethanolamine, monitored at 450 nm.)

With reduced H_2O content (20 % H_2O-CH_3CN), a similar strong 440 nm transient was observed under either N_2 or O_2 purging. However, the transient lifetime under O_2 (41 ns) was shorter than under N_2 (63 ns). Curiously, residual signals recorded 400 ns after the laser pulse were substantially different than those observed in 1:1 H_2O-CH_3CN. The residual transient under N_2 has λ_{max} = 400 nm with τ = 2.3 μs (Fig. 3.5, top), while the one observed under O_2 (Fig. 3.5, bottom) has λ_{max} = 390, 410 nm and τ = 3.7 μs, similar to the one observed in 1:1 H_2O-CH_3CN.

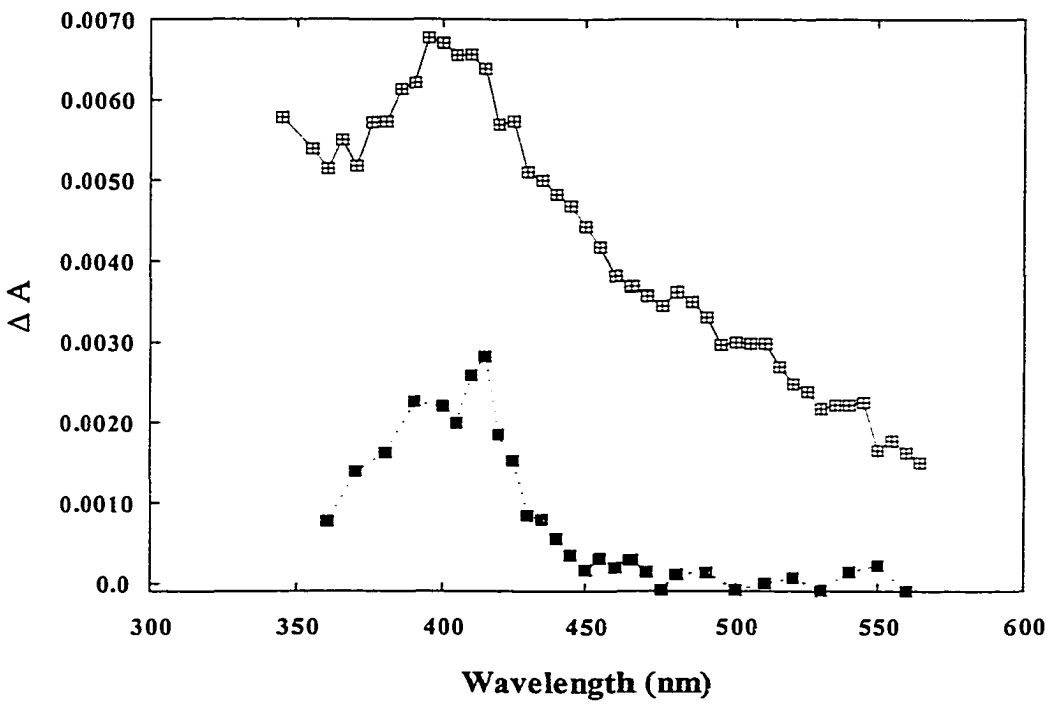

Fig. 3.5 Residual transient absorption spectra from **115** recorded 400 ns after the laser pulse in 20% H_2O-CH_3CN. Top: under N_2, Bottom: under O_2.

LFP of **115** in neat CH_3CN under N_2 gave two strong signals at 330 nm and 410 nm respectively, both of which disappeared with O_2 purging. No 440 nm transient was

observed. The decay of either band is better-fitted to the sum of two single exponentials, with lifetimes of ~ 9 μs and ~ 3 μs. The band shape of the transient absorption at 410 nm is similar to the residual transient observed in aqueous solution under N_2.

LFP of *m*-methoxybenzhydrol (**157**) generated a short-lived transient with lifetime of 75.5 ns and a long-lived one of 6.3 μs lifetime (λ_{max} = 428 nm) in 1:1 H_2O-CH_3CN (O_2). Similar LFP study of *m*-benzylphenol (**159**) gave a weak but long-lived transient at around 400 nm and a short-lived one at 750 nm. Both long-lived species from **157** and **159** might be the radical cation formed from an ejecting electron, which is not the same as either transient from **115**.

The yield of the 440 nm transient from **115** increased with the addition of water in O_2 purged CH_3CN (Fig. 3.6), by monitoring ΔA at 440 nm, which reached a maximum at around 70% H_2O concentration in CH_3CN. These results are similar to those observed for *o*-hydroxybenzhydrols at water content of > 10 % (Fig. 2.11, 2.18).

The lifetime of this transient decreased with the increasing water content. Additionally, the increase of log k_{obs} at low water concentration is slower than that observed above ~ 75% water concentration (Fig. 3.7).

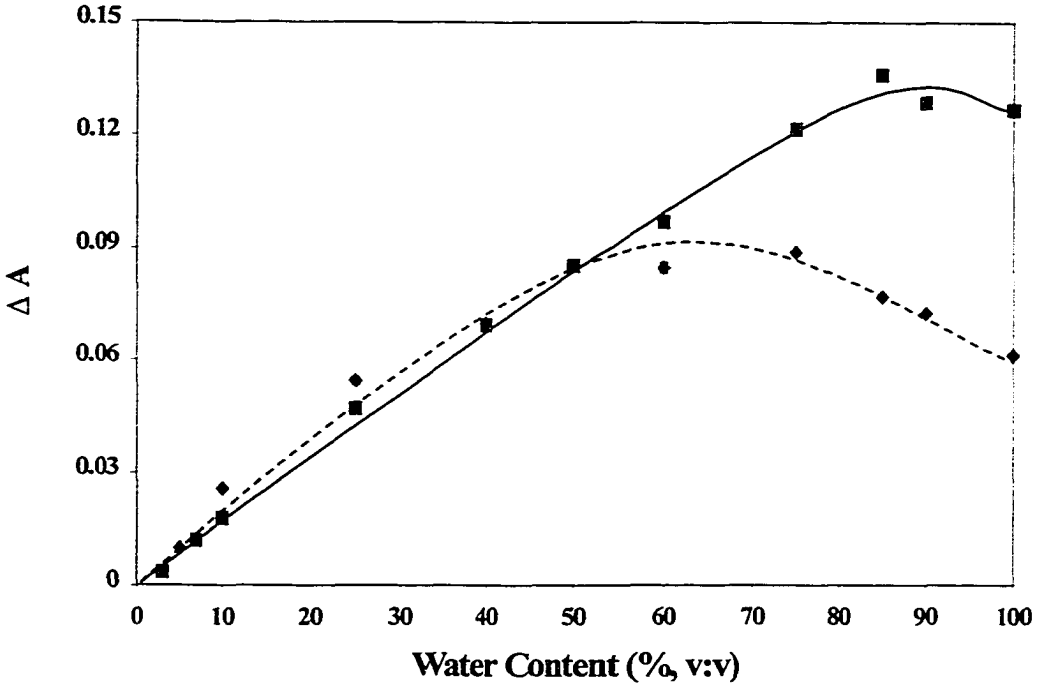

Fig. 3.6 Relative quantum yield of the formation (as measured by ΔA) of transients from **115** (♦) and **120** (■) as a function of water content in CH_3CN (O_2).

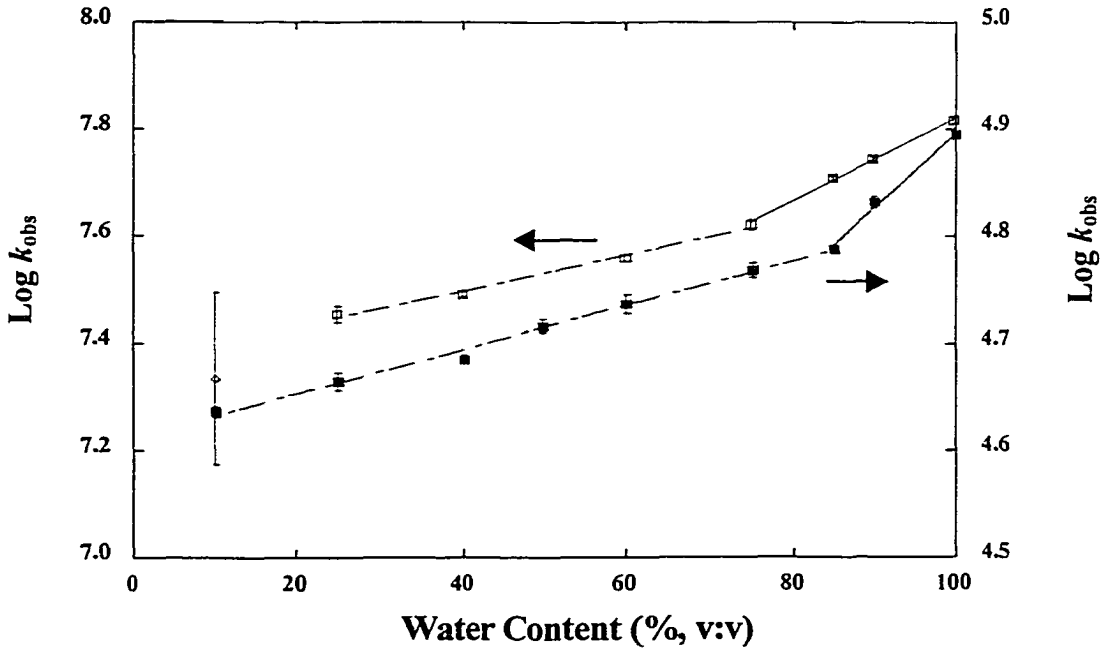

Fig. 3.7 Observed first order rate constants for decay transients from **115** (□) and **120** (■) as a function of water content in CH_3CN.

3.4.1.2 pH Effect

LFP of **115** in basic aqueous solution (pH = 13.7, 1:1 H_2O-CH_3CN, N_2 or O_2 saturated) showed a strong absorption at 440 nm which was identical to that obtained in neutral solution (Fig. 3.4). This transient decayed to a clean baseline rapidly (τ = 31 ns). The same 440 nm transient was observed at ~ pH 2 under both N_2 and O_2, along with weaker residual signals with λ_{max} at around 400 nm. These residual signals were the same as those shown in Fig. 3.5.

The relative quantum yield of formation of the 440 nm transient increased with increasing pH. The sigmoid plot of ΔA_{440} vs. pH (Fig. 3.8) showed two "titration curves" in both acidic solution (inflection point at pH ~ 2.2)[90] and basic solution (pH ~ 10). The first inflection point approximately corresponds to the $pK_a(S_1)$ of phenols and the second one to the $pK_a(S_0)$ of phenols. The lifetimes of the 440 nm transient were too short-lived in 100% H_2O to be measurable (< 15 ns, the limit of the laser system). Therefore, these experiments were repeated in 1:1 H_2O-CH_3CN with the quoted pH value being of the water portion. The resulting plot of ΔA_{440} vs. pH showed a titration curve in basic pH at a higher apparent $pK_a(S_0)$ value (Fig. 3.9). That is, the "titration curve" showed an inflection point at pH ~ 12, instead pH ~ 10 in 100 % H_2O. A plot log k_{obs} vs. pH in 1:1 H_2O-CH_3CN (Fig. 3.10) showed that the lifetimes were unchanged between pH 4 and 11, and were shortened in either acidic or basic media. Apparent slopes of –0.26 and 0.03 were calculated for pHs lower than 4 and higher than 11, respectively.

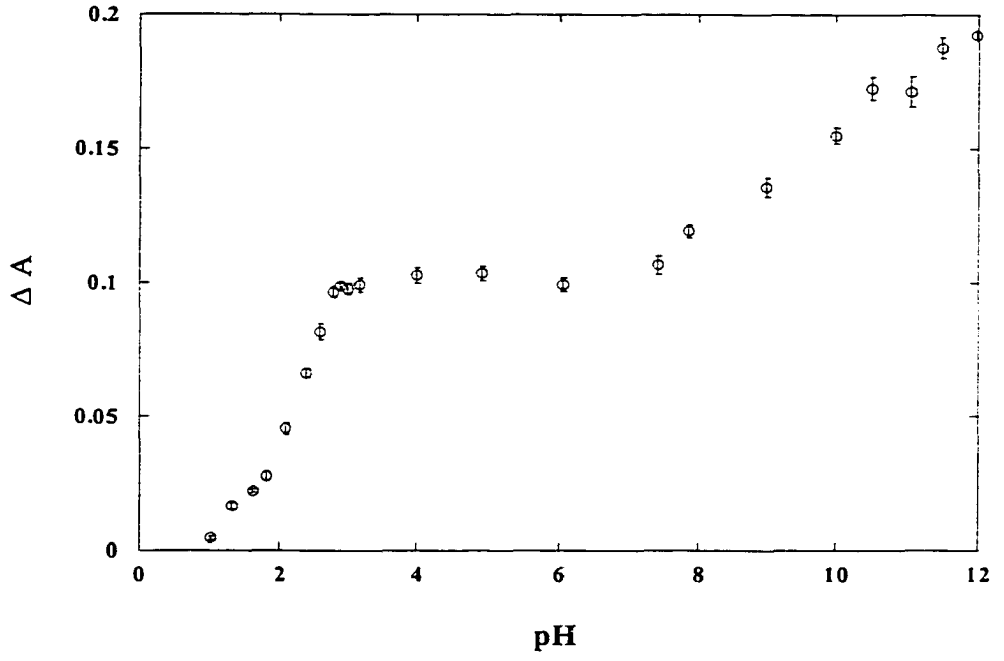

Fig. 3.8 Relative quantum yields (ΔA) for formation of transient observed for **115** vs. pH, monitored at 440 nm in 100% water.

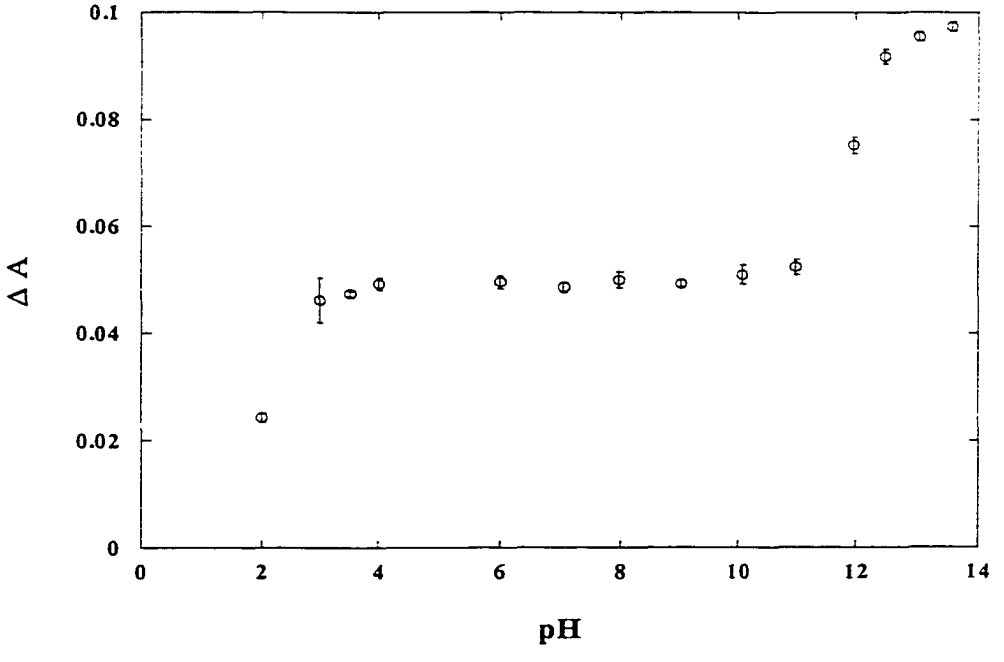

Fig. 3.9 Relative quantum yields (ΔA) for formation of transient observed for **115** vs. pH, monitored at 440 nm in 1:1 H_2O-CH_3CN (pH is of the water portion).

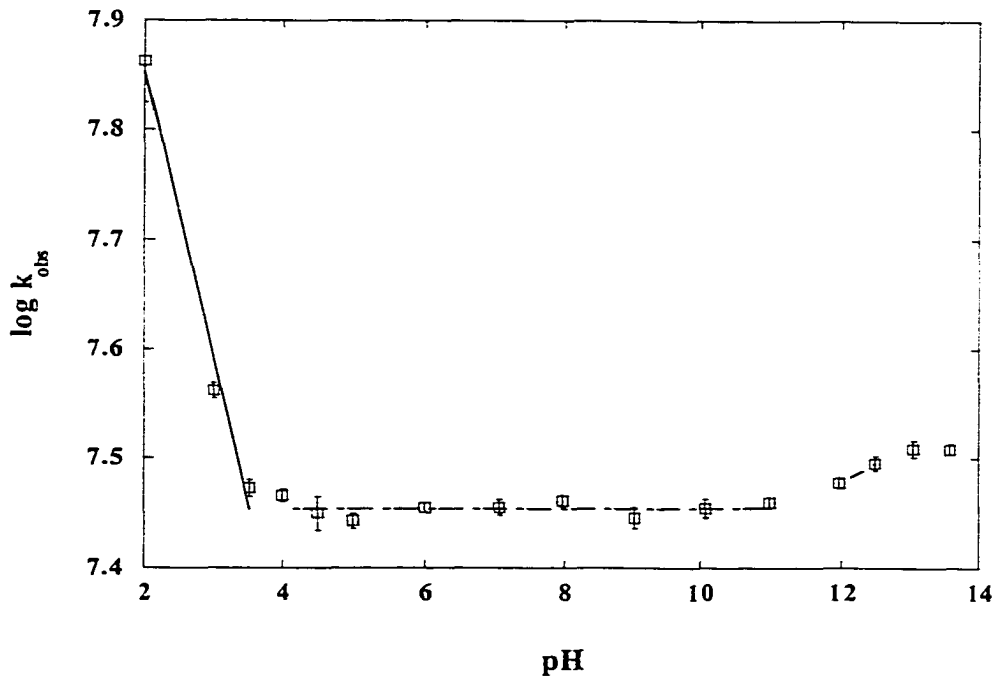

Fig. 3.10 A plot of log k_{obs} vs. pH (monitored at 440 nm) for the transient observed from **115** 1:1 H_2O-CH_3CN (pH is of the water portion).

As discussed in Chapter 2, $k_{obs} = k_{H+}[H^+]$ in acidic solution and $k_{obs} = k_{OH-}[OH^-]$ in basic solution, assuming that $k_{H2O}[H_2O] << k_{H+}[H^+]$ and $k_{H2O}[H_2O] << k_{OH-}[OH^-]$. A fit of the data using log $(k_{obs} - k_{H2O}[H_2O]) = \log k_{H+} + \log [H^+] = \log k_{H+} - pH$ (Fig. 3.11) at low pH gave a straight line with slope = -1 and $k_{H+} = 4.51 \times 10^9\ s^{-1}$. However, fitting the data at high pH to log $(k_{obs} - k_{H2O}[H_2O]) = \log k_{OH-} + \log [OH^-] = (\log k_{OH-} + 14) + pH$ did not give a slope of unity (was 0.36) and hence k_{OH-} could not be derived. The interference of CH_3CN to the pH values might have contributed to this anomaly.

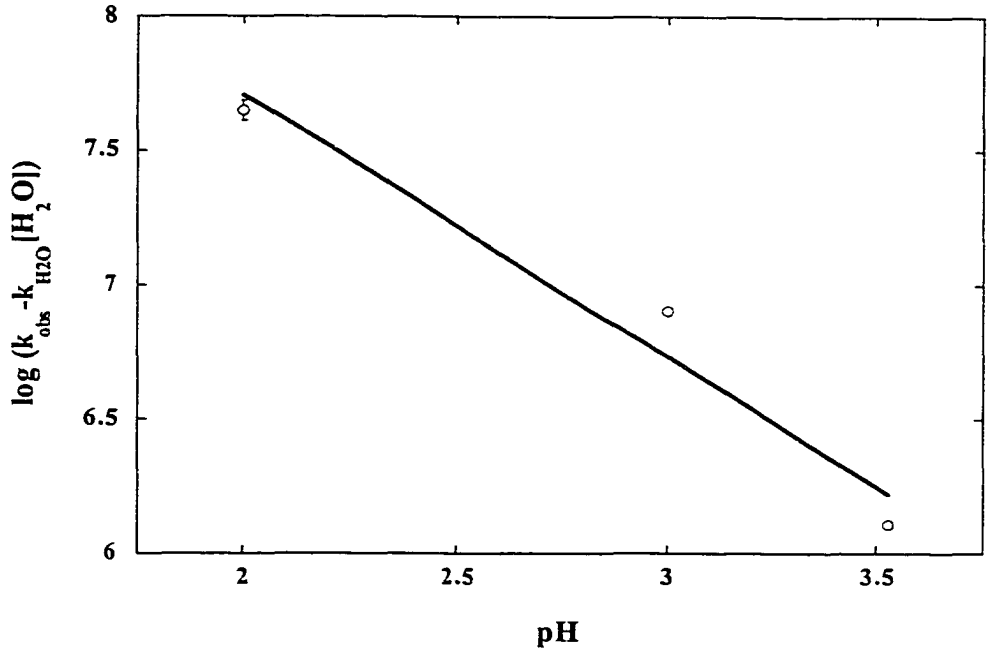

Fig. 3.11 A plot of log ($k_{obs} - k_{H2O}[H_2O]$) vs. pH for the transient observed from **115** in acidic 1:1 H_2O-CH_3CN.

3.4.1.3 Ethanolamine Quenching

The UV-Vis spectra of **115** in 1:1 H_2O-CH_3CN showed the formation of the phenolate ion (λ_{max} shifted from 274 nm to 293 nm) with addition of ethanolamine concentration (Fig. 3.12). However, the LFP transient observed from **115** in 1:1 H_2O-CH_3CN was identical with or without ethanolamine (Fig. 3.4), indicating that the same transient was generated. The lifetime of this transient was reduced by 50% in 0.23 **M** ethanolamine. A plot of k_{obs} vs. [$NH_2CH_2CH_2OH$] gave a linear relatrionship with k_{amine}= 1.04×10^8 $M^{-1}s^{-1}$ and k_{H2O} [H_2O] = 3.0×10^7 s^{-1} for **115** (Fig. 3.13). Ethanolamine is believed to function as a nucleophile in the quenching of the transient.

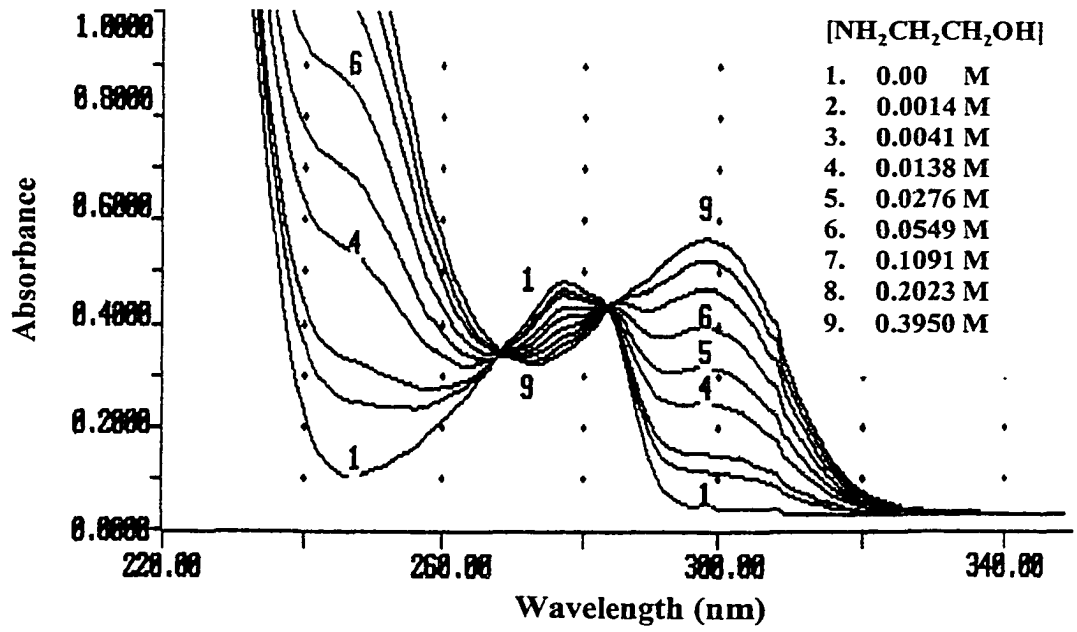

Fig. 3.12 Absorption spectra of **115** in 1:1 H_2O-CH_3CN upon addition of ethanolamine.

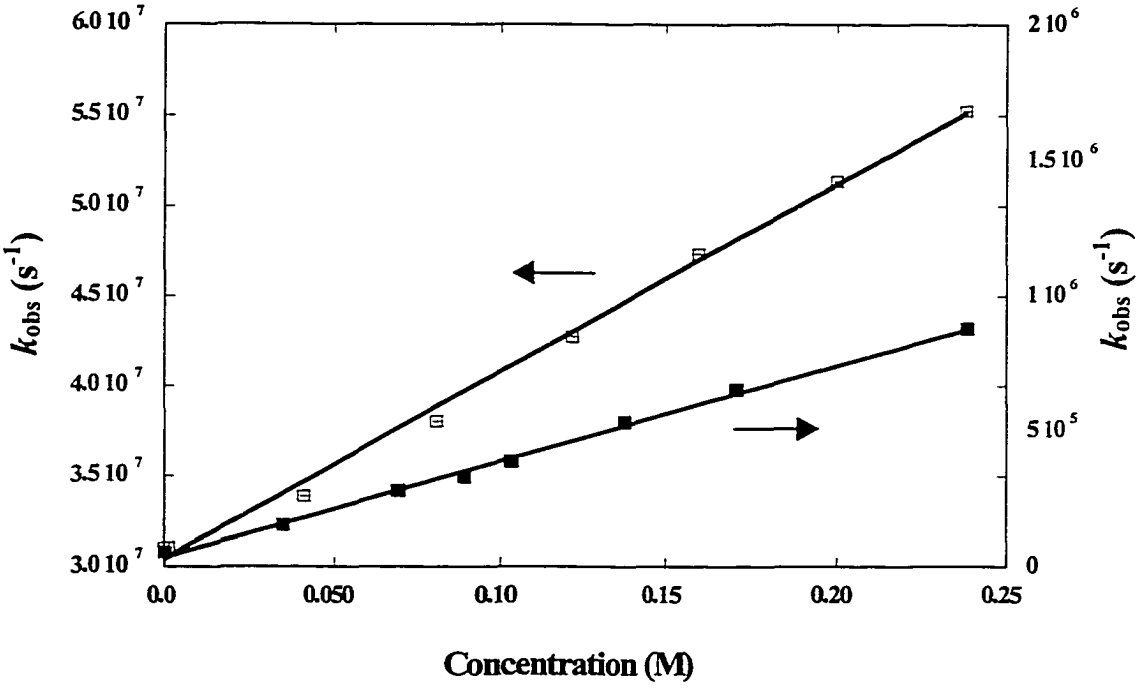

Fig. 3.13 Plot of k_{obs} vs. [$NH_2CH_2CH_2OH$] for the transient obtained from **115** (□) and **120** (■) in 1:1 H_2O-CH_3CN.

Curiously, the weak 440 nm transient from **115** (ΔA_{440} = 0.01) was observed in neat CH_3CN when in the presence of ethanolamine. A residual transient at 390 and 410 nm was also observed when the main transient had decayed, similar to that observed in acidic and neutral aqueous solution (Fig, 3.5, bottom trace).

3.4.1.4 Assignment of Transients

The λ_{max} and band-shape of the 440 nm transient observed on LFP of **115** is essentially identical to the corresponding diarylmethyl cations reported by McClelland et al.[66] Although they did not photogenerate the exact *m*-hydroxy-substituted cations, the lifetimes of those that were reported are informative. For example, diarylmethyl cations without strongly electron donating substituents have lifetimes of less than 10 ns in aqueous solution and are not detectable by standard nanosecond LFP; τ was estimated to be 1 and 5 ns for the diphenylmethyl and the (*p*-methylphenyl)phenylmethyl cations, respectively. Clearly, the transient observed from **115** is similar to an arylmethyl carbocation, but its lifetime is too long to be simply the (*m*-hydroxyphenyl)-phenylmethyl cation **168**.

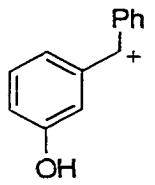

168

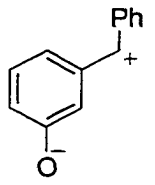

169b

Additional evidence available is that the methoxy derivative of **115** (**157**) did not produce any cationic transient by LFP. Moreover, **115** gave a significantly higher yield of the methyl ether product on photolysis in 1:1 MeOH-H_2O compared to **157**, with a quantum

yield (Φ_p = 0.40) only fractionally lower than that measured for the corresponding ortho isomer **112**. More importantly is the fact that the transient is quenchable both electrophilically and nucleophilically since its lifetime decreased in both acidic and basic media. The deprotonated hydroxy group (O^-) is electron-donating on the benzene ring, at a meta position (σ_m = - 0.47),[154] unlike the hydroxy group itself, which is electron withdrawing at the meta position (σ_m = + 0.12). If the transients from **115** were simply the cation **168**, its expected lifetime in aqueous solution, using data from McClelland et al.,[66] would be less than 1 ns and hence not observable using our LFP system. Its much longer observed lifetime (30 ns) is consistent with the hydroxyl group having deprotonated. We thus assign this transient as *m*-QM **169b**. Therefore, the present method offers a simple and efficient way for photogeneration of *m*-QMs in their zwitteironic singlet state.

The transient observed from **115** in pure CH_3CN under N_2 absorbs at 330 and 410 nm, and is quenchable by O_2. The residual signals recorded under N_2 in aqueous CH_3CN have λ_{max} at ca. 400 nm. Both transients in the 400 nm region have similar band shapes and lifetimes (2-3 μs). They are believed to belong to the same species. It is reasonable to assume that it is either the triplet, radical, or diradical (perhaps *m*-QM **169a**), but not a singlet or cationic species, which should have a much shorter lifetime and be insensitive to O_2. Studies of McClelland et al.[47] showed that the diphenylmethyl radical has λ_{max} = 330 nm and the corresponding singlet excited radical at 350 nm. While the (*p*-methoxyphenyl)phenylmethyl radical and singlet excited radical have λ_{max} = 340 and 360 nm, respectively. An electron-donating group appears to cause a red shift in the absorption

maximum of both radical and excited radical, which appear in pairs. The *m*-OH group is electron withdrawing which should result in a blue shift in the absorptions of the radical and the excited radical, relative to diphenylmethyl radical. The (*m*-hydroxyphenyl)phenylmethyl radical **170** could be responsible for the 330 nm absorption, but no corresponding excited radical absorption observed. Since the O^- group is strongly electron donating at the meta position, the radical **170a** should have λ_{max} at ca. 340 to 350 nm with λ_{max} of excited **170a** absorbing at 400 nm. However, there is no absorption at 340 to 350 nm regions. As a result, both **170** and **170a** can be excluded as transient candidates. Therefore, it is most likely that this transient is a triplet, either triplet **115** or triplet *m*-QM **169c** (diradical), both of which

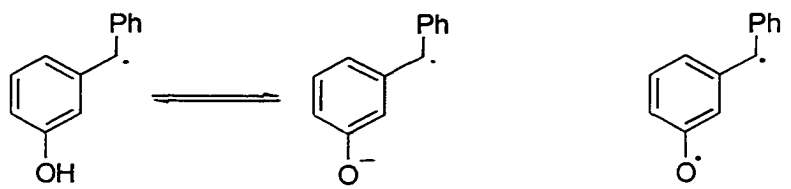

170 **170a** **169c**

are quenched by O_2. The possibility of a *m*-QM **169c** is consistent with the observation of EPR spectra of triplet *m*-QM **81c** and *m*-NQM **101c**, reported by Berson et al.,[126] and with the results of Goodman et al.,[145] who showed that *m*-NQM **101** has a triplet (diradical) as ground state.

The residual signal recorded under O_2 in aqueous CH_3CN is long-lived (3.7 μs). Again, it is probably a radical or triplet, since it is not quenchable by nucleophiles. This transient has a spectrum similar to that of a phenoxyl radical, which is known to have three

absorption bands at 365, 385 and 395 nm (Table 2.8), with a 15 nm red-shift. Therefore, it is likely to be a phenoxyl radical.

This transient was not observed in neat CH_3CN, which excludes the singlet **115**, abundant in neat CH_3CN, to be the precursor. And their absence in 1:1 H_2O (pH 13.7)-CH_3CN excludes the singlet phenolate ($[\mathbf{115}^-]^*$) and *m*-QM (**169a**), which are both abundant in basic solution. Therefore, the transient could be the O_2 quenching product **171** from either triplet **115** or triplet *m*-QM **169c** (Eq. 3.5).

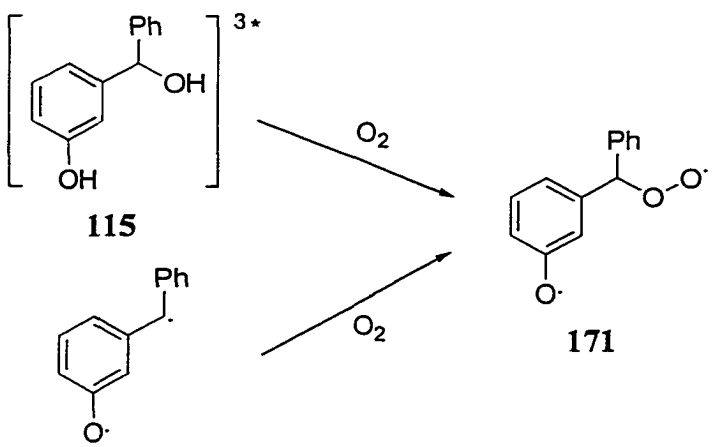

(3.5)

3.4.2 α-Phenyl-*m*-Hydroxybenzhydrol (120)

3.4.2.1 Transient Generation and Water Effect

LFP of **120** in 100% H_2O (pH 6, under O_2) gave a strong, broad absorption (λ_{max} = 430 nm) (Fig. 3.14). The decay to baseline was monitored at 380, 410 and 450 nm, respectively, and was best fitted to a sum of two single exponentials (τ = 11 ± 0.5 μs), (> 90%) and $\tau \sim 40$ μs, (< 10%)). No transient was observed from **120** in neat CH_3CN. The

addition of H_2O to CH_3CN solution resulted in increasing yield of transient along with a decreasing lifetime, similar to that observed for **115** (Figs. 3.6 and 3.7).

3.4.2.2 pH Effect

Transient spectra observed for **120** in acidic (pH 1-4) and basic (pH 9-14) solution had λ_{max} = 420 nm (Fig. 3.15a) and 445 nm (Fig. 3.15b), respectively, shifted from 430 nm observed in pH 6 solution. Both absorptions decayed cleanly to the baseline and fitted to a single exponential decay. The yield of the transient, as measured by ΔA (monitored at 425 nm), showed essentially no change in the pH 0-9 region, but an increase from pH 9 to 11 (Fig. 3.16).

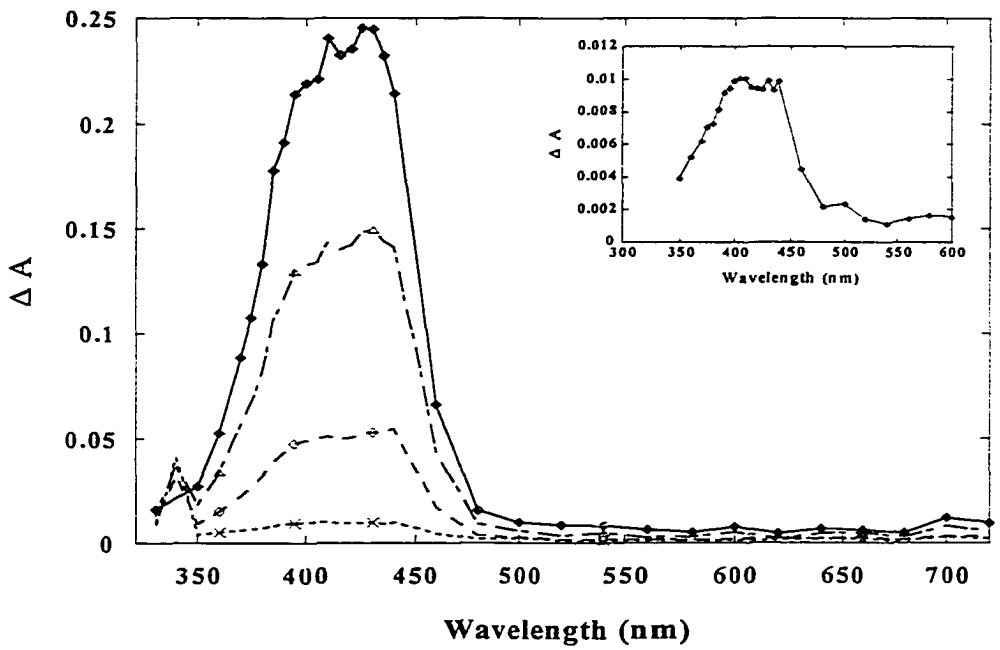

Fig. 3.14 Transient absorption spectra LFP of **120** in neat H_2O (under O_2). Recorded 1.5 μs (top), 7.5 μs, 24 μs and 73 μs (inset) after the laser pulse.

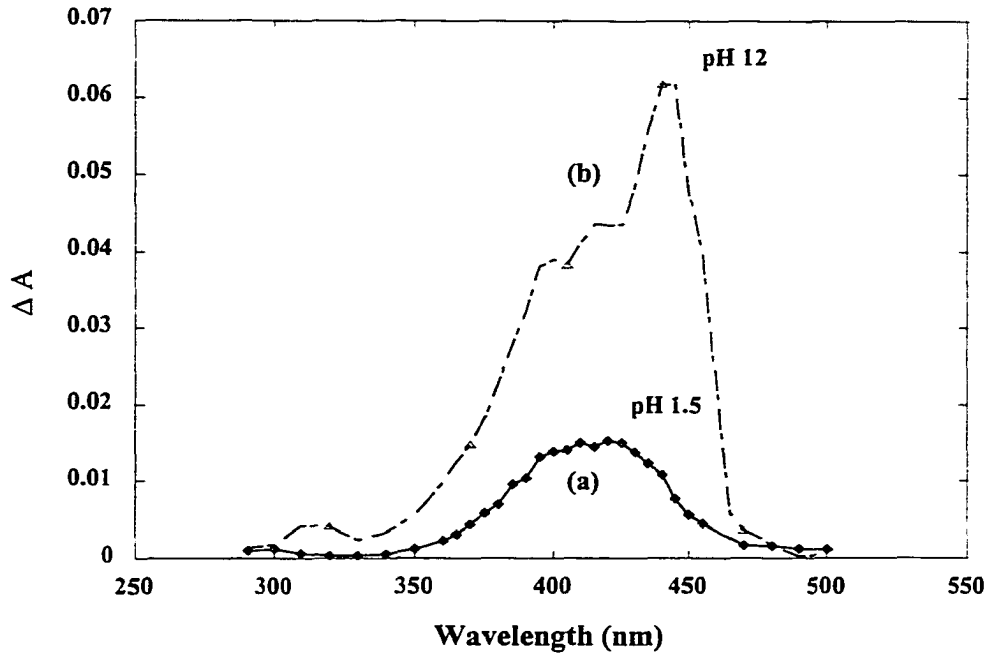

Fig. 3.15 Transient absorption spectra from LFP of **120** in neat H_2O (under O_2), measured 1.25 μs (pH 1.5) and 5 μs (pH 12) after the laser pulse.

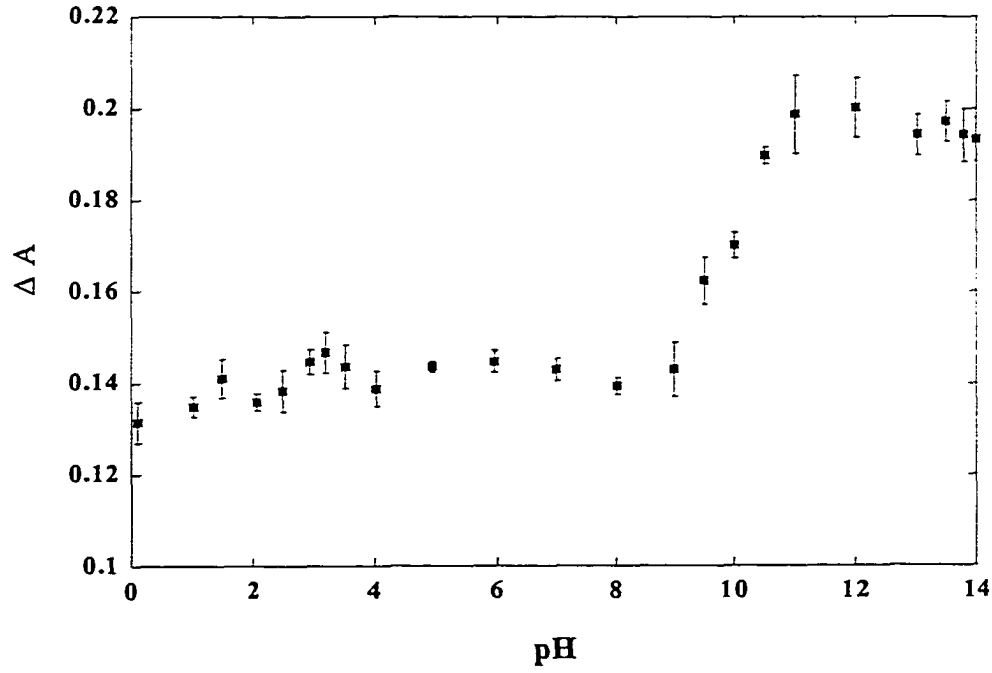

Fig. 3.16 Relative quantum yields (Δ A) for formation of transient for **120** vs. pH, monitored at 425 nm using LFP in neat H_2O (under O_2).

Decay rate constants vs. pH are shown in Fig. 3.17. Only one component was observed below pH 4 and above pH 9, whereas in pH 7-9 range, the decays are best fitted to a sum of two single exponentials. The lifetime of the transient generated below pH 4 is not affected by pH, with $k_{obs} = 1.6 \times 10^5\ s^{-1}$. In the pH 7-9 region, two species were observed, with $k_{obs} = 1.0 \times 10^5\ s^{-1}$ and $k_{obs} = 2.3 \times 10^4\ s^{-1}$. Above pH 12, the decay of the species showed a strong dependence on hydroxide ion concentration. A plot log (k_{obs} - $k_{H2O}[H_2O]$) vs. pH of this data gave a slope of unity and $k_{OH^-} = 7.5 \times 10^5\ s^{-1}$ (Fig. 3.18).

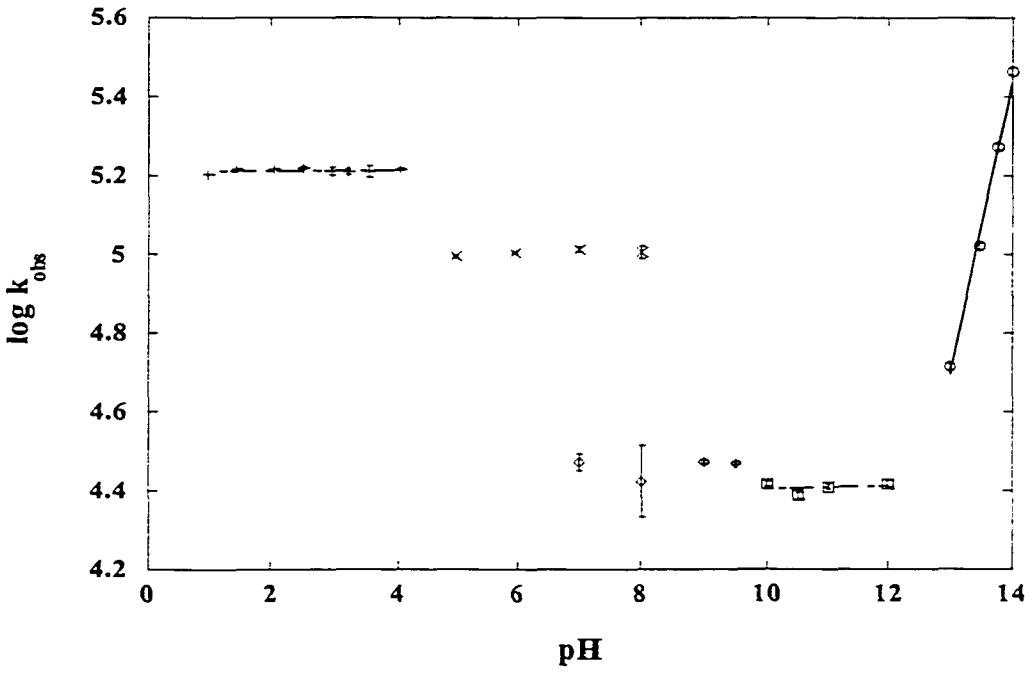

Fig. 3.17 A plot of log k_{obs} vs. pH for the transient observed from **120** in neat H_2O (under O_2).

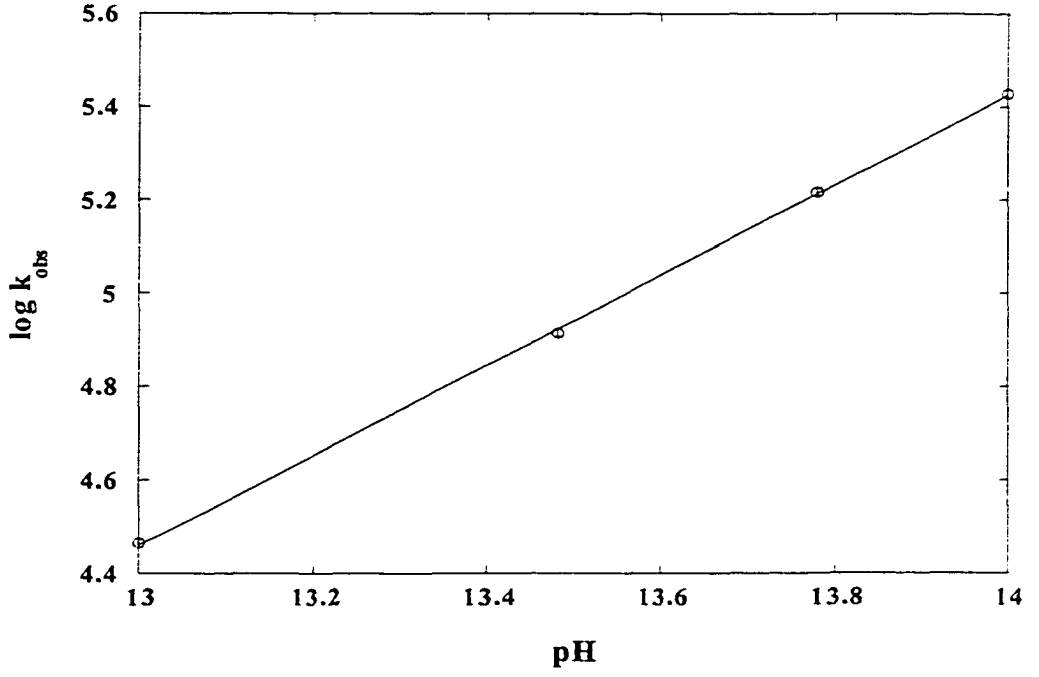

Fig. 3.18 A plot of log (k_{obs} - $k_{H2O}[H_2O]$) vs. pH for the transient from **120** in neat H_2O (under O_2).

LFP of α-phenyl-*m*-methoxybenzhydrol **158** in neutral 1:1 H_2O-CH_3CN gave only a weak signal at 430 nm (Fig. 3.19, pH 6). By decreasing the pH of the aqueous portion of the solvent (in 2:1 H_2O-CH_3CN), LFP of **158** gave stronger transient absorptions which also maximized at 430 nm with τ = 6 μs (Fig. 3.19, pH 1). The corresponding transient yield increase was shown in Fig. 3.19 inset. No change in lifetime was observed from pH 0 to 1 (Fig. 3.20). Decays above pH 1 are best fitted to a sum of two single exponentials, indicating that there is a new species present. McClelland et al.,[66] reported that the parent trityl (triphenylmethyl) cation **172** and (*m*-methoxyphenyl)diphenylmethyl cation **173** absorb between 400-500 nm with lifetimes of 7 and 6 μs (in 2:1 H_2O-CH_3CN), respectively.

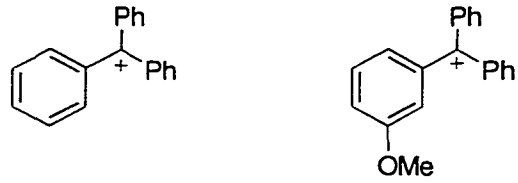

172 **173**

The band shape, λ_{max}, and lifetime of the transient observed for **158** are essentially identical to that reported for **173**. Therefore, the transient is assigned to carbocation **173**.

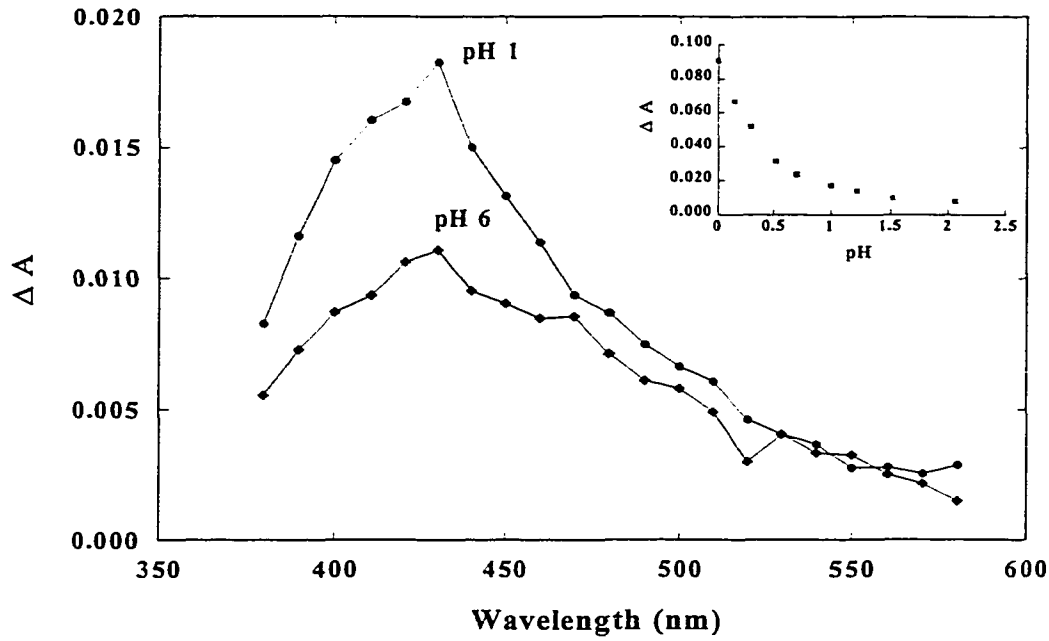

Fig. 3.19 Transient absorptions from **158** in 1:1 H_2O-CH_3CN. (Inset: relative quantum yields for transient formation vs pH.)

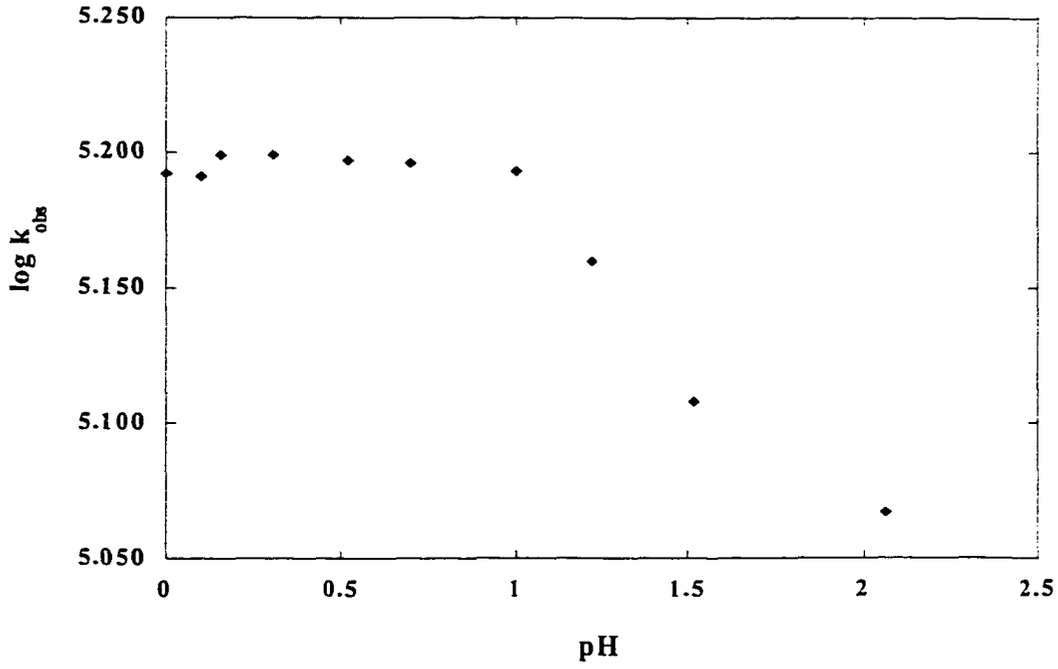

Fig. 3.20 Plot of log k_{obs} vs. pH for the transient from **158** in 1:1 $H_2O(H_2SO_4)$-CH_3CN. (Data above pH 1 are forced fits to a single exponential decay.)

3.4.2.3 Ethanolamine Quenching

The transient absorption spectrum from **120** in 1:1 H_2O-CH_3CN with the presence of ethanolamine was similar to the one observed in basic solution (Fig. 3.15). The UV spectra of **120** in 1:1 H_2O-CH_3CN showed formation of the phenolate ion with the addition of ethanolamine as observed for **115** (Fig. 3.12). The transient lifetime was reduced by 50% with 0.23 **M** ethanolamine. A plot of k_{obs} vs. $[NH_2CH_2CH_2OH]$ for **120** (Fig. 3.13) gave a straight line with $k_{amine} = 2.95 \times 10^6\ M^{-1}s^{-1}$ and $k_{H2O}[H_2O] = 3.5 \times 10^4\ s^{-1}$.

3.4.2.4 Assignment of Transients

The transients observed for **120** differ in both λ_{max} and τ depending on the pH. In basic solution (pH > 9), the transient has red-shifted λ_{max} and with generally longer lifetime. The yield of this transient showed a dramatic increase above pH 9 (Fig. 3.16), which corresponds to the $pK_a(S_0)$ of the phenol moiety in **120**. A plot of log k_{obs} vs. pH (Fig. 3.17) showed that both water and OH^- could quench the transient. Therefore, the transient must be a cationic species. However, it can not simply be cation **174**, as this cation (like **173**) would be much shorter lived in basic solution, i.e., < 6 μs instead of 35 μs. Using the same rational as used for **115**, the species must be the α-phenyl-*m*-QM **175**.

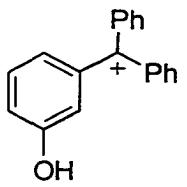

174

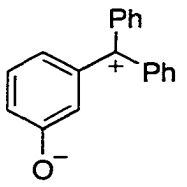

175

The related *m*-QM **169b** is the only transient observed throughout the whole pH region. If it is assumed that **175** is the only species generated in photolysis of **120** at all pHs, its yield would increase at low pH (pH < 4), level between pHs 4-8 and then increase above pH 9. However, a change in yield (as measured by ΔA in LFP experiments) was not observed at low pH and the transient observed for **120** has a similar band shape and lifetime as carbocation **173**. The lifetimes of this transient (Fig. 3.17) and those of **173** (Fig. 3.20) were both unchanged (~ 6 μs) at low pH. Considering that the OH and OMe groups have similar electron donating abilities, the transient from **120** in

acidic solution is assigned as cation **174** in place of the *m*-QM **175** (both of which have similar absorption characteristics).

In the pH 4-9 region, the transient yield stays constant but the observed decays are not always single exponential. The decay traces can be fitted to a single exponential at pHs 5 and 6 but better to a sum of two exponentials at pHs 7 and 8, where one of the components has a 35 μs lifetime. Thus, apparently, *m*-QM **175** is one of the transients generated in this pH region. Although a reasonable assignment for the other component ($\tau \cong 11$ μs) is the diaryl cation **174** generated via protonation of **175** (estimated pK_a of the phenol moiety of **174** is ≈ 7-8), its lifetime differs significantly from that observed in acid solution for this species. Additional studies are warranted before a final assignment can be made.

3.4.3 Solvent Effects on QM Formation

It is interesting to note that the yield of *m*-QM **169b** as measured by LFP shows a decrease on going from 70% H_2O-CH_3CN to neat H_2O (Fig. 3.6), which is accompanied by a faster increase of log k_{obs} vs. H_2O content (Fig. 3.7). McClelland et al.[15,66] have reported that first-order rate constants for the decay of diarylmethyl cations in aqueous acetonitrile have a "turning point" at around 20% H_2O-CH_3CN (Fig. 3.21) which they attributed to the requirement of H_2O at high CH_3CN concentration.

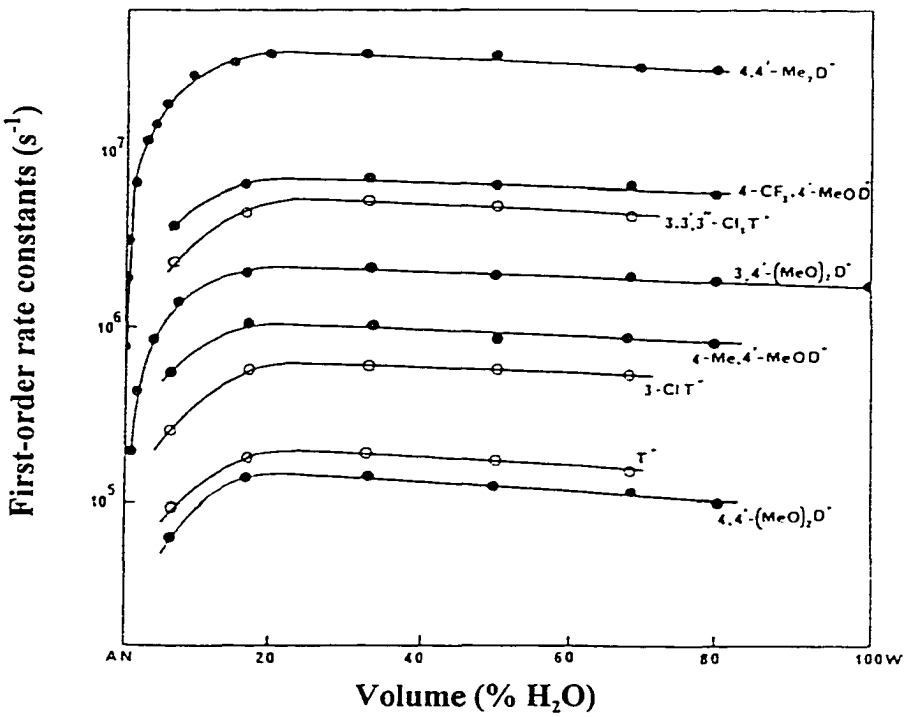

Fig. 3.21 First-order rate constants (s^{-1}, 20 °C) for the decay of substituted diarylmethyl cations (D^+) as a function of water content in acetonitrile. (Plot taken from ref. 66)

Obviously, other factors are probably involved behind this behavior observed in Figs. 3.6 and 3.7, since the "turning point" occurs at ~ 80% H_2O-CH_3CN. Factors such as solvation of the transient, changing of the water structure, and even the formation of water pools may be involved.[66] Indeed, water is considered as the most structured liquid.[153] It is generally accepted that liquid water has the short-range order of hydrogen-bonded, tetrahedrally coordinated structure of slightly expanded ice, with interstitial cavities filled by monomeric water, even though the precise nature of the structure of water still remains the subject of some controversy. Mixed aqueous solutions are even more complex. When small amounts (below 10 wt %) of alcohols, acetone, dioxane, or THF are added to water,

the water structure actually becomes reinforced, as in the case when non-polar solutes are dissolved. Therefore, the phenomena observed in Figs. 3.6 and 3.7 might be caused by the changing structure of water, although it is difficult to speculate on the details at the molecular level.

3.5 Steady State Fluorescence Measurements

3.5.1 Fluorescence Quantum Yields

3.5.2 Water and pH Effects

Steady state fluorescence spectra of **115** (Fig. 3.22) and **120** were taken in 100% CH_3CN, 1:1 H_2O-CH_3CN and 100% H_2O. Excitation at 270 nm in CH_3CN gave a strong emission band centered at 296.7 nm for **115** and 298.8 nm for **120**, respectively, which were red shifted upon the addition of H_2O as shown in Table 3.2. The fluorescence quantum yields (Φ_f) of both compounds, measured using anisole as a secondary standard, were drastically quenched by H_2O and only a weak emission band accompanied by a Raman band was observed in 100% H_2O solution (Fig. 3.22). Table 3.2 also summarizes emission maximum (λ_{max}) and quantum yields (Φ_f) for both **159** and **157**, as model compounds, in these solvent systems. The Φ_f decreased only 20% for **159** in 1:1 H_2O-CH_3CN, comparing to 62% for **115**, whereas Φ_f of **157** barely decreased.

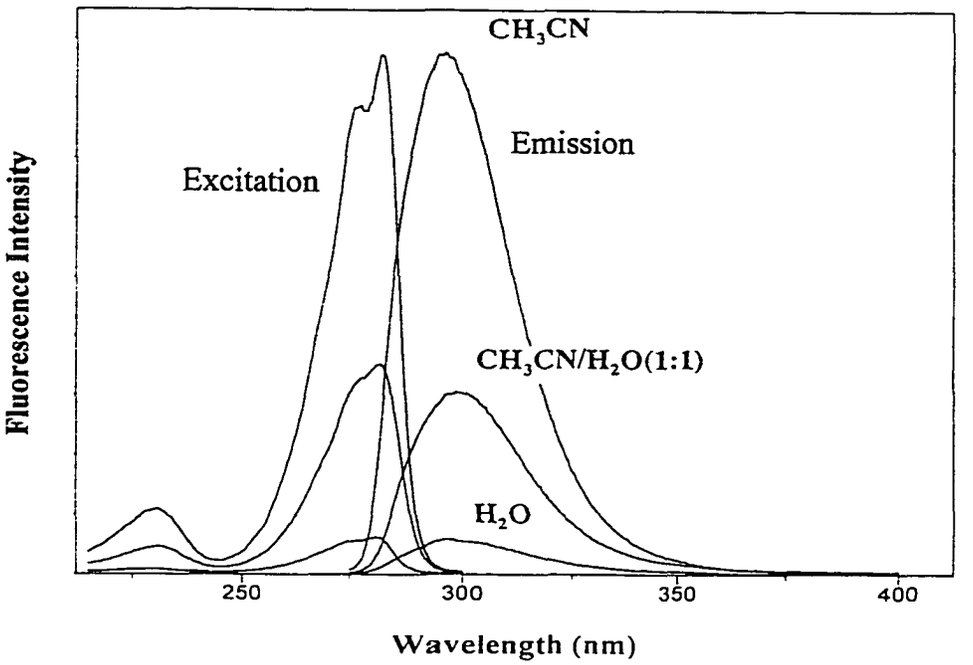

Fig. 3.22 Water quenching of the fluorescence of **115** in CH_3CN.

Fluorescence lifetimes (τ) of these *meta* substituted compounds were about the same in CH_3CN (Table 3.2). However, τ of **115** was reduced to 1.9 ns in 1:1 H_2O-CH_3CN. It was interesting to note that the lifetime of **159** was slightly shorter in 1:1 H_2O-CH_3CN than in 100% CH_3CN, whereas τ of **158** remained almost unchanged (Table 3.2). However, the lifetimes of both compounds were substantially quenched in 100% H_2O. Again, the overall water effect on fluorescence quenching followed the order of **115** $\approx$ **120** > **159** > **157** and the lack of a phenol moiety in **157** can be the reason of low fluorescence quenching efficiency.

Table 3.2 Effect of H_2O Content (in CH_3CN) on Emission Maximum (λ_{max}), Fluorescence Quantum Yields[a] (Φ_f) and Lifetimes[b] (τ) of *meta*-Substituted Compounds

	Solvent	**115**	**157**	**159**	**120**	**158**
λ_{max}	CH_3CN	296	295	293	299	--
	1:1 H_2O-CH_3CN	299	295	297	302	--
	H_2O	--	296	297	--	--
Φ_f[c]	CH_3CN	1 (0.22)	1 (0.21)	1 (0.25)	1 (0.21)	1
	1:1 H_2O-CH_3CN	0.38	0.95	0.79	0.46	--
	H_2O	0.08	0.67	0.24	0.13	--
τ[d] (ns)	CH_3CN	5.4	--	5.0	4.9	5.1
	1:1 H_2O-CH_3CN	1.9	--	4.5	--	5.0
	H_2O	< 1	--	1.3	< 1	3.2

[a] Excited at 270 nm. [b] Excited at 275 nm.
[c] Measured using anisole (Φ_f = 0.29 in cyclohexane) as secondary standard. Absolute quantum yield quoted in brackets. All other numbers are relative yields.
[d] Measured using PTI LS-1 Time-Correlated Single Photon Counting system (≥ 2 ns) or picosecond fluorescence system (< 2 ns)

The Φ_f for **115** was also affected by the pH value of the aqueous solution (Fig. 3.23). Similar emission bands were observed in neutral and acidic aqueous solutions (pH ~ 1) with only a slight lower Φ_f in the latter. However, the band is very broad and drastically quenched in basic solution (pH ~ 13). The absorption maximum was shifted in basic media to 292.8 nm for **115** (Fig. 3.1) and 293.6 nm for **120**, respectively, corresponding to the absorptions of their phenolate ions. Excitation at 290 nm gave rise to a new but very weak band at 350 nm (Fig. 3.24) for **115**. The 400 nm band was shown to come from the solvent. Clearly, the emission from excited phenol moiety (at ~ 300 nm) is predominant in acidic and neutral aqueous solutions, whereas fluorescence from excited phenolate ion (the weak 350 nm band) is very weak in basic media. Table 3.3 summarizes λ_{max} and the relative

fluorescence quantum yields Φ_f°/Φ_f (Φ_f° = fluorescence quantum yield at pH 7) in neutral, acidic, and basic solutions.

Table 3.3 pH Effect on Emission Wavelength (λ_{max}) and Relative Fluorescence Quantum Yields (Φ_f°/Φ_f)[a] of *meta* Compounds

	Solvent	**115**	**159**	**157**
λ_{max} (nm)	0.1 N H_2SO_4	300	297	297
	H_2O (pH 7)	300	297	297
	0.1 N NaOH	~ 350	~ 340	297
Φ_f°/Φ_f	0.1 N H_2SO_4	1	1	1
	H_2O (pH 7)	1.06	1.05	1.2
	0.1 N NaOH	~ 0	~ 0	0.9[b]

[a] Relative fluorescence quantum yuild where Φ_f° is the yield in neat CH_3CN. λ_{ex} = 270 nm.
[b] Estimated value.

Although bulk H_2O can dramatically quench the fluorescence of *meta*-hydroxybenzhydrols, Φ_f of **115** showed random fluctuation at low [H_2O]. As a consequence, Stern-Volmer analysis using relative fluorescence quantum yields Φ_f°/Φ_f was problematic. However, a plot of fluorescence lifetime τ_0/τ (τ_0 = lifetime in neat CH_3CN) vs. [H_2O] gave a good linear plot for **115** (Fig. 3.25), with slope = $k_q\,\tau_0$ = 0.073 M^{-1}. Hence, a quenching rate constant $k_q = 1.3 \times 10^7\ M^{-1}\ s^{-1}$ with τ_0 = 5.4 ns. Compound **120** behaved like **115** with $k_q = 1.2 \times 10^7\ M^{-1}\ s^{-1}$ (Table 3.4). It is worth mentioning here that λ_{max} red shifted as in higher H_2O content (Table 3.5).

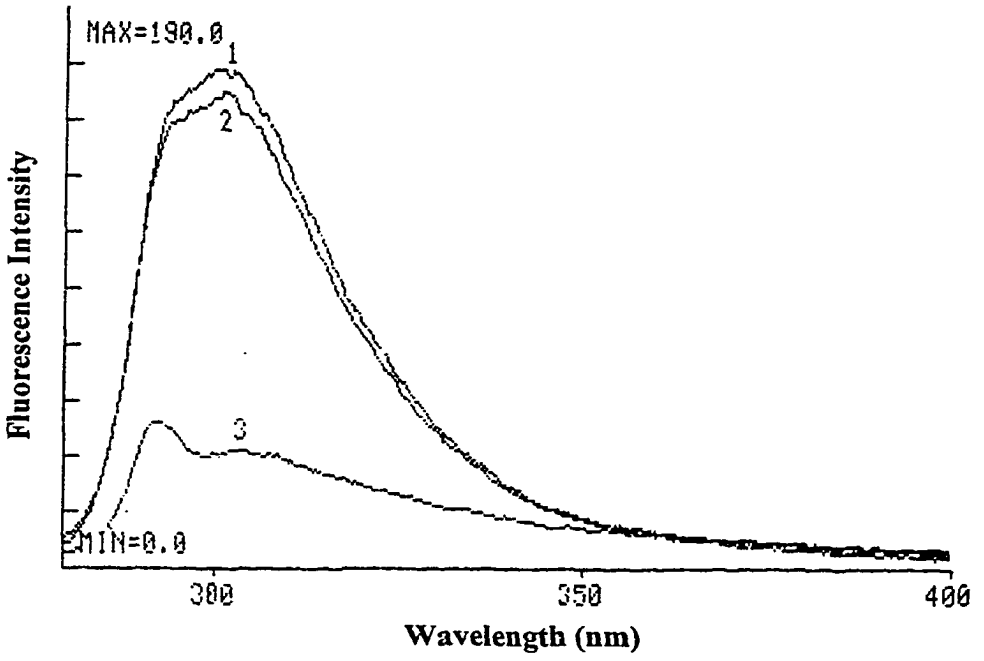

Fig. 3.23 Fluorescence emission spectra of **115** in H_2O. 1: pH 7.0; 2: pH 1.5; 3: pH 12.0 (λ_{ex} = 265nm, OD_{265}=0.038).

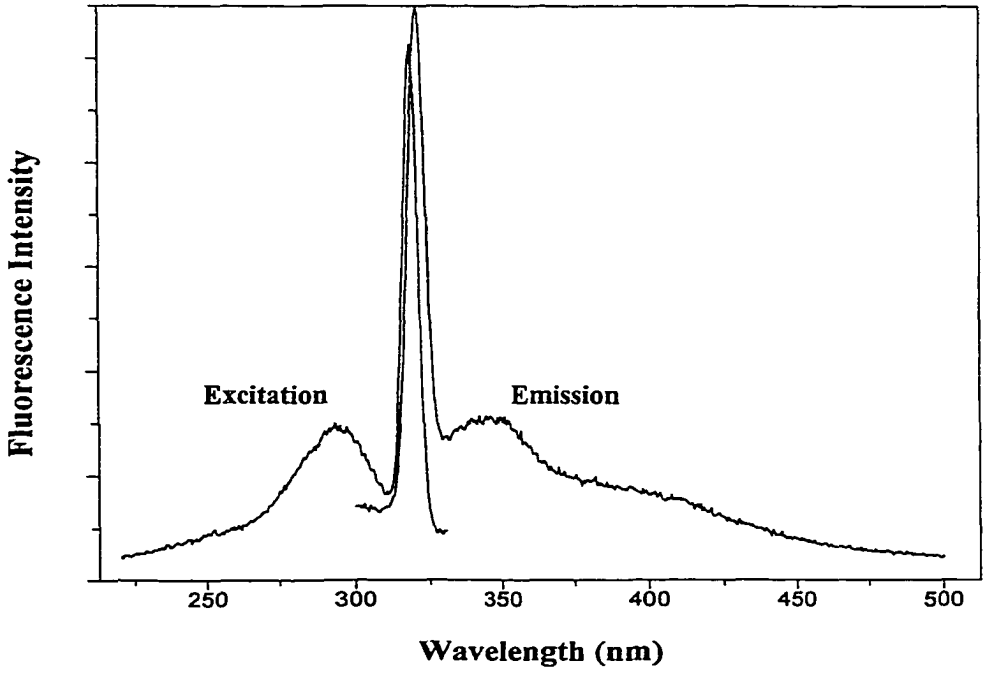

Fig. 3.24 Fluorescence emission of **115** in pH 13 (λ_{ex} = 290 nm).

Table 3.4 Fluorescence Quenching Rate Constant (k_q) of *m*-Hydroxybenzyl Alcohols

Quencher	k_q (M^{-1} s^{-1})	
	115	**120**
H_2O	1.3×10^7	1.2×10^7
$NH_2(CH_2)_2OH$	3.3×10^9	3.4×10^9

Table 3.5 Effect of H_2O Content on Fluorescence Emission of **115** in CH_3CN

$[H_2O]$, **M**	0	0.21	0.43	0.64	0.86	1.07	1.28	1.50	1.71
λ_{max}, nm	296.7	297.5	297.8	297.8	298.0	298.6	299.1	299.1	298.8
Φ_f^o / Φ_f	1	0.998	1.022	1.032	1.065	0.945	1.021	1.032	1.076

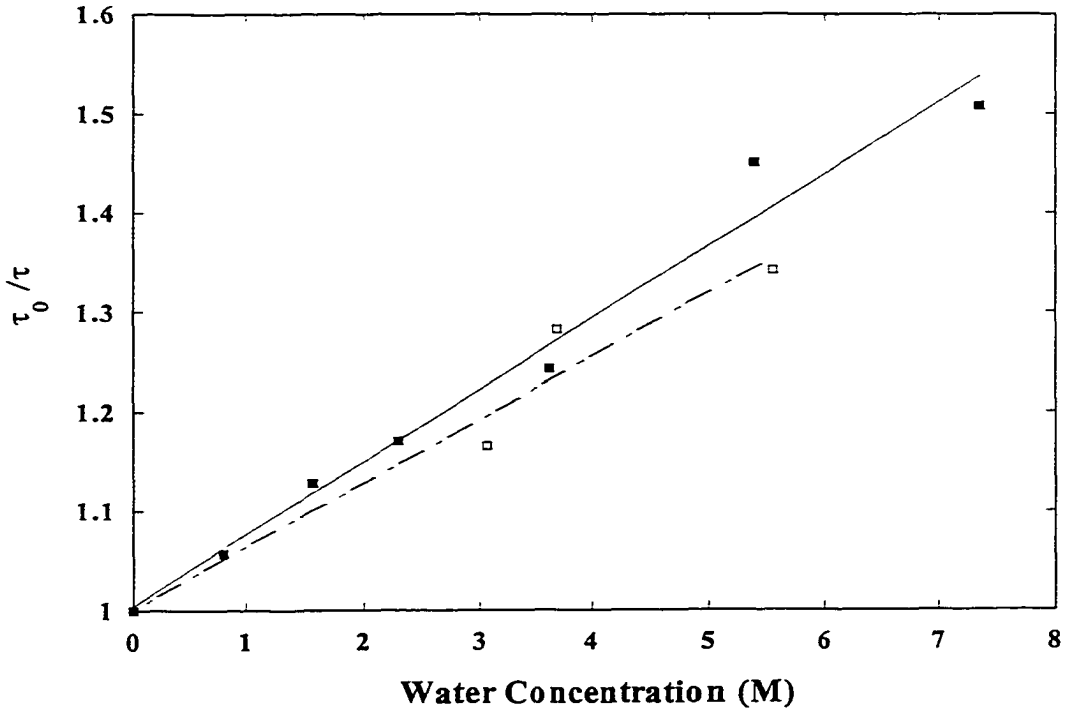

Fig. 3.25 Water effect on the fluorescence lifetimes of **115** (■) and **120** (□) in CH_3CN.

3.5.3 Ethanolamine Quenching

The fluorescence of **115** and **120** in acetonitrile were efficiently quenched by added ethanolamine. The Stern-Volmer plot of **115** showed a linear relationship for a plot of Φ_f^o / Φ_f vs. $[NH_2CH_2CH_2OH]$ with > 50% of the fluorescence intensity being quenched within 0.05 **M** ethanolamine (Fig. 3.26). A quenching rate constant $k_{sq} = 3.30 \times 10^9\ M^{-1}\ s^{-1}$ was obtained. A similar quenching efficiency was observed for **120** (Table 3.5, Fig. 3.26). In general, k_q for $NH_2CH_2CH_2OH$ are two orders higher than k_q for H_2O. It is worth noticing that the absorption spectrum of **115** undergoes some changes on the addition of ethanolamine (Fig. 3.27), indicating interactions between substrate and quencher in the ground state.

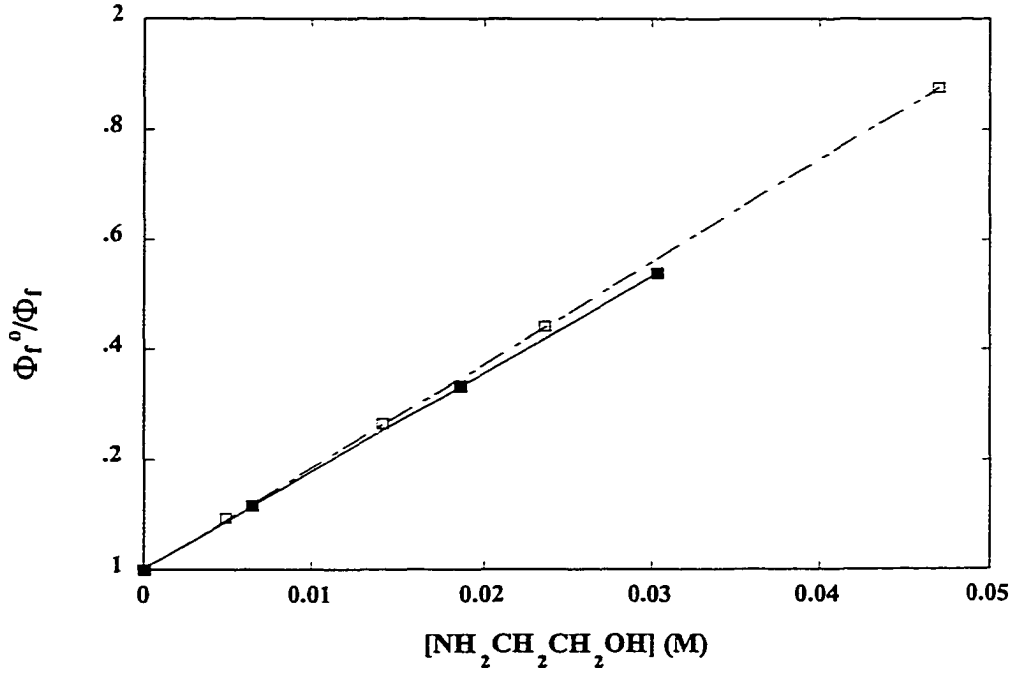

Fig. 3.26 Ethanolamine quenching on the fluorescence emission of **115** (■) and **120** (□) in CH_3CN.

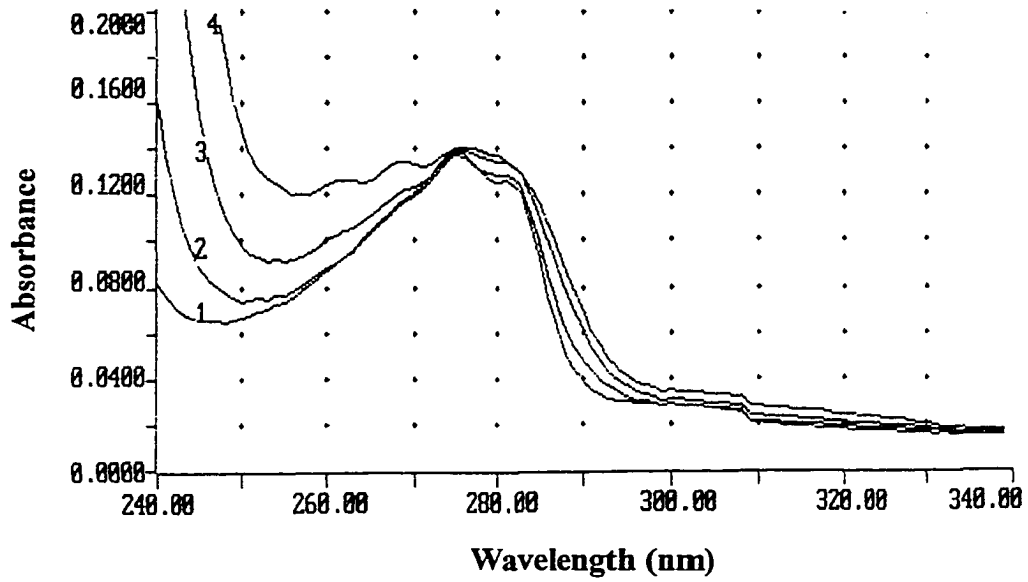

Fig. 3.27 Effect of ethanolamine on the UV absorption of **115** in CH_3CN. $[NH_2CH_2CH_2OH]$: **1**. 0 **M**; **2**. 0.01 **M**; **3**. 0.05 **M**; **4**. 0.14 **M**.

3.6 Mechanism

3.6.1 Mechanism of Formation of Transients

3.6.1.1 Transient Formation from 115

m-QM **169b** was identified as the main transient (λ_{max} = 440 nm) observed in the photolysis of *m*-hydroxybenzhydrol (**115**) in aqueous solution throughout the whole pH region. It was not generated in neat CH_3CN but was observed with increasing yields upon the addition of water (Fig. 3.6). Furthermore, the relative quantum yield of **169** showed two "titration curves" (Fig. 3.8) in acidic and basic pH regions, corresponding to pK_a (S_0) and pK_a (S_1) of the phenol moiety in **115**, respectively. Meanwhile, the fluorescence quantum yield decreased in the presence of water and drastically quenched in basic

solution. The weak phenolate ion emission in basic media also corroborates the involvement of the singlet phenolate ion in the mechanism. Parallel to the discussion in Chapter 2, the fluorescence of model compounds *m*-methoxybenzhydrol (**157**) and *m*-benzylphenol (**159**) were studied and showed that adiabatic deprotonation is probably the first step of the mechanism in neutral and acidic solution, followed by dehydroxylation to generate *m*-QM **169b** (Scheme 3.2).

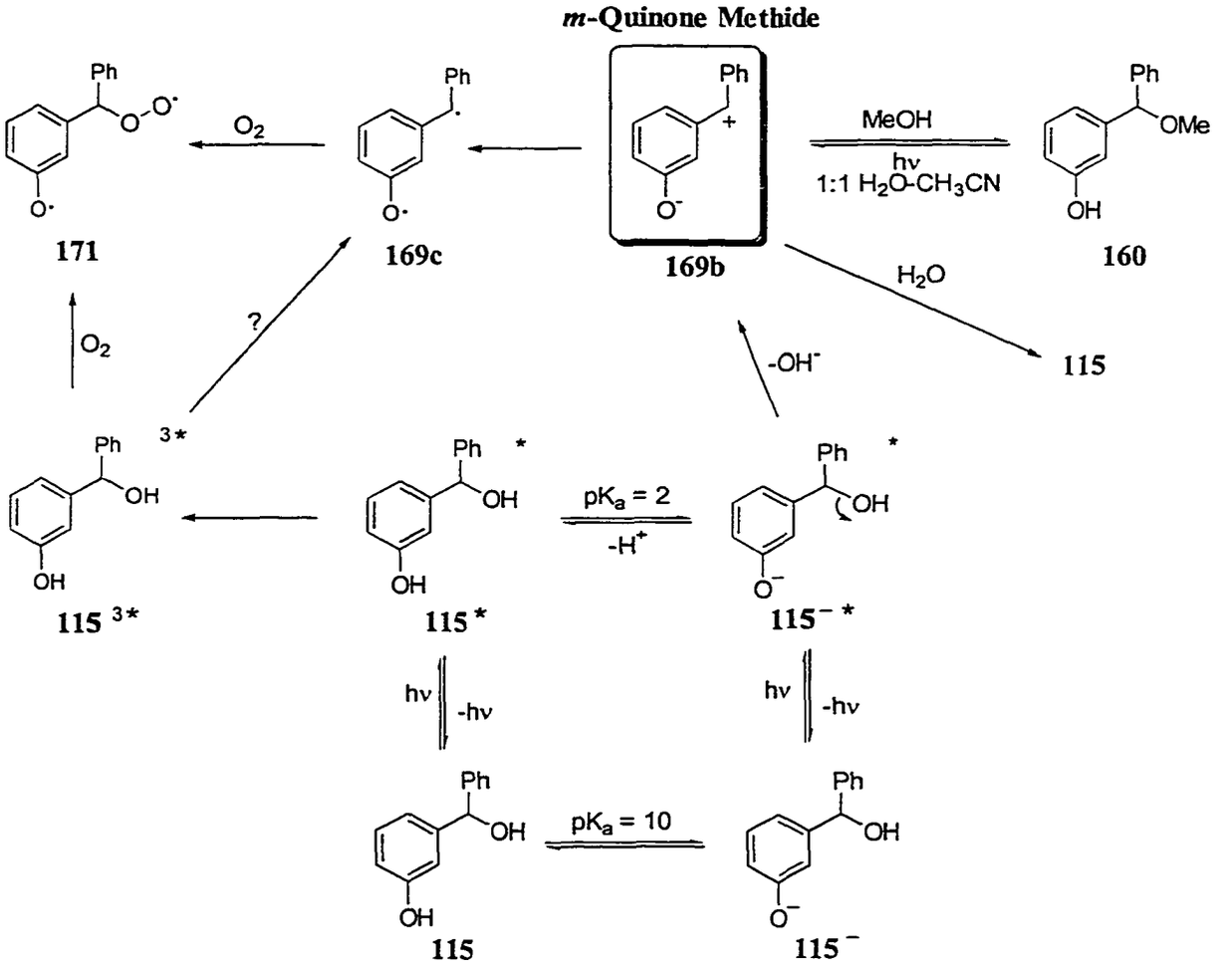

Scheme 3.2

Both the fluorescence emission and absorption spectra of **115** (Table 3.5 and Fig. 3.28) are affected by water, indicating that there are interactions between substrate and water molecules in the ground state. A linear relationship between τ_0/τ and $[H_2O]$ indicates that this is a dynamic quenching in S_1. There are physical and chemical dynamic processes in photochemistry. In physical dynamic quenching, the excited molecule forms an encounter complex with the quencher to dissipate heat and regenerate the ground state complex, which might persist in solution or dissociate immediately. Chemical dynamic quenching is used for the case when the reaction occurs through a dynamic process. In our case, both physical and chemical quenching processes are possibly occurring together.

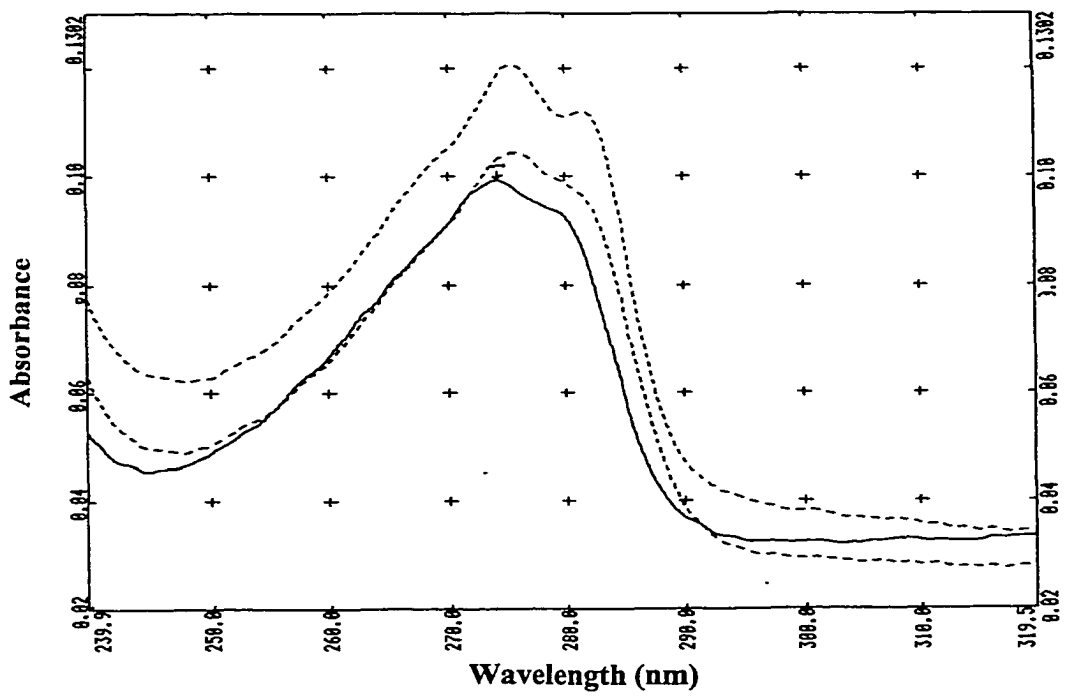

Fig. 3.28 Water effect on the UV-Vis absorption of **115** in 100 % CH_3CN (Top), 1:1 H_2O-CH_3CN and 100% H_2O (Bottom).

Long-lived transients observed under N_2 persisted after the decay of *m*-QM **169b**, which were assigned as triplet **115** (**115**^{3}*) or triplet *m*-QM **169c**, both of which would be quenched by O_2, possibly to **171**. It has also been shown that this transient (under N_2) was most abundant in the absence of water, whereas in aqueous solution, a higher yield was observed in low pH, opposite to that of *m*-QM **169b**. It is clear that **169b** is not the precursor of this transient. Moreover, singlet phenolate ([**115**$^{-}$]*) can be excluded since no N_2-transient was generated in 1:1 H_2O (pH13.7)-CH_3CN. Therefore, singlet **115** is the most probable precursor for the transient observed under N_2, although additional evidence would benefit on proposing a detailed mechanism.

Ethanolamine efficiently quenched the fluorescence of **115** and a Stern-Volmer plot showed a linear relationship between Φ_f° /Φ_f and [$NH_2CH_2CH_2OH$] (Fig. 3.26). Furthermore, compound **115** was readily deprotonated by ethanolamine in aqueous solution (Fig. 3.12) which generated *m*-QM **169b** as a transient on photolysis. Since ethanolamine quenching rate constants for **115** and **120** are about the same, the quenching probably involves only the phenol moiety. It is reasonable to suggest that static quenching is the dominating mechanism at low [$NH_2CH_2CH_2OH$], where ethanolamine interacts with **115** at the phenol hydroxyl moiety to form contact ion pairs (CIP), which are better solvated in neat acetonitrile but not as fluorescent as **115**. On excitation, the CIP dissociates to solvent solvated ion pairs (SSIP), i.e., excited phenolate ion of **115**, which gives rise to *m*-QM **169b** (Scheme 3.3).

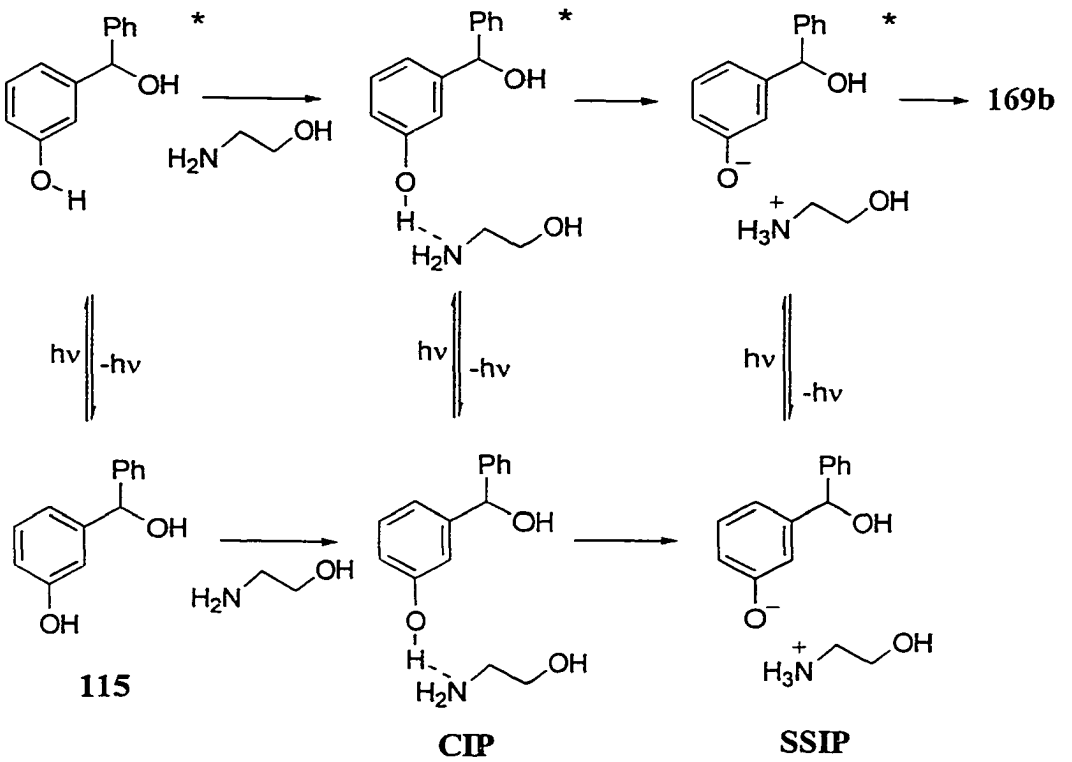

Scheme 3.3

3.6.1.2 Transients Formation from 120

Transients generated from photolysis of **120** are cation **174** in acidic solution (pH < 4) and α-phenyl-*m*-QM (**175**) in basic solution (pH > 9), while probably a mixture of **174** and **175** are present in intermediate pHs. There is no product formed and no transient observed in neat organic solution. With the addition of water, the transient yield (monitored at 440 nm, a wavelength where both **174** and **175** absorb) increased drastically, indicating that water is essential for the formation of both transients.

Following a similar rationale as that used for *m*-QM **169b** (from **115**), the mechanism for generation of **175** from **120** in basic solution is excitation of the phenolate

ion to S_1, which subsequently dehydroxylates to form the transient (Scheme 3.4). In acidic solution, the mechanism of formation of cation **174**, involves an acid catalyzed loss of hydroxide ion. Consistent with this proposal is the fact that studies of methoxy compound **158** showed that the yield of cation **173** decreased quickly with increase in pH; no cation was formed in neutral solution. Formation of cation **174** in neutral pH, if **174** is one of the transients, must be via an alternative pathway.

QMs can be quenched in two different ways to form either the corresponding phenolate ion or the carbocation, both of which eventually return to starting material. Because **175** has a significant lifetime in neutral solution, protonation to form cation **174**, which also absorbs in the same wavelength, occurs. This is why the decay at these pHs consist of two species: a fast equilibrium between **175** and **174** is probably established, which is not possible for the much shorter lived **169b** (Scheme 3.4).

No products derived from initial bond homolysis were observed in the photolysis and no radicals were observed in aqueous solution in LFP studies. McClelland and coworkers[47] have reported that photolysis of benzhydrol generated short-lived diphenylmethyl cation accompanied with diphenyl radical in 2:1 H_2O-CH_3CN, the former was not observed in neat CH_3CN, which is consistent with our results. Although substituted benzhydrols have not been studied, results of para-substituted diarylmethyl chlorides showed that the ratio of [cation] to [radical] increased with the presence of an electron-donating group on the phenyl ring. One conclusion reached in the Thesis is that the strongly electron-donating O^- favors formation of only cationic transients. This might

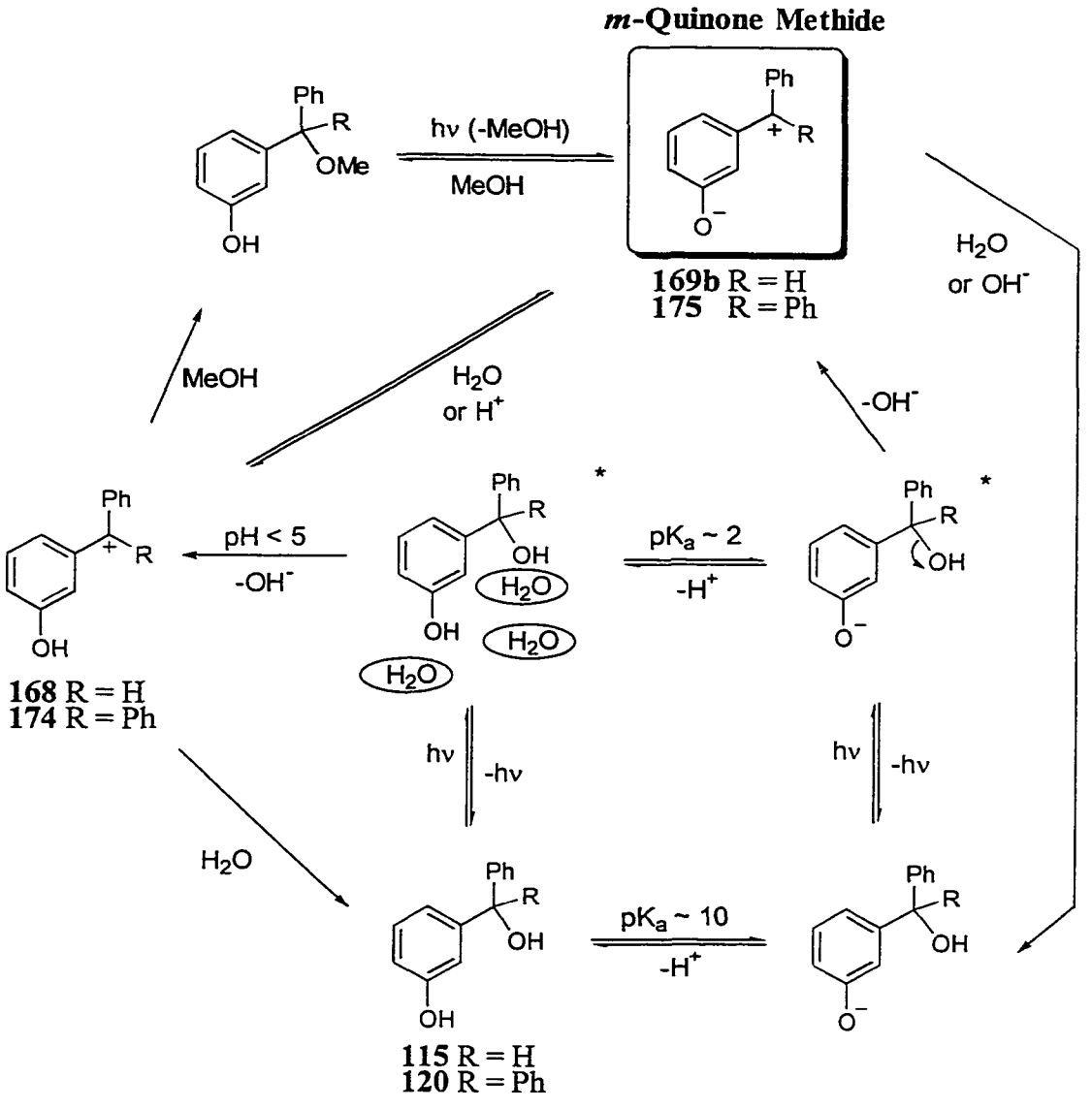

Scheme 3.4

be the reason why no radicals were observed. Peters et al.[23] have demonstrated using ps LFP that singlet trityl methanol failed to generated any cation while the 4,4'-NMe_2-substituted derivative cleaved heterolytic (within 300 ps). However, they did not record absorptions below 500 nm where radical absorption would appear. Later on, Peters et al.[50]

determined k_{ET} (electron transfer rate constant) from radical pair to ion pair for diphenyl chloride and derivatives which were in the 10^9 to 10^{10} range (beyond the limit of the LFP system used in this Thesis). Thus, initial homolysis followed by a fast electron transfer to give ion pairs cannot be strictly ruled out.

3.6.2 Mechanism for Generation of Condensation Product

Product studies of **120** in basic aqueous solution give condensation products (Scheme 3.1). Since the phenol of **120** is deprotonated in base, the resulting phenolate is nucleophilic and can attack the positive benzylic carbon of photogenerated *m*-QM **174**. Wan and Hennig[131] in their study of *o*-hydroxybenzyl alcohol **48** in base showed that a photocondensation product (phenol-formaldehyde type oligomers) was observed (Scheme 1.13), in which the phenolate attacks via the benzene ring. Such a mode of attack is not observed for **120**. Rather, the condensation product observed for **120** arises via attack of the phenolate oxygen. Scheme 3.5 illustrates the proposed mechanism for photogeneration of condensation products for **120**. Phenolate **120**$^-$ is the predominant species in basic solution. Upon irradiation of **120**, α-phenyl-*m*-QM (**174**) is generated which is then trapped by either OH^- to give **120**$^-$, or by **120**$^-$ to give the phenolate of **164**. In wholly aqueous solution, **164** precipitates from solution, which is the product characterized in this solvent. In basic 1:1 H2O-CH3CN. **164** (or its phenolate) is soluble and further photocondensation occurs to give oligomeric **165**.

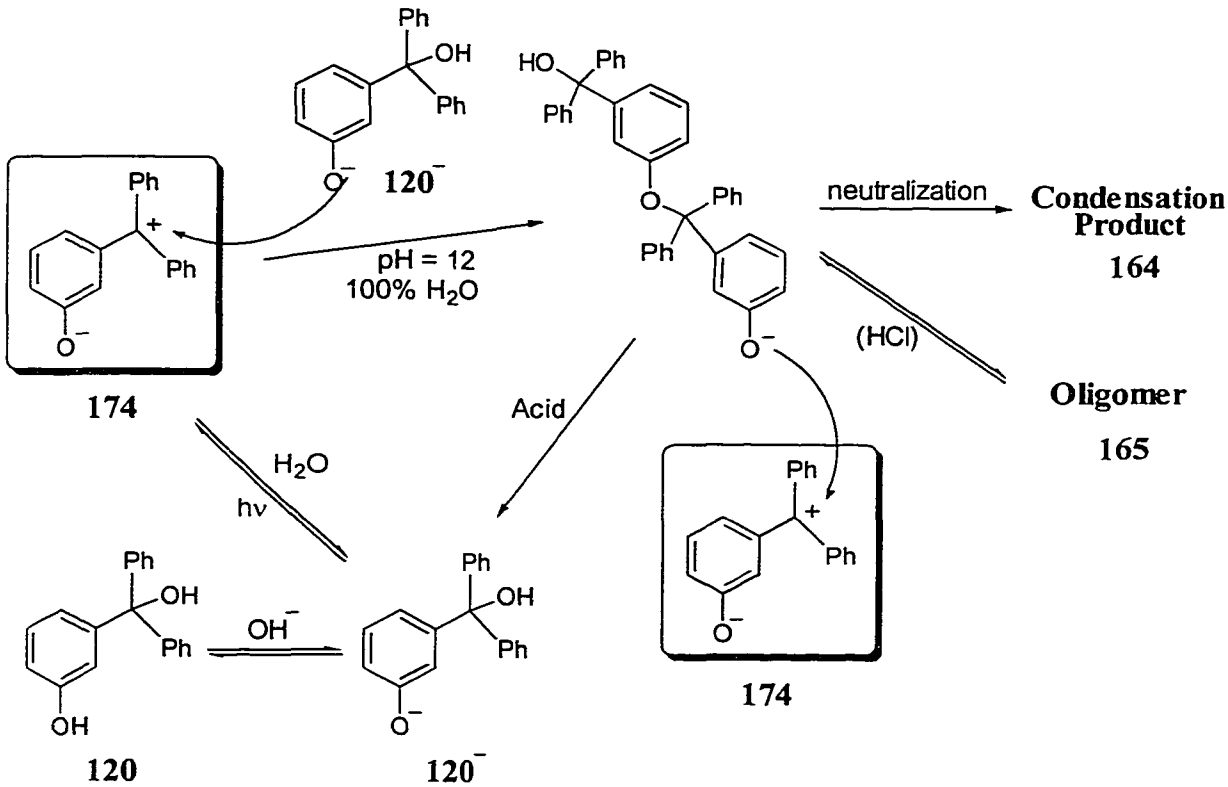

Scheme 3.5

3.7 Summary

Meta-hydroxybenzyl alcohols are only reactive upon photolysis in aqueous solution. Parallel to the ortho and para isomers, product studies gave corresponding methyl ether in high quantum yield in aqueous methanol, while no methyl ether products were observed for the corresponding methoxy analogues. Interestingly, methyl ether **160** also showed reactivity upon photolysis in aqueous acetonitrile to afford *m*-hydroxybenzhydrol. LFP generated strongly absorbing transients, the quantum yields of which increased with the addition of water, corresponding to the decrease of the fluorescence quantum yield. The lifetimes of these species were much longer than similar

diarylmethyl cations observed by McClelland et al.[47,66] Also, the transients generated can be quenched by both nucleophiles and electrophiles (H^+), which were subsequently identified as *m*-QMs. The water-assisted mechanism offered in Chapter 2 is proposed to be operating for the generation of *m*-QMs, which is supported by the observation of weak phenolate ion emission and the fluorescence behavior of model compounds.

The relative product quantum yields from hydroxybenzhydrols are summarized in Table 4.1, which shows that the quantum efficiencies for QMs generations are in the order of $o > m >> p$, in agreement with Zimmerman's *ortho-meta* activation theory.

A polymerization reaction of *m*-QMs has been discovered in basic media during investigations of their chemistry. In spite of the low concentration and short lifetime of *m*-QMs, phenolates of hydroxybenzhydrols gave condensation products by nucleophilic attack under basic condition. It is clear that the photochemistry of hydroxybenzyl alcohols in aqueous solution is a source of rich chemistry, which requires further investigations.

Chapter 4

Experimental

4.1 General

^{1}H NMR spectra were recorded on either a Perkin-Elmer R32 (90 MHz), a Bruker AC 300 (300 MHz) or a Bruker AM 360 (360 MHz) instrument using chloroform-*d*, acetonitrile-d_3 or acetone-d_6 as solvents. Tetramethylsilane (TMS) was used as an internal standard on the 90 MHz instrument. Chemical shifts were reported in ppm downfield from TMS and splitting patterns were designated as s, singlet; d, doublet; t, triplet; q, quartet; m, multiplet and b, broad. Mass spectra were taken on either a Finnigan 3300 (CI) or a Kratos Concept H (EI and FAB) instruments. Melting points were determined on a Koefler hot stage microscope (uncorrected). UV-Vis spectra were recorded either on a Phillips PU 8740, Varian Cary 1 or Cary 5 or a Pye Unicam SP8-400 spectrophotometer, or using nanosecond laser flash photolysis (LFP) with a Spectra Physics YAG laser Model GCR-12 (266 nm, ≤70 mJ/pulse) as excitation source. Steady state fluorescence spectra (uncorrected) were recorded on a Perkin-Elmer MPF-66 or Photon Technology International (PTI) A-1010 fluorimeter. Fluorescence lifetime was obtained by a PTI LS-1 Time-Correlated Single Photon Counting system or picosecond fluorescence system equipped with Ti:Sapphire laser. Sonication was done on Bransonic 220 ultrasonic cleaner (50/60 Hz). pH Measurements were performed on a Corning 140 pH meter. Analytical thin layer chromatogaphy (TLC) was performed on precoated silica

gel plates (Macherey-Nagel, Sil/UV-Vis_{254}), using solvent systems as indicated in each experiment. Preparative TLC was carried out on 20 cm × 20 cm silica gel GF 1000 micrometer Uniplates (Analtech).

4.2 Materials

4.2.1 Commercially Available Reagents

Methylene Chloride (A.C.S., reagent grade) was distilled before use. Anhydrous THF was obtained by distillation over potassium. Acetonitrile was either HPLC grade for photolysis, UV and LFP studies or freshly distilled over CaH_2 under N_2 for steady state fluorescence measurements. HPLC grade MeOH was stirred with $NaHCO_3$ for at least one hour to remove any trace of acid prior to photolysis. Ethanol (95%) and cyclohexane (HPLC) were used as received. Deuterated solvents, including D_2O, $CDCl_3$, $(CD_3)_2CO$ and CD_3CN were purchased from Cambridge Isotopes (99.9% D). Standard buffers were purchased from Fisher. Aqueous solutions of the appropriate pH were used directly or diluted from standardized stock of NaOH or H_2SO_4 with known concentration. Prior to photolysis, pH values were checked by a pH meter.

Hydroxybenzyl alcohols **48**, **49**, and **111** and benzofuran-2(3*H*)-one (**113**) were purchased from Aldrich and re-crystallized before use (**48** and **49** from toluene; **111** from benzene; **113** from 95% ethanol in an acetone/dry ice bath). 2,5-Dihydroxyphenylacetic-γ-lactone (**148**) and *o*-benzylphenol (**126**) were also Aldrich Reagents and used as received. ^1H NMR and GC analysis showed that they were > 98% pure. Ethyl vinyl ether (EVE) (Aldrich) was refrigerated prior to use. Ethanolamine (Aldrich) was distilled before

use. *o*-Methoxybenzhydrol (**125**) was available in the laboratory: MS (CI) m/z 197 (M^+-17, base peak), 215 (M^++1); (EI) 214 (M^+); ^{1}H NMR (300 MHz, acetone-d_6) δ 3.8 (s, 3H), 4.6 (d, 1H, D_2O exchangeable), 6.1 (d, 1H), 6.8-7.6 (m, 9H).

4.2.2 Synthesis

Grignard reaction. Magnesium was washed with dilute HCl to remove magnesium oxide and thoroughly dried. Pre-dried PhBr was dissolved in freshly distilled THF and added drop wise (under N_2) to magnesium/THF (a pinch of I_2 added) in an ice bath, which was then vigorously stirred. After the addition, the reaction mixture was refluxed for 1 hour and cooled to room temperature. The reacting PhMgBr was transferred to a dropping funnel and added drop wise to a THF solution of the approprate carbonyl compound. After addition, the solution was refluxed and reaction progress monitored by NMR. Work-up consisted of the addition of saturated aqueous NH_4Ac to a cooled solution to quench excess PhMgBr. Diluted HCl was also used to further acidify the solution if required. The solution was then extracted with CH_2Cl_2.

$NaBH_4$ reduction. Following the standard procedure,[155] the ketone or aldehyde was dissolved in 50-100 mL MeOH and cooled in an ice bath. To this stirred solution, a suspension of $NaBH_4$ in ice water was added dropwise. The solution was then heated to 40-50 °C for 1-2 h. After cooling by ice, the solution was neutralized with aqueous NH_4Cl and extracted with 3 × 50 mL CH_2Cl_2. The organic solvent was removed using a rotary evaporator and residue was dried on a vacuum pump.

3-Methoxy-4-hydroxybenzyl alcohol (128). Using the $NaBH_4$ reduction method, 5 g (0.033 mole) of 3-methoxy-*p*-hydroxybenzaldehyde was reduced by 1.25 g (0.033 mole) $NaBH_4$. The crude product was re-crystallized from ligroin to give pure **128**, mp. 110-112 °C; MS (CI) m/z 137 (base peak, (M^+-17), 155 (M^++1); ^{1}H NMR (300 MHz, acetone-d_6) δ 3.8 (s, 3H), 4.0 (t, 1H, D_2O exchangeable), 4.5 (d, 2H), 6.7 (t, 2H), 7.0 (s, 1H), 7.4 (s, 1H, D_2O exchangeable).

3,5-Di-*t*-butyl-4-hydroxybenzyl alcohol (129). Using the $NaBH_4$ reduction mechod, 5 g (0.021 mole) of 3,5-di-*t*-butyl-*p*-hydroxybenzaldehyde was reduced by 5 g $NaBH_4$ (0.132 mole) following the general procedure. Pure **129** was obtained by recrystallization from hexane, mp. 139-142 °C; MS (CI) m/z 219 (base peak, (M^+-17), 237 (M^++1); ^{1}H NMR (300 MHz, acetone-d_6) δ 1.4 (s, 18H), 4.0 (t, 1H, D_2O exchangeable), 4.5 (d, 2H), 5.9 (s, 1H, D_2O exchangeable), 7.2 (s, 2H).

***o*-Hydroxybenzhydrol (112).** Method A: To a stirred solution of salicyaldehyde (Aldrich, 2.0 g, 17.9 mmole) in 50 mL of dry THF, 30 mL of 1.8 **M** phenyllithium solution (54 mmole) was added under nitrogen in a dry ice-acetone bath. After reflux (4 h), the reaction mixture was cooled to room temperature and 50 mL of wet THF was added carefully followed by a further 10 min reflux to decompose the excess phenyllithium. The reaction mixture was then transferred to a 500 mL erlenmeyer flask and 100 mL of ice water was added and the solution acidified with saturated NH_4Cl. The solution was extracted with diethyl ether (3 × 70 mL). Removal of the ether afforded an oil (3.2 g, 90%), which solidified overnight. Method B: Following the general procedure

described above for making PhMgBr, 10 g salicyaldehyde (0.08 mole) was reacted with PhMgBr (0.24 mole). The crude yellow solid was re-crystallized from 1:1 toluene-hexane to afford pure **112** as white crystal, mp. 86-87 °C (literature: 54-55 °C,[103] yellow crystal); MS (CI) m/z 183 (base peak, (M^+-17); ^{1}H NMR (300 MHz, acetone-d_6) δ 4.3 (b, 1H, D_2O exchangeable), 6.1 (s, 1H), 6.7-7.3 (m, 9H), 8.6 (b, 1H, D_2O exchangeable).

3-Phenylisocoumaranone (121). The compound was made according to the procedure of Padwa and coworkers.[127b] To an ice-cooled mixture of finely pulverized phenol (26.5 g) and mandelic acid (30.45 g) was added 80 mL of a 70% sulfuric acid solution. The mixture was stirred at 0 °C until dissolution was nearly obtained and then heated at 115 °C for 45 min. The mixture was cooled to room temperature, poured into 400 mL of ice water slurry, and extracted with three 100 mL portions of methylene chloride. The combined organic layers were washed with 100 mL of a saturated aqueous sodium bicarbonate solution and dried over magnesium sulfate. The evaporation of the solvent under reduced pressure gave a red liquid as the crude product. When placed under vacuum, crystals slowly formed. White crystals were obtained after recrystallization from 95% ethanol, mp. 111-114 °C (literature: 113-114 °C[127b]); MS (CI) m/z 211 (M^++1, base peak), 183 (M^+-28); ^{1}H NMR (300 MHz, acetone-d_6) δ 5.2 (s, 1H), 7.1-7.5 (m, 9H).

***m*-Hydroxybenzhydrol (115).** Method A: Crude **115** was obtained by reducing *m*-hydroxybenzophenone (2.6 g, 0.013 mole) with $NaBH_4$ (0.75 g, 0.019 mole) following the general procedure. Method B: Following the general procedure using PhMgBr, 4.3 g Mg (0.18 mole) and 27.4 g PhBr (0.18 mole) were used to make the Grignard reagent,

which was reacted with 7 g of *m*-hydroxybenzaldehyde (0.057 mole) to give a brownish solid. The crude product was re-crystallized from 8:1 toluene-ligroin to afford white fine needle-like crystals, mp. 115 °C; MS (CI) m/z 183 (M^+-17, base peak), 201 (M^++1); ^{1}H NMR (300 MHz, acetone-d_6) δ 4.7 (d, 1H, D_2O exchangeable), 5.7 (d, 1H), 6.4-7.5 (m, 9H), 8.2 (s, 1H, D_2O exchangeable).

α-Methoxy-*m*-hydroxybenzhydrol (160). This compound was made via exhaustive photosolvolysis (≈ 30 min) of 200 mg of **115** in 200 mL 1:1 H_2O-MeOH (1 mL 1 **M** NaOH added) (≈ 70% yield). It was purified by preparative TLC (1:9 CH_3CN-CH_2Cl) and **160** was recovered as a yellow liquid which was dried on a vacuum pump; MS (CI) m/z 183 (M^+-31, base peak), 214 (M^+), 215 (M^++1); ^{1}H NMR (300 MHz, acetone-d_6) δ 3.3 (s, 3H), 5.2(s, 1H), 6.6-7.5 (m, 9H), 8.2 (s, 1H, D_2O exchangeable).

***m*-Methoxybenzhydrol (157).** Using the general procedure for PhMgBr, 10 g of *m*-anisaldehyde (0.074 mole) was reacted with PhMgBr (0.24 mole). The crude product (yellow oil) was distilled under reduce pressure to afford pure **157** (clear oil); MS (CI) m/z 197 (M^+-17, base peak), 215 (M^++1); ^{1}H NMR (300 MHz, acetone-d_6) δ 3.7 (s, 3H), 4.8 (d, 1H, D_2O exchangeable), 5.8 (d, 1H), 6.7-7.5 (m, 9H).

***p*-Hydroxybenzhydrol (116).** Following the general procedure for $NaBH_4$ reduction, *p*-hydroxy-benzophenone (1.98 g, 0.01 mole) was reduced by $NaBH_4$ (0.75 g, 0.02 mole). The crude product was re-crystallized from toluene to afford **116**, mp. 159-162 °C; MS (CI) m/z 183 (M^+-17, base peak), 201 (M^++1); ^{1}H NMR (300 MHz, acetone-

d_6) δ 4.6 (d, 1H, D_2O exchangeable), 5.7 (d, 1H), 6.4-7.5 (m, 9H), 8.2 (s, 1H, D_2O exchangeable).

3-Methoxy-4-hydroxybenzhydrol (117). Following the general procedure for PhMgBr, 1 g Mg (0.042 mole) and 6.54 g (0.042 mole) PhBr were used to produce PhMgBr which was subsequently reacted with 1.27 g (0.008 mole) of 3-methoxy-4-hydroxybenzaldehyde. On work-up, the resulting yellow oil was twice eluted through a silica gel column (CH_2Cl_2) which afforded **117** as a pure clear oil: MS (CI) m/z 213 (M^+-17), 231 (M^+); ^1H NMR (300 MHz, acetone-d_6) δ 3.4 (s, 3H), 4.6 (d, 1H, D_2O exchangeable), 5.7 (d, 1H), 5.9 (d, 1H, D_2O exchangeable), 7.0-7.5 (m, 8H).

3,5-Dibutyl-4-hydroxybenzhydrol (118). Following the general procedure for PhMgBr, 1 g Mg (0.042 mole) and 6.54 g (0.042 mole) PhBr were used to produce PhMgBr which was subsequently reacted with 3.36 g (0.014 mole) of 3,5-di-*t*-butyl-4-hydroxybenzaldehyde. The crude product was obtained as an orange solid which was re-crystallized in ligroin to give white crystals, mp. 123-124 °C; MS (CI) m/z 295 (M^+-17, base peak), 313 (M^++1); ^1H NMR (300 MHz, acetone-d_6) δ 1.4 (s, 18H), 4.6 (d, 1H, D_2O exchangeable), 5.7 (d, 1H), 5.9 (d, 1H, D_2O exchangeable), 7.0-7.5 (m, 7H).

***p*-Methoxybenzhydrol (127).** *p*-Methoxybenzophenone (2 g, 0.01 mole) was reduced using $NaBH_4$ (4.29 g, 0.13 mole) according to the general procedure. The crude product was re-crystallized from petroleum ether to give a white crystalline solid, mp. 59-62 °C; MS (CI) m/z 197 (M^+-17, base peak), 215 (M^++1); (EI) 214 (M^+); ^1H NMR (300

MHz, acetone-d_6) δ 3.7 (s, 1H), 4.7 (d, 1H, D_2O exchangeable), 5.8(d, 1H), 6.7-7.5 (m, 9H), 8.2 (s, 1H, D_2O exchangeable).

α,α-Diphenyl-*o*-hydroxybenzyl Alcohol (119). Following the general procedure for PhMgBr, Mg (4.2 g, 0.17 mole) and PhBr (27 g, 0.17 mole) were used to make the PhMgBr, which then reacted with *o*-hydroxybenzoic acid methyl ester (4.5 g, 0.03 mole). The crude product was re-crystallized from toluene to afford a white crystalline solid, mp. 148-150 °C; MS (CI) m/z 259 (M^+-17, base peak); ^{1}H NMR (360 MHz, acetone-d_6) δ 6.4 (s/b, 1H, D_2O exchangeable), 6.4-7.5 (m, 14H), 9.1 (s/b, 1H, D_2O exchangeable); (300 MHz, $CDCl_3$) δ 3.7 (s, 1H, D_2O exchangeable), 6.4-7.4 (m, 14H), 8.1 (s, 1H, D_2O exchangeable).

α,α-Diphenyl-*m*-hydroxybenzy Alcohol (120). The methyl ester of m-hydroxy-benzoic acid was prepared by refluxing 20 g of *m*-hydroxybenzoic acid in 400 mL MeOH with 1 mL conc. H_2SO_4 for 10 h. After cooling to room temperature, 2-4 g of $NaHCO_3$ was added with stirring and most of the MeOH evaporated. To this was added 200 mL of CH_2Cl_2 and the solution back-washed with water and saturated aqueous $NaHCO_3$. Crude *m*-hydroxybenzoic methyl ester was obtained after removal of the solvent and used without further purification.

Using the Grignard reaction procedure, 2 g of *m*-hydroxybenzoic methyl ester (0.013 mole) was reacted with PhMgBr produced from 2 g Mg (0.083 mole) and 13 g PhBr (0.084 mole), to generate a yellow gel as the crude product. The product was re-crystallized from CH_3CN to give white crystals, mp. 151-152 °C; MS (CI) m/z 199 (M^+-

77, base peak), 277 (M^++1); ^{1}H NMR (300 MHz, acetone-d_6) δ 5.2 (s, 1H, D_2O exchangeable), 6.6-7.4 (m, 14H), 8.2 (s, 1H, D_2O exchangeable).

α,α-Diphenyl-*m*-methoxybenzy Alcohol (158). The methyl ester of *m*-anisic acid was propared by reducing 15 g of *m*-anisic acid in 400 mL MeOH with 1 mL conc. H_2SO_4 for 19 h. A similar work-up as above gave *m*-methoxybenzoic acid methyl ester as product. Using the general Grignard reaction procedure, 2.5 g (0.015 mole) *m*-methoxybenzoic acid methyl ester was reacted with PhMgBr produced from 2 g Mg (0.083 mole) and 13 g PhBr (0.084 mole) to generate a yellow gel as product. The crude product was eluted with CH_2Cl_2 through a silica column and then re-crystallized from $CHCl_3$–hexane to give a mixture of transparent crystals and white precipitate. The transparent crystals, which were separated by hand, were pure **158**, mp. 84-87 °C; MS (CI) m/z 273 (M^+-17, base peak), 291 (M^++1); ^{1}H NMR (300 MHz, acetone-d_6) δ 3.7 (s, 3H), 5.3 (s, 1H, D_2O exchangeable), 6.7-7.4 (m, 14H).

***m*-Benzylphenol (159).** A THF solution of 2.0 g of **115** was shaken under H_2 (2 atm) for 30 h. The product mixture was eluted by CH_2Cl_2 in a silica column which gave the initial crude product. Colorless **170** was obtained by distillation under reduced pressure: MS (CI) m/z 185 (M^++1); ^{1}H NMR (300 MHz, acetone-d_6) δ 3.9 (d, 2H), 6.6-6.8 (m, 3H), 7.0-7.4 (m, 6H), 8.2 (s, 1H, D_2O exchangeable).

4.3 Product Studies

All preparative photolysis were carried out in a Rayonet RPR 100 photochemical reactor equipped with 254 lamps, using quartz tubes (100-200 mL) which were cooled

with an internal cold finger (tap water, < 15 °C). Solutions were continuously purged with a stream of argon via a stainless steel syringe needle for 10 min before and during the irradiation, to effect stirring and deoxygenation. The length of photolysis varied from 3-60 min depending on the conversion desired. After photolysis, work-up involved adding a saturated aqueous solution of NaCl and extracting with 5 × 75 mL portions of CH_2Cl_2. The organic extracts were then combined and dried over $MgSO_4$. Filtration of the $MgSO_4$ and evaporation of CH_2Cl_2 under reduced pressure provided crude photochemical products, which were then separated by preparative TLC if necessary and characterized by ^{1}H NMR and mass spectroscopy. Control experiments were repeated in the absence of light at room temperature (≈ 22 °C). Possible thermal reactions in photomethanolysis were eliminated by the addition of a pinch of $NaHCO_3$.

Photolysis *o*-hydroxybenzhydrol (112). A solution of 40 mg **112** in 100 mL 1:1 H_2O-MeOH ($NaHCO_3$ treated) was photolyzed at 254 nm. ^{1}H NMR analysis showed that ether **123** was the only product in low conversion runs and *o*-benzylphenol **126** was formed only in high conversion runs. Preparative TLC separation afforded pure **123**: MS (CI) m/z 183 (M^+ -31, base peak); ^{1}H NMR (300 MHz, acetone-d_6) δ 3.3 (s, 3H), 5.7 (s, 1H), 6.7-7.4 (m, 9H), 8.5 (s, 1H, D_2O exchangeable). The identity of **126** was confirmed by comparison with an authentic sample.

For time dependent studies, a solution of 75 mg of **112** dissolved in 150 mL of 1:1 H_2O-MeOH. After photolysis at set time periods, 20-25 mL was taken out, worked-up and analyzed by ^{1}H NMR.

pH Studies used 1:1 H_2O-MeOH as solvent with the pH measured for the aqueous portion. Typically, 40 mg of **112** was dissolved in 100 mL solvent and photolyzed for 3 min. It showed that dark reaction is inevitable below pH 5. The only photoproduct in basic solution was **123**.

Photolysis *p*-hydroxybenzhydrol (116). A solution of 40 mg of **116** in 100 mL 1:1 H_2O-MeOH ($NaHCO_3$ treated) was photolyzed at 254 nm for 3 min.. Methyl ether **130** was the only product purified by preparative TLC: MS (CI) m/z 121 (M^+ -93, base peak), 183 (M^+ -31), 215 (M^+ +1); ^1H NMR (300 MHz, acetone-d_6) δ 2.9 (s, 3H), 5.2 (s, 1H), 6.6-7.4 (m, 9H), 8.3 (b, 1H, D_2O exchangeable).

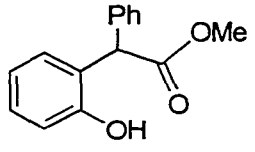

176

Photolysis of 3-phenylisocoumaranone (121). A solution of 40 mg of **121** in 100 mL 1:1 H_2O-MeOH ($NaHCO_3$ treated) was photolyzed at 254 nm for 3 min. Product **176** (100%) was formed with ^1H NMR (300 MHz, acetone-d_6) δ 3.7 (s, 3H), 5.4 (s, 1H), 6.6-7.6 (m, 9H), 8.7 (s, 1H, D_2O exchangeable); MS (CI) m/z 243 (M^++1, base peak), 211 (M^+-31). It appears that the addition of $NaHCO_3$ introduced an alternative chemistry.

A solution of 40 mg **121** in 100 mL 1:1 H_2O-MeOH was photolyzed at 254 nm for 3 min. The ^1H NMR of the product mixture showed that ≈ 3% of **123** was formed, as

indicated by the characteristic methoxy singlet at δ 3.3 (s, 3H) and methine singlet at δ 5.7 (s, 1H).

Photolysis of α,α-Diphenyl-*o*-hydroxybenzyl Alcohol (119). A solution of 55 mg **119** in 100 mL 1:1 H_2O-MeOH ($NaHCO_3$ treated) was photolyzed at 254 nm for 3 min. The product was its methyl ether **135** (28%), purified by preparative TLC: MS (CI) m/z 259 (M^+ -31, base peak); ^1H NMR (300 MHz, acetone-d_6): δ 3.2 (s, 3H), 5.6 (s, 1H), 6.4-7.8 (m, 14H), 8.7 (s, 1H, D_2O exchangeable).

A solution of 30 mg **119** was dissolved in 100 mL H_2O (pH 7 and 12), with 25 mL of CH_3CN as co-solvent. Solutions were photolyzed 10 min. at 254 nm. The product mixture in base was neutralized before work up. The ^1H NMR showed that starting material was recovered for both runs.

Photolysis *m*-hydroxybenzhydrol (115). A solution of 100 mg of **115** was dissolved in 100 mL 1:1 H_2O-MeOH and photolyzed at 254 nm for 5, 30 and 60 min, respectively. An additional sample was photolyzed for 20 min with the addition of 1 mL of 1N NaOH. Resulted product mixture contained **160** (methoxy singlet δ 3.3 (s, 3H)) and **159** (methine δ 3.9 (d, 2H)) (Table 3.1), purified by preparative TLC (See synthesis). Trace amount of dimers (< 2%) were also separated from 60-min run product mixture. Compound **163**: ^1H NMR (300 MHz, acetone-d_6) δ 3.2 (s, 3H), 5.2 (s, 1H), 6.3 (s, 1H), 6.8-7.8 (m, 18H), 8.3 (s, 1H, D_2O exchangeable); MS (FAB/LSIMS, mNBA as Matrix) m/z 395 (M^+-1, base peak). Product **162**: ^1H NMR (300 MHz, acetone-d_6) δ 3.9 (s, 2H),

6.3 (s, 1H), 6.6-7.6 (m, 18H), 8.3 (s, 1H, D_2O exchangeable); MS (FAB/LSIMS, mNBA as Matrix) m/z 365 (M^+-1, base peak).

A solution of **115** (100 mg) in 100 mL 1:9 H_2O-CH_3CN with 5 mL EVE was photolyzed for 1 h. No product was found other than EVE polymers. Using 4:1 H_2O-CH_3CN solvent, two aldehydes were separated as major products in low yields (< 5%). *m*-hydroxybenzaldehyde (**166**) (< 5%): ^1H NMR (300 MHz, acetone-d_6) δ 10.0 (s, 1H), 8.7 (s, 1H, D_2O exchangeable), 7.0-8.5 (m, 4H); MS (CI) m/z 123 (M^++1). Aldehyde **167** (~ 9%): ^1H NMR (300 MHz, acetone-d_6) δ 9.7 (t, 1H), 8.3 (s, 1H, D_2O exchangeable), 6.6-7.8 (m, 9H), 4.6 (t, 1H), 3.1 (dd, 1H); MS (CI) m/z 183 (M^+-43, base peak), 227 (M^++1).

Photolysis of α-phenyl-*m*-hydroxybenzhydrol (120). A solution of 55 mg **120** in 100 mL 1:1 H_2O-MeOH ($NaHCO_3$ treated) was photolyzed at 254 nm for 3 min. Product was methyl ether **161** (10%), purified by preparative TLC: MS (CI) m/z 259 (M^+ -31, base peak), 291 (M^++1); ^1H NMR (300 MHz, acetone-d_6) δ 3.0 (s, 3H), 6.6-7.4 (m, 14H), 8.2 (s, 1H, D_2O exchangeable).

Solutions of 20 mg **120** were dissolved in 1:1 H_2O-MeOH with water portion pH as 1, 6 and 13, respectively and photolyzed for 10 min to give 41% (acid), 59% (neutral) and 83% (base) methyl ether **161**.

A solution of 200 mg **120** was dissolved in 200 mL neat water (pH 12) and photolyzed at 254 for 30 min (vigorous Ar purge) which resulted in very cloudy (milky) solution. The product mixture was worked up by adding large amounts of aqueous NH_4Cl

to aggregate the fine, pale yellowish precipitate, which was then filtered out of the solution and allow to dry on the filter paper. ^{1}H NMR (300 MHz, acetone-d_6) showed that a new product was formed (> 80%) which was identified as condensation product **164**: δ 5.1 (s, 1H, D_2O exchangeable), 6.4 (t, 1H), 6.6-7.4 (m, 27H), 8.2 (s, 1H, D_2O exchangeable); MS (CI) m/z 199 (M^+-77, base peak), 277 (M^++1); (Negative FAB/LSIMS, mNBA as Matrix) m/z 533 (M^+-1, base peak).

A solution of 100 mg **120** in 100 mL 1:1:2 1 **M** NaOH solution-H_2O-CH_3CN was photolyzed at 254 nm for 30 min. A clear and pale yellow solution was obtained. To this solution, 320 mL of water was added to give milky solution, which aggregated upon the addition of aqueous NH_4Cl. The yellow precipitate thus obtained was filtered out and allowed to dry on a filter paper. ^{1}H NMR (300 MHz, acetone-d_6) showed no starting material: δ 5.1 (s, D_2O exchangeable), 6.4 (t), 6.5-7.4 (m), 8.4 (s, D_2O exchangeable), where the proton number could not be resolved because of the large number of aromatic protons. MS (CI) m/z 183 (M^+-93, base peak), 277 (M^++1); (Negative FAB/LSIMS, mNBA as Matrix) 258 (M^+-18, base peak), n × 258 + 275 (n from 1 to 10, Fig.3.3). Therefore, the product was identified as a mixture of oligomer **165**.

Photolysis of α-methoxy-*m*-hydroxydiphenyl methane (160). A solution of 25 mg **160** in 50 mL 1:1 H_2O-CH_3CN was photolyzed for 20 min. The resulting mixture, separated by preparative TLC, had **115** as major product (66.5%), along with 3% reduced product **159** (methine δ 3.9 (d, 2H)) and 0.7% of aldehyde **166** (δ 10.0 (s, 1H)). 20 min further irradiation gave 86% of **115**, 3.8% **159** and 1.2% of aldehyde **166**.

Product quantum yields of the photomethanolysis. The product quantum yield (Φ_p) for the methyl ether formation from **112** in 1:1 H_2O-MeOH was measured by Yang[146] ($\Phi_p = 0.46 \pm 0.03$). This Φ_p value was used as a secondary actinometric standard for the determination of Φ_p's for the rest of the parent and triphenyl alcohols in the same solvent system. Solutions of 40 mg benzhydrols (including **121**) or 55 mg triphenyl alcohols in 100 mL 1:1 H_2O-MeOH ($NaHCO_3$ treated) were photolyzed at 254 nm for 3 min (low conversion irradiation). ^1H NMR integration was employed for calculating the product conversions (Table 4.1).

Table 4.1 The Product Quantum Yield (Φ_p)[a] of Methyl Ether from Methanolysis of Hydroxybenzhydrols and Related Compounds

Compound	Φ_p	Compound	Φ_p	Compound	Φ_p
112	0.46 ± 0.03	**115**	0.40	**116**	0.19
125	0.11	**157**	0	**127**	0
121	~0.08				
119	0.76	**120**	0.27		
		158	0		

[a] Using the Φ_p for the methyl ether formation from **112** in 1:1 H_2O-MeOH, measured by Yang[146] ($\Phi_p = 0.46 \pm 0.03$) as a secondary actinometric standard.

4.4 Transient Absorption and Lifetime Measurements

Transient absorption and lifetime were recorded using Phillips PU 8740, Varian Cary 1 or Cary 5 or a Pye Unicam SP8-400 spectrophotometer. The concentrations of all the samples were ~10^{-2} **M**, with the absorbance at the excitation wavelength kept < 1. Before irradiation, a sample (in a quartz cuvette) was cooled in an ice bath. After irradiation

(no longer than 30 sec), the transient absorption spectrum was recorded and corresponding half lifetime (> 1 s) was determined.

4.5 Steady State Fluorescence and Lifetime Measurements

Steady state fluorescence spectra (uncorrected) were recorded on a Perkin-Elmer MPF-66 (1-2 nm) or Photon Technology International (PTI) A-1010 fluorimeter (0.5-1 nm slit).

Fluorescence lifetimes in ns range (> 2 ns) were obtained by PTI LS-1 Time-Correlated Single Photon Counting (SPC) system using a hydrogen flash lamp as the excitation source (λ_{ex} = 270 nm), with data fit using the iterative reconvolution program. Shorter lifetimes were measured utilizing picosecond fluorescence system equipped with Ti:Sapphire laser (Coherent Mira 900-F) pumped by an Ar ion laser (Coherent Innova 400, 13W).[156] The repetition rate is set with a pulse picker (Coherent 9200) to values which are smaller than the time window being monitored by the Hamamatsu streak camera, which is triggered by a small portion (< 4%) of the IR beam after the pulse picker is split into the photodiode (Thorlabs Inc. 201/579-7227). The rest of the beam is passed through a tripler (CSK SuperTripler 8315) in order to obtain the UV excitation source. The excitation beam is directed from the bottom of the cell to minimize reflections.

Data was acquired using the Hamamatsu Photolumi 2.45f program in the binarization mode, where the intensity of the light collected above a set threshold was measured for each pixel and caused the intensity for each photon blurred over several pixels. As a consequence, the best χ^2 value was 6, larger than unity, for our streak camera.

The sensitivity of the streak camera is not constant over the whole area of the detector and a correction for "shading" (set in the Hamamatsu program) was performed. The shading correction file was acquired for each slit width and wavelength range. To ensure that no photon pile up occurs, i.e. detection of more than one photon per measurement, the number of counts per cycle (CPC) was controlled at < 0.05 (Eq. 4.1), calculated at the emission maximum. The streak camera acquired a number of sequential pulses with frame per cycle set at 30 before the data is transferred to the frame grabber. For each emission decay of the sample, an instrument response function (IRF) profile was also measured with the cell containing solvent. Hamamatsu raw data (both IRF and sample trace) were transformed into PTI fitting software readable files by Labview 4 (National Instruments) program written in house. Excitation wavelength was 285 nm and the sweep range were 2 ns, 5 ns and 20 ns.

$$\text{CPC (Bin)} = \frac{\text{Intensity recorded}}{\text{number of } \lambda \text{ channels} \times \text{frame per cycle} \times \text{number of cycles}} \qquad \textbf{(4.1)}$$

Each sample (~10^{-5} **M**, OD < 0.02) was prepared in 3.0 mL four sided suprasil quartz cuvette with flat transparent bottoms and saturated with a stream of Ar (10 min) prior to the measurement. Samples were stable in fluorimeters and SPC, but decomposed in less than 5 min in ps system, where fresh sample was prepared for each data point.

Absolute fluorescence quantum yields (Φ_f) were measured in CH_3CN, using anisole (Φ_f = 0.29 in cyclohexane)[157] as external standard, for the analysis of observed

decays (Table 4.2). Excitation wavelength was 275 nm. OD_{275} was measured for individual sample and kept at ~0.1. Refractive index was not corrected.

Table 4.2 Fluorescence Quantum Yield[a] Φ_f of Hydroxybenzhydrols and Related Compounds in CH_3CN

Compound	Φ_f	Compound	Φ_f	Compound	Φ_f
112	0.13	**117**	0.22	**118**	0.13
127	0.28	**168**	0.21	**129**	0.15
128	0.25	**170**	0.25		
119	0.09	**122**	0.21		

[a] Measured using anisole ($\Phi_f = 0.29$ in cyclohexane)[157] as external standards.

4.6 Laser Flash Photolysis (LFP) Studies

Nanosecond laser flash photolysis (LFP) experiments were carried out at the University of Victoria LFP Facility at 20 ± 2 °C.[158] A Spectra Physics YAG laser Model GCR-12 (266 nm, ≤ 70 mJ/pulse) was used as excitation source, which is directly aligned on to the sample holder. The laser pulse energies are typically attenuated to less than 20 mJ/pulse by adjusting the high voltage for the flash lamp to avoid multiple photon process. The analyzing beam employed consists of a pulsed 150 W xenon lamp (Oriel housing Model 66057, PTI power supply Model LPS-220) or a DC lamp for lifetimes longer than 5 μs, both 90° angled with the excitation source (laser). The output of the Xe lamp is increased significantly for 4 ms in a wavelength-dependent manner by using a custom-made pulser. Light intensities at fixed wavelengths are detected using a photomultiplier (PMT, Hamamatsu R446, five dynodes)/monochromator (CVI Digikrom 240) system. The high voltage for the PMT tube is set by a custom built programmable

power supply interfaced to the computer. Signals from the PMT are fed into a base line compensation circuit that incorporates a sample and hold amplifier with digital memory based on a published circuit. This unit offsets the background intensity of the Xe lamp. On receiving a trigger pulse, it holds the value of the background intensity (V_0) constant and provides a dc output proportional to its magnitude. The remained transient signal (V_t) can then be measured with high precision using a Tecktronix TDS 520 digital oscilloscope (50 Ω input impedance for transmission experiments) or a Tektronix SCD 1000 digitizer for lifetimes below 100 ns. Spectrally resolved data are recorded with an intensified dual diode array system from Princeton Instruments (DIDA 700/RG, detector controller ST 116, high-voltage gating pulse generator PG200 and ISA spectrometer HR-320). The transient absorption signals were corrected for fluorescence from the sample or for slope in the base line when a total data collection time is equal or longer than 20 μs, depending on the experimental conditions. The correction shot was performed after each signal shot; i.e., for fluorescence correction the lamp shutter remained closed, whereas for base line correction the laser shutter remained closed. The system is fully integrated to a Macintosh IIci computer with a program written using Labview 3.1.1, which could transform the data collected (V_t) into absorbance values (ΔA = -log(1-corrected V_t/V_0)).

Generally, a solution of $OD_{266} \leq 0.3$ was prepared by dilution from a stock solution, followed by 10-min prepurge of oxygen or nitrogen. Experiments were carried out in a flow system (7mm × 7mm quartz cell) with continuous purge of oxygen or nitrogen, to ensure that a fresh solution was irradiated each time in order to avoid

complications from long-lived intermediates and/or photoproducts. The flow rate was set from 2-3 for spectra recording and 5-8 for sample decays.

The absorption spectra of a transient were collected within four time windows, specified according to the signal decay trace obtained at the maximum absorption of the transient. Therefore, the determined ΔA at fixed wavelength was the average of the absorbances within each time frame, while the first trace had the shortest delay and the forth one recorded after the longest delay among the four. Each relative quantum yield of the transient was determined by averaging ΔA_{max} from 4-6 decay traces and a standard deviation was employed as error. When data collecting during one continuous period was not possible, i.e., laser system has to be turned off between experiments, one or two conditions were repeated in the second period under exactly same conditions, including the ground state absorption, flow rate etc.. Thus, the laser power difference could be compensated and a set of comparable results obtained.

4.7 X-Ray Crystallography

X-Ray crystallographic analyses were carried out by Mr. Angus Mackinnon and Professor Judith Howard, Department of Chemistry, University of Durham, U.K.. Crystals of **112** were grown from toluene and **119** from $CHCl_3$-petroleum ether. Crystallographic data are summarized in Table 4.3. Details will be published in due course.

Table 4.3 Crystallographic Data for *o*-Hydroxybenzhydrol (**112**) and α,α-Diphenyl-*o*-Hydroxybenzyl Alcohol (**119**)[a]

Compound	**112**	**119**
Formula	$C_{13}H_{12}O_2$	$C_{19}H_{16}O_2$
MW	199.22	277.33
crystal system	Monoclinic	Monoclinic
space group	P2(1)/n	P2(1)/c
cell dimensions		
a, Å	6.0934(3)	8.3505(2)
b, Å	19.8321(8)	15.0020(2)
c, Å	8.7691(3)	11.4333(3)
α, deg	90	90
β, deg	92.557(2)	95.5050(10)
γ, deg	90	90
V, $Å^3$	1058.65(8)	1425.69(5)
Z	4	4
T, K	150(2)	293(2)
ρ_{calcd}, mg m^{-3}	1.250	1.292
μ, mm^{-1}	0.084	0.083
R (F_0)	0.0809	0.0507
R_w (F_0)	0.1539	0.0837
wavelength, Å	0.71073	0.71073

[a] Data from A. MacKinnon and J. Howard, Department of Chemistry, University of Durham. Details to be published in due course.

References

1. (a) Kagan, J. *Organic Photochemistry: Principles and Applications*; Acacemic Press: San Diego; 1993. (b) Barltrop, J. A.; Coyle, J. D. *Excited states in Organic Chemistry*; John Wiley & Sons Inc.: London; 1975. (c) Calver, J. G.; Pitts, Jr., J. N. *Photochemistry*; John Wiley & Sons Inc.: New York; 1966, pp. 22-23.
2. (a) Strehlow, H. *Rapid Reactions in Solution*; VCH: Weinheim, **1992**. (b) Dorfman, L. M.; Sujdak, R. J.; Bockrath, B. *Acc. Chem. Res.* **1976**, *9*, 352. (c) Wang, Y.; Tria, J. J.; Dorfman, L. M. *J. Phys. Chem.* **1979**, *83*, 1946.
3. Hughes, E. D.; Ingold, C. K.; Patel, C. S. *J. Chem. Soc.* **1933**, 526.
4. Steigman, J.; Hammett, L. P. *J. Am. Chem. Soc.* **1937**, *59*, 2536.
5. Olah, G. A. *Angew. Chem. Int. Ed. Engl.* **1973**, 12, 173.
6. Olah, G. A.; Schleyer, P. V. P. (Eds.) *Carbonium Ions*; Wiley Interscience: New York; 1976, *Vols. 1-5*.
7. Brouwer, D. M.; Hogeveen, H. In *Progress in Physical Organic Chemistry*; Streitwieser, A., Taft, R. W., Eds.; Wiley Interscience: New, York; 1972, Vol. 9.
8. Streitwieser, Jr. A. *Solvolytic Displacement Reactions*; McGraw Hill Book Co.: New York; 1962, P. 42.
9. Turro, N. J. *Modern Molecular Photochemistry*; Benjamin/Cummings, Menlo Park: California; 1978.
10. Neckers, D. C. *Mechanistic Organic Photochemistry*; Reinold: New York; 1976.
11. Coyle, J. D. *Introduction to Organic Photochemistry*; Wiley: New York; 1986.

12. (a) Cristol, S. J.; Bindel, T. H. *Organic Photochemistry* **1983**, *6*, 327. (b) Wan, P.; Yates, K. *Rev. Chem. Intermed.* **1984**, *5*, 157. (c) Kropp, P. J. *Acc. Chem. Res.* **1984**, *17*, 131.

13. Das, P. K. *Chem. Rev.* **1993**, *93*, 119.

14. Zimmerman, H. E.; Sandel, V. R. *J. Am. Chem. Soc.* **1963**, *85*, 915.

15. McClelland, R. A. *Tetrahedron* **1996**, *52*, 6823.

16. (a) Lifschitz, J. *Ber.* **1919**, *52*, 1919; (b) Lifschitz, J.; Joffé, Ch. L. *Z. Physik. Chem.* **1921**, *97*, 426.

17. Weyde, E.; Frankenburger, W. *Trans. Faraday Soc.* **1931**, *27*, 561.

18. (a) Harris, L.; Kaminsky, J. *J. Am. Chem. Soc.* **1935**, *57*, 1154; (b) Calvert, J. G.; Rechen, H. J. L. *ibid.* **1952**, *74*, 2101; (c) Fischer, G. L.; LeBlanc, J. C.; Johns, H. E. *Photochem. Photobiol.* **1967**, *6*, 757.

19. (a) Holmes, E. O. *J. Phys. Chem.* **1957**, *61*, 434. (b) Holmes, E. O. *J. Phys. Chem.* **1958**, *62*, 884.

20. Herz, M. L. *J. Am. Chem. Soc.* **1975**, *97*, 6777.

21. (a) Brown, R. G.; Cosa, J. *Chem. Phys. Letts.* **1977**, *45*, 429. (b) Knauer, K. –H.; Gleiter, R. *Angew. Chem. Internat. Ed.* **1977**, *16*, 113.

22. Cremers, D. A.; Cremers, T. L., *Chem. Phys. Lett.* **1983**, *94*, 102.

23. Peters, K. S.; Manring, L. E. *J. Phys. Chem.* **1984**, *88*, 3516.

24. Spears, K. G.; Gray, T. H.; Huang, D. *J. Phys. Chem.* **1986**, *90*, 779.

25. Havinga, E.; De Jong, R. O.; Dorst, W. *Recl. Trav. Chim. Pays-Bas* **1956**, *75*, 378.

26. Zimmerman, H. E.; Somasekhara, S. *J. Am. Chem. Soc.* **1963**, *85*, 922.

27. (a) Havinga, E.; Kronenberg, M. E. *Pure Appl. Chem.* **1968**, *16*, 137. (b) De-Jongh, R. O.; Havinga, E. *Recl. Trav. Chim. Pays-Bas* **1968**, *87*, 1318. (c) Havinga, E.; Cornelisse, J. *J. Chem. Rev.* **1975**, *75*, 353.

28. Zimmerman, H. E. *J. Am. Chem. Soc.* **1995**, *117*, 8988.

29. (a) Wan, P.; Chak, B.; Krogh, E. *J. Photochem Photobiol. A:* **1989**, *46*, 49. (b) Wan, P.; Chak, B. *J. Chem. Soc. Perkin Trans.* **1986**, *2*, 1751.

30. Ivanov, V. L.; Ivanov, V. B.; Kuz'min, M. G. *J. Org. Chem. U.S.S.R. (Eng. Tran.)* **1972**, *8*, 1263.

31. Ivanov, V. L.; Ivanov, V. B.; Kuz'min, M. G. *Mol. Photochem.* **1974**, *6*, 125.

32. (a) Pincock, J. A. *Acc. Chem. Res.* **1997**, *30*, 43. (b) Hilborn, J. W.; Macknight, E.; Pincock, J. A.; Wedge, P. J. *J. Am. Chem. Soc.* **1994**, *116*, 3337. (c) Pincock, J. A.; Wedge, P. J. *J. Org. Chem.* **1994**, *59*, 5587. (d) Pincock, J. A. In *Handbook of Organic Photochemistry and Photobiology*; Horspool, W. M., Song, P. -S. (Eds.); CRC Press: Boca Raton, FL, 1995; p. 393.

33. DeCosta, D. P.; Pincock, J. A. *J. Am. Chem. Soc.* **1989**, *111*, 8948. (b) Hilborn, J. W.; Pincock, J. A. *J. Am. Chem. Soc.* **1991**, *113*, 2683. (c) DeCosta, D. P.; Pincock, J. A. *J. Am. Chem. Soc.* **1993**, *115*, 2180.

34. (a) Jaeger, D. A., *J. Am. Chem. Soc.* **1975**, *97*, 902. (b) Jaeger, D. A.; Angelos, G. H. *Tetrahedron Lett.* **1981**, 803.

35. Cristol, S. J.; Schloemen, G. C. *J. Am. Chem. Soc.*, **1972**, *94*, 5916.

36. Cristol, S. J.; Greenwald, B. E. *Tetrahedron Lett.* **1976**, 2105.

37. Ivanov, V. B.; Ivanov, V. L.; Kuz'min, M. G. *Zh. Org. Khim.* **1973**, *9*, 340; *J. Org. Chem. USSR* **1973**, *9*, 345.

38. Hyömäki, J.; Koskikallio, J. *Acta Chem. Scand.* **1977**, *A31*, 321.

39. Appleton, D. C.; Bull, D. C.; Givens, R. S.; Lillis, V.; McKenna, J.; McKenna, J. M.; Thackeray, S.; Walley, A. R. *J. Chem. Soc., Perkin Trans. 2* **1980**, 87.

40. (a). Lillis, V.; McKenna, J.; McKenna, J. M.; Smith, M. J.; Taylor, P. S.; Williams, J. H. *J. Chem. Soc., Perkin Trans. 2* **1980**, 83. (b) Lillis, V.; McKenna, J.; McKenna, J. M.; Smith, M. J.; Williams, J. H. *J. Chem. Soc., Chem. Comm.* **1974**, 473.

41. (a). Appleton, D. C.; Bull, D. C.; Givens, R. S.; Lillis, V.; McKenna, J.; McKenna, J. M.; Thackeray, S.; Walley, A. R. *J. Chem. Soc., Perkin Trans. 2* **1980**, 77. (b) Appleton, D. C.; Bull, D. C.; Givens, R. S.; Lillis, V.; McKenna, J.; McKenna, J. M.; Walley, A. R. *J. Chem. Soc., Chem. Comm.* **1974**, 474.

42. Cristol, S. J.; Bindel, T. H. *J. Org. Chem.* **1980**, *45*, 951.

43. Cristol, S. J.; Bindel, T. H. *J. Am. Chem. Soc.* **1981**, *103*, 7287.

44. Ilenda, C. S.; Daughenbaugh, R. J.; Cristol, S. J. *Mol. Photochem.* **1976**, *7*, 287.

45. Stern, O. V.; Volmer, M. *Phisik. Zeitscher.* **1919**, *26*, 183.

46. Lamola, A. A.; Hammond, G. S. *J. Chem. Phys.* **1965**, *43*, 2129.

47. Bartl, J.; Steenken, S.; Mayr, H.; McClelland, R. A. *J. Am. Chem. Soc.* **1990**, *112*, 6918.

48. Peters, K. S.; Li, B. *J. Phys. Chem.* **1994**, *98*, 401.

49. Lipson, M.; Deniz, A. A., Peters, K. S. *J. Phys Chem.* **1996**, *100*, 3580.

50. Lipson, M.; Deniz, A. A., Peters, K. S. *J. Am. Chem. Soc.* **1996**, *118*, 2992.

51. Liler, M. *Reaction Mechanism in Sulfuric Acid*; Academic Press: London, **1971**.

52. Freedman, H. H. In *Carbonium Ions*, Olah, G. A., Schleyer, P. V. R. (Eds.); Wiley: New York, **1973**; *Vol. IV*, Chapter 28.

53. Rosenfeld, T.; Alchalal, A.; Ottolenghi, M. *Chem. Phys. Lett.* **1973**, *20*, 291.

54. (a) Blatz, P. E.; Pippart, D. L. *J. Am. Chem. Soc.* **1968**, *90*, 1296. (b) Blatz, P. E.; Pippart, D. L., *Chem. Commun.* **1968**, 176.

55. (a) Lin, C. I.; Singh, P.; Ullman, E. F. *J. Am. Chem. Soc.* **1976**, *98*, 6711. (b) Lin, C. I.; Singh, P.; Ullman, E. F. *J. Am. Chem. Soc.* **1976**, *98*, 7848.

56. Brown, G. H. *Techniques of Chemistry*; Wiley: New York; **1971**, *Vol. 3*.

57. Manchair, R. N. *Photochem. Photobiol.* **1967**, *6*, 779.

58. Irie, M. *J. Am. Chem. Soc.* **1983**, *105*, 2078.

59. (a) Turro, N. J.; Wan. P. *J. Photochem.* **1985**, *28*, 93. (b) Wan, P.; Yates, K.; Boyd. M. K. *J. Org. Chem.* **1985**, *50*, 2881.

60. Wan, P. *J. Org. Chem.* **1985**, *50*, 2583.

61. Hall, B.; Wan, P. *J. Photochem Photobiol. A:* **1991**, *56*, 35.

62. Parman, T.; Pincock, J. A.; Wedge, P. J. *Can. J. Chem.* **1994**, *72*, 1254.

63. Griffin, C. E.; Kaufman, M. O.; *Tetrahedron Lett.* **1965**, 773.

64. Maycock, A. L.; Berchtold, G. A. *J. Org. Chem.* **1970**, *35*, 2532.

65. Arnold, B.; Donald, L.; Jurgens, A.; Pincock, J. A. *Can. J. Chem.* **1985**, *63*, 3140.

66. McClelland, R. A.; Kanagasabapathy, V. M.; Banait, N. S.; Steenken, S. *J. Am. Chem. Soc.* **1989**, *111*, 3966.

67. Zimmerman, H. E.; Schuster, D. I. *J. Am. Chem. Soc.* **1961**, *83*, 4486.

68. Zimmerman, H. E.; Schuster, D. I. *J. Am. Chem. Soc.* **1962**, *84*, 4527.

69. Barltrop, J. A.; Schofield, P. *J. Chem. Soc.* **1965**, 4758.

70. Pincock, J. A.; Wedge, P. J. *J. Org. Chem.* **1995**, *60*, 4067.

71. Ivanov, V. L.; Ivanov, V. B.; Kuz'min, M. G. *J. Org. Chem. U.S.S.R. (Eng. Tran.)* **1972**, *8*, 626.

72. Ratcliff, Jr. M. A.; Kochi, J. K. *J. Org. Chem.* **1971**, *36*, 3112.

73. (a). Appleton, D. C.; Brocklehurst, B.; McKenna, J.; McKenna, J. M.; Thackeray, S.; Walley, A. R. *J. Chem. Soc., Perkin Trans. 2* **1980**, 87. (b) Appleton, D. C.; Brocklehurst, B.; McKenna, J.; McKenna, J. M.; Smith, M. J.; Taylor, P. S.; Thackeray, S.; Walley, A. R. *J. Chem. Soc., Chem. Comm.* **1977**, 108.

74. Alonso, E. O.; Johnston, L. J.; Scaiano, J. C.; Toscano, V. G. *J. Am. Chem. Soc.* **1990**, *112*, 1270.

75. Pross, A.; Shaik, S. S. *Acc. Chem. Res.* **1983**, *16*, 363.

76. McClelland, R. A.; Kanagasabapathy, V. M.; Steenken, S. *J. Am. Chem. Soc.* **1988**, *110*, 6913.

77. Chateauneuf, J. *J. Chem. Soc., Chem. Commun.* **1991**, 1437.

78. Mecklenburg, S. L.; Hilinski, E. F. *J. Am. Chem. Soc.* **1989**, *111*, 5471.

79. McClelland, R. A.; Mathivanan, N.; Steenken, S. *J. Am. Chem. Soc.* **1990**, *112*, 4857.

80. McClelland, R. A.; Chan, C.; Cozens, F.; Modro, A.; Steenken, S. *Angew. Chem. Int. Ed. Engl.* **1991**, *30*, 1337.

81. (a) Richard, J. P. *J. Am. Chem. Soc.* **1989**, *111*, 1455. (b) Richard, J. P.; Amyes, T. L.; Bei, L.; Stubblefield, V. *J. Am. Chem. Soc.* **1990**, *112*, 9513. (c) Richard, J. P. *J. Am. Chem. Soc.* **1991**, *113*, 4588. (d) Amyes, T. L.; Stevens, I. W.; Richard, J. P. *J. Org. Chem.* **1993**, *58*, 6057.

82. McClelland, R. A.; Cozens, F. L.; Steenken, S.; Amyes, T. L.; Richard, J. P. *J. Chem. Soc., Perkin. Trans. 2* **1993**, 1717.

83. Johnston, L. J.; Kwong, P.; Shelemay, A.; Lee-Ruff, E. *J. Am. Chem. Soc.* **1993**, *115*, 1664.

84. Schepp, N. P.; Wirz, J. *J. Am. Chem. Soc.* **1994**, *116*, 11749.

85. Chiang, Y.; Eliason, R.; Jones, J.; Kresge, A. J.; Evans, K. L.; Gandour, R. D. *Can. J. Chem.* **1993**, *71*, 1964.

86. Steenken, S.; McClelland, R. A. *J. Am. Chem. Soc.* **1989**, *111*, 4967.

87. Okuyama, T.; Haya, N.; Takane, S.; Ueno, K.; Fueno, T. *Bull. Chem. Soc. Jpn.* **1991**, *64*, 2751.

88. Arnaut, L. G.; Formosinho, S. J. *J. Photochem. Photobiol. A: Chem.* **1993**, *75*, 1 & 21.

89. (a) Ireland, J. F.; Wyatt, P. A. H. *Adv. Phys. Org. Chem.* **1976**, *12*, 131. (b) Martynov, I. Y.; Demyashkevich, A. B.; Uzhinov, B. M.; Kuzmin, M. G. *Russ. Chem. Rev.* **1977**, *46*, 1.

90. Wan, P.; Shukla, D. *Chem. Rev.* **1993**, *93*, 571.

91. Huppert, D.; Gutman, M.; Kaufman, K. J. In *Photoselective Chemistry*; Jortner, J., Levine, R. D., Rice, S. A. Eds; Wiley: New York, 1981; Part 2.

92. (a) Webb, S. P.; Yeh, S. W.; Philips, L. A.; Tolbert, L. M.; Clark, J. H. *J. Am. Chem. Soc.* **1984**, *106*, 7286. (b) Webb, S. P.; Philips, L. A.; Yeh, S. W.; Tolbert, L. M.; Clark, J. H. *J. Phys. Chem.* **1986**, *90*, 5154.

93. (a) Lee, J.; Robinson, G. W.; Webb, S. P.; Philips, L. A.; Clark, J. H. *J. Am. Chem. Soc.* **1986**, *108*, 6538. (b) Harris, C. M.; Selinger, B. K. *J. Phys. Chem.* **1980**, *84*, 891. (c) Harris, C. M.; Selinger, B. K. *J. Phys. Chem.* **1980**, *84*, 1366.

94. (a) Krishnan, R.; Fillingim, T. G.; Lee, J.; Robinson, G. W. *J. Am. Chem. Soc.* **1990**, *112*, 1353. (b) Syage, J. A.; Steadman, J. *J. Chem. Phys.* **1991**, *95*, 2497.

95. Weller, A. *Prog. React. Kinet.* **1961**, *1*, 189.

96. Clark, J. H.; Shapiro, S. L.; Winn, K. R. C. *J. Am. Chem. Soc.* **1979**, *101*, 746.

97. (a) Gutman, M.; Huppert, D. *J. Biochem. Biophys. Methods* **1979**, *1*, 9. (b) Gutman, M.; Nachliel, E.; Huppert, D. *Eur. J. Biochem.* **1982**, *125*, 175. (c) Politi, M. J.; Brandt, O.; Fendler, J. H. *J. Phys. Chem.* **1985**, *89*, 2345. (d) Lee, J. *J. Am. Chem. Soc.* **1989**, *111*, 427.

98. (a) Frater, G.; Schmid, H. *Helv. Chim. Acta* **1967**, *50*, 255. (b) Horspool, W. M.; Pauson, P. L. *J. Chem. Soc., Chem. Commun.* **1967**, 195. (c) Houry, S.; Geresh, S.; Shani, A. *Isreal J. Chem.* **1973**, *11*, 805. (d) Geresh, S.; Levy, O.; Markovits, Y.; Shani, A. *Tetrahedron* **1975**, *31*, 2803. (e) Morrison, H. *Org. Photochem.* **1979**, *4*, 143. (f) Koch-Pomeranz, U; Schmid, H.; Hansen, H. J. *Helv. Chim. Acta* **1977**, *60*, 768.

99. Chow, Y. L.; Zhou, X. –M.; Gaitan, T. J.; Wu, Z. –Z. *J. Am. Chem. Soc.* **1989**, *111*, 3813.

100. (a) Turner, A. B. *Q. Rev.* **1964**, *28*, 347. (b) Wagner, H. -U; Gompper, R. *The Chemistry of the Quinonoid Compounds*; Patai, S., Ed.; Wiley: New York, **1974**; Part 2.

101. Fiswick, C. W. G.; Jones, D. W. *The Chemistry of the Quinonoid Compounds*; Patai, S., Rappoport, Z., Ed.; Wiley: Chichester, **1988**; Part 1, pp 403-453.

102. Kann, K.; Fries, K. *Ann.* **1907**, *353*, 335.

103. Fries, K.; Brandes, E. *Ann.* **1939**, *542*, 48.

104. Gardner, P. D.; Sarrafizadeh, R. H.; Brandon, R. L. *J. Am. Chem. Soc.* **1959**, *81*, 5515.

105. Cook, C. D.; Norcross, B. E. *J. Am. Chem. Soc.* **1956**, *78*, 3797; *J. Am. Chem. Soc.* **1959**, *81*, 1176.

106. (a) Berson, J. *The Chemistry of the Quinonoid Compounds*; Patai, S., Rappoport, Z., Ed.; Wiley: Chichester, 1988. Part 1, pp 455-536. (b) Berson, J. A. *Acc. Chem. Res.* **1997**, *30*, 238.

107. (a) Desimoni, G.; Tacconi, G. *Chem. Rev.* **1975**, *75*, 651. (b) Boger, D.; Weinreb, S. N. *Hetero Diels-Alder Methodology in Organic Synthesis*; Academic Press: New York, 1987. (c) Fringuelli, F.; Taticchi, A. *Dienes in the Diels-Alder Reaction*; Wiley: New York, 1990.

108. Chapman, O. L.; Engel, M. R.; Springeer, J. P.; Clardy, J. C. *J. Am. Chem. Soc.* **1971**, *93*, 6696.

109. Marino, J. P.; Dax, S. L. *J. Org. Chem.* **1984**, *49*, 3671.

110. (a) Génisson, Y.; Tyler, P. C.; Young, R. N. *J. Am. Chem. Soc.* **1994**, *116*, 759. (b) Génisson, Y.; Young, R. N. *Tetrahedron Lett.* **1994**, *35*, 7747.

111. Roper, J. M.; Everly, C. R. *J. Org. Chem.* **1988**, *53*, 2639.

112. (a) Angle, S. R.; Arnaiz, D. O.; Boyce, J. P.; Frutos, R. P.; Louie, M. S.; Mattson-Arnaiz, H. L.; Rainer, J. D.; Turnbull, K. D.; Yang, W. *J. Org. Chem.* **1994**, *59*, 6322. (b) Angle, S. R.; Arnaiz, D. O. *J. Org. Chem.* **1992**, *57*, 5937. (c) Angle, S. R.; Arnaiz, D. O. *J. Org. Chem.* **1992**, *57*, 6883.

113. (a) Leary, G. J. *Wood Sci. Technol.* **1980**, *14*, 21. (b) Shevchenko, S. M.; Apushkinskii, A. G. *Russ. Chem. Rev.* **1992**, *61(1)*, 105.

114. (a) Thompson, D. C.; Thompson, J. A.; Sugumaran, M.; Moldeus, P. *Chem.-Biol. Interact.* **1992**, *86*, 129.

115. (a) Tomasz, M.; Chawla, A. K.; Lipman, R. *Biochemistry* **1988**, *27*, 3182. (b) Egbertson, M.; Danishefsky, S. J. *J. Am. Chem. Soc.* **1987**, *109*, 2204.

116. (a) Li, T.; Zeng, Q.; Rokita, S. E. *Bioconjugate Chem.* **1994**, *5*, 497. (b) Chatterjee, M.; Rokita. S. E. *J. Am. Chem. Soc.* **1994**, *116*, 1690. (c) Boger, D. L.; Nishi, T.; Teegarden, B. R. *J. Org. Chem.* **1994**, *59*, 4943.

117. Janda, K. D.; Lo, L.-C.; Lo, C.-H. L.; Sim M.-M.; Wang, R.; Wong, C.-H.; Lerner, R. A. *Science*, **1997**, *275*, 945.

118. (a) Bolon, D. A. *J. Org. Chem.* **1970**, *35*, 3666. (b) Jurd, L. *Tetrahedron* **1977**, *33*, 163. (c) Zanarotti,, A. *J. Org. Chem.* **1985**, *50*, 941. (d) Dyall, L. K.; Winstein, S. *J. Am. Chem. Soc.* **1972**, *94*, 2196.

119. Filar, L. J.; Winstein, S. *Tetrahedron Lett.* **1960**, *25*, 9.

120. Arduini, A.; Bosi, A.; Pochini, A.; Ungaro, R. *Tetrahedron* **1985**, *41*, 3095.

121. Yato, M.; Ohwada, T.; Shudo, K. *J. Am. Chem. Soc.* **1990**, *112*, 5341.

122. (a) Chambers, J. D.; Crawford, J.; Williams, H. W. R.; Dufresne, C.; Scheigetz, J.; Bernstein, M. A.; Lau, C. K. *Can. J. Chem.* **1992**, *70*, 1717. (b) Bissada, S.; Lau, C. K.; Bernstein, M. A.; Dufresne, C. *Tetrahedron Lett.* **1994**, *35*, 3691.

123. (a) Longuet-Higgins, H. C. *J. Chem. Phys.* **1950**, *18*, 265. (b) Hund, F. *Linienspektren Periodisches System der Elemente*, Springer-Verlag: Berlin, 1927, p. 124. (c) Hund, F. *Z. Phys.* **1928**, *51*, 159.

124. Borden, W. T.; Iwamura, H.; Berson, J. A . *Acc. Chem. Res.* **1994**, *27*, 109.

125. (a) Benson, S. W., *Thermochemical Kinetics*, 2nd ed., Wiley-Interscience: New York, 1976. (b) Liebman, J. F.; Greenberg, A. *Chem. Rev.* **1976**, *76*, 311.

126. Rule, M.; Matlin, A. R.; Hilinski, E. F.; Dougherty, D. A.; Berson, J. A. *J. Am. Chem. Soc.* **1979**, *101*, 5098.

127. (a) Chapman, O. L.; McIntosh, C. L. *J. Chem. Soc. Chem. Commun.* **1971**, 383. (b) Padwa, A.; Dehm, D.; Oine, T.; Lee, G. *J. Am. Chem. Soc.* **1975**, *97*, 1837.

128. (a) Hamai, S.; Kokubun, H. *Bull. Chem. Soc. Jpn.* **1974**, *47*, 2085; (b) Hamai, S.; Kokubun, H. *Z. Phys. Chem.* (Frankfurt) **1974**, *88*, 211.

129. (a) Padwa, A.; Lee, G., *J. Chem. Soc. Chem. Commun.* **1972**, 795; (b) Lenoble, C.; Becker, R. S.; *J. Photochem.* **1986**, *33*, 187; **1986**, *34*, 83.

130. (a) Creed. D. *J. Chem. Soc. Chem. Commun.* **1976**, 121. (b) Creed, D.; Hales, B. J.; Porter, G. *Proc. R. Soc. London, Ser. A:* **1973**, *334*, 505. (c) Gandhi, R. P.; Ishar, M. P. S.; Srivastave, R.; Sarin, R. *J. Photochem. Photobiol. A:* 1994, *78*, 153.

131. Wan, P.; Hennig, D. *J. Chem. Soc. Chem. Commun.* **1987**, 939.

132. Isaks, M.; Yates, K.; Kalanderopoulos, P. *J. Am. Chem. Soc.* **1984**, *106*, 2728.

133. Kalanderopoulos, P.; Yates, K. *J. Am. Chem. Soc.* **1986**, *108*, 6290.

134. Huang, C.–G.; Shukla, D.; Wan, P. *J. Org. Chem.* **1991**, *56*, 5437.

135. Huang, C.–G.; Beveridge, K. A.; Wan, P. *J. Am. Chem. Soc.* **1991**, *113*, 7676.

136. (a) Shi, Y.; Wan, P. *J. Chem. Soc. Chem. Commun.* **1995**, 1217. (b) Shi, Y. *Ph.D. Thesis*, University of Victoria, 1997.

137. Fisher, M.; Shi, Y.; Wan, P. Unpublished results.

138. Seeger, D. E.; Hilinski, E. F.; Berson, J. A. *J. Am. Chem. Soc.* **1981**, *103*, 720.

139. Rule, M; Matlin, A. R.; Seeger, D. E.; Hilinski, E. F.; Dougherty, D. A.; Berson, J. A. *Tetrahedron* **1982**, *38*, 787.

140. (a) Lahti, P. M.; Berson, J. A. *J. Org. Chem.* **1989**, *54*, 958. (b) Lahti, P. M.; Rossi, A. R.; Berson, J. A. *J. Am. Chem. Soc.* **1985**, *107*, 2273.

141. (a) Platz, M. S.; Carrol, G.; Pierrat, F.; Zayas, J.; Auster, S. *Tetrahedron* **1982**, *38*, 777. (b) Platz, M. S.; Burns, J. R. *J. Am. Chem. Soc.* **1979**, *101*, 4425.

142. Matlin, A. R.; Inglin, T. A.; Berson, J. A. *J. Am. Chem. Soc.* **1982**, *104*, 4954.

143. Goodman, J. L.; Peters, K. S., Lahti, P. M.; Berson, J. A. *J. Am. Chem. Soc.* **1985**, *107*, 276.

144. Seeger, D. E.; Lahti, P. M.; Rossi, A. R.; Berson, J. A. *J. Am. Chem. Soc.* **1986**, *108*, 1251.

145. Khan, M. I.; Goodman, J. L. *J. Am. Chem. Soc.* **1994**, *116*, 10342.

146. Yang, C. *M.Sc. Thesis*, University of Victoria, **1994**.

147. Yang, C.; Wan, P. unpublished results.

148. (a) Bowden, S. T.; Beynon, *J. Chem. Soc.* **1957**, 4244. (b) Gomberg, M.; Nishida, D. *J. Am. Chem. Soc.* **1923**, *45*, 190.

149. (a) Chatgilialoglu, C. *Handbook of Organic Photochemistry*, Vol. II, Chapter 1, Scaiano, J. C., Ed. (b) Neta, P.; Schuler, R. H. *J. Am. Chem. Soc.* **1975**, *97*, 912.

150. Berlman, I. B. *Handbook of Fluorescence Spectra of Aromatic Molecules*, 2nd ed., Academic press: New York, 1971.

151. Land, E. J.; Porter, G., Strachan, E. *Trans. Faraday Soc.* **1961**, *57*, 1885.

152. Dobson, G.; Grossweiner, L. I. *Trans. Faraday Soc.* **1965**, *61*, 708.

153. Popovych, O.; Tomkins, R. P. T. *Nonaqueous Solution Chemistry*, John Wiley & Sons: Toronto, 1981, p18.

154. Murov, S. L.; Carmichael, I.; Hug, G. L. *Handbook of Photochemistry*, 2nd ed., Marcel Dekker: New York, 1993, p345.

155. Murphy, R. S.; Barros, T.C.; Barnes, J.; Mayer B.; Marconi, G.; Bohne, C. *J. Phys. Chem.* Accepted.

156. Furniss, B. S.; Hannaford, A. J.; Rogers, V.; Smith, P. W. G.; Tatachell, A. R., *Vogel's Textbook of Practical Organic Chemistry*, 5th ed., Longman: London and New York, 1989, p. 552.

157. Berlman, I. B. *Handbook of Fluorescence Spectra of Aromatic Molecules*, Academic Press: New York, 1971.

158. Liao, Y.; Bohne, C. *J. Phys. Chem.* **1996**, *100*, 734.